Theoretical Investigations of the Electronic Processes in Organic Photovoltaics

by

Shane Robert Yost

B.S., University of California, Santa Barbara (2008)

Submitted to the Department of Chemistry
in partial fulfillment of the requirements for the degree of

Doctor of Philosophy

at the

MASSACHUSETTS INSTITUTE OF TECHNOLOGY

June 2013

Author ....
Department of Chemistry
May 14, 2013

Certified by ....
Troy Van Voorhis
Associate Professor
Thesis Supervisor

Accepted by ....
Robert W. Field
Chairman, Department Committee on Graduate Theses

This doctoral thesis has been examined by a Committee of the Department of Chemistry as follows:

Professor Jianshu Cao ....
Chairman, Thesis Committee
Professor of Chemistry

Professor Troy Van Voorhis ....
Thesis Supervisor
Associate Professor of Chemistry

Professor Marc A. Baldo ....
Member, Thesis Committee
Associate Professor of Electrical Engineering

Theoretical Investigations of the Electronic Processes in Organic Photovoltaics

by

Shane Robert Yost

Submitted to the Department of Chemistry
on May 14, 2013, in partial fulfillment of the
requirements for the degree of
Doctor of Philosophy

Abstract

The design of more efficient organic photovoltaics starts with an increase in understanding of the fundamental processes related to organic photovoltaics, such as the charge separation processes at the organic/organic interface, which can only be remedied by a combined theoretical and experimental effort. In this thesis we use a variety of computational techniques to address current questions in the field or organic photovoltaics. Applying the ΔSCF method to a test set of conjugated organic molecules we find it has an error of ± 0.3 eV, and by using the ΔSCF wavefunctions for a multi-reference basis we construct a new perturb then diagonalize multi-reference perturbation theory method that performs well for both ground and excited state potential energy surfaces, called ΔSCF(2). Our computed singlet fission rates are in near quantitative agreement with experimental measurements in a variety of pentacene derivatives, and we find that the singlet fission mechanism proceeds through a non-adiabatic to adiabatic transition. By combining *ab initio* rate constants and Kinetic Monti-Carlo we get an accurate prediction of triplet diffusion and show that only a small decrease occurs when the crystal becomes highly disordered, and no significant traps exist. Our models of the organic/organic interface reveals that the the simple picture of constant HOMO and LUMO levels throughout an organic photovoltaic device is only qualitatively accurate at best. At the organic/organic interface effects such as change in the dielectric constant, decreased packing efficiency, and molecular multipole moments all can contribute to changing the HOMO and LUMO levels at the interface by over 0.2 eV, which is large enough to drive apart thermally relaxed charge transfer states at the interface. The work in this thesis provides insight into how to achieve better exciton diffusion and charge separation in organic photovoltaics, as well as insight into a number of electronic processes relevant to organic photovoltaics.

Thesis Supervisor: Troy Van Voorhis
Title: Associate Professor

Acknowledgments

The work presented in this thesis could not have been completed without the help and support of many people. I would first just like to thank my adviser Troy Van Voorhis for all of his guidance. He has provided a lot of help for all of my different research projects over the years. I have had many fruitful discussions with Troy, and without which I would not have been able to finish all of the projects presented in this Thesis. Troy has been an excellent adviser and I will always be grateful for my experiences in his group.

I would like to thank previous and current group members Tim Kowalczyk, Ben Kaduk, Lee-Ping Wang, Seth Difley, Laken Top, Sina Yeganeh, Oleg Vydrov, Eric Hontz, Michael Mavros, Matt Welborn, Helen Xie, Jiahao Chen, David McMahon, and Takashi Tsuchimochi for both scientific and non-scientific discussions. For the older group members I would like to thank them for answering my many questions throughout the years. Thank you to my office-mates Lee-Ping and Eric for putting up with my pestering and me talking with myself throughout the years, as well as being my good friends.

In particular I would like to thank Tim for his help on the work on ΔSCF and ΔSCF(2). Tim contributed equally on both projects with me and helped a lot with the implementation of the ΔSCF(2) formulas. Thank you Lee-Ping and Seth for creating the foundations for the organic/organic interface project by creating a method of constructing and running the quantum mechanics/molecular mechanics calculations. Thank you Sina for getting the Kinetic Monti-Carlo code together for the triplet diffusion project and Eric for helping compute the hopping rates. Thank you David for working with me on computing the ΔSCF and CDFT states to compute the couplings for the singlet fission project.

Though not directly related with research I would like to thank the other system-administrators for our group cluster, Ben, Lee-Ping, and Matt for the group cluster for putting up with my lack of computer knowledge. I would also like to thank the members of the Zoo for many enjoyable lunches and fun discussions.

I would like to thank my experimental collaborators Marc Baldo, Jiye Lee, Priya Jadhav, Carlijn Mulder, Sebastian Reineke, Nick Thompson, Dan Congreve, Tony Wu, Phil Reusswig, Matthias Bahlke, and Mark Wilson, with out them I would not know much about organic electronics or the implications of many of my results. In particular I would like to thank Marc Baldo for many helpful discussions and the opportunity to collaborate with many members in his group. I would like thank Jiye for the close collaboration on many projects, in particular the singlet fission work.

I would like to thank my thesis chair, Jianshu Cao, and former thesis chair, Bob Silbey, for their help as well as very useful and insightful lectures during my first year at MIT.

For all of their support throughout my graduate career and beforehand I would like to thank my family members, especially my parents Garold, Susan, and Barbara Yost. My graduate studies were made easier with knowing that I always had a family to help me if I asked. I would also like to thank Sandy and John Rankin for the many wonderful visits down to their house. It was a great help to have a place I could go and be with family. Thank you Casandra Cox for being my very good friend. Your friendship has helped me enjoy my life outside of work. Thank you to my roommates Nate Brandt and Andrew Horning for dealing with all of my venting when I arrive home. My work has been made easier by having a very relaxing environment at home and I am grateful for that. Finally, thank you to my caring wife Alejandra Nehme for your love and support. Even though my work made for some late nights I always knew I had your support, and I am very grateful to have you as a permanent inspiration in my life.

To any of those I have forgotten to mention, thank you for your support, help, and friendship.

Contents

List of Figures

List of Tables

Chapter 1

Introduction

The role of photovoltaic (PV) materials in today's energy market is continually expanding.[5,6] The main challenge in keeping this trend is to continue to increase the efficiency at which solar energy is converted to electricity in a PV device. The original photovoltaic type systems are contained in cells in plants and bacteria that perform very efficient photosynthesis.[7–12] In these different natural systems many proteins in a cell are used to perform the steps in photosynthesis that, in the end, store the suns energy in chemical bonds. Man-made devices, on the other hand, combine all of the photovoltaic steps into one system, but are not nearly as efficient. In a photovoltaic device sunlight is first absorbed and then converted into an excited electron and hole, which must separate to different electrodes in order to create any electrical work. For inorganic semiconductors, the absorbed photon immediately creates an electron and hole pair with a binding energy on the order of kT, and therefor it requires very little effort to separate them. The typical inorganic photovoltaic system is made of p- and n-doped silicon layers next to each other. The doping in the silicon causes the Fermi levels to be different, so when they are brought into electrical contact electrons transfer from the n-doped silicon into the p-doped silicon. This charge transfer creates a dipolar electric field at the interface between the two silicon layers, and it is this electric field that helps create efficient charge separation in silicon PVs.[13]

The most efficient single-junction, crystalline silicon PV device convert 25% of the suns solar power into electricity,[14] approaching the maximum thermodynamic limit given by Shockley and Queisser[15] of 33%. Silicon PVs need to be very thick in order to absorb all of the sunlight hitting the device[17] in order to achieve their maximum efficiency. Despite their efficiency, silicon PVs are still not widely used because the processing and instillation costs combined with their average lifetime make them too expensive to compete in today's energy market.[16]

In order to get over this road-block researchers have been looking into a wide range of PV materials including organic/organic[6,18,19] and hybrid inorganic/organic based[20,21] PVs. Unlike in the case of the inorganic PVs, organic photovoltaics (OPVs) can be made with cheap processing techniques and are light weight, but their efficiency is currently limited to 12%.[22] When sunlight is absorbed in OPV devices the organic semiconductor (OSC) materials do not generate free charge carriers upon absorption, but instead create a coulombically-bound electron-hole pair (known as an exciton).[23–26] Excitons are the result of a small dielectric screening between the electron and hole, which leads to a large binding energy between the charges.[23] In OPVs, this exciton binding energy is overcome due to the energy offset at an interface of two OSC materials.[27,28]

The photovoltaic process in a functioning OPV starts when (i) sunlight is absorbed and forms an exciton, (ii) then the exciton diffuses to an interface; (iii) at the interface, the exciton forms a charge transfer (CT) state, where now the electron and hole are on two different molecules; (iv) finally the electron and hole separate and diffuse to the cathode and anode, respectively.[23,27] In order for OPV devices to reach the Shockley-Queisser limit,[29] each one of the four processes needs to be optimized, which requires a fundamental understanding of each process to guide device engineering.

There are a number of current limitations in OPVs. One issue is that despite the much stronger absorption in OPV devices they are not able to be made thick enough to absorb all of the incident sunlight.[30] The main reason for the size limitation of OPV devices is the diffusion length of the singlet exciton.[31] So when an OPV is made thicker to absorb more sunlight it reaches a point where the added excitons do not reach the interface to form charges. One way to try and resolve this issue is by engineering different device structures, such as bulk-hetero-junction OPVs,[32–35] and optimizing contacts at the electrodes.[36] Another problem is that while experimentalists have found that charge separation at the organic/organic interface can be very efficient,[19,37,38] the processes governing this fast breakup of the charges are not fully understood. The lack of understanding of charge separation at the organic/organic interface makes it difficult to know before making a device if the charges will be able to separate and make it to the electrodes efficiently.

The key to rational design of fast and efficient exciton break up at the organic/organic interface is understanding the interplay between molecular properties and device performance. At an organic/organic interface, the key properties are the highest occupied molecular orbital (HOMO) and lowest unoccupied molecular orbital (LUMO) levels of each material, the offset between the LUMOs (ΔL) and HOMOs (ΔH), and the difference between the acceptor LUMO and donor HOMO (E_{gap}), all of which are represented in Figure 1-1. The HOMO and LUMO levels are equivalent to the ionization potential (IP) and electron affinity (EA) of the material, respectively. The energy gap, E_{gap}, is the maximum limit to the open-circuit voltage (V_{OC}), and is reduced by the relative efficiency of charge separation vs. recombination.[39]

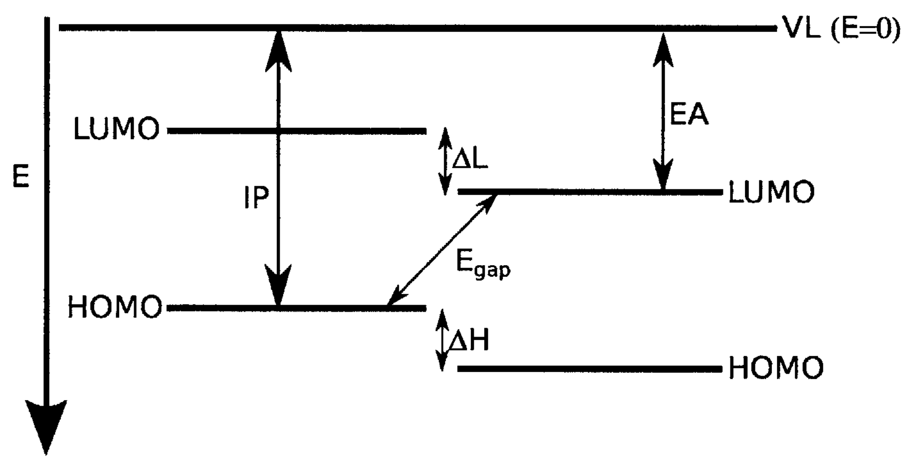

Figure 1-1: General band diagram for an OPV device with the donor (red) and acceptor (blue) HOMO/IP and LUMO/EA levels. All of the energies are relative to the vacuum level (VL). The energy difference ΔL between the LUMO of the donor and acceptor provide the driving force for charge formation, and E_{gap} is the maximum possible open-circuit voltage from an organic photovoltaic device.

A number of papers have been published on potential ways to optimize the properties of organic semiconductors in order to achieve a better OPV device.[29,40–42] Almost all of these studies, however, focus on optimizing the HOMO and LUMO levels with respect to those of Phenyl-C61-butyric acid methyl ester (PCBM), while keeping the band gap of the polymer small to use in bulk hetero-junction polymer/PCBM OPV device.[43–45] Optimization of the bulk HOMO and LUMO levels is a straightforward goal, but in actual devices factors such as polymer morphology and charge recombination complicate the optimization.[46] To avoid unforeseen problems when making an OPV device with a new material we need an improved molecular understanding of the static properties and dynamic processes in OPV devices.

1.1 Singlet Fission

A significant loss process that is part of the Shockley-Queisser limit is the energy lost to heat as a high energy exciton relaxes to the band gap of the material. The most obvious way to try and fix this issue is to extract the excitons energy and create charges before the excitons are able to relax down to the band gap,[47,48] but this is very difficult because of the fast relaxation time scale. Another way to solve this problem is to create multiple excitons of lower energy from a higher energy exciton, that is known as multi-exciton-generation (MEG). MEG has been observed since the 60's in organic acene molecules,[49,50] and has more recently be proposed to occur in quantum dot systems.[51,52] In the organic materials the MEG process is called singlet fission because one singlet exciton splits up into two triplet excitons that are at half of the singlet energy. Including singlet fission molecules in an OPV device can increase the Shockley-Queisser limit to above 40%,[53] and can give internal quantum efficiencies above 100%,[54] since two electrons can be created from one photon.

Unfortunately, like charge separation at the organic/organic interface, the mechanism for singlet fission is not fully understood. Once the singlet excited state is formed, Figure 1-2 left, it has two possible routes to form the triplet-triplet dimer state, Figure 1-2 right. The singlet can go through an intermediate charge transfer state, Figure 1-2 top, before reaching the triplet-triplet state,[55] or the singlet can directly form the triplet-triplet state through a two electron transfer process. Both of the mechanisms are possible and will depend on the coupling and energy differences between the different excited states. If the coupling is large enough between the singlet and charge transfer state then the excited bright state could be a coherent mixture of the two states. In which case, the coupling for the direct mechanism would be increased due to the mixing of the charge transfer state, this is called super-exchange.[53,56–58] Given a large enough singlet and triplet-triplet coupling the initial bright state could be a coherent mixture of both states, and the triplet-triplet state would then just be formed by the bright state decohering into the triplet-triplet state.[59,60]

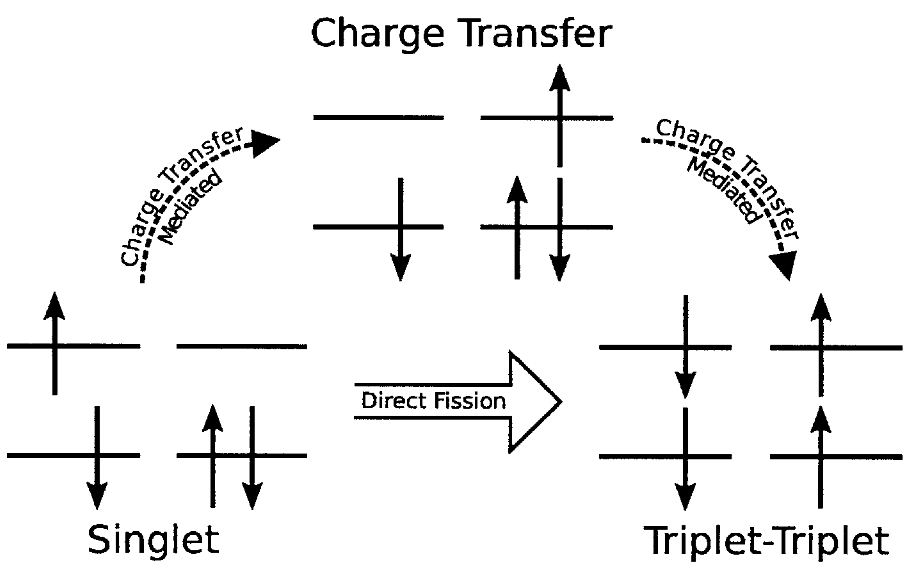

Figure 1-2: The mechanism for a singlet excited state converting into two triplet excited states can happen either through a direct two electron transfer process, or through an indirect one electron transfer process where the charge transfer state is an intermediate state.

Using time resolved transient absorption measurements[61–63] researchers have been able to measure singlet fission rates in many different organic molecules. In the case of the pentacene molecule the fission process occurs on the order of 80 fs,[59,61] which indicates that a more direct mechanism of singlet fission is more likely. The singlet fission rate for tetracene thin films have been measured between 1-100 ps.[53] Unlike pentacene, the energetics in tetracene are such that the triplet-triplet state is a little above the singlet state, which makes it very dependent on minor changes in the singlet energy. The variation in measured tetracene thin film fission rates might then be caused by variation in the crystallinity of the measured thin films because the singlet energy depends greatly on the delocalization lengths, as seen in the difference between solution and thin film spectra.[64]

More recently measurements using time resolved photo-electron spectra (TR-2PPE) were performed on tetracene and pentacene.[59,60] In both of these measurements the authors found a low energy peak, associated with ionization of the triplet state, that rose with the singlet peak on the time resolution of the experiment, $\sim$25 fs. The interpretation of these measurements are that the singlet and triplet-triplet excited states are coherently mixed together upon excitation. Theoretical models have not found couplings between the singlet and triplet-triplet state to support a coherent energy transfer process.[56–58,65] The different calculations have reported varying coupling strength between the singlet, triplet-triplet, and charge transfer state depending on what approximations are made and what type of quantum chemistry calculations are performed.

At the moment there is no agreement on what the dominant mechanism for singlet fission is in a given molecule, let alone across a wide variety of different singlet fission molecules. The complexity of the fission process has made it difficult for researchers to agree on an accurate and reliable theoretical or experimental method for determining the fission rate. This leaves a lot of opportunity for experimental and theoretical studies to further the understanding of the singlet fission mechanism in different systems. Given a better understanding of the singlet fission mechanism, new molecules can be created from improved design principles that can be used to drastically increase the efficiency of OPVs.

1.2 Exciton Diffusion

Another concern for OPVs is the limited diffusion length of the singlet exciton. In most OPV devices if the active organic layers are made too thick then a large number of excitons will not reach the organic/organic interface and just decay radiatively or non-radiatively back to the ground state.[30] In typically OPV devices the diffusion length of the singlet exciton limits the optimal thickness of the donor or acceptor layer to 10-20 nm,[30,31,66] which is not thick enough to absorb all incident photons. One way to alleviate this problem is to avoid it altogether by using device architectures like that of a bulk-heterojunction, so that no matter where the exciton is formed in the organic materials it does not have far to travel to reach an organic/organic interface. While using the bulk-heterojunction architecture helps resolve the exciton diffusion problem, it creates a number of new issues with things like charge extraction.[46] The more direct way to increase OPV thicknesses is to try and increase the exciton diffusion length through molecular design.

Optimizing the exciton diffusion length has proven difficult because it depends on monomer properties, molecular packing, and it is not easy to measure experimentally. The diffusion length of singlet and triplet excitons are mainly measured using photoluminescence[66–69] or photocurrent[70–72] methods, but measurements on the same molecule can sometimes disagree by orders of magnitude for triplet[72–74] and singlet[75–77] excitons. One common complication that can alter the measured exciton diffusion length is the emission of a photon that is then waveguided in the crystal and reabsorbed by another molecule. This waveguide effect can incorrectly increase the measured diffusion length.[78] Furthermore, photocurrent studies can over estimate the diffusion length due to metal penetration into the organic layer[79] and optical interference near the metal interface.[80] While the method for measuring the exciton diffusion length is improving[66] there is plenty of room for computations to help in our ability to measure and control exciton diffusion lengths.

One question in the area of exciton diffusion is how important quantum coherence is to the diffusion of the exciton. While the contribution of quantum coherence in photosynthetic systems is still up for debate,[81–83] a number of experiments and theoretical models have found that only at low temperatures or in highly ordered systems does quantum coherence impact the motion of excitons.[84–87] Very little theoretical work has been done on modeling the motion of triplet excitons in OPVs, mainly because it is not relevant in most OPVs and it is assumed that the disorder in these systems makes it very difficult for the very localized triplet exciton to diffuse. For the case of singlet fission materials it is important to determine how much the triplet diffusion length is hindered by disorder because if the triplet excitons formed can not reach the organic/organic interface then the overall singlet fission process will not help increase the device efficiency. In general there is still the issue of how much can the diffusion length of singlet or triplet excitons be increased. If there is some underlying limit to their diffusion length then one must rely on device architecture to circumvent the problem.

1.3 Organic/Organic Interface

Once the exciton reaches the organic/organic interface and forms a charge transfer state, the electron and hole still need to separate to the electrodes. Coulombs law tells us that the electron and hole formed in the acceptor and donor material, respectively, must be bound by some amount of energy. In most OPV systems the binding energy for the charge transfer state is around 0.2-0.4 eV, much larger than the available thermal energy of 0.03 eV. However, many OPVs are nearly 100% efficient at creating a free charge from an exciton,[37,38] which is counter intuitive to the idea that there is not enough thermal energy to separate the charges from the organic/organic interface. The experimental trend that ΔL and ΔH (from Figure 1-1) needs to be at least 0.2 eV for efficient OPV performance has led some to believe that the excess energy from the exciton goes into vibrationally[88,89] exciting the charge transfer state. The idea is then the high charge separation efficiency is due to thermal storage of excess energy[89,90] into vibrational energy (resulting in what are known as hot charge transfer states), which then provides the energy necessary to overcome the binding energy between the electron and hole of the charge transfer state. It has also been suggested that the charge transfer binding energy is overcome by storing the excess exciton energy in low-lying (0.2-0.4 eV) electronic excited states in the anion state of fullerene derivatives.[91] Contradictory research has shown that in efficient OPV systems the formation of a hot charge transfer state makes no significant difference in the charge separation rate when compared to thermally relaxed charge transfer states.[92,93] The conflicting experimental reports suggest that other possible mechanisms might be contributing to the efficient charge separation.

If the excess exciton energy does not go into creating a hot charge transfer state, then it could go into creating an initially delocalized charge transfer state.[91,94,95] If the charge transfer state is more delocalized, then it will have a much smaller binding energy, making it easier to separate. A recent study by Jailaubekov and co-workers using both experimental and computational methods found fast charge separation at the copper phthalocyanine (CuPc)/C_{60} interface.[94] The initial charge transfer state that is found to lead to quick charge separation is one where the electron and hole are not located on nearest-neighbors. The similarity in energy between delocalized charge transfer state and the singlet excited state makes the energy transfer rate between these two states significantly faster.

The work of McMahon *et al.* provides a similar view through the use of an atomistic model of the interface between a poly(3-hexylthiophene-2,4-diyl) (P3HT)/PCBM interface, where the exciton was proposed to undergo direct dissociation into relatively delocalized charge carriers.[96] In addition, it was found that due to an increase in the disorder of the polymer at the interface relative to the bulk, there is an increase in the band-gap of the polymer at the interface. The increased stability of the charge carriers away from the interface and delocalized nature of the charges was proposed as a possible explanation for the increased efficiency and low charge recombination rate observed in devices based on P3HT/PCBM blend. The calculations are backed by the findings of Guo, who, in a study on regio-regular P3HT and regio-random P3HT, found that most excitons can dissociate at the interface, but only in regio-regular P3HT do the majority of excitons lead to free carriers.[97] This has been further studied in the work of Bakulin *et al.*, in which the authors suggest that charge-separation in highly efficient devices occurs through delocalized band states, as opposed to energy-gradient driven intermolecular hopping.[93] These delocalized states help suppress charge-recombination due to the increased distance between the charge carriers and the reduced binding energy of the resultant delocalized states.

Another possible explanation for the fast separation of charge transfer states at the organic/organic interface is that the HOMO and LUMO levels bend in such a way that the electrons and holes are driven away from the interface. This idea is similar to how inorganic PVs function, and as in inorganic PVs, partial charge transfer has been measured in organic/organic interfaces to match the charge neutral levels of the materials.[98,99] The amount of charge transferred at the organic-inorganic interface can be significant, while very little to no charge transfer typically occurs at organic/organic interfaces.[100] The lack of partial charge transfer at organic/organic interfaces does not mean that the HOMO and LUMO levels in an OPV are the same throughout the device. The electron and hole states can be highly dependent on their environment, which can be drastically different at the organic/organic interface than in a bulk OSC material.[101–106]

There is still no set consensus on how charges form and separate efficiently at the organic/organic interface. The complex nature of the organic/organic interface, coupled with the lack of accurate experimental techniques with which to probe the charge transfer state at the interface, necessitates further use of simulations and theory in order to help determine the dominant, if any, charge separation mechanism for different OPV devices.

1.4 Quantum Chemistry Methods

Almost all of the steps in the photovoltaic processes occur in molecular excited states. The type of excited states that are important are the low lying singlet, triplet, and charge transfer (CT) excited state. The singlet excited state will determine the absorption and exciton diffusion properties of an OSC. Depending on the properties of the triplet excited state, the singlet excited state can intersystem cross or undergo singlet fission to form triplet states. Forming a triplet excited state could potentially be a loss or a gain process in an OPV depending on the diffusion properties of the triplet exciton and its energy. Then at the organic/organic interface the singlet or triplet exciton must form a CT excited state. The performance of an OPV depends heavily on the energetic and kinetic properties of the molecular excited states.

Almost all excited state methods require to first compute the ground state wavefunctions or density. One of the more original approximate methods used to compute the ground state is the Hartree-Fock (HF) method,[107] though the most commonly used ground state method now is Köhn-Sham density functional theory (DFT).[108–111] The Köhn-Sham equations reduce to a solving a set of one electron equations

$$\left[-\frac{1}{2}\nabla^2 + \nu(\mathrm{r})_{ext} + \int \frac{\rho(\mathrm{r'})}{|\mathrm{r} - \mathrm{r'}|} d\mathrm{r'} + \nu_{xc}(\mathrm{r})\right] \psi_i = \epsilon_i \psi_i \tag{1.1}$$

Where the first term on the LHS is the Kinetic energy operator, $\nu(\mathrm{r})_{ext}$ is an external potential, the third term is the coulombic potential, and ν_{xc} is a potential that is quantum mechanical in nature (called the exchange-correlation potential). In theory, solving the Köhn-Sham DFT equations will yield the exact solution to the Schrödinger equation, but in practice approximations are required because the exact functional form of the exchange correlation potential (xc-functional) is unknown. The xc-functional describes all of the complex two-electron interactions in a DFT calculation. Many different approximations to the xc-functional exist.[112–116] The different approximate functionals include pure functionals, such as LDA[108] and PBE,[117] which only use properties of the electron density itself. Hybrid functionals, such as PBE0[118] and B3LYP,[119] incorporate some amount (specific to the functional) of exact HF exchange. Additionally, a recent class of functionals, known as long-range-corrected (LRC) functionals, smoothly separate electron interactions into short-range and long-range components and treat the short-range component using a typical functional and the long-range component using only HF exchange.[120–123]

If the right xc-functional is chosen for a given problem, DFT can perform very well.[124–127] One major error that plagues DFT is the fact that for most xc-functionals the electron repels itself.[128,129] The self repulsion of the electron causes the electrons in a molecule to over delocalize, and while for small molecules this isn't a problem it does start to become an issue for large π-conjugated systems like polymers. Issues like excess partial charge or spin transfer can occur.[129,130] In conjugated polymer based systems the HOMO $\rightarrow$ LUMO gap is under predicted using most xc-functionals.[131] The more recent LRC functionals do provide some potential fix to the self-repulsion issue, though it may be due to a cancellation of errors between DFT and HF because the exact HF potential has the opposite effect of over localizing the electrons.

The main issue in the HF method is that it is a single determinant method that does not include any correlation interactions between the electrons, and as such has limited accuracy.[132,133] The missing electron correlation can be split into two main categories, static and dynamic correlation. Static correlation is mainly due to the true wavefunction having significant contribution from multiple HF-like determinants, and dynamic correlation is due to weak interactions between the occupied and high lying virtual orbitals. Higher level wavefunction-based methods such as couple cluster,[134–136] configuration interaction,[107,137,138] and active space based[139–141] methods include multiple determinants to incorporate some of the electron-electron correlation. Perturbation theory methods, such as second order Møller-Plesset perturbation theory,[142] go beyond the HF method by perturbatively adding dynamic electron correlation. Many of these correlated wavefunction-based methods have well-defined ways in which they approach the exact solution to the Schrödinger equation and thus have the potential to be extremely accurate, but this accuracy comes at a very high computational cost.[143]

To compute the excited state from these ground state based methods one typically applies a linear response approach to the time dependent form of the method, for example time dependent density functional theory (TDDFT). Linear response TDDFT[144–146] is the most commonly used excited state method, due to its low computational cost and decent accuracy of ± 0.3 eV.[125,147,148] The accuracy of TDDFT depends not only one the choice of xc-functional but also on the type of excited state being calculated. For most OSC small molecules or polymers the singlet excited state is a HOMO $\rightarrow$ LUMO excitation because the extended π-conjugation creates a low band gap between the π bonding and π anti-bonding orbitals. This is useful for TDDFT since those types of excited states are ones where it is most accurate. However, if we try and compute Rydberg type excited states or charge transfer excited states then TDDFT significantly fails.[146,149]

The self-interaction error already mentioned also causes issues when computing excited state properties using TDDFT. Because of the self-interaction error, the CT state predicted out of TDDFT for a HOMO $\rightarrow$ LUMO excitation reduces down to the orbital energy differences between the HOMO and LUMO (assuming the electron and hole are spatially separated). The self-interaction error also creates errors in the orbital energies. The combination of these two errors gives rise to the drastic underestimation of the CT state energy in TDDFT, as well as causes a non $1/R$ decay in the CT state energy with separation distance. The LRC functionals discussed above seem to work much better for troublesome systems in TDDFT and achieve more accurate CT state energies.[150]

For methods like linear response time dependent Hartree-Fock (TDHF) and configuration interactions singles (CIS) there is no self-interaction error due to the exact treatment of the exchange interaction. However, the lack of correlation in TDHF and CIS causes these methods to have very limited accuracy for both singlet excited states and CT states. Which is why TDDFT is still more commonly used to compute excited state energies.

An old method, but relatively unused, called ΔSCF is a time-independent method capable of computing excited states.[151] In the ΔSCF method the excited state is computed by selecting a non-Aufbau occupation of the wavefunction/density, Figure 1-3 middle, and enforcing that non-Aufbau occupation during a HF or DFT calculation until it converges onto the final ΔSCF state, Figure 1-3 right. It can be sometimes difficult to stay in the correct non-Aufbau excited state during the minimization, and as such schemes like the maximum overlap method[152] are very useful to insure convergence onto the right ΔSCF state. The excited state determinant computed using this method will not be an eigenfunction of the spin operator, and will require an extra step in order to obtain spin pure singlet excited states.

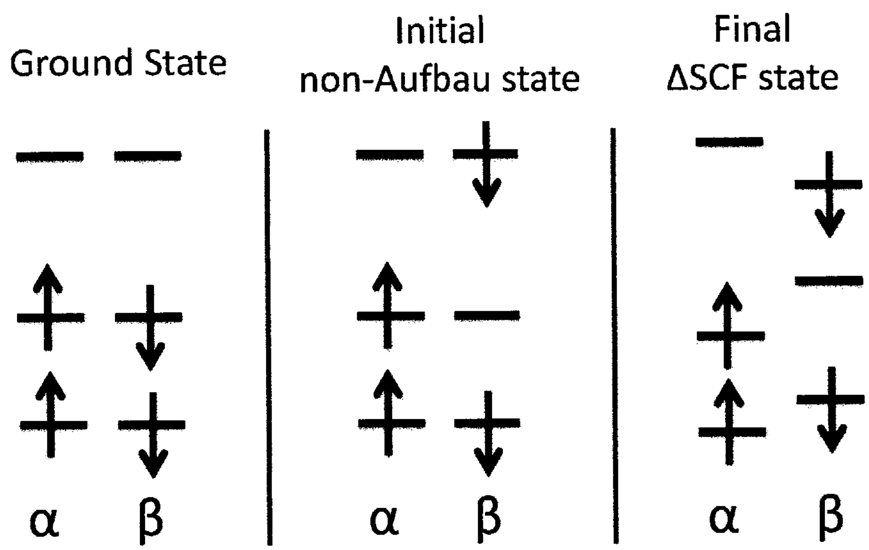

Figure 1-3: The ΔSCF method computes excited states by first taking the ground state (left),applying a non-Aufbau occupation (middle), and minimizing the wave-function/density under the enforced non-Aufbau configuration until the ΔSCF excited state is converged (right).

Except for some groups using ΔSCF to compute core excitations for X-ray spectra,[152] ΔSCF has not been tested for these molecules used in OPVs. The HOMO → LUMO nature of the lowest energy excited state for OSC materials lends itself to this type of calculation, though the accuracy of ΔSCF has not been studied using recent DFT functionals.

In order to compute CT states more directly and accurately one can employ another time-independent method called constrained DFT (CDFT),[153–155] which works by performing a constrained minimization of the density such that specified regions of the system have certain amounts of charge and spin. If for example, one wants a CT state with an extra electron on an acceptor molecule and one less electron on a donor molecule, then in CDFT an electrostatic potential is applied at each minimization step such that the density on the acceptor molecule has one extra electron and the density on the donor has one less electron. The CDFT method has been applied to a number of different inter- and intra-molecular charge transfer systems with high accuracy.[156–158] The only drawback of CDFT is that you need to have an idea as to how much charge should be transfered in order to perform the calculation, but for OPV systems the electronic states have either no net charge or one more/less electron so this is not an issue.

The other important electronic states for an OPV system is the cation of the donor and the anion of the acceptor, which are used to compute the ionization potential (IP) and electron affinity (EA) of a material. The HOMO and LUMO energies in Figure 1-1 are exactly equivalent to the IP and EA of the material, respectively. For non polymeric systems, we can typically make the reasonable approximation that the disorder in an OSC material and the low coupling between molecules causes very localized states, and as such, we can use the IP and EA of a single molecule. Because of the self-interaction error in DFT accurate IP/HOMO and EA/LUMO energies are usually computed using IP $= E(\text{cation}) - E(\text{ground})$ and EA $= E(\text{ground}) - E(\text{anion})$. It is important to emphasize, however, that the IP/HOMO and EA/LUMO in the bulk can vary substantially from what a gas-phase QM calculation predicts, due to the environment and delocalization effects.

Multi-reference wavefunction based methods like the coupled cluster method and configuration interactions method can also be used to compute excited state properties.[159–162] These methods can obtain accurate ground state and excited state properties no matter what type of excited state is being computed. But they are greatly hindered by the size of the system, typically less than 100 heavy atoms, that can be computed due to very poor scaling of the methods with the basis set size. One method that has been shown to get both accurate energies and is more computationally feasible on larger systems is the complete active space self consistent field method (CASSCF).[140] CASSCF works by defining an active space of orbitals, say the HOMO and LUMO, and minimizing the orbital coefficients and CI coefficients within the active space. CASSCF obtains a lot of the static correlation, but it does not get much of the dynamic correlation. In order to add on dynamic correlation Roos and co-workers choose to add a second-order perturbation theory correction to the ground and excited states of the CASSCF wavefunctions.[163,164] This CAS method with perturbation theory, called CASPT2, can compute even more accurate excited state energies. However, CASSCF and CASPT2 are limited to an active space of typically 12-13 orbitals, and in CASPT2 there is no set definition for the zeroth-order Hamiltonian used to apply the perturbation theory correction to.[165,166] Work is continually being done to try and create a multi-reference perturbation method that is both fast and highly accurate for excited states due to their importance in many molecular systems.[167–170]

1.5 Condensed Phase Simulations

All of the above computational methods do not include the environment in which the molecules exists for OPV models. The molecular packing in OPVs is typically disordered, due to the weak Van der Waals intermolecular interactions holding the molecules together[23] and the processing techniques used to make the devices, such as spin-casting.[171,172] The interplay between structural disorder, molecular distance, and orientation significantly affect the electronic properties in an OPV, which in turn affects the nature and mechanism by which free charge carriers can be generated. Without the inclusion of these considerations, any computational study will be incapable of accurately describing the performance of OPV materials. The geometry, electronic structure, and energetics of an isolated molecule are defined by its gas-phase Hamiltonian, but the surrounding molecules in an OPV cause perturbations through electrostatic and polarization interactions. Thus, the singlet, triplet, CT, HOMO, and LUMO energies can be highly dependent upon the configuration of the surrounding molecules or, more importantly, the proximity to the interface. Disorder also affects intermolecular couplings and charge transfer state energies, because they are highly dependent upon the distance between and the relative orientation of the molecules involved.

Unlike the case for triplet excited states, which are very local and have no significant multipole moment, the surrounding environment can greatly impact the energy and properties of the singlet and CT excited states. The main environmental impact on the singlet excited state is the amount of disorder, which will change how well the singlet excited state is able to delocalize over many molecules. In the case of a homo-dimer the two monomer excited states, (ψ_1, ψ_2), can couple together to produce two dimer excited states $\Psi_+ = \frac{1}{\sqrt{2}}(\psi_1 + \psi_2)$ and $\Psi_- = \frac{1}{\sqrt{2}}(\psi_1 - \psi_2)$. The transition dipoles of the monomer excited states can add or subtract in the same way. When the monomers are placed head-to-tail Ψ_+ is the only excited state that has a non-zero transition dipole and is the lower energy state. When they are placed parallel to each other Ψ_+ is still the only excited state with a non-zero transition dipole moment, but it is now the higher energy state. Any orientation between these two will make it so that both Ψ_+ and Ψ_- have non-zero transition dipole moments. In a thin film or crystalline environment these effects are amplified due to coupling between many monomers causing effects like J-aggragation, H-aggragation, and Davydov splitting to appear in the absorption and emission spectra.[23,173]

The most straight-forward way to compute these coupled excited states, or aggregate states, would be to just apply our favorite procedure, say TDDFT, to a system composed of many monomers. This, however, is not very feasible due to the limitations on the number of atoms that can be treated for even methods like TDDFT. Furthermore, in TDDFT the self-interaction error will become even worse and the excited state manifold will be plagued with numerous fictitious CT states. One way to try and get around this issue is to apply semi-empirical type methods. The spirit of semi-empirical methods is to partially (or fully) ignore or approximate the two-electron integrals of HF theory, which are, by far, the most expensive part of the calculation.[174–178] Most semi-empirical methods parameterize some aspect of the calculation, using parameter values tuned to reproduce experimental or high-level computational data. They are typically less accurate than DFT and correlated wavefunction methods, and just like choosing the proper functional in DFT, their performance can depend on which type of semi-empirical approximation is used.[179–181]

They are reasonably accurate at predicting charge distribution in a large system and can be used to determine the energetics of a charge or CT state in a polarizable environment,[182,183] such as an interface.[106,184]

Another approach is to break up the system into monomer and dimer calculations. By computing the energy of each molecule/monomer and the electronic coupling between them, one can construct a Hamiltonian and the eigenstates of which are the delocalized states of the system.[182] This is exemplified by the work of McMahon *et. al.* in which they compute the electronic structure of P3HT at the interface with amorphous PCBM[96] through the use of a localized molecular orbital method[185] to obtain the eigenstates of the system containing thousands of atoms with a quantum chemical level of detail. Each individual calculation is feasible using this method, but the number of dimer calculations quickly grows with the system size. To make things simpler and drastically cheaper, one can take a Hückel-type approach and consider only nearest-neighbor couplings. These types of simulations can provide a good qualitative estimate on the amount of delocalization within an OPV device.

Unlike the singlet and triplet excited states, the CT state, HOMO level, and LUMO level significantly depend on the environment they are located in. Since all of these states are composed of charged molecules, or charged fragments of a molecule, their energy will be greatly affected by the electrostatic environment. One important environmental factor in the condensed phase is the surrounding dielectric, which stabilizes charges. A simple option for incorporating effects from the environment into a QM calculation is to use a dielectric continuum model.[186–188] The electronic structure calculation is solved self-consistently in response to the surrounding dielectric. The calculation only requires the input geometry of the QM system and a few parameters, such as the effective dielectric constant of the surroundings. Unfortunately, an effective dielectric constant of the system is not always available, and the calculated charge state energy can be sensitive to the choice. In addition, a continuous dielectric is a poor model for the environment of a molecule very near to an interface, since there are two different types of polarizable molecules surrounding it.

One of the more common methods to obtain a detailed description of the environment is to use classical forces to describe the surroundings. In this classical technique the environment is modeled with molecular mechanics (MM) force fields in order to simplify the simulations. Instead of explicitly treating all the electrons of a system, MM force fields treat each atom as a particle with a Van der Waals radius, constant effective charge, and polarizability. The force field contains potential energy functions that define the energy of bonds, angles, and dihedrals within a molecule. Additionally, force field parameters are not generally transferable between different molecules. Currently, force fields exist for very few OPV molecules, so one must usually create a new force field for a given OSC molecule.[189] The typical scheme for creating force fields involves matching the parameters to QM calculations and, sometimes, available experimental data (such as the material density).[190] Difficulties arise in the parameterization of force fields for polymers, because QM is too expensive and experimental data can be difficult to trust, due to the existence of multiple possible structures and morphologies, which can depend on the molecular weight and even how the material was processed (e.g. two known crystal phases of P3HT exist[191,192]).

By calculating energies using force fields, rather than approximate solutions to the Schrödinger equation, MM simulations can handle extremely large system sizes with thousands to millions of atoms, depending on the complexity of the force field. Unfortunately, the accuracy of MM force fields can be quite low compared to QM methods, and energies of excited states and couplings cannot be calculated through MM. Though, MM simulations do provide snapshots of nuclear geometries that can be used in QM or semi-empirical calculations. Currently, high-level calculations cannot be run on the large system cell, so a combined quantum mechanics/molecular mechanics (QM/MM) method is typically used to incorporate the effects of the molecular environment and disorder. In the QM/MM method, the simulation is divided into system and bath regions, the chosen system being small enough to afford the use of an accurate QM calculation. The bath then interacts with the system during the QM calculation through electrostatic and Van der Waals interactions, unless the system and bath regions are divided across a bond (e.g. for a large polymer), in which case linker-atoms are necessary.[193] MM atoms are represented in the QM calculation as static charges and oscillating dipoles, the specifics of which are determined by the force field.

There are a few different things to consider with the QM/MM method. One major issue is selecting the set of MM parameters to represent the MM region, since only a few molecules related with OPVs have existing parameters, for example C_{60}[194] and P3HT.[195] The choice of MM parameters, especially the polarizability parameters, can greatly alter the results. The results can also depend on the size of the QM region because delocalization can only occur in the QM region, and so one must be careful that delocalization in the system and states is not a significant effect, otherwise a large QM region is needed. For small molecule OPV devices the QM/MM method is very useful approximation to the system because all of the states except for the singlet excited state are very localized in the disordered environment. The detailed description of the environment and quantum description of the system make the QM/MM method a very useful method to investigate the energetics at the organic/organic interface. Through careful study of the effect of the molecular geometries and the impact of structural disorder on the electronic structure, a better understanding of OPV devices can be gained.

1.6 Dynamic Simulations

In order to study the dynamics of singlet fission and exciton diffusion in OPVs one needs to compute the electronic coupling between different excited states. For triplet excitons the CDFT method with configuration interactions (CDFT-CI) can be applied to compute the electronic coupling.[196,197] Here we can define two diabatic states, one with the triplet exciton on the donor molecule and one with the triplet exciton on the acceptor molecule. Then using these two diabatic states we can compute the electronic coupling between them. While CDFT-CI can be applied to many types of energy transfer problems, it is still limited by the requirement that the electronic states need to be defined by some localization of spins and charges. One method that relies on the TDDFT method to get couplings for singlet and triplet excitons is the fragment excitation difference method,[198,199] which uses the transition densities to calculate the coupling between different excited states.

It is well understood that the coupling for singlet excitons will typically be much larger than the coupling for triplet excitons because of how they transfer the energy. Singlet excitons transfer their energy from one molecule to another through a non-radiative energy transfer process. The simplest approximation to this energy transfer process is the Förster energy transfer approximation.[200,201] Förster energy transfer approximates the interaction as a dipole-dipole interaction, which decays as R^{-6}, and is fairly accurate for energy transfer at distances greater than a few nanometers.[202,203] Triplet excitons on the other hand require a two-electron transfer process, typically called Dexter energy transfer, in order to hop from one molecule to the next.[204,205] Dexter energy transfer depends on the overlap of the wavefunctions on the donor and acceptor molecules, and therefore is typically not very large and decays as $exp(-R)$.

In most dynamic processes in OPVs the energy transfer occurs through an incoherent hopping type mechanism due to the large molecular and thermal disorder. For triplet and singlet exciton diffusion the excited state moves from one location to another by hopping, and in the case of hopping transport the diffusion length (L_{D}) is composed of two molecular parameters: the hopping rate (k_{D}) and the exciton lifetime (τ). The lifetime is composed of a radiative and non-radiative part, both of which can be the dominant factor depending on the molecule and if the exciton is a singlet or triplet. The hopping rate of an exciton from a donor molecule to an acceptor molecule can be approximated using the well known Marcus Theory rate.[206]

$$k_{\mathrm{da}} = \frac{2\pi}{\hbar} |V_{\mathrm{da}}|^2 \sqrt{\frac{1}{4\pi k_{\mathrm{B}} T \lambda}} \exp\left[-\frac{(\Delta G^\circ + \lambda)^2}{4\lambda k_{\mathrm{B}} T}\right] \tag{1.2}$$

Here, the three important molecular parameters are the coupling between the donor and acceptor states V_{da}, the free energy change ΔG°, and the reorganization energy λ.

While one can relate the hopping rate and lifetime directly to the diffusion length[78] it typically requires a number of assumptions, such as only nearest neighbor hopping and specific packing directions. In order to more accurately model diffusion in a realistic system we need to apply the Kinetic Monte-Carlo (KMC) method.[207] KMC works by taking in a list of hopping sites and the rates between each site, and then using the rates a random site is chosen to hop to. After hoping the time in the simulation is evolved based on the rate between the initial and final sites. This process is then repeated over and over to propagate an exciton or charge until the simulation is stopped. The combination of the KMC code and quantum chemistry methods can make it easier to determine what molecular properties are controlling the diffusion length of the exciton in OPVs.

All of the different types of static and dynamic computational methods can be used together to model and further our understanding of the excitonic properties and the separation of charges from the organic/organic interface in OPVs.

1.7 Thesis Outline

The body of this thesis is concerned with topics related to modeling the condensed phase properties of organic photovoltaics. Chapter 2 and 3 focus on refining and developing computational methods for the use of computing excited state properties of organic semiconductors. The rest of the thesis focuses on modeling different electronic processes in an OPV device on the molecular level in order to gain further understanding of how OPVs work.

The focus of chapter 2 is on the assessment of an alternative DFT approach to excited states, ΔSCF, for organic dyes. The ΔSCF method is a time-independent based method for computing excited states, and as such it provides a potentially simpler and faster way of computing excited states. For a test set of vertical excitation energies of 16 chromophores, we observe surprisingly similar accuracy for the ΔSCF and TDDFT approaches over a wide range of DFT functionals. In light of this performance, we reconsider the *ad hoc* ΔSCF prescription and demonstrate that it formally obtains the exact stationary density within the adiabatic approximation, partially justifying its use. The relative merits and future prospects of ΔSCF for simulating individual excited states are discussed.

While the performance of both TDDFT and ΔSCF are similar, they both still can not obtain accuracies greater than 0.3 eV for the singlet excited state. In order to try and improve upon the limited accuracy of these methods in chapter 3 we present a new excited state method, ΔSCF(2), that has similarities to the CASPT2 method. In ΔSCF(2) we take a set of ground and excited non-Aufbau determinants as our active space. We then apply a second order Møller-Plesset perturbation correction to the wavefunctions, and in this new active space we diagonalize the Hamiltonian. The ΔSCF(2) method avoids a number of problems in CASPT2, such as the choice of state-averaging weights and what zeroth-order Hamiltonian to use for the perturbation correction. We find similar accuracy to multi-reference excited state methods with a reduced cost and smaller active space. Thus making the ΔSCF(2) a potentially useful new way to compute accurate excited state properties.

Our focus then shifts from method development to modeling molecular properties important for the performance of OPV devices. In chapter 4 we investigate the exciton fission process, which is where one singlet exciton splits into two independent triplets.[53] Because fission generates two triplet excitons from a single high energy photon, fission-based solar cells can produce quantum yields in excess of 100%[54] and could lead to single junction photovoltaics with power conversion efficiencies above 40%.[53] Here, experimental collaborators measure the fission dynamics using ultrafast photoinduced absorption, and we derive a first principles expression that successfully predicts the rate of fission for a range of materials with vastly different structures. Our results show that the experimental rates are consistent with a non-adiabatic Marcus-like mechanism in weakly interacting systems and an adiabatic, coupling independent pathway at larger interaction strengths. For a range of electronic couplings covering almost three orders of magnitude, we predict near unit fission efficiency in any material where fission is energetically favored. This is confirmed experimentally, as we observe high fission yields even in materials where molecules are oriented orthogonal to one another at large separations (>5 Å). We conclude that singlet exciton fission in thin films is robust against variations in molecular structure. The success of this kinetic model simplifies the rational design of materials capable of fission. Crucial molecular properties such as solubility and energy level alignment can be safely tailored by functionalizing an active core while maintaining a high quantum yield.

Once singlet or triplet excitons are formed in an OPV device they must diffuse to the organic/organic interface. In chapter 5 we present a discussion of the limits to the diffusion lengths of both singlet and triplet excitons. The diffusion length of excitons sets an upper bound on the efficiency of OPV devices because current bilayer OPVs cannot be made thick enough to absorb all incident solar radiation due to the short diffusion lengths ($\approx$ 10 nm) of singlet excitons.[31,66] By contrast, triplet excitons can have very long diffusion lengths (as large as 10 microns) in organic solids, leading some to speculate that triplet excitonic solar cells could be more efficient than their singlet counterparts.[68,74,208] We demonstrate that while there are fundamental physical upper bounds on the distance singlet excitons can travel by hopping, there are no corresponding limits on triplet diffusion lengths. This conclusion strongly supports the idea that triplet diffusion should be more controllable than singlet diffusion in organic photovoltaics. To validate our predictions, we model triplet diffusion by purely *ab inito* means in various crystals, achieving good agreement with experimental values. We further show that in at least one example (tetracene) triplet diffusion is fairly robust to disorder in thin films, due to the formation of semi-crystalline domains and the high internal reorganization energy for triplet hopping. These results support the potential usefulness of triplet excitons in achieving maximum organic photovoltaic device efficiency.

In chapter 6 we present models on the organic/organic interface and their implications on the charge separation process. Exciton dissociation at organic semiconductor interfaces is an important process for the design of future organic photovoltaic (OPV) devices, but at present it is poorly understood. On the one hand, exciton breakup is very efficient in many OPVs. On the other, electron-hole pairs generated by an exciton should be bound by Coulombic attraction, and therefore difficult to separate in materials of such low dielectric. We start by investigating the band levels and CT states at the interface between two organic semiconductors, metal-free phthalocyanine (H_2Pc) and 3,4,9,10 perylenetetracarboxylic bisbenzimidazole (PTCBI), using a combined QM/MM technique. Near the organic/organic interface significant changes from the bulk, as large as 0.2 eV, are found in the excited state energies, ionization potentials, and electron affinities. We highlight several electrostatic effects that appear commonly at organic/organic interfaces and can cause such band bending effects. Using QM/MM simulations we demonstrate that the electric fields generated in this fashion are large enough to overcome typical electron-hole binding energies, creating a system where the CT states at the interface can be on average higher in energy than fully separated charges in the bulk materials despite having a typical local binding energy of 0.15 eV. Furthermore, we find that thermal fluctuations can induce variations of up to 0.1 eV in the CT binding energy. These results suggest that it is possible for bound interfacial CT states to dissociate in a barrier-less fashion without involving "hot" CT states, and that the classical picture of flat bands at organic/organic interfaces is only qualitatively correct. These observation have direct relevance to the design of more efficient organic photovoltaics.

Finally in chapter 7 we conclude with describing the key findings of the thesis and how they relate together in the broader context of understanding and improving OPV devices. Some further discussion is also provided on ongoing work and future work for these topics.

Chapter 2

Assessment of ΔSCF density functional theory for electronic excitations in organic dyes

2.1 Introduction

Conjugated organic dyes have found widespread use: from lasers, paints, and inks to more exotic technologies such as dye-sensitized solar cells,[209–211] organic light-emitting devices,[6,212–214] organic transistors,[215] and organic solar cells.[30,216] The performance of these materials relies heavily on the careful tuning of their electronic properties. Specifically, in organic solar cells the singlet excited state in conjugated molecules and polymers are tuned to both increase solar absorption while maintining the correct energy level allignment for charge formation.[40,42] Consequently, there is growing interest in the development and application of computational methods for characterizing electronic excitations in condensed-phase organic materials.[217,218]

Among the earliest approaches to this challenge were semiempirical molecular orbital methods such as complete neglect of differential overlap[219] and the Pariser-Parr-Pople approach.[220] As computational resources expanded, *ab initio* methods such as time-dependent Hartree-Fock and configuration interaction singles became feasible for molecules of moderate size.[146] None of these methods are expected to give quantitative results, but often they are sufficient to predict trends. More recently, methods such as complete active space self-consistent field[221] and equation-of-motion coupled cluster[222] havebeen developed, which promise quantitative results for excited states. Unfortunately, at present, these are too expensive for routine use on organic dyes that typically have 50–100 atoms. A modern method that offers a good compromise between accuracy and efficiency is time-dependent density functional theory (TDDFT).[144,146,223]

TDDFT within the adiabatic approximation (AA) (Refs. 224 and 225) has been the workhorse method for computing excitation energies in organic molecules over the last decade. TDDFT excitation energies with commonly employed exchange-correlation functionals are usually accurate to within 0.3 eV for localized valence excitations in organic molecules.[147] However, TDDFT is less reliable for excitations with long-range character, such as Rydberg[226,227] and charge transfer excitations[228,229] as well as excitations in large conjugated molecules.[230–232] Recently developed long-range corrected functionals have addressed these issues with promising success.[123,148,150,233] Several time-independent alternatives for computing excitation energies within a density functional theory (DFT) framework have been proposed,[234–236] but many of these methods pose significant implementation challenges[237] or are too computationally expensive compared to TDDFT.

The ΔSCF-DFT (or simply ΔSCF) method, one of the earliest such time-independent methods,[151] is straightforward to implement and offers low computational cost. This method is also known in the literature as excited state DFT[238] or constrained DFT[239] (not to be mistaken for the method of the same name[153] in which constraints are applied to the density). The ΔSCF procedure employs non-Aufbau occupations of the Kohn–Sham orbitals to converge the SCF equations to an excited state that might have other states of the same symmetry beneath it. Because SCF algorithms are geared toward energy minimization, they can sometimes cause a collapse to these lower energy states during the SCF iterations. Techniques such as the maximum overlap method[152] have been developed to address these convergence issues, thereby rendering the ΔSCF method an efficient potential alternative to TDDFT for excited state geometry optimizations and molecular dynamics. Analytical excited state Hessians, which are needed to obtain infrared or vibrationally resolved electronic spectra, are also readily accessible from the ΔSCF approach, in contrast to the current situation for TDDFT — though progress in this area has been rapid in recent years.[240] ΔSCF was recently associated with the fourth-order correction to a "constricted" variational approach to TDDFT,[241] but here we focus on its use as a stand-alone method.

Although ΔSCF has gained some traction recently as a DFT-based alternative to TDDFT for excited states,[152,227,242–244] the performance and range of validity of the method remain poorly understood. This paper addresses this gap in understanding in two ways: first, by comparing excitation energies computed by TDDFT and ΔSCF with experimental values for a representative set of conjugated organic molecules; and second, by providing new insight into the approximations that are made when computing excitation energies from ΔSCF.

The rest of the chapter is arranged as follows. First, we construct a set of organic dye molecules that we use as a benchmark test set. Next, we present TDDFT and ΔSCF excitation energies and discuss the performance of the two methods relative to experiment. We find that the two approaches are quite comparable, which we find surprising given the lack of formal justification for ΔSCF. We therefore spend some time in the discussion examining the theoretical underpinnings of TDDFT and ΔSCF in order to determine if there might not be a deeper reason for the success of ΔSCF. Finally, we conclude our analysis and suggest some potential future directions.

2.2 Test Set

It is of course impossible to construct a single test set that characterizes the quality of a given functional for excited states. The wide variety of behaviors of different functionals for Rydberg states,[226] charge transfer states,[229] excited states of conjugated organic molecules[229,231–233,245] and core excitations[152] suggests a more modest goal:

to design a test set that assesses a functionals utility for a given purpose. Because of our interest in organic electronics, we are most keenly interested in testing TDDFT and ΔSCF for the low- lying singlet excited states of common dye molecules. Other test sets consisting of small conjugated organic molecules have been constructed to assess the performance of TDDFT, with typical errors of roughly 0.2−0.3 eV for the best-performing functionals.[125,148,246] Our chosen test set is tabulated in Tables 2-1 and 2-2. In each case, E_{ex} is the energy of the lowest maximum in the experimental absorption spectrum.

There were a number of criteria that we used to select the molecules in the test set. First, they were required to have a significant absorption in the visible region. This typically requires extensive π conjugation over most of the molecule, resulting in low-lying $\pi \rightarrow \pi^*$ transitions. Further, as can be seen in Tables 2-1 and 2-2, all of the excitations are predominantly HOMO → LUMO. This restriction is not essential, but leads to more robust SCF convergence than, say, HOMO → LUMO + 1 would. The single-reference character of the excited states helps us circumvent the general problem that some excited states require a multireference approach. We make no restriction on the degree of charge transfer present in the excited state. However, in order to control for solvatochromic effects, we selected molecules for which experimental absorption spectra are available in gas phase, thin film, or nonpolar solvent. Ideally, all of the experimental results would be in gas phase, but this restriction would only leave us with five molecules in our test set, which would be insufficient. We therefore must accept some degree of inequivalence between the experimental observable (absorption maximum in a weak environment) and the calculated quantity (vertical excitation in the gas phase). We should note that methods exist to attempt to correct theoretical gas phase excitation energies for dielectric[247] and vibrational[246] effects to obtain solvent-corrected $0-0$ excitation energies, but such shifts will in any case be smaller than the errors due to the approximate nature of the density functional.

Despite the fact that all of the molecules satisfy the criteria given above, our test set includes molecules covering a wide range of current applications. Some molecules

dye	structure	environment	E_{ex} (eV)	% H → L
1	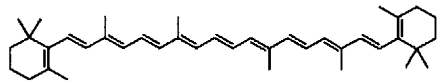	pentanes	2.50[a]	100.0
2	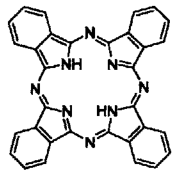	gas phase	1.82[b]	95.3
3	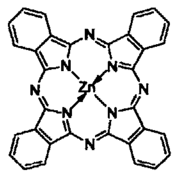	gas phase	1.88[b]	91.9
4	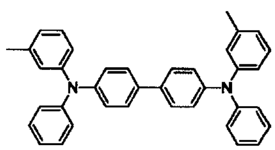	thin film	3.46[c]	97.5
5	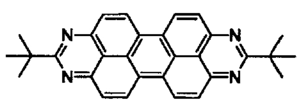	toluene	2.87[d]	95.7
6	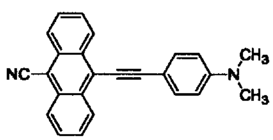	thin film	2.59[e]	99.5
7	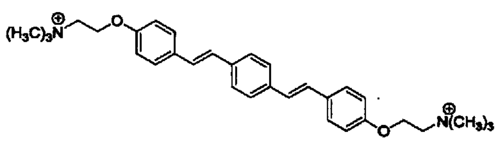	thin film	3.55[f]	99.6
8	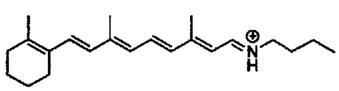	gas phase	2.01[g]	95.2

Figure 2-1: Test set, molecules **1**–**8**: chemical structure, absorption maximum measured in the specified environment, and TD-B3YLP HOMO → LUMO character of the lowest singlet excited state. Experimental excitation energies: [a]Ref. 248; [b]Ref. 249; [c]Ref. 250; [d]Ref. 251; [e]Ref. 252; [f]Ref. 253; [g]Ref. 254.

are found in biological systems (**1**, **8**, **9**, **13**, **14**), others are used for organic electronics

dye	structure	environment	E_{ex} (eV)	% H → L
9	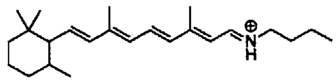	gas phase	2.36^a	99.7
10	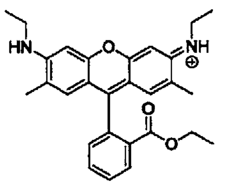	thin film	2.26^b	98.0
11	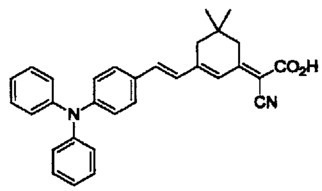	thin film	2.58^c	98.6
12	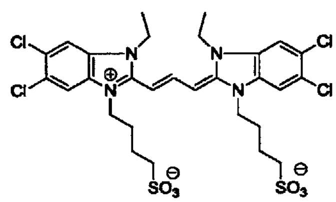	thin film	2.11^d	74.6
13	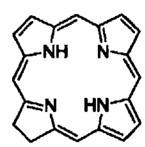	benzene	1.94^e	72.1
14	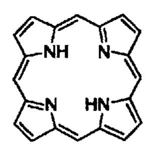	gas phase	2.01^f	57.0
15	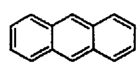	trichlorobenzene	3.21^g	98.0
16	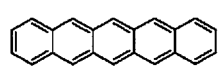	trichlorobenzene	2.06^g	100.0

Figure 2-2: Test set, molecules **9**–**16**: chemical structure, absorption maximum measured in the specified environment, and TD-B3YLP HOMO → LUMO character of the lowest singlet excited state. Experimental excitation energies: [a]Ref. 254; [b]Ref. 255; [c]Ref. 256; [d]Ref. 257; [e]Ref. 258; [f]Ref. 259; [g]Ref. 260.

(**2**, **3**, **4**, **15**, **16**), and some as synthetic organic dyes (**5**, **6**, **7**, **10**, **11**, **12**). Thus, we have made an effort to select a structurally diverse set of molecules that can answer the question: how accurate are ΔSCF and TDDFT for organic dyes?

2.3 Computational Methods

All geometries were optimized at the B3LYP/6-31G* level in the gas phase; these geometries are provided in Appendix C. TDDFT and SCF excitation energies were computed in the 6-311+G* basis set with an array of exchange-correlation functionals. An SRSC pseudopotential was employed for Zn.[261] The functionals were chosen because of their widespread use, and the hybrid functionals intentionally represent a wide variation in the fraction of exact (Hartree–Fock) exchange. The SCF calculations include two additional M06 functionals[126] for which TDDFT excitation energies were unavailable. An additional functional consists of 60% PBE exchange and 40% Hartree–Fock exchange with PBE correlation and will be denoted PBE4.

The ΔSCF procedure was carried out as follows. Starting with the molecular orbital coefficients of the ground state as an initial guess, the Kohn–Sham equations were solved using a modified SCF procedure in which the lowest $N-1$ orbitals and the $(N+1)$th orbital were occupied at each update of the density matrix. The shifting of orbital energies during this procedure occasionally caused the density to collapse to the ground state. In these cases, the maximum overlap method[152] provided a way to retain the target configuration through convergence.

The non-Aufbau electronic state obtained from this procedure is not a spin eigenfunction. To obtain the energy of the singlet excited state, we use the common spin purification formula,[151]

$$E_S = 2E_{\uparrow\downarrow} - E_{\uparrow\uparrow}$$

Both the spin-mixed ($\uparrow\downarrow$) and spin-pure energies are of interest, so we include both in our analysis. All computations were performed with a modified version of the Q-Chem 3.2 software package.[262]

2.4 Results

Deviations of computed TDDFT and ΔSCF vertical excitation energies from experiment are presented in Table 2.1, with a more detailed description of the PBE0 results in Table 2.2. Typical mean absolute errors (MAEs) in TDDFT excitation energies are 0.3 eV, with B3LYP and PBE0 outperforming their counterparts with greater or lesser exact exchange. The magnitude of these deviations is in line with that observed in previous TDDFT benchmarking studies.[147,263]

For ΔSCF with spin purification, the results parallel the TDDFT results quite closely for all functionals: B3LYP and PBE0 perform best, with MAE and RMSD similar to those of the corresponding functionals in the TDDFT approach. This similarity suggests an argument in favor of applying the spin purification procedure. In keeping with Beckes assertion that the fraction of exact exchange reflects the independent-particle character of the system,[119] the appropriate fraction of exact exchange in Kohn–Sham DFT should be a characteristic of the system, not of the method (TDDFT, ΔSCF, or another approach) chosen to compute excitation energies. Of course, it is also convenient from a practical standpoint that TDDFT and spin-purified ΔSCF perform similarly for the same functionals.

The energy of the mixed state in ΔSCF systematically underestimates experimental energies when the employed functional possesses a conventional fraction of exact exchange (20%–30%). Functionals with twice as much exact exchange (BH&H and M06-2X) give mixed states that are more accurate, performing comparably to the best functionals for TDDFT excitation energies. The satisfactory performance of spin-contaminated ΔSCF with a larger fraction of exact exchange can be interpreted as a convenient cancellation of errors. The energy of the mixed state underestimates the singlet energy by half the singlet–triplet splitting. The addition of surplus exact exchange systematically increases the singlet–triplet gap. Therefore, the energy of the mixed state tends to increase with increasing exact exchange. At least on average, one can thus raise the fraction of exact exchange such that the energy of the mixed state with surplus exact exchange matches the energy of the pure singlet with the original

		Mean error	
Functional	TDDFT	ΔSCF_{mixed}	ΔSCF_{pure}
PBE	-0.23	-0.72	-0.56
B3LYP	0.08	-0.47	-0.16
PBE0	0.15	-0.42	-0.05
LC-ωPBE0	0.23	-0.26	0.24
PBE4	0.28	-0.26	0.26
BH&H	0.33	-0.14	0.45
M06-2X		-0.08	0.41
M06-HF		0.52	1.47
		MAE	
Functional	TDDFT	ΔSCF_{mixed}	ΔSCF_{pure}
PBE	0.39	0.72	0.58
B3LYP	0.27	0.49	0.25
PBE0	0.27	0.45	0.21
LC-ωPBE0	0.27	0.32	0.26
PBE4	0.31	0.33	0.30
BH&H	0.35	0.27	0.45
M06-2X		0.27	0.42
M06-HF		0.52	1.47
		RMSD	
Functional	TDDFT	ΔSCF_{mixed}	ΔSCF_{pure}
PBE	0.46	0.81	0.66
B3LYP	0.32	0.57	0.32
PBE0	0.32	0.52	0.28
LC-ωPBE0	0.33	0.38	0.32
PBE4	0.38	0.38	0.37
BH&H	0.42	0.31	0.50
M06-2X		0.30	0.48
M06-HF		0.74	1.69

Table 2.1: Test set statistics for the three different excited state methods. All values are in eV.

Molecule	Exp.	TDDFT	ΔSCF$_{\text{mixed}}$	Mixed $\langle S^2 \rangle$	ΔSCF$_{\text{pure}}$	Triplet $\langle S^2 \rangle$
1	2.50	2.25	1.64	1.015	2.08	2.088
2	1.82	2.08	1.55	1.029	1.91	2.021
3	1.88	2.08	1.54	1.029	1.96	2.047
4	3.46	3.40	3.16	1.017	3.37	2.017
5	2.87	2.96	2.34	1.009	2.84	2.067
6	2.59	2.51	2.01	1.009	2.47	2.027
7	3.55	3.15	2.61	1.008	3.00	2.034
8	2.01	2.42	1.41	1.062	1.72	2.023
9	2.36	2.71	1.68	1.048	2.05	2.020
10	2.26	2.89	2.08	1.056	2.28	2.014
11	2.58	2.49	2.05	1.024	2.38	2.022
12	2.11	2.75	2.06	1.055	2.16	2.009
13	1.94	2.29	1.93	1.046	2.21	2.015
14	2.01	2.30	2.26	1.019	2.63	2.050
15	3.21	3.29	2.71	1.008	3.32	2.024
16	2.06	1.96	1.49	1.009	2.02	2.037

Table 2.2: PBE0 energies and spin multiplicities for the test set. All energies are in eV.

functional. Functionals with roughly 50% exact exchange achieve this cancellation in our test set.

The functional LC-ωPBE0 ($\omega = 0.1$ bohr^{-1} , $c_{\text{HF}} = 0.25$) was included in our study to assess the performance of long-range corrected density functionals. Given that these functionals are optimized (in part) to give accurate TDDFT vertical excitation energies,[123] it is somewhat surprising to note that LC-ωPBE0 performs best neither for TDDFT nor for ΔSCF. We suspect this arises from the fact that these excited states are bright, which selects against the charge transfer excitations (which tend to be dark) for which LC-ωPBE0 would outperform all other tested functionals.

It is important to note that while ΔSCF and TDDFT have statistically similar accuracy for the singlet states, it does not follow that ΔSCF and TDDFT predict similar results for a given molecule. For example, as illustrated in Table 2.2, the ΔSCF and TDDFT vertical excitation energies with PBE0 can often differ by as much as 0.6 eV for the same molecule. These fluctuations cancel out, on average, and the MAEs of ΔSCF and TDDFT excitation energies differ by only 0.06 eV over the whole set. Further, the $\langle S^2 \rangle$ values from the table clearly justify the use of spin purification for these states.

2.5 Discussion and Analysis

Based on the results of Section 2.4, it would appear that ΔSCF and TDDFT predict vertical excitation energies of organic dyes with approximately equal accuracy, with ΔSCF being perhaps slightly better when the best functionals are used. If we combine this information with existing evidence that ΔSCF is effective for Rydberg states[238] core excitations,[152,264] solvent effects[265] and double excitations[266] we are led to the pragmatic conclusion that SCF is a powerful tool for excited states. Is this just a coincidence? Or are there deeper reasons why SCF is so effective? To answer these questions, we must unpack the approximations inherent to TDDFT and ΔSCF calculations.

2.5.1 Linear response TDDFT

According to the Runge–Gross theorem,[144] there exists a one-to-one correspondence between the time-dependent density, $\rho(x,t)$, and the time-dependent potential, $v_{\text{ext}}(x,t)$. Thus, one can formulate an equation of motion that involves $\rho(x,t)$ alone, where x contains spatial and spin coordinates, $x \equiv (r,\sigma)$:

$$\dot{\rho}(x,t) = F[\rho]$$

where F must be defined. In the Kohn-Sham (KS) formulation of TDDFT, the exact density is constructed out of a set of time-dependent orbitals,

$$\rho(x,t) = \sum_{i=1}^{\text{occ}} |\phi_i(x,t)|^2$$

The KS orbitals, in turn, obey a Schrödinger equation,

$$i\dot{\phi}_i(x,t) = \left(-\frac{1}{2}\nabla^2 + v_{\text{ext}}(x,t) + \int \frac{\rho(x',t)}{|\mathbf{r}-\mathbf{r}'|}\,dx' + v_{\text{xc}}[\rho](x,t)\right)\phi_i(x,t) \equiv \hat{H}_{\text{KS}}\phi_i(x,t)$$

where the external potential, v_{ext}, is augmented by the classical Coulomb potential and the unknown exchange-correlation potential, $v_{\text{xc}}[\rho]$. According to the Runge–Gross theorem, v_{xc} exists and is uniquely determined by the density. Thus, $v_{\text{xc}}(x,t)$ is a functional of $\rho(x,t)$, justifying the notation $v_{\text{xc}}[\rho]$. The major challenge in TDDFT is determining accurate approximations to the exchange-correlation potential.[150,267–273]

Now, in principle, $v_{\text{xc}}(x,t)$ can depend on $\rho(x,t)$ at any point r in space and any time t in the past. In practice, it is very difficult to obtain approximations to $v_{\text{xc}}(x,t)$ that obey causality and possess all the proper time translation invariance properties.[274,275] As a result, nearly all existing approximations to $v_{\text{xc}}(x,t)$ are strictly local in time — $v_{\text{xc}}(x,t)$ depends only on the density of the system at time t. This approximation is known as the adiabatic approximation (AA). It greatly simplifies the construction of approximate potentials, and from this point forward, our manipulations will assume the AA.

In order to obtain excitation energies from TDDFT, the most common route is to employ linear response (LR).[225,276] Here, one first performs a traditional DFT calculation to obtain the ground state density. Next, one subjects the system to a small time-dependent external potential, $\delta v(x,t)$, that induces a small change in the density, $\delta\rho(x,t)$, and a corresponding small change in the exchange correlation potential, $\delta v_{\text{xc}}(x,t)$. One then uses the time-dependent KS equations to connect the different linear variations and computes excitation energies as the poles in the frequency-dependent response function.[223] The resulting equations can be cast as a generalized eigenvalue problem:

$$\begin{pmatrix} \mathbf{A} & \mathbf{B} \\ -\mathbf{B} & -\mathbf{A} \end{pmatrix} \begin{pmatrix} \mathbf{X}_M \\ \mathbf{Y}_M \end{pmatrix} = \omega_M \begin{pmatrix} \mathbf{X}_M \\ \mathbf{Y}_M \end{pmatrix}$$

Here, $\mathbf{X}_M$ and $\mathbf{Y}_M$ are vectors of length (occupied) $\times$ (unoccupied) that represent the density response and the **A** and **B** matrices are given by

$$\begin{aligned} A_{ia;jb} &\equiv (\epsilon_a - \epsilon_i)\delta_{ij}\delta_{ab} + B_{ia;jb} \\ B_{ia;jb} &\equiv \int \phi_i(x_1)\phi_j(x_2)\left(\frac{1}{r_{12}} + \frac{\delta v_{\rm xc}(x_1)}{\delta\rho(x_2)}\right)\phi_a(x_1)\phi_b(x_2)\,dx_1\,dx_2 \end{aligned}$$

where i, j (a, b) index occupied (unoccupied) orbitals. In principle, the eigenvalues ω_M are the exact (within the AA) transition energies between the ground electronic state and the various excited states: $\omega_M = E_i - E_0$. Meanwhile the eigenvectors, $\mathbf{X}_M$ and $\mathbf{Y}_M$ contain information about the intensity of the transition.

2.5.2 ΔSCF densities

Now, because quantum mechanics is linear, linear response in Hilbert space starting from any two different reference states will give equivalent transition energies. However, since most density functionals have a nonlinear dependence on the density, the excitation energy obtained from LR-TDDFT depends on the reference state one chooses. Thus, for example, in certain cases it is advantageous to choose a reference state with a different spin multiplicity.[277–281]

Instead of sifting for excitations in the density response, an alternative approach is to search directly for the excited state density in TDDFT. Here, one recognizes that every eigenstate Ψ_i of the Hamiltonian is a stationary state. Hence, $\rho_i(x,t)$ is constant in time and

$$\dot{\rho}(x,t) = F[\rho] = 0 \tag{2.1}$$

Within the KS formulation, the density is invariant if each KS orbital changes by a phase factor

$$\phi_j(x,t) = e^{-i\epsilon_j t}\phi_j(x)$$

so that

$$\begin{aligned} i\dot{\phi}_j(x,t) &= \epsilon_j\phi_j(x,t) \\ \hat{H}_{\rm KS}\phi_j(x,t) &= \epsilon_j\phi_j(x,t) \end{aligned}$$

Thus, the equations obeyed by stationary densities within TDDFT are *exactly the same as the SCF equations for traditional KS-DFT*. Viewed in this light, it is clear that ΔSCF states — which solve the traditional KS-DFT equations with non-Aufbau occupations of the orbitals — have a rigorous meaning in TDDFT: they correspond to stationary densities of the interacting system. Further, these stationary densities have a clear connection with excited states of the molecule. This connection between TDDFT and ΔSCF comes tantalizingly close to rigorously justifying the use of ΔSCF-DFT for excited states: ΔSCF-DFT gives stationary densities that are exact within the AA.

Before moving on, we note how the AA is expected to influence Eq. 2.1. The above derivation is so concise that it almost seems as if no approximation has been made at all. However, we note that in Eq. 2.1 the density is constant at all times. Thus, the system must have been *prepared* in the desired eigenstate. This assumption violates the terms of the Runge–Gross theorem, which applies only to different densities that originate from the same state (usually assumed to be the ground state at $t = -\infty$). Only within the AA can different initial densities be justified.[282]

The ΔSCF scheme implied by Eq. 2.1 is exact within the AA because the system has no memory of how it was prepared. If our functional has memory, Eq. 2.1 states that $F[\rho_i(x,t)] = 0$ when applied to a particular density, $\rho_i(x,t)$, that is constant in time. To put it another way, Eq. 2.1 depends only on the zero frequency ($\omega = 0$) part of F. In many ways, this is the ideal scenario within the AA. Any adiabatic functional is time-local and thus frequency independent. However, it is trivial for a frequency-independent kernel to be correct at one frequency (i.e. $\omega = 0$) and so one suspects that the AA could be well-suited to the ΔSCF approach. In contrast, within linear response one relies on the ω-independent kernel being a good approximation to the true kernel at every excitation energy. It is clear that, except in special cases, the latter condition cannot hold and thus LR-TDDFT would seem more limited by the AA.

2.5.3 ΔSCF energy expressions

ΔSCF gives us a rigorous route to obtain a stationary density in TDDFT. But how should we associate an energy with this density? Since there is no Hohenberg–Kohn theorem for excited states,[283] there can be no single density functional that gives the correct energy for all excited states. Instead, one must tackle the problem of defining different functionals for different excited states[234,236] or else make the functional depend on more than just the density.[284,285] The simplest procedure is to evaluate the ground state energy expression using the ΔSCF orbitals

$$E^{\text{ex}} = E\left[\phi_i^{\text{ex}}(x)\right] \tag{2.2}$$

and this is the "mixed" ΔSCF energy used above. It should be noted that this energy expression is not a functional of the density, but rather an explicit functional of the orbitals. If we used the excited state density (rather than the orbitals), we would need to derive a corresponding set of KS orbitals to compute the kinetic energy, $T_s[\rho]$. By definition, these orbitals would be obtained by constrained search[286] and the resulting orbitals would give a different energy than the excited state orbitals. The orbital dependence lends some measure of robustness to the ΔSCF predictions.

In practice, it is necessary to correct Eq. 2.2 because Eq. 2.1 is necessary but not sufficient: not all stationary densities correspond to excited states even though all excited states give stationary densities. To see this, suppose you have a state that is a linear combination of two eigenstates:

$$|\Psi\rangle \propto |\Psi_1\rangle + |\Psi_2\rangle$$

Then the time evolving wavefunction is

$$|\Psi(t)\rangle \propto e^{-iE_1 t}|\Psi_1\rangle + e^{-iE_2 t}|\Psi_2\rangle$$

and the density is

$$\begin{aligned}\rho(\mathbf{r}) &\equiv \langle\Psi(t)|\delta(\mathbf{r}-\hat{\mathbf{r}})|\Psi(t)\rangle \\ &\propto \langle\Psi_1|\delta(\mathbf{r}-\hat{\mathbf{r}}|\Psi_1\rangle + \langle\Psi_2|\delta(\mathbf{r}-\hat{\mathbf{r}}|\Psi_2\rangle \\ &\quad + e^{-i\Delta Et}\langle\Psi_1|\delta(\mathbf{r}-\hat{\mathbf{r}})|\Psi_2\rangle + e^{i\Delta Et}\langle\Psi_2|\delta(\mathbf{r}-\hat{\mathbf{r}})|\Psi_1\rangle\end{aligned}$$

where $\Delta E = E_1 - E_2$. If ΔE is not zero, we do not have an eigenstate and in general the density is not stationary. However, suppose the transition density between the two excited states is zero everywhere. That is, suppose that

$$\rho_{12} \equiv \langle\Psi_1|\delta(\mathbf{r}-\hat{\mathbf{r}}|\Psi_2\rangle = 0$$

In this situation, the oscillating piece of the density is zero and the density is stationary even though the wavefunction is not an eigenstate. Thus, it is, in principle, possible for Eq. 2.1 to locate densities that do not correspond to eigenstates.

How does this affect ΔSCF in practice? Note that ρ_{12} is zero only if no one particle potential can drive the $1 \to 2$ transition. The most common situation where this occurs is if the eigenstates have different total spin (e.g. the transition density for singlet–triplet transitions is always rigorously zero in the absence of spin-orbit coupling). Thus, any linear combination

$$|\Psi\rangle \propto c_S\,|\Psi_S\rangle + c_T\,|\Psi_T\rangle$$

of a singlet eigenstate (Ψ_S) and a triplet eigenstate (Ψ_T) will have a stationary density and could lead to spurious ΔSCF solutions. In practice, this indeterminacy leads to spin contamination of the KS eigenstates in the following way. Suppose we have a singlet ground state and we are interested in the HOMO → LUMO transition. The singlet and one of the triplet states require two determinants:

$$\begin{aligned}|\Psi_S\rangle &\propto \left|\ldots\psi^{\uparrow}_{\mathrm{HOMO}}\psi^{\downarrow}_{\mathrm{LUMO}}\right\rangle - \left|\ldots\psi^{\downarrow}_{\mathrm{HOMO}}\psi^{\uparrow}_{\mathrm{LUMO}}\right\rangle \\ |\Psi_T\rangle &\propto \left|\ldots\psi^{\uparrow}_{\mathrm{HOMO}}\psi^{\downarrow}_{\mathrm{LUMO}}\right\rangle + \left|\ldots\psi^{\downarrow}_{\mathrm{HOMO}}\psi^{\uparrow}_{\mathrm{LUMO}}\right\rangle\end{aligned}$$

but KS-DFT biases us toward states that are well-represented by a single determinant.[287] Thus, rather than obtaining a pure singlet or a pure triplet we obtain a broken symmetry solution like

$$|\uparrow\downarrow\rangle = \left|\ldots\psi^{\uparrow}_{\mathrm{HOMO}}\psi^{\downarrow}_{\mathrm{LUMO}}\right\rangle \propto |\Psi_S\rangle + |\Psi_T\rangle$$

When employed in Eq. 2.2, this mixed spin state gives an energy somewhere between the singlet and triplet excitation energies. Thus, we are led to the purification formula

$$E_S = 2E_{\uparrow\downarrow} - E_{\uparrow\uparrow}$$

This scheme has a long history in predicting exchange couplings,[288,289] and the results above suggest that it predicts singlet HOMO→LUMO transitions in line with intuition. We thus see that the projection of excited state energies arises directly from the indeterminacy of the ΔSCF equations in the presence of spin degeneracy. We can also explicitly solve the case of three unpaired electrons to obtain two doublet energies:

$$\begin{aligned} E_D^{\pm} &= \frac{1}{2}\left(E_{\downarrow\uparrow\uparrow} + E_{\uparrow\downarrow\uparrow} + E_{\uparrow\uparrow\downarrow} - E_{\uparrow\uparrow\uparrow}\right) \\ &\quad \pm\sqrt{\frac{1}{2}\left(E_{\downarrow\uparrow\uparrow} - E_{\uparrow\uparrow\downarrow}\right)^2 + \frac{1}{2}\left(E_{\uparrow\downarrow\uparrow} - E_{\uparrow\uparrow\downarrow}\right)^2 + \frac{1}{2}\left(E_{\downarrow\uparrow\uparrow} - E_{\uparrow\downarrow\uparrow}\right)^2} \end{aligned}$$

The projection scheme can be further generalized to an arbitrary number of unpaired electrons,[290] although the ensuing equations are overdetermined.[291]

A more sophisticated scheme for dealing with spin would involve introducing a multideterminant reference state into the KS calculation. This is the idea behind the ROKS and REKS methods[292–294] which will be addressed in the next chapter. As we will see, techniques of this sort are certainly more elegant than *post facto* energy projection, but they also fundamentally change the equations being solved.

2.6 Conclusion

We have revisited the approximations that define the ΔSCF approach to excited states in DFT. The performance of the method was assessed by comparing ΔSCF excitation energies for several organic dyes with TDDFT and experimental excitation energies. We found that deviations of spin-purified ΔSCF excitation energies from experimental values are comparable to those of TDDFT for all functionals tested. Spin-contaminated ΔSCF energies were found to require more exact exchange to achieve similar accuracy. As a partial justification of these results, we demonstrated that ΔSCF densities are precisely the stationary densities of TDDFT within the adiabatic approximation, and the necessity of purifying the energies arises from the indeterminacy of the stationary equations with respect to different spin states.

While this study establishes some expectations regarding the range of applicability of the ΔSCF approach, there remain several unanswered questions to be explored in future work. We have shown that ΔSCF performs well for HOMO → LUMO excitations, but it remains to be determined how it performs for higher energy excitations. It will also be interesting to compare and contrast the performance of a spin-adapted approach such as ROKS with the spin purification approach presented here.

Several possible extensions and applications of ΔSCF methodology also deserve attention. ΔSCF gradients are readily available from ground-state SCF codes. Therefore, if the excited state potential energy surface (PES) obtained from ΔSCF is reasonably parallel to the true Born–Oppenheimer PES, ΔSCF could provide an efficient alternative to TDDFT and other wavefunction based methods for geometry optimization and molecular dynamics on excited states.[295–297] Furthermore, ΔSCF also provides an affordable route to the excited state Hessian, from which one could construct vibrationally resolved absorption and emission spectra.[298,299] It is also a simple matter to incorporate solvation effects in ΔSCF.[189,265] Together, these features could provide an affordable way to calculate full absorption and emission spectra in different environments for large molecules for photovoltaic applications. It will be intriguing to see if the robustness of ΔSCF for low-lying excited states extends across a wide enough range of excited state properties to make these simulations worthwhile.

2.7 Acknowledgment

The work described in this chapter was carried out jointly with Tim Kowalczyk, who is a co-author of Ref. 300.

Chapter 3

An efficient and balanced treatment of ground and excited states within multireference perturbation theory

3.1 Introduction

The ΔSCF method discussed and studied in chapter 2 gave an example of another fast method with reasonable accuracy (≈0.3 eV). However, if we want to go beyond the 0.3 eV accuracy limit, and more importantly, if we want probe excited state dynamical processes such as singlet fission (discussed in chapter 4) in organic photovoltaics then we need a more accurate method.[301–303] The properties of electronically excited states are also very important in many different aspects of chemistry, such as photoinduced electron transfer,[304,305] and solar thermal electrics.[306–308] Our ability to accurately and affordably compute the properties of molecular excited states is still not where we would like it to be. A standard approach that only requires knowledge of the ground state wavefunction is linear response, in which excitation energies are identified with poles in the linear response function due to electromagnetic perturbation.[309] However, linear response time-dependent Hartree-Fock (TDHF) provides only limited accuracy for excited state energies and potential energy surfaces (PES).[146] Its counterpart within density functional theory (DFT), linear response time-dependent DFT[144,145] (TDDFT) is a relatively affordable way to compute excited states; but its success with currently available exchange-correlation functionals is limited to certain classes of excited states. For well-behaved systems, accuracy of around 0.3 eV can be anticipated, but for charge transfer or Rydberg excitations TDDFT is significantly worse.[146] TDDFT fares even worse for excited state PES,[231,310] making it unreliable when searching for a reaction barrier or propagating dynamics in the excited state. The perennial issue with TDDFT and other DFT-based methods for excited states is the quality of the exchange-correlation functional. Efforts to improve on these approximations are ever ongoing,[127,311–313] but the roadmap to chemical accuracy for excited states in TDDFT remains blurry.

Wavefunction based methods building on the HF determinant, on the other hand, provide a more systematic way to generate high-quality ground and excited state wavefunctions. Due to the mean field approximation of HF, the HF wavefunction lacks all electron correlation. Static correlation can be recovered through the use of a multireference wavefunction, while the dynamic correlation is often more convenient to treat perturbatively.[165,166]

A multi-determinant solution to the Schrödinger equation, capable of recovering both static and dynamic correlation, can be obtained by applying single, double, and possibly higher order excitation operators to the ground state HF determinant. The improved ground state wavefunction is a linear combination of these wavefunctions, and its coefficients are obtained by variational minimization. Configuration interaction (CI) and coupled-cluster (CC) methods are examples of this scheme.[107,134,314] The variational theorem guarantees that including higher-order excitations gives a wavefunction at least as accurate as one obtained with only lower-order excitations; but the computational cost of including these excitations grows rapidly. Excited state methods rooted in this approach, such as equation-of-motion CCSD,[159] CC2,[160,161] and QCISD,[162] are even more computationally demanding and are unaffordable for excited state dynamics of more than ~10-electron systems.

One formalism that efficiently captures static correlation while reducing computational costs relative to CI is the complete active space self consistent field (CASSCF) approach.[140] In CASSCF, CI is applied to an active space of molecular orbitals, usually a small number of occupied and virtual orbitals, instead of the full set, the CI coefficients and orbitals in the active space are then optimized self consistently. The typical notation is (n, m)-CASSCF, where n indicates the number of electrons in the active space and m indicates the number of orbitals in the active space. As with full-CI, the cost of CASSCF grows combinatorially with the size of the active space. There exist various active space reduction strategies, such as restricted active space SCF (RASSCF),[315] to manage the balance between accuracy and cost. However, even with these tools, CAS methods are not black-box, and in practice one needs to closely monitor the orbitals during PES scans and dynamics to ensure the consistency of the active space, and thus the accuracy of the calculation.[165,166]

The CASSCF method lacks most of the dynamic correlation. Roos and coworkers extended the CASSCF method to include a second order perturbative expansion to the CASSCF energies, called the CASPT2 method.[163,164] There are several choices to be made in the development of such a formalism, and so a variety of multireference perturbation theories have since been developed.[167,316–319] While CASPT2 and related methods perform well, they all face two key potential problems. First, the perturbation series is not guaranteed to converge,[320–322] and in particular second order perturbation thoery can accumulate an unbounded error in the case of orbital near-degeneracies;[323] typically this is fixed using an empirical correction factor. The other, more intricate issue is that the perturbation correction is applied after the CASSCF calculation, which creates some ambiguity regarding what to define as the zeroth-order Hamiltonian for the perturbation theory.[168,324–326] To treat excited states in CASPT2, an additional ambiguity arises in the prescription for the state averaging procedure used to select the optimal set of orbitals. CASPT2 energies can depend significantly on the state averaging procedure used.[327] Finally, the accuracy of CASPT2 depends on how large of an active space is used, which is typically limited by computational resources.

While state-averaged, or state-specific, CASPT2 is the most widely used multi-reference perturbation theory method, many other multi-reference perturbation theory methods exist. Multi-reference Møller-Plesset[167] and n-electron valence space perturbation theory[168] are similar to CASPT2 in that they are "diagonalize then pertrub" theories, but they differ in the nature of the applied perturbation. Other methods based on the concept of an effective Hamiltonian which, when diagonalized, only gives some of the exact eigenvalues of the exact Hamiltonian[170,328,329] take the alternative "perturb then diagonalize" approach to the multi-reference perturbation theory problem. Still other multi-reference methods use coupled-cluster theory instead of perturbation theory to add dynamic correlation to the total energy.[169,330–332] Like CASPT2 these methods can be accurate, but can depend on the choice of active space and suffer from intruder state problems.

As shown in chapter 2, recently we[300] and others[333] have shown that the ΔSCF-DFT method[334] can often perform as well as TDDFT for a given choice of exchange-correlation functional. While the ΔSCF-DFT method only yields estimates of excited state properties of roughly the same quality as TDDFT,[300] the underlying strategy of ΔSCF-DFT suggests a unique opportunity to approach the multi-reference purturbation theory problem from a new direction. In HF theory as in Kohn-Sham DFT, the ΔSCF approach can be used to enforce a selected non-Aufbau orbital occupation pattern during SCF energy minimization and converge onto an excited state determinant. In this chapter, we introduce a second-order multireference perturbation theory rooted in the ΔSCF approach, which we denote ΔSCF(2). In this "perturb then diagonalize" method, the reference states are composed of the HF ground state wavefunction and a number of non-Aufbau HF excited state wavefunctions, each dressed with a perturbative correction in the spirit of second order Møller-Plesset perturbation theory (MP2). Due to the equal treatment of the ground and excited states the ΔSCF(2) method is designed to require a small number of wavefunctions and use a perturb-then-diagonalize strategy to obtain ground and excited states.

In the remainder of this chapter, we describe in detail the ΔSCF(2) method, and then we present applications to some minimal models of bond breaking and a conical intersection to assess its strengths and weaknesses.

3.2 Theory

In the ΔSCF(2) method, the HF ground-state wavefunction and several non-Aufbau, stationary HF wavefunctions ($|\Phi_A^0\rangle \equiv |A^{(0)}\rangle$) are used to construct a basis in which the final ground- and excited-state wavefunctions ($|\Psi_n\rangle$) are to be determined via CI,

$$|\Psi_n\rangle = \sum_A c_n^A \, |A\rangle \tag{3.1}$$

To account for dynamic correlation within the HF and ΔSCF wavefunctions, we apply second-order perturbation theory with the Fock operator as the zeroth-order Hamiltonian, which generates a first-order correction for each wavefunction,

$$\begin{aligned} |A\rangle &= |A^{(0)}\rangle + |A^{(1)}\rangle \qquad (3.2)\\ &= |A^{(0)}\rangle + \frac{1}{4}\sum_{\substack{ij\\ab}} t_{ij}^{ab}|A_{ij}^{ab}\rangle \qquad (3.3) \end{aligned}$$

where $|A_{ij}^{ab}\rangle$ is the double excitation $i \to a, j \to b$ from $|A^{(0)}\rangle$ and its amplitude t_{ij}^{ab} is the standard MP2 amplitude,

$$t_{ij}^{ab} = \frac{|\langle ij||ab\rangle|^2}{\epsilon_a + \epsilon_b - \epsilon_i - \epsilon_j} \tag{3.4}$$

We use indices i, j, k, l for occupied orbitals, a, b, c, d for virtual orbitals, and p, q, r, s for either type of orbital. We also use index notation, so in the following expressions there is an implicit sum over repeated indices. Each wavefunction in this basis is derived from an independent solution to the HF equations, with an independent set of optimized molecular orbitals (MOs) for each state. In this sense, all states in ΔSCF(2) are determined at the same level of theory, in contrast to CAS methods which generate excited states from constituent orbitals of the ground state, or from a single set of orbitals determined by state-averaging. The orbital relaxation that occurs in the non-Aufbau excited states during convergence avoids the need for a state-averaging procedure; instead, all orbitals are chosen by self-consistent minimization of each state's energy. Furthermore, because the basis states in ΔSCF(2) are designed to resemble the many-electron states of interest (e.g. ground and low-lying excited states), far fewer basis states should be required to represent the target wavefunctions, compared to the relatively large active spaces usually required in CAS methods. However, since the non-Aufbau wavefunctions are independently obtained solutions to the HF equations, orbitals obtained from different states will generally be nonorthogonal.

The MP2-corrected ground state and non-Aufbau states define the basis of single-determinant wavefunctions for the ΔSCF(2) method. We can then perform CI in this basis, i.e. we find the eigenvalues and eigenfunctions of

$$\mathbf{Hc} = E\mathbf{Sc} \tag{3.5}$$

where the Hamiltonian and overlap matrix elements are

$$H_{AB} = \langle A|\hat{H}|B\rangle = \langle A^{(0)}|\hat{H}|B^{(0)}\rangle + \frac{1}{2}\left(\langle A^{(0)}|\hat{H}|B^{(1)}\rangle + \langle A^{(1)}|\hat{H}|B^{(0)}\rangle\right) \tag{3.6}$$

$$S_{AB} = \langle \Phi_A|\Phi_B\rangle = \langle A^{(0)}|B^{(0)}\rangle + \frac{1}{2}\left(\langle A^{(0)}|B^{(1)}\rangle + \langle A^{(1)}|B^{(0)}\rangle\right) \tag{3.7}$$

We do not include matrix elements such as $\langle A^{(1)}|\hat{H}|B^{(1)}\rangle$ because they are fourth-order in the perturbation expansion, and we are only interested in perturbation to second order. We take an average of the two terms on the RHS of Eqs. 3.6 and 3.7 so that the diagonal Hamiltonian matrix elements will reproduce the MP2 energy and the off-diagonal terms will be symmetric. The zeroth-order terms in Eqs. 3.6 and 3.7 are straightforward to evaluate, despite the nonorthogonality of molecular orbitals of A and B.[335,336] To evaluate the second-order terms $\langle A^{(0)}|\hat{H}|B^{(1)}\rangle$ and $\langle A^{(0)}|B^{(1)}\rangle$, we must address the issue that the MO bases of $|A^{(0)}\rangle$ and $|B^{(0)}\rangle$, $\{\phi_p^A\}$ and $\{\phi_p^B\}$, respecitvely, are not orthogonal to each other.

In the MO basis, the overlap matrix S' between two ΔSCF determinants $|A\rangle$ and $|B\rangle$ will in general have non-zero off diagonal matrix elements in all blocks (occupied-occupied, occupied-virtual, and virtual-virtual). In order to simplify the evaluation of $\langle A^{(0)}|\hat{H}|B^{(1)}\rangle$ and $\langle A^{(0)}|B^{(1)}\rangle$ we rotate the orbitals, t_{ij}^{ab}, and two electron integrals into a basis that diagonalizes the occupied-occupied block of the overlap matrix S'_{occ},

$$S'_{\text{occ}} = U S_{\text{occ}} V^{-1} \tag{3.8}$$

In this new basis, which is called the corresponding orbital basis,[337,338] the matrix elements of the overlap are

$$\langle \phi_i^A | \phi_j^B \rangle = S_i \delta_{ij} \tag{3.9}$$

$$\langle \phi_a^A | \phi_b^B \rangle = S_{ab} \tag{3.10}$$

$$\langle \phi_i^A | \phi_a^B \rangle = S_{ia} \tag{3.11}$$

$$\langle \phi_a^A | \phi_i^B \rangle = S_{ai} \tag{3.12}$$

The occupied-occupied block is then diagonal, which simplifies the evaluation of the Hamiltonian and overlap matrix elements. The diagonal elements in the occupied-occupied block are well defined up to an overall sign, which we select such that the product of the determinants of U and V is positive, $|U||V| > 0$. This choice preserves the overall sign of the occupied-occupied block.

In the corresponding orbital basis, the second-order terms in Eq. 3.6 can now be written as

$$\langle A^{(0)}|\hat{H}|B^{(1)}\rangle = \frac{1}{4} E_A \langle A^{(0)}|B_{ij}^{ab}\rangle t_{ij}^{ab} + \frac{1}{16}\langle kl\|cd\rangle \langle A_{kl}^{cd}|B_{ij}^{ab}\rangle t_{ij}^{ab} \tag{3.13}$$

Here E_A is the Hartree-Fock energy of state A. Evaluating Eq. 3.13 using a brute force approach requires computational effort that scales as $N_{\text{occ}}^4 \times N_{\text{virt}}^4$.

To greatly improve the scaling behavior of Eq. 3.13, we express $\langle A^{(0)}|B_{ij}^{ab}\rangle$ and $\langle A_{kl}^{cd}|B_{ij}^{ab}\rangle$ in terms of the matrix elements of the overlap matrix in the corresponding orbital basis, given in Eq. 3.12. For example, the overlap between $A^{(0)}$ and B_{ij}^{ab}, $\langle A^{(0)}|B_{ij}^{ab}\rangle$, in the corresponding orbital basis set is $\frac{\langle A^{(0)}|B^{(0)}\rangle}{S_i S_j}(S_{ai}S_{bj} - S_{aj}S_{bi})$. Using the symmetry relations of the two electron integrals and t_{ij}^{ab} matrix elements the first term on the RHS of Eq. 3.13 becomes

$$\frac{1}{4}E_A\langle A^{(0)}|B_{ij}^{ab}\rangle t_{ij}^{ab} = \frac{1}{2}E_A\frac{S_{ai}S_{bj}}{S_i S_j}\langle A^{(0)}|B^{(0)}\rangle t_{ij}^{ab} \tag{3.14}$$

where $\langle A^{(0)}|B^{(0)}\rangle = \prod_k^N S_k$, and our final expression scales as $N_{\text{occ}}^2 \times N_{\text{virt}}^2$. We repeat this procedure in order to obtain the rest of the terms on the RHS of Eq. 3.13.

In order to simplify the expressions for the second term on the RHS of Eq. 3.13, we define the following two projected-overlap quantities,

$$S_{pr}^{ij} = \langle\phi_p^A|1 - \sum_{k\neq i,j}\frac{|\phi_k^B\rangle\langle\phi_k^A|}{S_k}|\phi_r^B\rangle \tag{3.15}$$

$$S_{pr}^{i} = \langle\phi_p^A|1 - \sum_{k\neq i}\frac{|\phi_k^B\rangle\langle\phi_k^A|}{S_k}|\phi_r^B\rangle \tag{3.16}$$

The expression for the overlap between doubly-excited determinants $\langle A_{kl}^{cd}|B_{ij}^{ab}\rangle$ depends on how many occupied orbitals the states have in common, so we break up $\langle A_{kl}^{cd}|B_{ij}^{ab}\rangle$ into three cases according to the number of common indices: (1) two common indices, $i = k$ and $j = l$; (2) one common index, $i = k$ and $j \neq l$; and (3) no common indices, $i \neq k$ and $j \neq l$. For each case we give the simplified expression for the second term on the RHS of Eq. 3.13.

Case 1: $i = k$, $j = l$

$$\frac{1}{2}\frac{\left[\langle ij||cd\rangle S_{ac}^{ij}\right]\left[t_{ij}^{ab}S_{bd}^{ij}\right]\langle A^{(0)}|B^{(0)}\rangle}{S_i S_j} \tag{3.17}$$

We place terms in brackets to indicate where they can be summed independently to decrease the scaling. Eq. A.10 scales as $N_{\text{occ}}^2 \times N_{\text{virt}}^3$.

Case II $i = k$, $j \neq l$

$$\left[\frac{\langle il\|cd\rangle S_{ld}}{S_l}\right]\left[\frac{t_{ij}^{ab}S_{bj}}{S_j}\right]\frac{S_{ac}^{i}\langle A^{(0)}|B^{(0)}\rangle}{S_i} - \left[\frac{\langle ij\|cd\rangle S_{jd}}{S_j}\right]\left[\frac{t_{ij}^{ab}S_{bj}}{S_j}\right]\frac{S_{ac}^{i}\langle A^{(0)}|B^{(0)}\rangle}{S_i} \quad (3.18)$$

The second term of Eq. A.11 corrects for the inclusion of $j = l$ in the first term. While this expression is more complex than the one obtained by restricting the implicit sum in the first term, it permits evaluation with a better scaling, namely $N_{\mathrm{occ}}^3 N_{\mathrm{virt}}^2$.

Case III $i \neq k$, $j \neq l$

$$\frac{1}{4}\left[\frac{\langle kl\|cd\rangle S_{kc}S_{ld}}{S_k S_l}\right]\left[\frac{t_{ij}^{ab}S_{ai}S_{bj}}{S_i S_j}\right]\langle A^{(0)}|B^{(0)}\rangle - \left[\frac{\langle il\|cd\rangle S_{ic}S_{ld}}{S_i S_l}\right]\left[\frac{t_{ij}^{ab}S_{ai}S_{bj}}{S_i S_j}\right]\langle A^{(0)}|B^{(0)}\rangle$$
$$+\frac{1}{2}\left[\frac{\langle ij\|cd\rangle S_{ic}S_{jd}}{S_i S_j}\right]\left[\frac{t_{ij}^{ab}S_{ai}S_{bj}}{S_i S_j}\right]\langle A^{(0)}|B^{(0)}\rangle \quad (3.19)$$

Again, the second and third terms in this expression are correction factors which could be avoided if restrictions were placed on the sums in the first terms; but evaluation of the expression is more efficient in this form, scaling as $N_{\mathrm{occ}}^2 \times N_{\mathrm{virt}}^2$.

Eqs. 3.13–A.12 allow us to compute the matrix elements of the Hamiltonian and overlap in the basis of perturbed non-Aufbau states. The second-order overlap matrix elements are equal to the second term on the RHS of Eq. 3.13 divided by the energy E_A. An important practical consideration is that some diagonal matrix elements of the overlap in the corresponding orbital basis, S_i, may be nearly zero, i.e. the overlap matrix may be singular. In this case, the derivation of Eqs. 3.14-A.12 requires further modification. One way to circumvent the singular overlap matrix problem is to drop terms where $|S_i|$ falls below a threshold value, but this is only an approximate solution. In order to avoid further approximations, we have derived additional sets of equations, given in the Appendix A, which specially address cases where some $S_i = 0$. These considerations do not increase the computational cost of the method, but they do increase the complexity of the equations.

Given these expressions for the Hamiltonian and overlap matrix elements in the basis of perturbed ΔSCF states, we can diagonalize the Hamiltonian to obtain ΔSCF(2) energies and wavefunctions for the ground and excited states. In the next section, we test the method on some simple systems.

3.3 Excited State Potential Energy Surfaces

To test our new approach to a multi-reference MP2 method we consider ground and low-lying excited states of the H_2, FH, and tetrahedral H_4 molecules. The H_2 and FH molecules provide simple test systems for discerning the performance of ΔSCF(2) at dissociation and for comparing to established methods, while tetrahedral H_4 provides a simple test case for conical intersections. The ΔSCF(2) calculations use a modified version of Q-Chem 4.0,[262] and we use an in-house full-CI code. The convergence of the ΔSCF states is aided by the maximum overlap method (MOM).[339] To avoid intruder-state problems at dissociation in the FH and H_2 dissociation curves,[323] we replaced the energy difference in the denominator, $\Delta\epsilon = \epsilon_a + \epsilon_b - \epsilon_i - \epsilon_j$ with a Lorentzian approximation that removes the divergence, $\frac{1}{\Delta\epsilon} \approx \frac{\Delta\epsilon}{\Delta\epsilon^2+\delta^2}$. We use threshold values for the Lorentzian, δ, of 0.3 and 1.0 Hartree for H_2 and FH, respectively; no modification is needed for the H_4 calculations.

For both H_2 and FH we compute the dissociation curves for the ground and lowest lying excited states. In the case of H_2 we use the 6-311G basis set. The basis states consist of the ground state, the α- and β-spin HOMO→LUMO non-Aufbau states, and the doubly excited HOMO→LUMO non-Aufbau state. The dissociation curves for both ΔSCF(2) and full-CI are shown in Figure 3-1, with a table of the results for the ΔSCF(2) states given in Appendix A. The four different potential energy curves plotted are the ground state (S_0), triplet state (T_0), singlet excited state (S_1), and the doubly excited state (S_2). We are able to compute the triplet excited state and singlet excited state since they are simple linear combinations of the two broken-symmetry HOMO→LUMO ΔSCF states. Just as in CAS calculations, the ΔSCF(2) method gets the correct shape of the potential energy surfaces, but lacking some of the dynamic correlation, it is consistently above the full-CI curve.[221,340] The excited states show accuracy similar to that of the ground state, with T_0 having the smallest mean absolute error (MAE) with full-CI (4 mHartree) and S_2 having the largest MAE (12 mHartree).

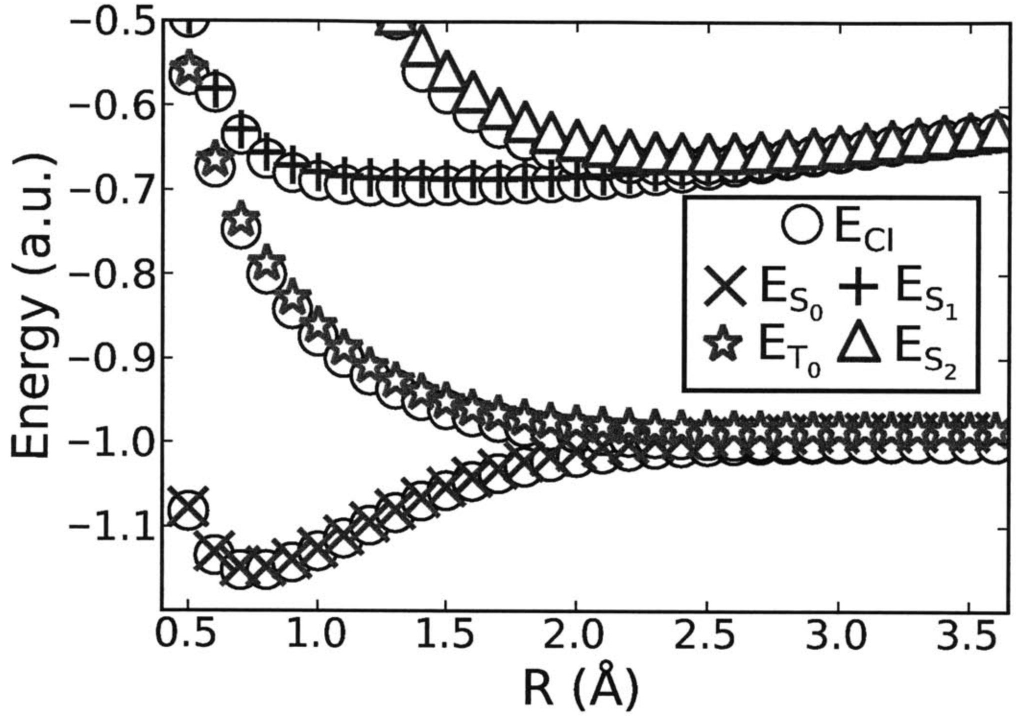

Figure 3-1: H_2 dissociation potential energy curves computed with full-CI (circles) and ΔSCF(2). The ΔSCF(2) method performs well for both the ground, singly, and doubly excited states over the entire potential energy surface.

Interestingly, we find the S_0 state from ΔSCF(2) is above the full-CI results by 4 mHartree near the equilibrium distance and 13 mHartree at the dissociation limit, which is the opposite of the effect one would expect from errors due to dynamic correlation. For example, the CASSCF method has an error of 7 mHartree near equilibrium and less than 0.001 mHartree at the dissociation limit. The reason the ΔSCF(2) methods is worse for H_2 at dissociation is due to the orbital relaxation in the doubly excited ΔSCF state. At dissociation distances the CASSCF calculation can yield the exact energy, $2\times E_{\mathrm{H}}$, while due to relaxation of the orbitals in the ΔSCF procedure, the ΔSCF(2) method cannot reproduce the exact dissociation limit. Using the ΔSCF(2) wavefunctions at the dissociation limit would be like using state-averaged CASSCF to get the ground and doubly excited state. The H_2 molecule provides an extreme example of this problem. At the dissociation limit with a minimal basis set, the full-CI expansion yields exactly the ground state and the doubly excited state, both constructed from the same molecular orbital basis, and while these two states are both included in the ΔSCF(2) calculation, the relaxation in the doubly excited-state molecular orbitals introduces an error into the calculation. Across the potential energy curve, the ΔSCF(2) method performs about equally well for the ground and excited states of H_2.

One important property for an excited state method is its ability to locate conical intersections. Conical intersections are very important for many systems, since in many molecules the dynamics in an excited state proceeds through a conical intersection. To test the ability of ΔSCF(2) to describe conical intersections, we consider a tetrahedral H_4 molecule with the 6-311G basis. Plotted in Figure 3-2 are the ground state and lowest lying excited state PES of H_4 according to ΔSCF(2). The conical intersection is located at the symmetric tetrahedral geometry, which is not the minimum geometry of the system. To obtain the conical intersection we use a set of six non-Aufbau determinants that are symmetry equivalent at the symmetric tetrahedral geometry. The six states come from the four-choose-two combination of two unique spins distributed over four sites.

For H_2 and H_4 we find similar non-parallelity errors (NPE) of roughly 2-4 mHartree for all of the different electronic states. The NPE is computed as NPE= $\text{avg}(\Delta E - \Delta E_{\text{avg}})$, where ΔE is the difference between ΔSCF(2) and full-CI. Just like in CAS methods the error can typically be reduced if the number of basis states (e.g. for CASSCF, the size of the active space) is increased. For example, if we add the HOMO$\rightarrow$LUMO+1 double excitation and the HOMO$\rightarrow$LUMO+2 double excitation to the H_2 ΔSCF(2) calculation, the NPE is reduced by a factor of 2.

Finally we compare the ΔSCF(2) method to existing multi-reference methods by calculating different electronic states during the dissociation of the FH molecule. The ground state, Σ singlet and triplet excited states, and Π singlet and triplet excited states of the FH molecule are computed using the valence double-zeta Dunning-Hay

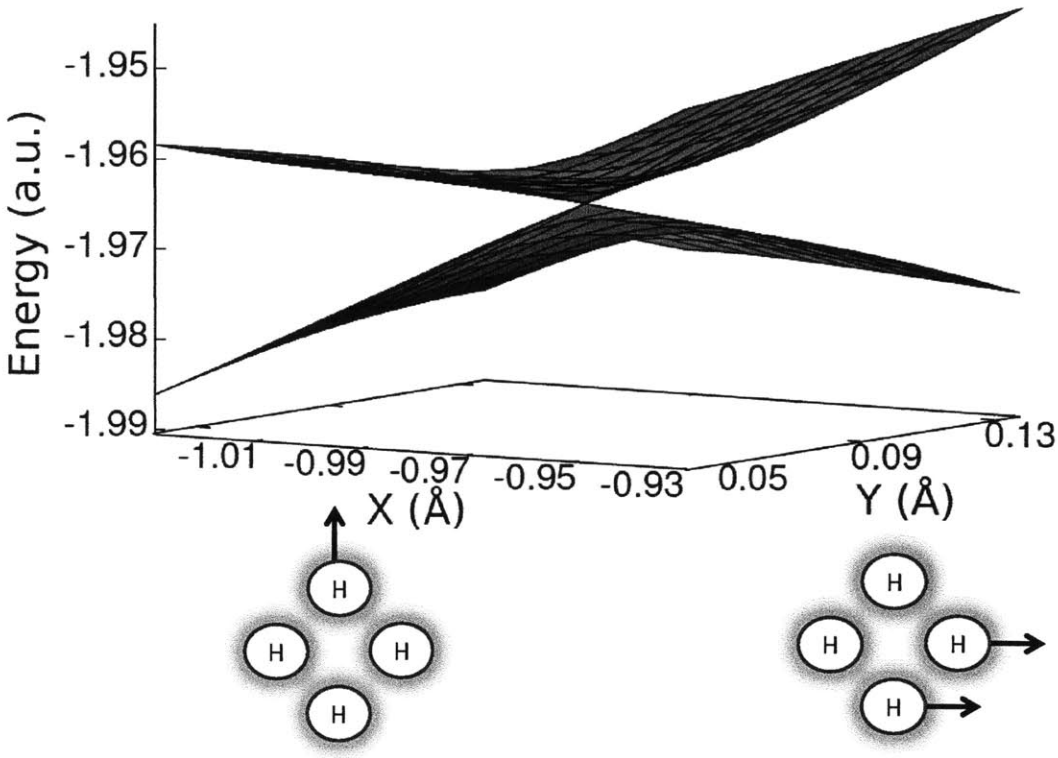

Figure 3-2: ΔSCF(2) reproduces the conical intersection in the tetrahedral H_4 molecule with a NPE relative to full-CI of roughly 2 mHartree for both the ground and excited state.

basis, as implemented in GAMESS.[341] At equilibrium, the Σ excited states are made up of a HOMO−2 →LUMO transition; both of these are σ orbitals. The Π excited states come from the degenerate HOMO→LUMO transition, which are π orbitals and a σ orbital, respectively. The wavefunction basis in the ΔSCF(2) calculations is made up of the HF ground state and nine ΔSCF states. The nine ΔSCF states are made up of two single and one double transition: HOMO→LUMO, HOMO−1 →LUMO, and HOMO−2 →LUMO. We plot the deviation of ΔSCF(2) from the average difference with full-CI for the FH molecule in Figure 3-3, a table of the ΔSCF(2) states can be found in Appendix A. For reference, the full-CI equilibrium bond distance for FH is 0.917 Å.

Overall, with a minimum set of 10 determinants, the ΔSCF(2) method stays fairly parallel to full-CI. In Figure 3-3 we can see that the ΔSCF(2) method does not

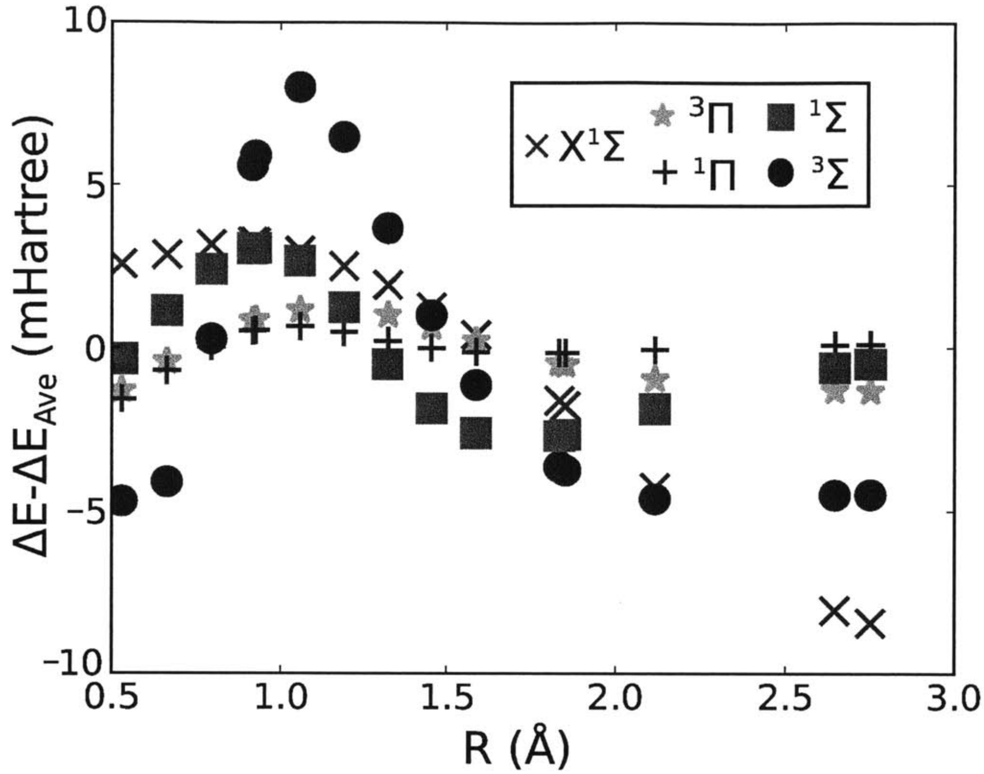

Figure 3-3: Deviation of the ΔSCF(2) potential energy from full-CI for FH as a function of bond length. The ΔE variable is $\Delta E = E_{\Delta\text{SCF(2)}} - E_{\text{Full-CI}}$. The ΔSCF(2) ground and excited state average errors very between 6 and 16 mHartree. All of the states display the most significant deviation with full-CI near the equilibrium distance (0.917 Å) because of the lack of the full dynamical correlation energy in the MP2 treatement.

perform as well at short distances due to the increased dynamical correlation at short distances. This is different from H_2 because now the full dissociation limit is not two independent one-electron systems. Such larger errors at short distances have also been found for CASPT2 and CASSCF methods since the small active space for the methods makes it much more difficult to pick up all of the dynamic correlation.[331] This error is even more prevalent for the S_2 excited state in the H_2 molecule and the $^3\Sigma$ excited state in the FH molecule.[331] The drop in the ground state at long distances in Figure 3-3 is due to the errors in MP2 at long range, and if we increase the δ parameter to above 1.0 then the drop in the ground state is reduced. .

We can compare the ΔSCF(2) method for FH with two different CASPT2 calculations from Ref. 340. In Ref. 340 the authors compute the ground state of FH using a valance and a 1:1 active space in the 6-31G** basis. The valance active space for FH has 8 electrons and 3011 active determinants per irreducible representation of the largest Abelian subgroup, and the 1:1 active space consists of 8 electrons and 4022 determinants. The average error of CASPT2 in the valance and 1:1 active space is 8.2 and 5.6 mHartree, respectively. The average error in the ground state for our 10-wavefunction basis set is 10 mHartree, very similar to CASPT2 errors with a much smaller number of reference determinants.

More importantly, with our small number of non-Aufbau states and basis set, we are able to achieve similar accuracy for the ground and excited states. The MAEs of ΔSCF(2) for the FH dimer are between 6 and 16 mHartree for the different states, and while the MAEs are not smaller than those of most multi-reference methods, the ΔSCF(2) excited states are fairly parallel to the full-CI excited states.[332] In Figure 3-3 the NPE is as small as 0.3 and 0.9 mHartree for the $^1\Pi$ and $^3\Pi$ states, and the largest NPE of 4.12 mHartree is in the $^3\Sigma$ state. This is not too surprising since the Σ states are less accurate in many multi-reference methods.[332] With the ΔSCF(2) method we gain accuracy in the ground state and other excited states by computing more excited states. That is not always the case for state-averaged CASPT2 methods, where one needs to have a large enough basis set and active space to make sure accuracy is not lost through the state averaging procedure.

The test cases presented here show that there is promise for the ΔSCF(2) method for computing ground and excited state potential energy surfaces. The NPEs for the different molecular systems ranged from 0.3 to 7 mHartree for all the electronic states. Like CASPT2, we do not get all of the dynamic correlation when we use a small number of non-Aufbau states. ΔSCF(2) is not a black box method because like CASPT2 we need to choose a proper set of non-Aufbau states, and for ΔSCF(2) we then need to converge all of the non-Aufbau states. Given this caveat however, the ΔSCF(2) method provides a new and potentially very accurate way to efficiently compute excited states in molecular systems.

3.4 Conclusion

Here we have presented a new type of multi-reference perturbation theory method that treats the ground and excited states equally. The use of ΔSCF wavefunctions for the excited states allows for the ground and excited states to have their own individually optimized set of molecular orbitals. Adding the perturbation before mixing the ground and excited state wavefunctions allows us to incorporate the popular MP2 level of dynamic correlation. We have showed how to simplify the computation of matrix elements in this method such that terms scale no worse than $N_{\text{occ}}^2 \times N_{\text{virt}}^3$. By modeling a few simple systems we have found that the ΔSCF(2) method is able to locate conical intersections and obtains ground and excited state PES to similar degrees of accuracy. The ΔSCF(2) method also obtains similar accuracy to CASPT2 with only a small number of ΔSCF states.

Just like picking the active space for CASSCF and CASPT2, the main difficulty with the ΔSCF(2) method is that one needs to determine which ΔSCF states are most important, and then converge those ΔSCF states. The nature of the ΔSCF(2) method makes it easy to parallelize since each ΔSCF calculation is independent, as well as the computation of the Hamiltonian and overlap matrix elements. Since the ΔSCF(2) method uses MP2 corrections, the total energies can in principle diverge when the orbital energies become degenerate, thus making it desirable to develop a non-emperical remedy for this problem. Future work will explore the ΔSCF(2) description of excited states in larger and more complicated systems, such as open-shell radicals, in order to further asses the abilities and limitations of ΔSCF(2), though the present results indicate significant potential for ΔSCF(2) to compute excited states with high accuracy.

3.5 Acknowledgement

The work described in this chapter was carried out jointly with Tim Kowalczyk.

Chapter 4

Universal Mechanism for Singlet Exciton Fission

4.1 Introduction

The optimum efficiency for an single junction organic solar panel is 33%.[15] One of the major loss mechanisms that limits the efficiency to 33% is the energy loss that occurs when a high energy exciton relaxes to the band gap of the device. This means that even if we are able to get perfect performance in all of the aspects of the energy conversion process in an organic solar panel we will still be at 33%. However, if we are able to reduce the loss due to relaxation of high energy excitons we can increase the maximum efficiency above 40%. One way this can be achieved is through a process called singlet fission. The singlet fission process takes one high energy exciton and converts it into two lower energy excitons. This means that all of the energy that would have been lost to heat is now converted into creating another charge in the system.

Singlet exciton fission was first observed in crystalline acene materials in the 1960s.[50] It has since been observed in a handful of materials several acene derivatives,[50,54,59,61,342,343] an isobenzofuran[344] and some carotenoids.[345] Progress toward new materials for singlet fission-based devices has been slow in part because the mechanism of singlet fission is not well understood.[53] Numerous time-resolved studies have confirmed that fission can occur very quickly on timescales as short as 80 fs[59,61] and can be very efficient.[346] However, it is not clear why it is so fast or what material properties must be controlled to ensure efficient fission. In the simplest physical picture, fission involves electronic states of a dimer in the material. Labeling the monomer electronic states as S_0, S_1 and T,

$$S_0S_0 \xrightarrow{h\nu} S_0S_1 \xrightarrow{k_{fis}} TT \tag{4.1}$$

The coupling, $V = \langle S_1S_0|\hat{H}|TT\rangle$, between the initial singlet excited state and the final triplet pair state plays a key role in understanding the rate of fission. Accurately computing this coupling is a challenge for electronic structure theory, in part because the TT state is a doubly excited state.[146,347] Early calculations[348] suggested V was too small to account for the observed ultrafast fission rates. As a result, it has been proposed that either activated charge hopping[55] or CT-mediated superexchange[53,56–58] could potentially be accelerating the fission rate. On the other hand, recent experiments have been interpreted as implying that V is so large that the bright state is a coherent superposition of S_1S_0 and TT.[60]

In order to determine which mechanism singlet fission uses we study the fission rate in a number of pentacene derivatives using a combined theoretical and experimental approach. The fission rates are experimentally measured using transient absorption techniques. We calculate the coupling for each molecule and use it to compute a theoretical fission rate, which agree with experimental fission rates over two orders of magnitude change in the fission rate. The fission process undergoes a transition from non-adiabatic energy transfer in the low coupling regime to adiabatic energy transfer in the high coupling regime. Therefor, the fission rate is not very sensitive the electronic coupling and can have a fission rate in the ps time regime with a coupling only as large as a few meV.

The rest of the chapter is organized as follows. The set of pentacene derivatives is introduced and their corresponding properties such as crystal packing and their absorption spectrum are discussed. The computational procedure is then outlined and discussed. Using the experimental and theoretical data the mechanism for singlet fission in the pentacene derivatives and its implications are considered.

4.2 Pentacene Derivatives

In order to quantify which of these models is correct, we study thin films of the six different pentacene derivatives shown in Figure 4-2: pentacene, 6,13-bis(triisopropylsilylethynyl) pentacene (TIPS-P), 6,13-diphenylpentacene (DPP), 6,13-di-biphenyl-4-yl-pentacene (DBP), 6,13-di(2-thienyl)pentacene (DTP), and 6,13-di-benzothiophene-pentacene (DBTP). The crystal structures were either obtained from the literature[349,350] or determined from X-ray crystallography. As is clear from the Figure 4-2, while chemically similar, these compounds adopt radically different crystal structures from one another. Pentacene packs in a herringbone arrangement, TIPS-P creates a 2D π-stacked structure, DTP shows cofacial 1D π-stacking, while in DBP, DPP and DBTP the side-chains prevent significant π overlap between the pentacene cores. We expect that crystals are a valid structural model for dimer pairs in the poly and nano-crystalline thin films that we study experimentally below.[351] The structural variations in these materials are expected to have a dramatic impact on the electronic coupling between monomers, leading to significant variation of k_{fis}. The expected variation in coupling is validated in part by the 100 nm range of redshifts measured in these films[1] (See Figure 4-1).

Presented in Figure 4-1 is the absorption spectra of the pentacene derivatives in solution and in thin-film states. Pentacene and TIPS-P feature large red shifts and significant broadening of their absorption peaks as the structure changes from solution to thin films. Also, we observe considerable changes in relative intensities of peaks in vibronic progressions. On the contrary, DBTP, DBP, and DPP show almost no change in absorption spectra as the state changes from solution to solid-state, except for a small redshift of ~0.05 eV. On each film we studied the effects of annealing. The absorption of DTP thin films became red-shifted and broadened upon annealing. In contrast, we observed a blue-shift of the absorption peak of DBP thin

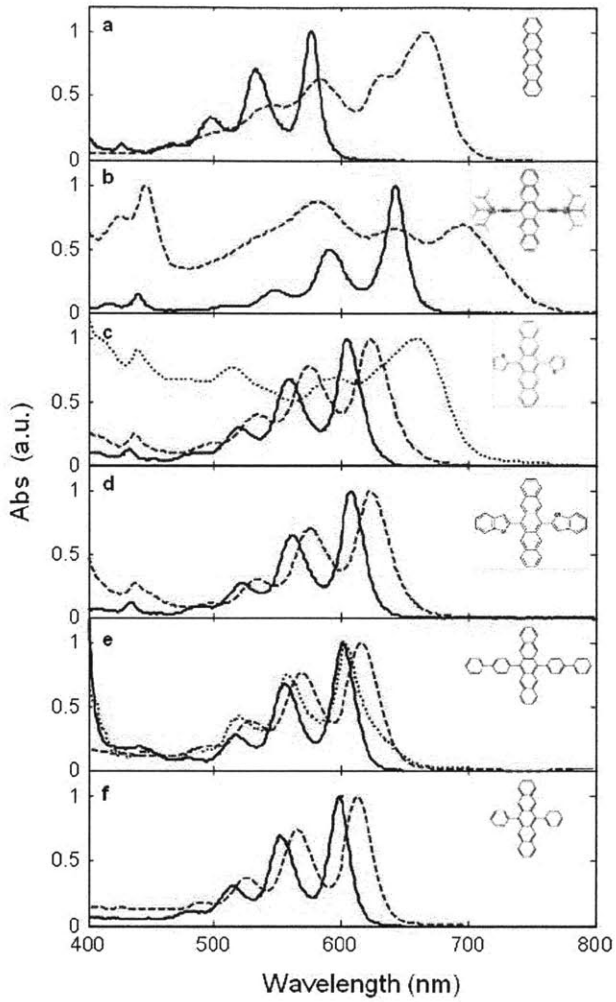

Figure 4-1: Absorbance spectra of toluene solutions (blue solid) and thin-films (green dashed) of (a) pentacene, (b) TIPS-P, (c) DTP, (d) DBTP, (e) DBP, and (f) DPP. The red dotted lines in (c) and (e) show the spectra of annealed DTP and DBP thin-films, respectively

films after annealing. The subsequent change in fission dynamics is discussed below. As the thin films with lower-energy absorption peaks are likely to have morphology closer to crystal structures, we chose annealed DTP and non-annealed DBP films for reporting fission rates. The other pentacene derivatives showed no discernible change in absorption upon annealing

Following photoexcitation to the bright state, the formation of triplets is probed by monitoring the intensity of $T_1 \rightarrow T_2$ (~880 nm) or $T_1 \rightarrow T_3$ (~530 nm) transitions

	Pentacene	TIPS-P	DTP	DBTP	DBP	DPP
Crystal Structure	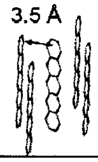	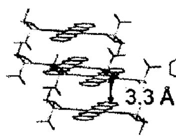	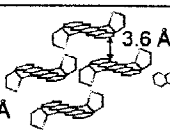	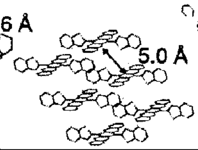	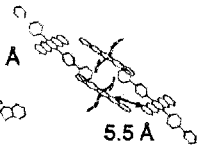	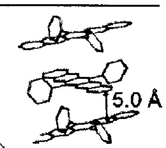
Structure Type	Herringbone	2D π stack	Slip stacked	Displaced slip stack	Displaced slip stack	Orthogonal π stacked
V (meV)	19	56	10	5.6	2.4	1.4
$\bar{V}$ (meV)	84	72	16	5.4	2.0	0.82
k_{fis} (ps^{-1})	12.5	10	6.25	1.11	0.26	.085

Figure 4-2: Pentacene derivatives examined in this study along with their crystal structures, structure types, coupling energies with ($\bar{V}$) and without (V) charge transfer mixing, and measured fission rates (k_{fis}).

at various time delays[1].[61,62] We obtain the rate of singlet fission by fitting the TA signal to a single exponential in time. Figure 4-3 presents the kinetics of triplet formation in a series of pentacene derivatives. The peak of the $T_1 \rightarrow T_3$ ($T_1 \rightarrow T_2$) photoinduced absorption feature was chosen for DBTP, DBP and DPP (pentacene, TIPS-P and DTP). The pump intensity was 5-45 J/cm^2, and we verified the absence of singlet-singlet annihilation by confirming the independence of the transient shape on intensity dependence. The time-resolved photoinduced absorption of singlet excitons for DPP presented in the inset in Figure 4-7 was obtained by averaging over the probe wavelengths of 465-475 nm. As singlet fission in pentacene is exothermic and thus unidirectional (unlike tetracene[64,343,352]), we obtained the rate of singlet fission by fitting a mono-exponential curve to the data. Fission time constants for DBP thin films increased from 3.8±0.2 ps to 19.5±0.6 ps upon annealing; slowed singlet fission in annealed DBP films is consistent with the blue-shift of absorption spectrum (Figure 4-1), both meaning reduced intermolecular interaction. The time constant of singlet fission rate in the pentacene derivatives studied here are summarized in Figure 4-2.

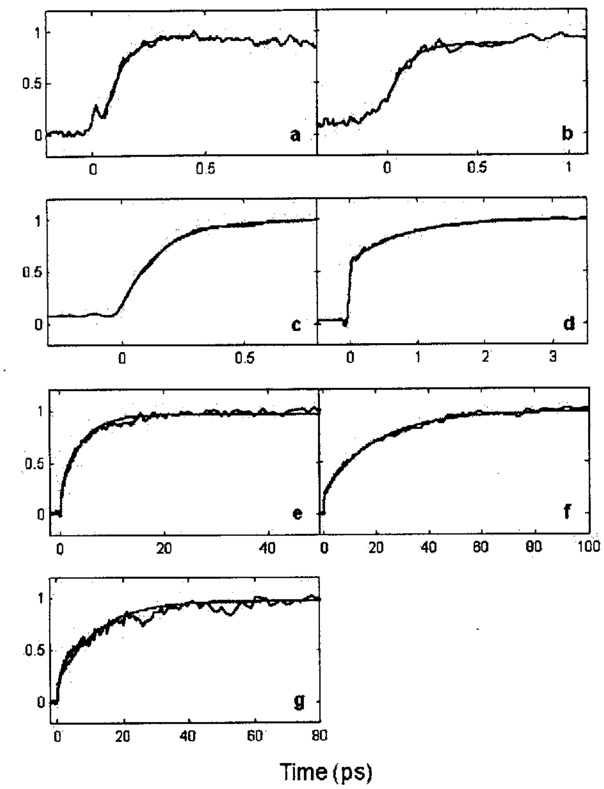

Figure 4-3: Transient absorption kinetics of triplets (blue) for (a) pentacene (850-870 nm), (b) TIPS-P (790-813 nm), (c) DTP (annealed) (760-810 nm), (d) DBTP (520-530 nm), (e) DBP (non-annealed) (525-535 nm), (f) DBP (annealed) (525-535 nm) and (g) DPP (525-535 nm). Kinetics were averaged over the wavelength ranges specified. Green lines are exponential fittings for the corresponding data. Kinetics taken from the $T_1 \rightarrow T_3$ transition often display a vertical offset due to overlapping spectral features.

4.3 Theoretical Modeling

For each material, we compute V using constrained density functional theory (CDFT).[154,155] Using the crystal structure of each material we select dimer pairs for the density functional theory (DFT) calculations, and model the electronic states of a dimer embedded in the crystal electrostatic field. Monomer geometries are optimized in the gas phase using the 6-31G* basis and the PBE0 functional. The monomer geometry are then placed in maximum coincidence with the crystal structure to remove artifacts from imprecise determination of monomer structures in the diffraction fit, and can be found in Appendix C. The QM/MM environment is obtained from a force field parametrized to quantum chemical calculations and experimental data, and the final force field parameters can be found in Appendix B. Note that in some cases more than one dimer pair can conceivably be involved in fission. In these situations, all the reasonable dimer pairs are computed following the procedure below and only the largest coupling (corresponding to the fastest rate) is reported. For pentacene, two different dimers (A and B, See Figure 4-4) corresponding to translation along different axes of the herringbone plane, are found to have comparable couplings. Data are shown for both of these cases in what follows.

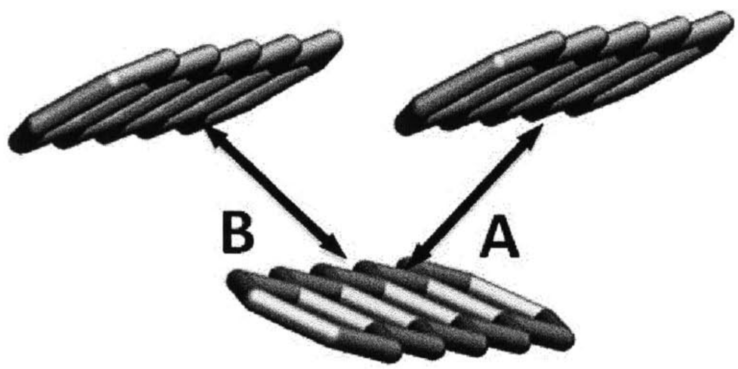

Figure 4-4: Pentacene dimer coupling directions considered in this work.

4.3.1 CDFT States

The electronic states were calculated using ΔSCF[300] and Constrained-DFT[197] on a dimer. Some dimer pairs are computed using the promolecule feature in Constrained-DFT in order to correct for the wave function overlap between the monomers. For each dimer, we obtain ten localized, broken symmetry, diabatic-like states by constraining the charge and spin of each monomer (M) to match the appropriate physical state: S_1S_0, S_0S_1, M^+M^-, M^-M^+, TT (See Figure 4-5). Note that in some cases, a tiny dipolar electric field of 0.0007 debye is applied in order to aid convergence to a localized state. The coupling between $\uparrow\downarrow$ and $\downarrow\uparrow$ on a single monomer is extracted from the computed PBE0/6-31G* singlet-triplet gap of the monomer.[151] All other couplings and overlaps between the ten states are computed using constrained-DFT based configuration interaction (CDFT-CI).[197]

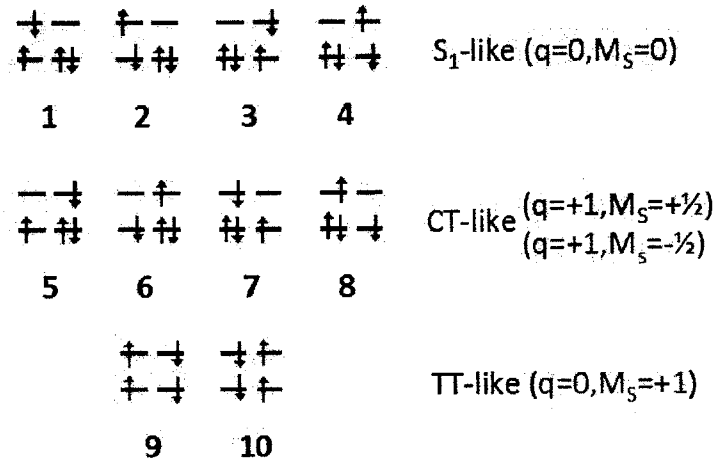

Figure 4-5: CDFT states computed for each dimer. For each dimer, the ten broken symmetry CDFT states shown are computed and used as an active space for expanding the wave functions involved in the fission process. For the S_1 states, CDFT is employed with non-Aufbau occupation of the orbitals (i.e. a constrained ΔSCF procedure). For all other cases, traditional Aufbau occupations are used.

In order to obtain spin eigenstates, we make appropriate linear combinations of the symmetry broken configurations: 1+2 $\rightarrow S_1S_0$; 3+4 $\rightarrow S_0S_1$; 5+6 $\rightarrow M^+M^-$; 7+8 $\rightarrow M^-M^+$; 9+10 $\rightarrow TT$. Note that in the case of the TT state, we are only able to obtain two of the three spin components required to obtain a pure singlet (we miss the component with S=1, $M_S = 0$ on each monomer). Thus our TT state is actually 2/3 singlet and 1/3 quintet. We account for this in what follows by multiplying the computed TT couplings by $\sqrt{3/2}$ before using them in the fission rate expression. The result of the spin adaption is to reduce the active space to five configurations, as described in the text: S_1S_0, S_0S_1, M^+M^-, M^-M^+ and TT. The energies of these five states for all materials considered in this work are presented in Table 4.1. For reference, the S_1 energy of pentacene in a film (solution) is 1.8 (2.1) eV, twice the T energy is approximately 2×0.86 eV[353] = 1.73 eV and the CT energy in the thin film is estimated from electroabsorption to be ~0.3-0.6 eV above the singlet (2.1-2.4 eV).[354]

As noted previously, the computed energies are only expected to be accurate to

Energy (eV)	S_1S_0	S_0S_1	M^+M^-	M^-M^+	TT
Pentacene (A)	2.32 (2.08)	2.32 (2.09)	1.80 (2.54)	4.73(2.58)	2.49 (1.92)
Pentacene (B)	2.30 (2.07)	2.31(2.10)	1.82 (2.56)	4.74(2.58)	2.50(1.93)
TIPS-P	1.69	1.77	2.11	2.15	1.42
DTP	1.94	2.03	2.63	2.47	1.82
DBTP	1.98	1.98	3.09	3.17	2.08
DBP	2.11 (1.99)	2.16(2.00)	2.03(2.66)	3.17(2.71)	1.96 (1.84)
DPP	2.06	2.05	2.79	2.56	1.99

Table 4.1: CDFT Energies of spin adapted states. The energies of the five relevant CDFT states are shown in eV relative to the ground state. Results in parentheses show the result of using the promolecule prescription to obtain the constrained states.

±0.3 eV[300] and so they will not be used to predict, e.g., the driving force for the reaction. However, the fact that the energies of these states are typically within the expected error bars of the experiment serves to justify that these states are physically reasonable representations of the states in question. A few notes concerning these energies:

- For pentacene, the herringbone arrangement leads to significant overlap of the monomer wavefunctions. DBP also contains significant overlap between the monomer wavefunctions due to the sidegroups attached to the pentacene core. Thus, the raw CDFT energies are not accurate. More reasonable energies can be obtained using the promolecule prescription of CDFT (results shown in italics). For consistency, we will use the non-promolecule data in what follows, although similar data could be obtained using the promolecule prescription for pentacene and DBP.

- For TIPS-P, the S_1 energy is lower than for the other derivatives, consistent with the acetylene linkers effectively increasing the conjugation length of the pentacene core.

- In principle, the S_1S_0/S_0S_1 and M^+M^-/M^-M^+ states should have identical energies due to translational symmetry. Our QM/MM simulations do not precisely preserve this symmetry, but the resulting energies typically agree to within a few hundredths of an eV.

From Table 4.1 we see that CDFT predicts the energy gaps $\Delta E_{\mathrm{CT}} = E_{S_0S_1} - E_{M^+M^-}$ to be fairly small (0.31.0 eV). Thus, charge transfer (CT) mediated superexchange might play a significant role in fission.[56–58] Indeed, the absorption spectra (see Figure 4-1) for pentacene, TIPS-P and DTP show the clear signature of CT mixing in the bright excited state.[355] We can account for CT-mediated and direct fission simultaneously by mixing the four states (S_1S_0, S_0S_1, M^+M^-, M^-M^+) to obtain four quasi-adiabatic states that account for superexchange-type CT mixing.

4.3.2 Electronic Coupling

In order to compute the raw coupling, $V = \langle S_1S_0|\hat{H}|TT\rangle$, we first compute the energy eigenstates in the basis spanned by S_1S_0 and S_0S_1. That is, we solve the 2×2 eigenvalue problem $\mathbf{Hc}=\epsilon\mathbf{Sc}$ to obtain the coefficients of the Frenkel exciton (FE) states $c_1 \cdot S_1S_0 + c_2 \cdot S_0S_1$. We then symmetrically orthogonalize those FE states to the TT state. In practice, this results in two distinct couplings, V_1 and V_2, and we report the average $V = \sqrt{\frac{V_1^2+V_2^2}{2}}$. Because both FE states are expected to be close in energy (less than $\sim kT$ apart) both will be thermally accessible. The resulting couplings are shown in Table 4.2.

In order to determine the extent of CT mixing in the dimers, we first compute the energy eigenstates in the basis spanned by S_1S_0, S_0S_1, M^+M^- and M^-M^+. That is, we solve the 4×4 eigenvalue problem $\mathbf{Hc}= \epsilon\mathbf{Sc}$ to obtain the coefficients of the bright states. We then symmetrically orthogonalize those four states to the TT state. We then select from among the four states the two bright states with significant S_1S_0 character. In practice, this again results in two distinct couplings and we report the average $\bar{V} = \sqrt{\frac{\bar{V}_1^2+\bar{V}_2^2}{2}}$ in the text. For the case of pentacene, we report $V = \sqrt{\frac{\bar{V}_{1A}^2+\bar{V}_{2A}^2+\bar{V}_{1B}^2+\bar{V}_{2B}^2}{2}}$. The resulting couplings are shown in Table 4.2.

Several features are worth noting:

- The couplings themselves obey the expected behavior that dimers that are further separated have smaller couplings, while those close together have larger couplings.

Coupling (meV)	V_1	V_2	V_1	V_2	%CT
Pentacene (A)	6.5	17.3	24.5	77.8	1.1% (5.8%)
Pentacene (B)	10.8	16.1	8.0	87.6	1.8% (9%)
TIPS-P	51.7	60.3	71.7	73.6	1.0%
DTP	8.1	12.5	8.3	21.5	13%
DBTP	7.3	2.9	7.1	2.8	0.1%
DBP	2.8	2.0	2.1	1.9	0.2% (0.1%)
DPP	2.0	0.6	1.0	0.6	0.3%

Table 4.2: Electronic Couplings computed as outlined in the text. The last column shows the percentage CT character of the lowest bright eigenstate as computed in the basis spanned by S_1S_0, S_0S_1, M^+M^- and M^-M^+. Numbers in parenthesis indicate the CT character of promolecule-based bright states.

- The effective couplings in DBTP, DBP and DPP are not significantly changed by including the interaction with CT states. This is consistent with the fact that the resulting bright states have little CT character (last column of Table 4.2) and that the experimental spectra do not show significant features of CT absorption. Two effects contribute to the suppression of superexchange-type mixing in these cases: 1) Because of the larger separation, ΔE_{CT} is larger in these dimers and 2) Because of the poor wavefunction overlap, the one electron hopping integrals required for superexchange-CT mixing are exponentially smaller.

- Surprisingly, superexchange actually marginally reduces the coupling for the DBTP, DBP and DPP. We attribute this to destructive interference between the direct and superexchange pathways in these dimers.

- Pentacene, TIPS-P and DTP all show appreciable increases in the coupling due to superexchange effects. This is consistent with the fact that these materials have the largest computed CT character and the most significant CT signatures in their absorption spectra.

- The percentage of CT mixing we obtain for pentacene is somewhat lower than that predicted based on detailed analysis of the polarized absorption spectra.[355] We attribute this to poor estimation of the ΔE_{CT} gap in our calculations. As noted previously, we only expect to predict this gap accurate to ± 0.3 eV. Our results are on the high side of the experimental estimate (i.e. we find $\Delta E_{\mathrm{CT}} \sim$ 0.5 eV). If we were to adjust this value to be toward the lower end of the experimental window (i.e. we shift the CT states down so that ΔE_{CT} 0.3 eV) we would obtain CT mixing more in line with previous results. However, as the CT mixing only changes the couplings that are already adiabatic, this would not change our rate predictions and so we do not employ this element of empiricism.

The couplings, V and $\bar{V}$, computed with CDFT-CI[196] in Table 4.2 span a range of almost three orders of magnitude for the materials in Figure 4-2. Our prescription to compute the couplings has been shown previously to quantitatively predict triplet hopping rates in acenes.[356] Because triplet hopping relies on a coupling ($V_{TT} = \langle TS_0|\hat{H}|S_0T\rangle$) that is physically similar to the fission coupling, one thus expects that these theoretical estimates should be reliable. For pentacene, our calculations are in semi-quantitative agreement with more recent theoretical estimates of V.[65] Furthermore, in agreement with the experimental spectra, we find that superexchange only appreciably changes the coupling for materials (Pentacene, TIPS-P and DTP) where CT mixing is significant in the bright state (See Table 4.2).

4.3.3 Rate Model

To model the rate of fission, we borrow from the extensive literature on electron transfer rates as a function of electronic coupling.[357,358] For weak coupling, k_{fis} is expected to follow the celebrated Marcus non-adiabatic rate expression: $k_{na} = \frac{2\pi}{\hbar}\bar{V}^2(DWFC) \approx \frac{2\pi}{\hbar}\bar{V}^2\frac{1}{\sqrt{4\pi\lambda kT}}e^{-\frac{(\Delta G+\lambda)^2}{4\lambda kT}}$. $DWFC$ is the density weighted Franck-Condon factor, which can be approximated classically for low frequency modes.[206] k_{na} assumes activated motion in the bright diabatic state and sudden, rare transitions to the TT state, as illustrated in Figure 4-6a. For large coupling, this non-adiabatic picture ceases to be appropriate. Instead, the system follows the adiabatic state, which evolves continuously from S_1-like to TT-like as the reaction progresses (Figure 4-6b). In the adiabatic limit, the rate is governed by the speed of nuclear rearrangement (which may or may not be activated) and thus k_{fis} will become independent of $\bar{V}$

for large enough $\bar{V}$. These two limits can be unified into a single rate expression as shown by Bixon and Jortner (BJ):[357]

$$k_{fis} = \sum_n \frac{\bar{V}^2 k_n}{1+\tau_n^{ad}\bar{V}^2}$$
$$k_n \equiv \sqrt{\frac{\pi}{\hbar^2 \lambda kT}} |\langle 0|n\rangle|^2 e^{-\frac{(\Delta G + n\hbar\omega + \lambda)^2}{4\lambda kT}} \qquad \tau_n^{ad} \equiv \frac{4\pi}{\hbar\lambda}\tau_{ad}|\langle 0|n\rangle|^2 \tag{4.2}$$

The BJ formula predicts k_{fis} will follow the non-adiabatic rate (k_n) when $\bar{V}$ is small but be limited by the adiabatic timescale (τ_{ad}) for large $\bar{V}$. This rate expression depends on several parameters the reorganization energy (λ), the driving force (ΔG), the frequency and displacement of the primary accepting mode (ω,Δ) all of which can be estimated based on experimental spectra and simple monomer calculations.

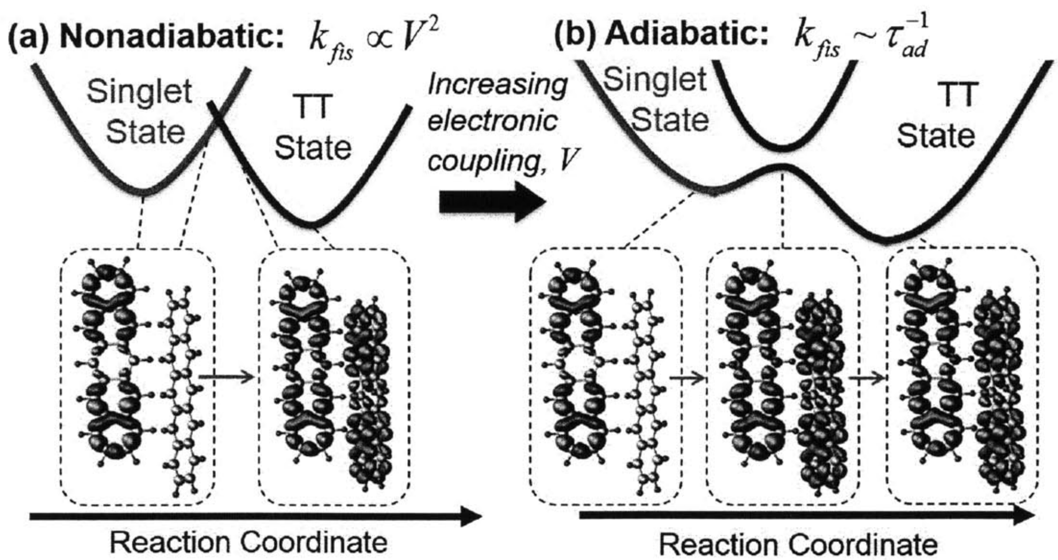

Figure 4-6: Kinetic model of singlet fission. As the coupling, V, between the S_1 and TT states increases the fission process transitions from non-adiabatic (a) to adiabatic (b) energy transfer. In the non-adiabatic regime the transition from one electronic state to the other is abrupt, and rate depends on the coupling squared. In the adiabatic case the electronic state changes continuously from S_1S_0 to TT, and the rate becomes independent of coupling.

In order to compute the BJ rate (Eq. 4.2), we first need to specify several pa-

	Pentacene	TIPS-P	DTP	DBTP	DBP	DPP
λ_{full} (meV)	138	103	141	140	137	133

Table 4.3: Reorganization Energies computed as outlined in the text. The energies here are for the full reorganization energy.

rameters. We fix ΔG based on the experimental estimates of the S_1-TT energy gap in pentacene: $\Delta G = -0.11\text{eV}$.[353,354] Meanwhile, we fix the frequency of the accepting mode based on the frequency of the vibrational progression in the S_1 absorption spectrum: $\omega = 1450$ cm^{-1}. Next, we estimate the displacement to be $\Delta \sim 0.3$, based on the vibrational progression in acene absorption and emission spectra.[359] Next, we compute the overall reorganization energy using PBE/6-31G* geometry optimizations of the S_0, S_1 and T states of each monomer in conjunction with the four point rule:[360]

$$\begin{aligned}\lambda_{full} &= \tfrac{1}{2}\left([S_1S_0|TT] + [TT|S_1S_0] - [S_1S_0|S_1S_0] - [TT|TT]\right) \\ \lambda_{full} &\cong \tfrac{1}{2}\left([S_1|T] + [S_0|T] + [T|S_1] + [T|S_0] - [S_1|S_1] - [S_0|S_0] - 2\,[T|T]\right)\end{aligned} \quad (4.3)$$

where $[A|B]$ means "the energy of state A at the relaxed geometry of state B". This results in the reorganization energies shown in Table 4.3. Since all the systems have similar reorganization energies, we use the same value of $\lambda_{full} = 0.13$ eV for all cases. The reorganization energy in the BJ formula is the total reorganization energy less the amount accounted for by the accepting mode: $\lambda = \lambda_{full} - h\omega\Delta$. Finally, we can estimate τ_{ad} (which is basically the attempt frequency) based on the C-C stretching frequency in acenes, so that $\tau_{ad} \sim 40$ fs.

We should note that while there are in principle five parameters here, in practice the five parameters only influence two physical features of the predicted rates. Changing ΔG, ω, λ, Δ and τ_{ad} can modify: 1) the DWFC factor that governs the rate at small coupling and 2) the plateau rate that determines the adiabatic rate of fission. All other features of the plot are insensitive to the choice of parameters. Thus, the parameter set outlined above is under-determined and the proposed parameters should only be considered estimates.

	V (meV)	k_{fis} (ps^{-1})	V (meV)	k_{fis} (ps^{-1})	k_{fis}^{exp} (ps^{-1})
Pentacene	18.9	10.1	84.9	17.3	12.5
TIPS-P	56.1	11.0	72.6	11.3	10.0
DTP	10.6	4.1	16.3	5.6	6.25
DBTP	5.6	1.5	5.4	1.5	1.11
DBP	2.4	0.34	2.0	0.24	0.263
DPP	1.4	0.13	0.82	0.041	0.085

Table 4.4: Fission Rates computed as outlined in the text. The final column shows the experimental rate for comparison.

Finally, in order to apply Eq. 4.2 to the materials here, we note that for a given singlet state, there will always be at least two equally likely final states after fission. If we expand our notation to include three monomers we see this clearly: $|S_0S_1S_0\rangle \rightarrow |S_0TT\rangle$ or $|TTS_0\rangle$. Since there are two equally likely final states, each generated with a rate according to Eq. 4.2, we assume the observed rate (which corresponds to the total rate of triplet generation) corresponds to the sum of the rates from the two initial bright states $k_{fis} = k_{BJ}\left(\bar{V}_1\right) + k_{BJ}\left(\bar{V}_2\right)$. In the case of pentacene, there are actually four possible final states (two each along the A and B directions) and so we assume $k_{fis} = k_{BJ}\left(\bar{V}_1^A\right) + k_{BJ}\left(\bar{V}_2^A\right) + k_{BJ}\left(\bar{V}_1^B\right) + k_{BJ}\left(\bar{V}_2^B\right)$. A more sophisticated treatment would involve proper treatment of the periodic boundary conditions and coupling of the manifold of delocalized excitonic states onto the manifold of final TT states, which is beyond the scope of the present work. The rates predicted by this model are shown in Table 4.4, using both V and $\bar{V}$.

We note several interesting features of the results.

- CT mixing has a minimal effect on the rates. The only couplings that change significantly due to CT mixing are pentacene (which speeds up, but is ultrafast in any case) and DPP (which slows down). Thus, superexchange does not appear to be the dominant mechanism promoting fission.

- The results obtained without CT mixing (first two columns) actually do a slightly better job of reproducing the experiment than the columns including CT mixing. This is likely due to a cancellation of errors, as in any case the agreement between theory and experiment is very good. On the whole, we expect the $\bar{V}$ couplings to contain more of the proper physics and so we use those in what follows.

- For pentacene, the presence of twice as many fission pathways means that fission is faster for pentacene than for TIPS-P, even though the individual monomers of TIPS-P are more strongly coupled.

- For DPP, it appears that our coupling is slightly underestimated. This may in part be due to the lack of diffuse functions in our basis set. A set of calculations in a larger basis might give slightly larger couplings for the well-separated systems like DPP without materially changing the coupling in a close packed system like pentacene. But as we have not previously benchmarked the basis set dependence of our scheme for computing the couplings we adhere to the established protocol, which uses a 6-31G* basis throughout.

4.4 Fission Mechanism

Now that we have the experimental and theoretical fission rates we can compare them to determine if the assumed Eq. 4.2 is an appropriate description for the singlet fission mechanism. The results are shown in Figure 4-7, which shows the comparison between the observed fission rates to the values of k_{fis} predicted by Eq. 4.2 for the compounds in Figure 4-2. The theoretical expression reproduces the experimental rates with impressive accuracy in all cases. For compounds with $\bar{V} < V_C \approx 20$ meV the rates increase as $\bar{V}^2$ while all materials with $\bar{V} > 20$ meV show essentially the same fission rate. Thus the experimental data are in quantitative agreement with the expected picture of a non-adiabatic-to-adiabatic transition in k_{fis}.

Our results are in qualitative agreement with recent theoretical predictions that superexchange can significantly increase the coupling[56–58] (i.e. $\bar{V}$ can be much larger than V). However, we do not find compelling evidence that superexchange is necessary for fast, efficient fission. Even neglecting the contributions of CT mixing, we find that direct coupling governed by V still results in fast fission rates in every material

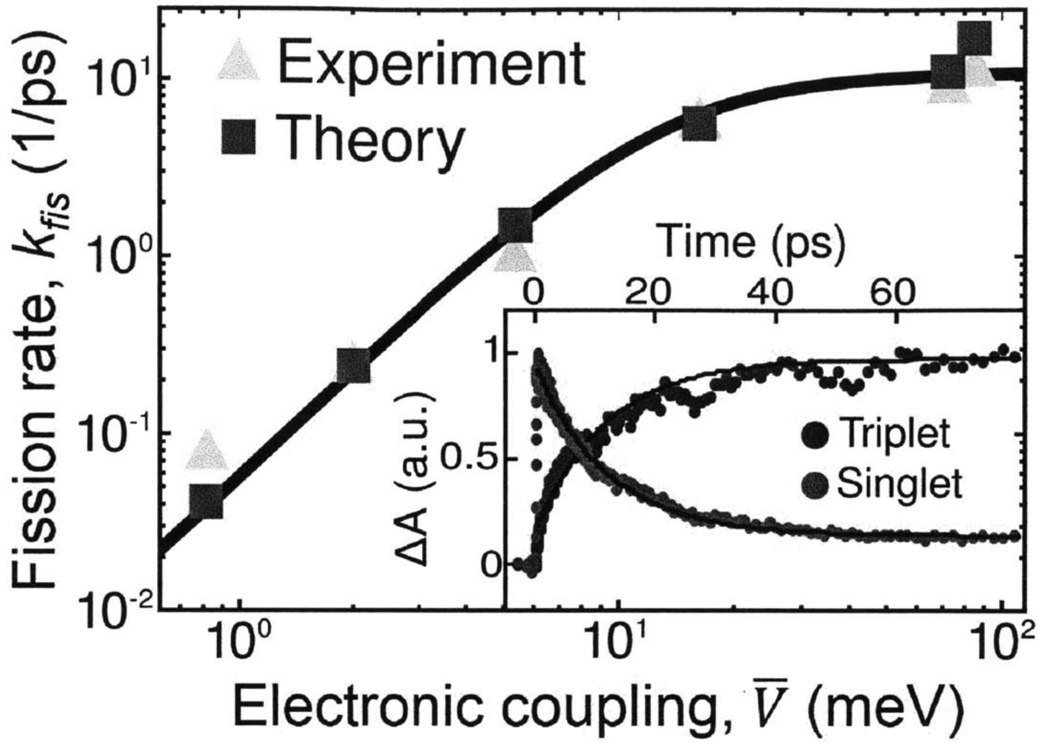

Figure 4-7: Prediction of fission rates for a variety of pentacene derivatives. Theoretical (red) and experimental (yellow) fission rates for the six materials in Figure 4-2. The theoretical fission rates (k_{fis}) are computed using the method outlined in the text (Eq. 4.2). The experimental fission rates are determined from ultrafast transient absorption (TA). The inset shows experimental TA data for DPP: fitting a single exponential (black) to the measured transient absorption of the triplet excited state (blue) gives the rate directly. The measured TA of the singlet excited state (green) decays with the same rate as the triplet excited state. Experimental data for other pentacene derivatives are given in Ref. 1.

studied (see Table 4.4). In particular, for cases where CT mixing increases the coupling (pentacene, TIPS-P, DTP) the reaction occurs adiabatically, so that changes in the coupling have a modest effect on the rate. This observation is significant for the purposes of rational design, as it implies that one need not control $\Delta E_{\rm CT}$ in order to ensure fast fission. A reasonably large V is sufficient.

While our predicted values of V are among the largest reported in the literature, they are typically an order of magnitude smaller than would be required to support coherent fission. We can estimate the TT character of the bright state by simply

	Pentacene	TIPS-P	DTP	DBTP	DBP	DPP
%TT	2.7%	1.6%	1.1%	0.1%	0.0%	0.0%

Table 4.5: TT character of bright states. For each material the largest TT character of either of the two bright states is given.

solving for the energy eigenstates in the basis spanned by all five CDFT states. The resulting percentage TT character for each material is shown in Table 4.5. For all the materials studied here, coherent coupling of the S_1S_0, CT and TT states at the ground state geometry results in less than 3% TT character in the bright state. This is at odds with the interpretation of time-resolved two-photon photoemission (TR-2PPE) spectra which show a high energy peak (associated with S_1 ionization) and a low energy peak (associated with T ionization) rising together within the time resolution of the measurement in both tetracene and pentacene[59].[60]

Clearly, all of the bright states have an extremely small contribution from TT, casting doubt on the validity of the coherent fission model. A few notes on these results:

- The TT character increases roughly as the dimer spacing gets smaller. In this respect, it mirrors both the increase of the coupling V and the %CT character of the materials.

- There is little chance of increasing the TT character by adjusting the energy of the TT state. The energies presented in Table 4.1 demonstrate that our computed TT energies are typically within ~0.1 eV of the S_1 energy, in agreement with experimental estimates.[361] Assuming a closer spacing of S_1 and TT would actually contradict experiment.

- There is some theoretical work suggesting that lowering the CT energies so that $\Delta E_{\text{CT}} \sim 0.1$ eV results in a resonance effect that allows the TT character to dramatically increase.[56–58] We will not use this kind of empirical adjustment here, but note that unusually small ΔE_{CT} values like this would only be plausible for the most closely packed dimers (e.g. pentacene, TIPS-P and perhaps DTP) as a small ΔE_{CT} implies a large electron-hole binding energy, which in turn requires a very small electron-hole separation, which can only happen for closely packed systems. So if the electroabsorption experiments[354] and our calculations of the CT energy are systematically too high, the only rates that could be affected are, again, the ones that are already exceptionally fast even neglecting any coherence effects.

Time resolved photoelectron spectra (TR-2PPE) of both tetracene and pentacene[59,60] show a high energy peak (associated with S_1 ionization) and a low energy peak (associated with T ionization) rising together with the time resolution of the experiment (~25 fs), which has been interpreted to mean that the initial excited state is some superposition of S_1S_0 and TT. Given the calculations here it seems likely that the prompt low energy signal arises from some other source. For example, ionization of the CT state, which is coherently mixed with S_1 in pentacene and tetracene,[355] could potentially lead to a prompt TR-2PPE signal at the same energy as TT ionization, as illustrated in Figure 4-8. If the bright state contains both S_1S_0 and M^+M^- character, there are clearly two different photoionization pathways: one that takes an electron out of a LUMO-like orbital and leaves behind a cation and a molecule in the ground state; and a second path that takes an electron out of a HOMO-like orbital and leaves behind a cation and a molecule in the triplet state. The latter photoelectron will have less kinetic energy and thus result in a lower energy peak in the photoelectron spectrum. Indeed, as long as $E_S \sim 2E_T$, the peak will come at $\Delta E = E_S - E_T - E_+ \approx E_T - E_+$. The latter energy is precisely the energy of triplet ionization and one would therefore expect this photoelectron peak to strongly overlap with the peak arising from true triplet ionization. Note that this interpretation is only one attempt at understanding the prompt TR-2PPE signal and there are other possible interpretations. In any case, coherence between S_1S_0 and TT is not required for efficient fission, as the maximum fission rate (k_{ad}) can be realized even when there is negligible coherence.

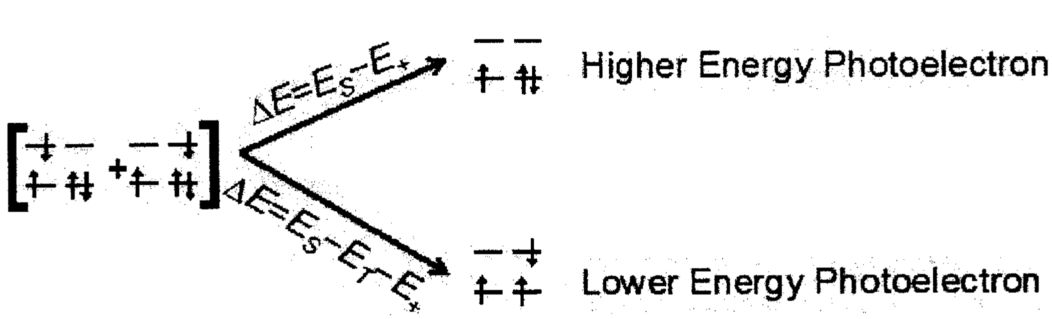

Figure 4-8: Interpretation of TR-2PPE prompt photoelectron peaks.

4.5 Conclusion

The most significant loss mechanism for singlet fission in pure materials is radiative decay from S_1, which typically occurs on the nanosecond timescale. Thus, every material in Figure 4-2 undergoes efficient fission, as confirmed by the low (<0.2%) photoluminescence quantum yield in every sample. Indeed, using Eq. 4.2 we can predict that $k_{fis} > 1$ ns^{-1} as long as $V \gtrsim 100$ μeV. This coupling is nearly an order of magnitude smaller than that for DPP, which itself has very poor wave function overlap due to the orthogonal alignment of the monomers. As a result, it seems clear that even materials with fairly poor monomer contact should be capable of efficient fission. This stands in contrast to the situation for multiple exciton generation (MEG), where exciton multiplication must out-compete thermal relaxation on a sub-picosecond timescale,[362] necessitating an ultrafast MEG mechanism analogous to coherent fission.[363] Thus, organic materials have a larger dynamic range and more freedom to accomplish carrier multiplication than their inorganic counterparts.

We have presented experimental confirmation of a fundamental model that correctly predicts the kinetics of singlet fission across a wide range of organic materials. Our results suggest that the rational design of novel fission materials should focus primarily on two features: 1) Making $E_{S_1} \gtrsim 2E_T$ and 2) Maintaining a reasonable coupling, $V \gtrsim 100$ μeV. For comparison, the best fission materials (like pentacene and TIPS-P) have couplings almost three orders of magnitude above this threshold. The broad applicability of this model opens up the possibility of creating photovoltaic devices in which fission is fast enough to out-compete potential loss mechanisms, such as direct charge separation, while retaining the ability to synthetically tune key material properties. With new derivatives, singlet exciton fission can now contribute to important technologies like solution-processed organic, and conventional inorganic solar cells.

4.6 Acknowledgment

The experimental work described in this chapter was lead by Jiye Lee from Marc Baldo's group in the electrical engineering department at MIT, who is a co-author of Ref. 1. The theoretical work described in this chapter was carried out with the help of David P. McMahon, who is an author in Ref. 1.

Chapter 5

Triplet Versus Singlet Energy Transfer in Organic Semiconductors: the Tortoise and the Hare

5.1 Introduction

Efficient energy transfer in condensed phases is an important phenomenon in both artificial and natural light harvesting systems. The photosynthetic process that sustains plants and bacteria requires an efficient transfer of energy from an absorption site to the chemical reaction center.[8] The natural light harvesting problem is solved by light harvesting architectures capable of reaching near 100% efficiency even under very low illumination conditions and in a disordered condensed phase environment.[9–11,364] In some cases, the high efficiency of some of these systems may be associated with coherent energy transfer.[81,82] Just as in photosynthetic systems, artificial photovoltaic devices rely on efficient conversion of harvested light energy to directly useful forms. In traditional organic photovoltaics (OPVs), light is absorbed in a thin film bilayer consisting of two organic semiconductors (OSCs). The exciton must then diffuse to the organic-organic interface in order to break up into charges.[27] In OPVs, coherent energy transfer has a less pronounced role because the thermal and static energy disorder localizes the exciton,[365] causing it to undergo incoherent energy transfer.[23,366] The efficiency of this excitation energy transfer process is what determines how thick an OPV can be, since any exciton created that does not diffuse to the interface is wasted. Thick OPVs are able to absorb more sunlight, but most OPVs rely on singlet excitons, which have diffusion lengths[31,66] (L_D) in the tens of nanometers, thus limiting the thickness of the devices[30] to $\approx$ 100 nm and making it impossible to absorb most of the incoming sunlight. There are potential ways of avoiding the exciton diffusion problem, most notably using bulk hetero-junction OPVs,[367] but these methods have other complications such as a significant morphology dependence[368] due to the difficulty of charge carrier extraction. The relatively consistent singlet diffusion length across a wide range of organic materials has led some to suspect a physical limit to L_D in these materials. On the other hand, triplet excitons have been shown to diffuse up to tens of micrometers[68,74,208] in single crystalline OSCs, orders of magnitude longer than singlet excitons. But will poor molecular packing and energetic disorder greatly reduce the diffusion length in thin film devices?

To address exciton diffusion one must understand the mechanisms of exciton migration in OSC materials. OPVs typically operate in the incoherent energy transfer regime. In this regime the singlet or triplet exciton is localized and hops from site to site. To lowest order in perturbation theory, using the Condon approximation to factorize the rate into an electronic and a vibrational part, the hopping rate is given by the familiar Fermi's Golden Rule:

$$k_{da} = \frac{2\pi}{\hbar} |V_{da}|^2 (\text{FCWD}) \tag{5.1}$$

The rate depends on the electronic coupling between the donor and acceptor states (V_{da}) and the Frank-Condon-weighted density of states (FCWD), which depends on the overlap of the density of states of the donor with that of the acceptor. The rate of exciton hopping is thus governed by an interplay between the energy landscape (via the FCWD) and the relative orientations of the monomers (via the coupling).

In this article, we explore the role of these molecular properties in singlet and triplet exciton diffusion to uncover possible future routes to more efficient OPVs. We first show that Eq. 5.1 implies a theoretical maximum for singlet diffusion in organic semiconductors due to a competition between the hopping rate and the radiative lifetime. There is no corresponding competition at work for triplets, suggesting that triplet diffusion lengths in OSCs are (in theory) unlimited. To test this hypothesis, we combine density functional theory (DFT) with kinetic Monte Carlo (KMC)[207] to model triplet diffusion in a purely *ab initio* manner. Triplet diffusion constants obtained through our procedure agree well with experimental data and also expose potential inaccuracies in some present experimental techniques. We further find that triplet diffusion constants in disordered thin films of tetracene are nearly isotropic and comparable in magnitude to the crystalline values. The formation of semi-crystalline domains plays a significant role in the continued efficiency of triplet diffusion in disordered systems. We conclude that the long triplet lifetime and apparent indifference to disorder make triplet excitons an ideal candidate for long range energy transfer.

5.2 Controlling Diffusion

Long diffusion lengths allow for thicker OSC layers that can absorb more sunlight, but what factors cause the differences in singlet versus triplet diffusion, and what are their potential maximum diffusion lengths? In order to arrive at theoretical maxima for the singlet and triplet diffusion lengths, we start by revisiting equation Eq. 5.1 and express the energy transfer rate in terms of physically relevant quantities. First, the FCWD factor can be defined in terms of the normalized overlap of the emission spectrum of the donor (I_D) and the absorption spectrum of the acceptor (ϵ_A).[369] If we assume the absorption and emission spectra are Gaussians of width $\sigma \approx 0.3$ eV and their centers are shifted by Δ_{da}, i.e. a Stokes shift, then the spectral overlap is given by[202]

$$(\text{FCWD}) = \int I_D \epsilon_A dv = \frac{\sqrt{\pi}}{2\sigma} \exp\left[-\frac{\Delta_{da}^2}{4\sigma^2}\right] \tag{5.2}$$

Within this approximation, then, the differences between singlet and triplet diffusion all arise from differences in the electronic coupling for the process. The electronic coupling V_{da} can be split into two parts, V_{Coulomb} and V_{Exchange}, where the Coulomb term is typically larger, especially at long range, and the exchange piece becomes relevant at separations less than 1 nm. The question is then which types of coupling are important for singlet and triplet excitons and how large are they?

5.2.1 Singlet Diffusion

The Coulomb operator can be expanded as a monopole series and approximated to lowest order with a dipole-dipole interaction. This approximation yields the familiar Förster coupling[200, 201] (in atomic units)

$$V_{\mathrm{da}} \approx V_{\mathrm{dip\,-\,dip}} = \frac{\kappa\mu^2}{n^2 R^3} \tag{5.3}$$

where we have assumed a homo-dimer situation (i.e. the donor and acceptor are chemically identical). In this expression, μ is the magnitude of the transition dipole moment, n is the refractive index of the material, and R is the magnitude of the center of mass separation between the donor and acceptor. Förster energy transfer is a radiationless energy transfer like that shown in Figure 5-1a, and the coupling's R^{-3} dependence makes it capable of transferring energy between molecules over fairly large distances. The orientational factor, κ, has a value between 0 and 2 and is determined by the relative orientation of the two transition dipoles and has the form

$$\kappa_{\mathrm{da}} = n_{\mathrm{d}} \cdot n_{\mathrm{a}} - 3\,(e \cdot n_{\mathrm{d}})\,(e \cdot n_{\mathrm{a}}) \tag{5.4}$$

Where n_{d}, n_{a}, and e are the normalized transition dipole of the donor, transition dipole of the acceptor, and displacement vector between the donor and acceptor, respectively.

The Förster coupling, Eq. 5.3, has been extensively studied[202, 369–371] for many molecules. A major problem with this approximation is that it overestimates the

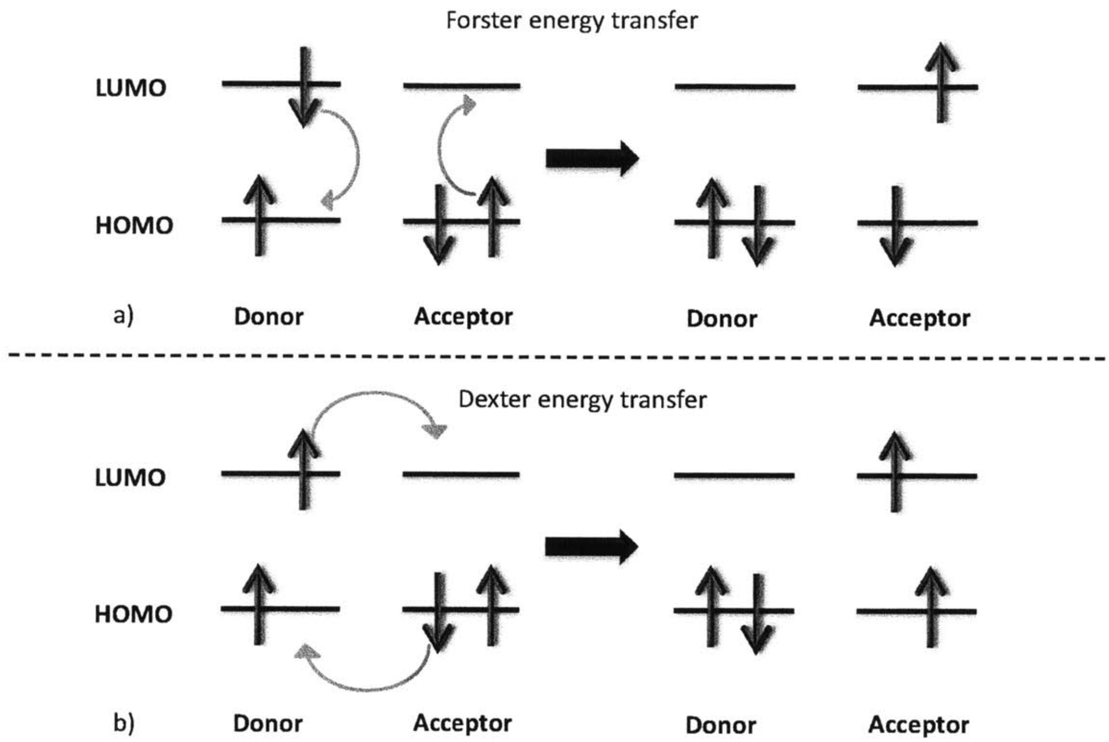

Figure 5-1: Radiationless Föster energy transfer (top) is the dominant mechanism for singlets, while the two electron Dexter energy transfer (bottom) is the dominant mechanism for triplets.

coupling at short distances,[202,203,372,373] where the separation distance is comparable to or smaller than the transition dipole. Given that the hopping rate is proportional to the coupling squared, we conclude that if we use Eq. 5.3 without correction, we will grossly overestimate the maximum singlet hopping rate. To get around this, we need a simple means of correcting the Förster result for the saturation of k_{da} at short range. Typical ways of refining this treatment are to include higher orders in the monopole expansion[369,374] or even the full Coulomb term calculated through DFT.[370,372] However, in reference 202 the authors pursue a simpler approach, showing that the full Coulomb coupling approaches a constant at small separations and suggest a modified functional form to fit to the full Coulomb coupling. Using this idea, we fit the following functional form to coupling curves computed with the fragment excitation difference (FED)[198] method on six different homo-dimers with large transition dipoles.

$$V_{\text{dip-dip}} \approx V_{\text{fit}}\left(R\right) = \frac{\kappa\mu^2}{n^2}\left(\frac{1}{\alpha\mu + R}\right)^3 \tag{5.5}$$

This functional form captures the asymptotic behavior of the Förster coupling as $R \to \infty$, while properly saturating to a constant as $R \to 0$. The geometries for the set of six homo-dimers used to obtain the α parameter can be found in Appendix C. Table 5.1 shows that α is fairly consistent over a range of molecules with different transition dipoles. We find that a value of $\alpha = 1.15$ reasonably reproduces the FED coupling values for the homo-dimers across a range of R values. We will thus take Eq. 5.5 as a rough approximation to the Coulomb coupling between donor and acceptor.

Molecule	μ	α	RMSD ($\times 10^{-7}$)
cyanine-3	5.3194	1.0335	2.2
cyanine-5	6.0474	1.1066	3.5
dcm	4.232	1.2181	0.39
thiophene	5.7966	1.1615	2.4
thiat	4.879	1.2385	0.66

Table 5.1: Calculated fitting parameter α for five different molecules along with their transition dipole (μ) and RMSD. All numbers are given in atomic units

Inserting equation Eq. 5.5 and Eq. 5.2 into equation Eq. 5.1 we arrive at a Förster-based expression for the rate

$$k_{\text{da}} \approx k_{\text{dip - dip}} = \frac{\kappa^2\pi^{\frac{3}{2}}\mu^4}{n^4(\alpha\mu + R)^6\sigma}\exp\left[-\frac{\Delta_{\text{da}}^2}{4\sigma^2}\right] \tag{5.6}$$

Thus, we have arrived at a rate dependent on the transition dipole, Stokes shift, and donor-acceptor separation. To gain estimates of the diffusion length, we need to be able to connect the site-to-site energy transfer rate to a diffusion constant. We do this by assuming a three dimensional diffusion with equal separation between molecules and equal hopping rates in every direction. We neglect non-nearest neighbor hopping, which is somewhat simplistic given the slow R^{-6} decay of the hopping rate. We will thus slightly underestimate the diffusion for larger transition dipoles. Under these conditions, the diffusion constant has the form,[78] $D = \frac{kR^2}{z}$, where z is equal to 2, 4, or 6 for one, two, or three dimensional diffusion, respectively.

Finally, to obtain the diffusion length, we need the lifetime of the excited state. The lifetime is determined by the nonradiative and radiative transition rates of the excited state by $\tau = 1/(k_{\text{rad}} + k_{\text{nonrad}})$. To capture the ideal theoretical limit on the diffusion length we assume only radiative losses. Singlet excitons then have the following lifetime:

$$\tau = \frac{1}{k_{\text{rad}}} = \frac{3c^3}{4E_{\text{S}}^3\mu^2} \tag{5.7}$$

Where E_{S} is the singlet excitation energy. It is important to point out that the lifetime also depends on the transition dipole, but inversely, so as μ increases the lifetime decreases. Combining all terms gives an approximate diffusion length, L_{D}, of:

$$L_{\text{D}} = \sqrt{D\tau} = \sqrt{\frac{3c^3\kappa^2\pi^{\frac{3}{2}}\mu^2R^2}{4zn^4E_{\text{S}}^3\left(\alpha\mu + R\right)^6\sigma}\exp\left[-\frac{\Delta_{\text{da}}^2}{4\sigma^2}\right]} \tag{5.8}$$

Thus we arrive at a final expression for L_{D} in terms of molecular and crystal properties.

There are quite a few different parameters in Eq. 5.8. This is misleading though; most of the parameters are essentially constant or have little effect on the diffusion length. Material parameters such as n, κ, and R do not change significantly between different OSCs. The molecular parameter E_{S} is fixed by the desire to have the singlet energy be in the visible range for optimal solar energy absorption, and Δ_{da} is already very small and will at most make the exponential term unity when optimized. That just leaves the transition dipole as the only significant way to alter the singlet diffusion length.

Considering then L_{D} only as a function of the transition dipole yields a maximum diffusion length. For small μ the diffusion length increases linearly with the transition dipole due to the coupled relationship of the lifetime and hoping rate on the transition dipole. At large μ though, the diffusion constant decays as μ^{-2}, and so at some value of μ the diffusion length must reach a maximum. A diagram of this effect is shown in Figure 5-2. As noted above, at large μ we somewhat underestimate the hopping rate, meaning that we somewhat underestimate the diffusion constant at large μ. However for qualitative purposes, this will not change the picture: it will merely shift the

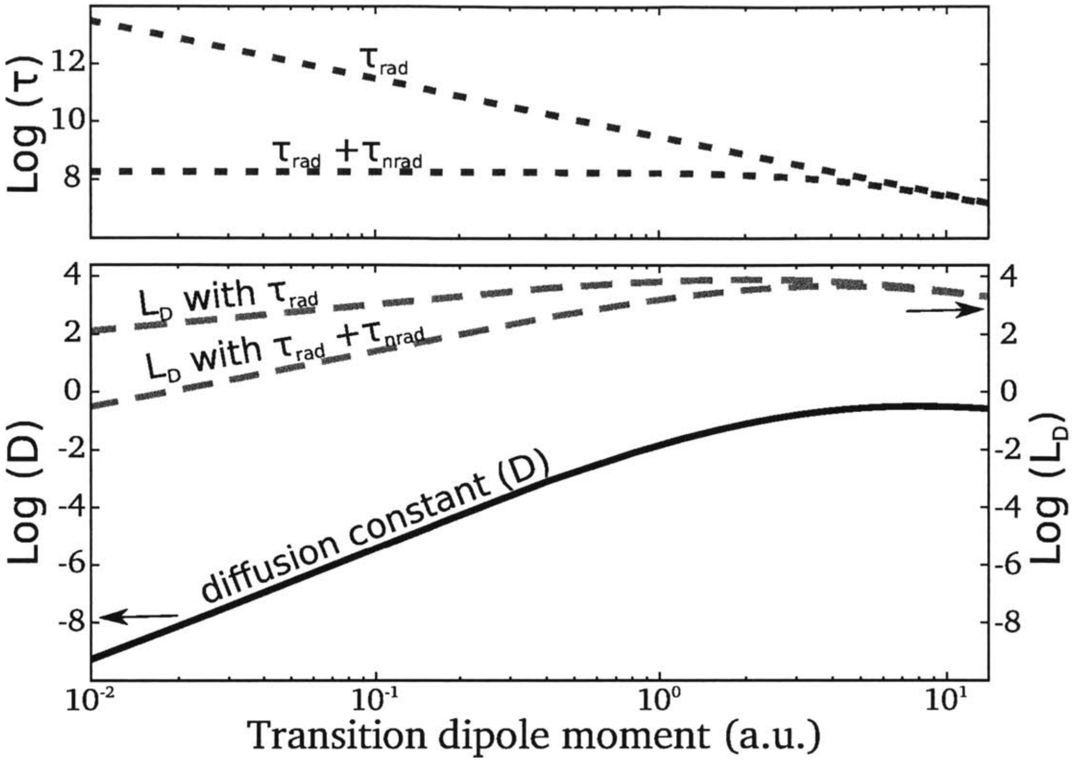

Figure 5-2: A rough depiction on a log-log scale of the dependence of the singlet diffusion length (green) on the transition dipole. Values were calculated using tetracene parameters from Table 5.2 and a nonradiative decay of 5 ns. Both cases of with and without nonradiative decay are included in the diffusion length. The lifetime (red) continually decreases with a slope of -2. At low transition dipoles the diffusion constant (black) has a slope of 4, but the slope decreases as the transition dipole grows, yielding a maximum diffusion length at some value of μ.

maximum to L_D to a slightly larger value. We should emphasize that our prediction of a theoretical maximum of L_D for singlets is predicated on the hopping model of energy transfer. For highly ordered systems (such as J-aggregates) where coherence effects are important, different behavior could be observed.

Using our ideal model for singlet hopping, Eq. 5.8, we can also calculate a rough maximum for the singlet diffusion length. Assuming no Stokes shift ($\Delta_{da} = 0$), a hopping distance, (R), of 0.45 nm and the optimal transition dipole of $\mu = 6$ along with other parameters shown in Table 5.2, we get a ideal diffusion length of 230 nm. In practice, the diffusion length of OSCs are a fraction of this due to non-ideal

Table 5.2: Theoretical singlet diffusion lengths (nm), L_D, for the fitted Coulomb coupling using Eq. 5.8 and values given in the text. Two examples are given, one with an optimal set of physical values and the other with values found for tetracene. The singlet energy (E_S) is in eV, and the transition dipole (μ) is in atomic units.

	κ	n	E_S	μ	L_D
optimal	2	2	2.0	6	230
tetracene	2	2	2.5	1	115

behavior in the orientation factors (κ), there will be a Stokes shifts, and there is nonradiative decay. Also shown in Table 5.2 is a maximum diffusion length for a more typical OSC material, tetracene, of 115 nm, significantly larger than what is observed in experiments, 12 nm.[375] As mentioned, we only included radiative decay and the radiative lifetime using Eq. 5.7 for tetracene is 60 nanoseconds, while the measured lifetime is closer to 0.15 nanoseconds,[73] a factor of four hundred times shorter. Using the experimental lifetime gives a diffusion length of 6 nm (instead of 115 nm), much closer to the measured singlet diffusion length,[66] indicating the significance of nonradiative decay. The effect of nonradiative decay is also shown in Figure 5-2. Nonradiative decay does not change the qualitative behavior of L_D but does make the maximal μ larger and the maximal L_D smaller. In the end, we find the diffusion length for singlet excitons is roughly limited to 100-200 nm.

The above results suggest the following ways to maximize the singlet diffusion length: large solution emission quantum yield, small Stokes shift, and reduced disorder to minimize the number of trap states and nonradiative decay channels; which all of these boil down to increasing the singlet lifetime to get longer diffusion lengths. Unfortunately, most of these properties are already optimized or are too costly to optimize for a typical OPV device.[6,376] The transition dipole can be optimized to increase the diffusion constant, but as shown above, there is a limit where it then starts to hurt the diffusion length. Therefore, existing devices are already close to the singlet diffusion limit, and even if they could be optimized more, we can not hope to achieve singlet diffusion lengths long enough to ensure full absorption of the solar spectrum.

5.2.2 Triplet Diffusion

Triplet excitons are not able to transfer energy via Coulomb coupling, because the triplet excited state to singlet ground state transition is a spin-forbidden process. Therefore, triplets can only transfer their energy through exchange coupling. Energy transfer through exchange coupling, also known as Dexter energy transfer,[204,205] occurs through the exchange of two electrons between the donor and acceptor, as shown in Figure 5-1b. Conveniently, this form of energy transfer implies that a material with good hole and electron conductance should also have a larger Dexter coupling,[377,378] which is already something that is beneficial for a OPV material. Dexter coupling relies on the overlap of the wavefunction of the donor with that of the acceptor and has the form

$$V_{\mathrm{da}} \approx V_{\mathrm{Dexter}} \approx A \exp\left[-\zeta R\right] \tag{5.9}$$

where $\zeta \approx 0.285\ \mathrm{nm}^{-1}$ describes the spatial extent of this overlap,[379] and A is an exponential prefactor whose value can be calculated using data from reference 379. Meanwhile, the radiative lifetime of the triplet exciton depends on the spin-orbit coupling,[380] which is very small unless the molecule contains a heavy atom. Thus we immediately see a difference between singlet and triplet energy transfer: whereas for singlets there was competition due to the fact that increasing μ affected both the lifetime and the energy transfer rate, for triplets there is no similar competition. The Dexter transfer depends on one set of parameters (Stokes shift, electron conductance, hole conductance, and wavefunction overlap) while the radiative lifetime depends on a disjoint set of parameters (spin-orbit coupling).[380] Thus we see immediately that there is *no theoretical maximum for triplet diffusion lengths in OSCs*

Using Eq. 5.9 with a R of 0.45 nm and the same parameters as in Table 5.2, the triplet diffusion constant is $3.2\times10^{-4}\ \mathrm{cm}^2/\mathrm{s}$. Not surprisingly it is much smaller than that for singlets at the same R, $0.17\ \mathrm{cm}^2/\mathrm{s}$. Dexter energy transfer decays exponentially with distance while Förster energy transfer decays as R^{-6}. On the other hand, the lifetimes for triplet excitons are of the order of a millisecond, while as described above for singlets, the lifetime is closer to a nanosecond. The drastic difference is due to the spin-forbidden phosphorescence decay of the triplet state to the singlet ground state. Using the above values, the triplet diffusion length is 6 μm while that of the singlet is 0.13 μm. The singlet exciton moves faster but also decays quickly, while the slower moving triplet exciton keeps its steady pace for a long time, in the end yielding a much longer diffusion length for the triplet exciton.

Even though triplets have an intermolecular coupling several hundred times smaller than singlets, they still diffuse greater distances thanks to lifetimes up to a million times larger. Analogously to singlets, properties like the non-radiative decay rate, and the energy disorder can be used to optimize the diffusion length. Unlike the case of singlets, where there is a theoretical maximum limit of a few hundred nanometers, there is no limit to the triplet diffusion length, because the coupling and lifetime of triplets are independent of each other. For example, the coupling can be increased (while not effecting the lifetime) by increasing the size of the molecule to increase the area for wavefunction overlap. Thus, triplet excitons offer two variables (overlap and spin-orbit coupling) that can be varied independently to optimize diffusion lengths.

5.3 Organic Crystals

Now, just because triplets *can* have long diffusion lengths, does not mean they will in practice. To analyze the feasibility of engineering long triplet diffusion in organic PVs, we begin by studying triplet diffusion in a few experimentally well-characterized cases. This will also allow us to investigate what molecular properties govern observed experimental trends and also provide a control experiment when we asses the impact of disorder on triplet diffusion. We choose to simulate diffusion lengths for crystalline anthracene,[69,208,381,382] tetracene,[74] stilbene,[68] naphthalene,[68] 1,4-dibromo-naphthalene,[68] and rubrene[71,383] for which the triplet diffusion length is experimentally known.

A rough schematic of how we obtain the diffusion constant for a crystal is shown in Figure 5-3. First, we start by creating a crystal large enough so there are no boundary effects and compute all unique intermolecular couplings between dimers that are separated by less than 1.5 nm. Then we use a KMC code developed in Ref. 207 to propagate a single triplet exciton for 0.5 ns at 300 K; we repeat this 25,000 times to calculate an average diffusion length. The geometries of the molecules studied can be found in Appendix C.

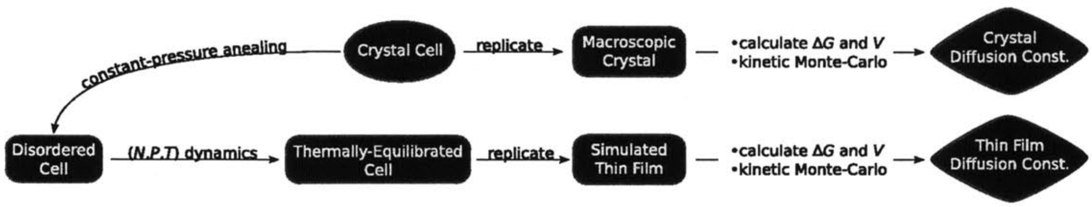

Figure 5-3: The computational procedure used to compute the triplet diffusion constant for molecular systems. The top describes our procedure for crystalline cells and the bottom describes our procedure for disordered cells.

To calculate the hopping rates for triplet energy transfer we need to express Eq. 5.1 in terms of parameters that can be readily obtained through DFT calculations. At high temperatures the FCWD term can be approximated by the classical Marcus[206] rate expression:

$$k_{\mathrm{da}} = \frac{2\pi}{\hbar} \left|V_{\mathrm{da}}\right|^2 \sqrt{\frac{1}{4\pi k_{\mathrm{B}} T \lambda}} \exp\left[-\frac{(\Delta G^{\circ} + \lambda)^2}{4\lambda k_{\mathrm{B}} T}\right] \tag{5.10}$$

Where the dependence on the temperature (T), change in free energy (ΔG°), and reorganization energy (λ) are explicitly seen in the rate equation. These parameters are obtained from DFT calculations using the 6-31G* basis and PBE or B3LYP functionals. ΔG° in equation Eq. 5.10 is zero, since all the molecules in a crystal are energetically equivalent. The reorganization energy can be split into two components: the relaxation of the molecules involved in the energy transfer -inner sphere (λ_i) - and the relaxation of the environment - outer sphere (λ_o). The triplet excitons for the molecules we study are localized states[384] with no charge or large dipole, and so λ is reasonably approximated by λ_i. We calculated the reorganization energy with the 6-31G* basis with the PBE functional using the four-point method.[356] The reorganization energies obtained for our test set range from 0.3 to 0.7 eV, shown in Table 5.3. Such large reorganization energies are due to the very localized nature of the triplet state.[384] Both constrained density functional theory (CDFT)[154,385] and FED methods are used to calculate V_{da}, and both give good agreement with experiments for triplet energy transfer rates.[130,379]

Our results for the six different crystals are displayed in Table 5.3 and show good agreement with experimental trends. The reported diffusion lengths are obtained using the experimentally measured crystal lifetimes and our computed diffusion constants, and we obtain nearly quantitative agreement with experiments using FED/PBE. The differences in diffusion lengths calculated with various functionals and coupling methods result from changes in wavefunction delocalization and thus overlap. PBE consistently gives the largest couplings, since as the amount of exact exchange is decreased, the electron self-interaction error increases, causing the wavefunction to become more delocalized than it should.[128] FED gives larger couplings than CDFT, since with currently used functionals, FED contains some fractional spin/charge error that increases the coupling.[130] Though not represented in Table 5.3, but shown in reference 379, if the basis set is increased, the wavefunction overlap, and thus the coupling, will increase. One should expect that with a larger basis set that functionals with less self-interaction error and methods like CDFT should yield more quantitative results.

Naphthalene, anthracene, and tetracene all have a herringbone crystal structure like that shown in Figure 5-4a, while rubrene and 1,4 dibromo-naphthalene form a different herringbone type structure, shown in Figure 5-4b. These packing motifs explain why diffusion in the C-axis is at least an order of magnitude smaller than in the A- or B-axis; diffusion in the C-axis occurs between a head to tail pair, which have very little wavefunction overlap. In fact, packing is a major determinant in the direction and efficiency of triplet diffusion. As an additional note, when the number of benzene rings increase across the acene series from naphthalene to tetracene, the amount of area for wavefunction overlap increases causing the square of the coupling to increase from 1.76×10^{-5} to 1.94×10^{-3} eV^2, respectively. The reorganization energy decreases from 0.65 to 0.33 eV from naphthalene to tetracene, which results in a further two orders of magnitude increase in k_{da}, both effects resulting in an increased

Table 5.3: Computed triplet diffusion lengths in μm show good agreement with experimental values, given in parentheses. The experimental lifetimes (τ) are in s and computed reorganization energies (λ) are in eV.

naphthalene , $\tau = 2 \times 10^{-1}$ Ref. 68, $\lambda = 0.64$

	CDFT		FED		
Axis	PBE	B3LYP	PBE	B3LYP	
A	1.10	0.38	5.04	5.78	(25.69)
B	1.32	0.49	10.41	10.53	(23.24)
C	0.27	0.07	4.46	4.88	
Total	1.74	0.63	12.40	12.97	(34.64)

anthracene , $\tau = 2.3 \times 10^{-2}$ Ref.381, $\lambda = 0.44$

	CDFT		FED		
Axis	PBE	B3LYP	PBE	B3LYP	
A	6.78	3.20	20.24	6.33	(18.57)
B	8.28	3.85	21.39	12.91	(20.35)
C	0.57	0.16	1.25	3.11	(5.25)
Total	10.72	5.01	29.48	14.71	(27.96)

tetracene , $\tau = 8 \times 10^{-4}$ Ref. 386, $\lambda = 0.33$

	CDFT		FED		
Axis	PBE	B3LYP	PBE	B3LYP	
A	6.28	3.37	19.78	6.07	
B	8.01	4.32	25.37	7.68	(17.89)
C	0.05	0.04	0.09	0.44	
Total	10.17	5.48	32.17	9.80	

1,4-dibromo-naphthalene , $\tau = 3 \times 10^{-3}$ Ref. 68, $\lambda = 0.60$

	CDFT		FED		
Axis	PBE	B3LYP	PBE	B3LYP	
A	2.82	1.58	5.61	2.94	(10.25)
B	0.08	0.02	0.67	0.83	
C	0.07	0.01	0.56	0.69	
Total	2.83	1.58	5.69	3.14	

stilbene , $\tau = 8 \times 10^{-3}$ Ref. 68, $\lambda = 0.70$

	CDFT		FED		
Axis	PBE	B3LYP	PBE	B3LYP	
A	1.22	0.41	2.83	2.01	(8.49)
B	0.57	0.19	1.46	0.91	(7.48)
C	0.25	0.04	0.78	1.33	
Total	1.37	0.20	3.27	2.57	(11.31)

rubrene , $\tau = 1 \times 10^{-6}$ Ref. 71, $\lambda = 0.32$

	CDFT		FED		
Axis	PBE	B3LYP	PBE	B3LYP	
A	0.02	0.004	0.03	0.02	
B	0.54	0.27	0.86	0.50	
C	$<$ 0.001	$<$0.001	$<$ 0.001	$<$ 0.001	(5.00)
Total	0.55	0.27	0.86	0.50	

diffusion constant and diffusion length in tetracene.

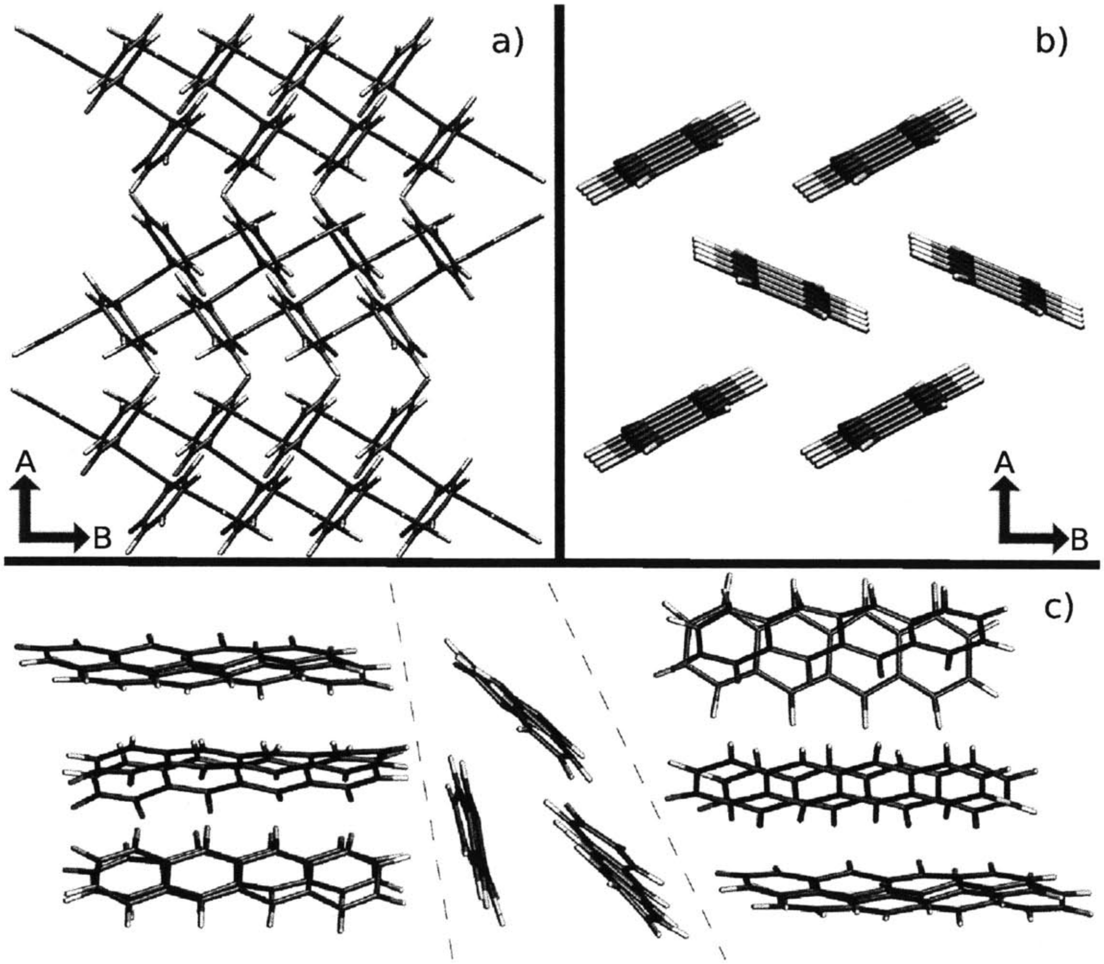

Figure 5-4: a) Rubrene crystal looking down the C axis. b) Tetracene crystal looking down the C axis, anthracene has identical crystal orientations. c) Disordered tetracene cell depicting three different semi-crystalline domains.

One noticeable disagreement is in the diffusion constant of rubrene. Our simulations predict a diffusion length of roughly 1 μm along the B-axis; in agreement with the diffusion length of 4 μm in the same direction from Ref. 383. On the other hand, in ref 71 the reported value is 5 μm along the C-axis. Due to the crystal packing there is almost no overlap between the donor and acceptor wavefunctions in the C-axis, and as such almost no diffusion in that direction. The diffusion length of singlet and triplet excitons are mainly measured using photoluminescence[66–69] or photocurrent[70–72] methods, but as in the case of rubrene discussed above, different experiments on the same molecule can often report diffusion lengths that vary by orders of magnitudes for both triplet[72–74] and singlet[75–77] excitons. One complication common among these methods is the emission of a photon that is then waveguided in the crystal and reabsorbed by another molecule, which can increase the measured diffusion length by a considerable amount.[78] This effect is likely the source of the large error in the experimental prediction of the C-axis diffusion length in rubrene crystals. In particular, this example shows how our simulations can help resolve discrepancies in experimental measurements of L_{D}.

Evidence of independence of triplet diffusion constants and lifetimes, as discussed earlier, is contained within Table 5.3. Rubrene's diffusion constant is only two times smaller than tetracene's, but its diffusion length is over an order of magnitude smaller due to its drastically shorter lifetime. Rubrene's shorter lifetime is most likely due to an increase in nonradiative decay resulting from its more complex structure. As the conjugation size increases from naphthalene to tetracene, the diffusion constant increases due to a decrease in the reorganization energy and an increase in the wavefunction overlap. The lifetime however decreases mainly due to the unique effect in the acenes of triplet-triplet fusion, which is more energetically favorable in tetracene. The diffusion constant in 1,4-dibromo-naphthalene is an order of magnitude larger than that of naphthalene, but the presence of bromine increases spin-orbit coupling, which decreases the triplet lifetime, so naphthalene still has a longer diffusion length. The above results highlight the independence of triplet diffusion constants and lifetimes and demonstrate the ability of our method to predict nonradiative triplet diffusion.

5.4 Amorphous Systems

The ability to cheaply process organic solar cells is what gives them a fighting chance against their highly ordered, expensively processed, but highly efficient inorganic solar cell competitors. Cheap processing, however, inherently leads to disorder within the cell, and disorder is typically considered to be an enemy of diffusion. Average intermolecular distances can increase, stacking arrangements can become less than optimal for good wavefunction overlap, and trap states can be formed if the energy disorder becomes comparable to the reorganization energy. However, the following results show how surprisingly robust triplet diffusion can be to disorder.

One thing to note immediately is that the difficulties inherent to measuring triplet diffusion in a crystal are compounded when dealing with a thin film. Thus, our computational procedure provides a relatively simple and reliable way to probe the effect of disorder. For this part of our study, we choose to model diffusion in amorphous tetracene, because its lack of side groups results in a smoother transition across the spectrum of disorder, from crystalline to amorphous. The parameters for the tetracene force-field were created using a procedure outlined in Ref. 189 and are given in Appendix B. Our procedure, illustrated in Figure 5-3, is as follows. We first obtain a disordered cell through a two-step procedure: using molecular mechanics, a crystal cell made up of 96 tetracene molecules is annealed from 150 to 730 K and back down on a 1.2 ns interval under constant pressure of 15 bar, after which it is equilibrated at constant temperature of 300 K and pressure of 1 bar. The crystal cell size was chosen to be 96 tetracene molecules because it gives 4560 unique dimer pairs and this number grows very quickly with increasing crystal size. Next, we calculate the couplings between all molecular pairs using PBE/FED. In a disordered system, ΔG° is no longer zero, so we use the difference in triplet exciton energy between the donor and acceptor, each computed individually. Using the same λ as in the crystal, we have all of the parameters needed to obtain hopping rates in the disordered system and to run a KMC simulation, using the same parameters as the crystal KMC simulations, to obtain the diffusion constant. We repeat this entire processes with over twenty tetracene cells of varying disorder, each obtained by applying additional constant pressure annealing.

To quantify the disorder of each of the twenty cells, we define an order parameter based on the intermolecular interaction energy. The interaction energy is the sum of the Van der Waals interactions and electrostatic interactions and is also known as the cohesive energy (E_{coh}). Our order parameter ΔE_{coh} is defined by

$$\Delta E_{\text{coh}} = \frac{E_{\text{coh}}^{\text{crystal}} - E_{\text{coh}}^{\text{cell}}}{N} \tag{5.11}$$

where N is the number of molecules in the cell. This gives the loss in cohesive energy per molecule in going from the crystal to a disordered system and directly corresponds to how well the cell is packed.

In what follows, we present our results here in terms of the diffusion constant, rather than the diffusion length, because the diffusion length depends on both the diffusion constant and the lifetime, and there is no reason to suspect that the lifetime will be the same in an amorphous system as in the crystal.[387] Figure 5-5 displays the effect of disorder on the total triplet diffusion constant in tetracene. As disorder is introduced, the diffusion constant decreases by only an order of magnitude, which corresponds to a three-fold decrease in the diffusion length. After this relatively small drop, the diffusion constant remains relatively unchanged as disorder increases. The average over all the total diffusion constants in the disordered cells agrees to within a factor of 10 with experimental measurements.[388] The range of disorder covered by our cells is much greater than kT (0.6 kcal/mol), and any typical device should easily be within the range of disorder covered here. These results show the triplet diffusion constant of tetracene to be robust to disorder.

We find that cells in our simulation contain semi-crystalline domains, which are sometimes rotated with respect to one another (see Figure 5-4c), sometimes with a few molecules inserted in the domain boundaries, like a wedge in a crack. The cells with larger ΔE_{coh} tend to have more of these domains, which have a smaller degree of crystallinity. Inspection of the nearest-neighbor couplings reveals that the molecules with the lowest couplings are not the ones wedged between the semi-crystalline domains. Rather, small couplings are common among molecules that are slipped along the long molecular axis out of their crystalline position thus decreasing their wavefunction overlap. Interestingly, the presence of these semi-crystalline domains and their rotation with respect to one another results in significantly more isotropic diffusion, as

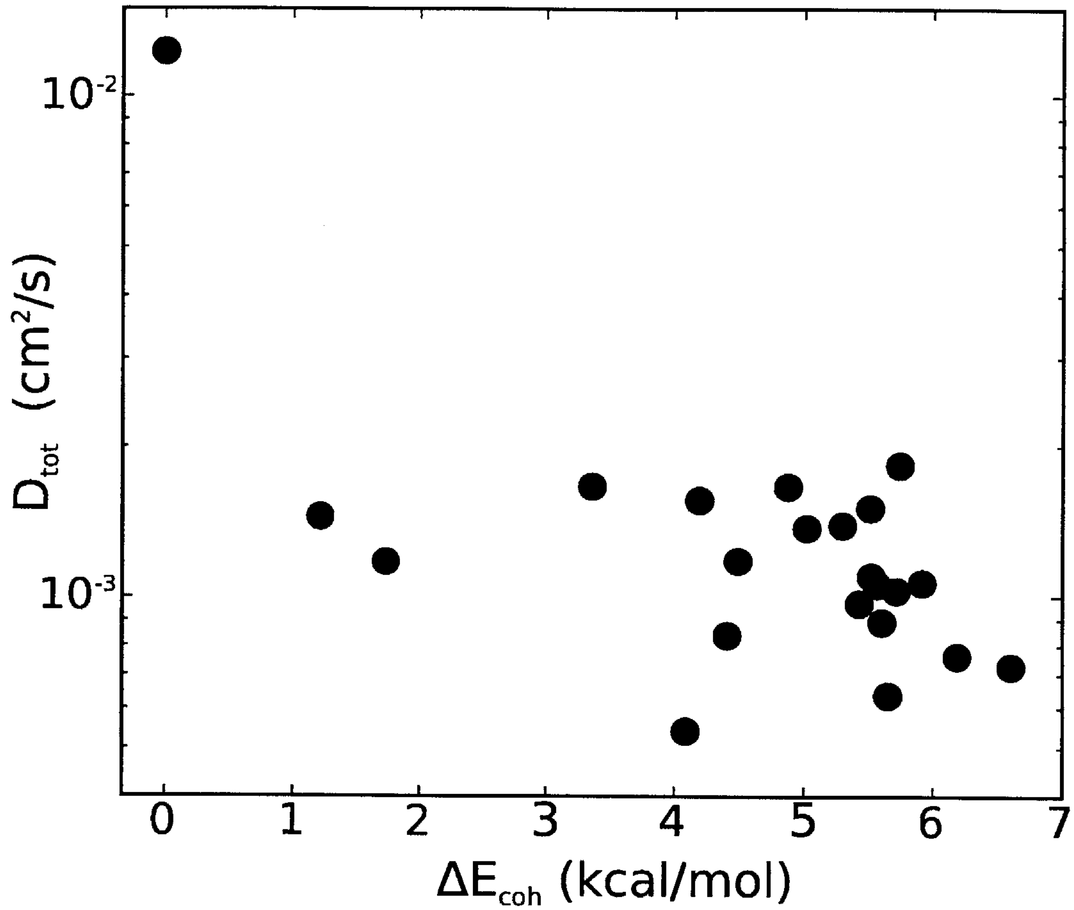

Figure 5-5: The total diffusion constant (D_{tot}) has no correlation to an increase in intermolecular disorder.

shown in Figure 5-6. As a measure of isotropy, we use the ratio between the diffusion constant in the direction with the greatest overall diffusion D_{large} to the diffusion constant in the direction with the smallest overall diffusion D_{small}, minus one. As shown, the characteristic two-dimensional diffusion of crystalline tetracene switches to an isotropic, three-dimensional diffusion as the cells become more disordered, in agreement with experiment.[387] This switch to isotropic diffusion is easily explained. Cells with greater disorder tend to have more randomly-oriented semi-crystalline domains, each containing two-dimensional diffusion, and diffusion over these randomly-oriented domains averages into an overall isotropic diffusion. Additionally, as stated above, hopping between crystalline domains is not a major bottleneck for the triplet exciton as it diffuses through the cell.

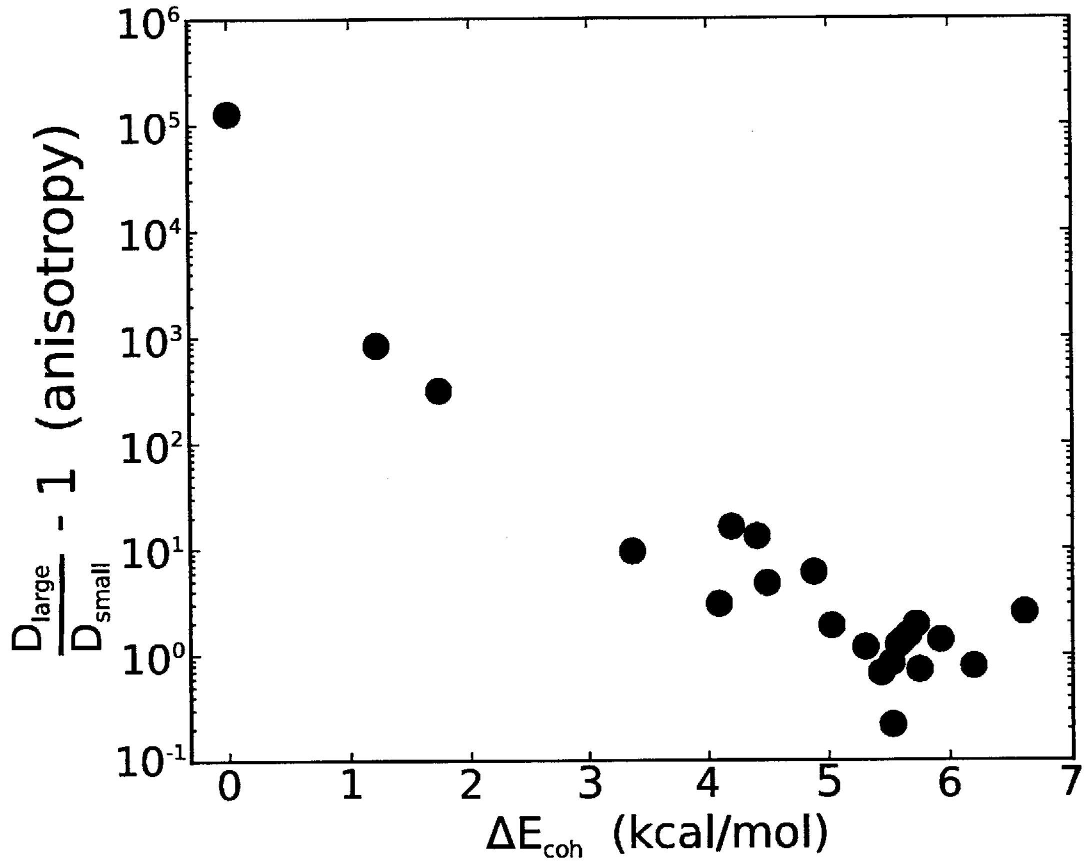

Figure 5-6: Triplet diffusion in tetracene goes from an anisotropic two-dimensional diffusion to an isotropic three-dimensional diffusion as crystal disorder is increased.

In addition to the effect of couplings, it is important for us to also address the possibility of site energies significantly decreasing the intermolecular hoping rates. Being a localized electronic state, triplet excitons are influenced little by their environment. This indifference to environment is why we find fluctuations in site energies staying below 80 meV across the wide range of disorder. Tetracene has a reorganization energy of 330 meV, an order of magnitude larger than the these energy fluctuations, so we are easily outside of the static trapping regime. Based on the reorganization energies shown in Table 5.3, with tetracene being the smallest, we expect that this result will hold for most organic semiconductors. In conclusion, we find the localized nature of the triplet exciton and the semi-crystalline structure of a thin film result in diffusion constants comparable to that found for the crystal.

5.5 Conclusions

In this article we have outlined the mechanisms for singlet and triplet exciton transport in OSCs and their potential limitations and advantages. For singlet excitons, the inability to increase the diffusion constant without decreasing the lifetime creates a fundamental upper bound on the diffusion length. For triplet excitons, the diffusion length and lifetime can be varied independently, and there is no theoretical maximum for diffusion. To demonstrate that these simple predictions are borne out in reality, we modeled triplet diffusion in crystalline environments, with good agreement to experiments. The triplet diffusion length is also robust to disorder; the total diffusion constant is only decreased by an order of magnitude when disorder is introduced and shows no trend with increasing disorder. Site energy fluctuations are an order of magnitude smaller than the reorganization energy, so the diffusion is not hindered by static traps. Additionally, the increase in disorder corresponds to an increase in the number of semi-crystalline domains, which are randomly oriented and result in more isotropic diffusion. Furthermore, while the hopping rate at the boundaries of these domains might be decreased by weaker couplings, it is not a major bottleneck for triplet exciton diffusion. Our simulations show that the Dexter coupling (which correlates to electron/hole conductance), while much smaller than Förster, is still large enough to allow triplets to traverse large distances during their long lifetimes. The results indicate that the measured triplet diffusion lengths of 2-10 μm should be possible for most OSC materials.

To utilize the long diffusion lengths of triplet excitons and make thicker OPV devices, different ways of creating triplet excitons in OPV devices should be explored. One possible route is to introduce guest molecules that have high intersystem crossing from the singlet excited state to the triplet excited state and that can also then energy transfer the triplet to the host material.[389] Using singlet fission with molecules like tetracene and pentacene offers both the ability of using triplet excitons and potentially getting two electrons from every photon.[49,54,390] One of the main potential pitfalls of using triplets is the difficulty of controlling non-radiative relaxation mechanisms.[23] The triplet diffusion length is only long if the triplets maintain lifetimes on the order of hundreds of microseconds, and so even very slow nonradiative quenching can be a significant hindrance. In particular, it is not clear if triplet-triplet annihilation places a fundamental limit on the triplet lifetime (and hence the triplet diffusion length) in thin film devices, and this is a question that deserves further study. In conclusion, our results show the long diffusion length of triplets offers a promising route to optically thick, efficient OPV devices.

5.6 Acknowledgment

The work described in this chapter was carried out with help from Eric Hontz and Sina Yeganeh, who are authors of Ref. 356.

Chapter 6

Study of the Electronic States and Electrostatic Effects at Organic/Organic Interfaces: A Mechanism for "Cold" Exciton Breakup

6.1 Introduction

The field of photovoltaics (PVs) continues to progress towards creating a device that is efficient enough to compete in today's energy market.[5] With this progress a wide range of PV materials have emerged, such as inorganic,[391–393] organic,[6,18,19] and hybrid dye-sensitized[21] photovoltaics. All photovoltaic devices operate under the same general physics in order to create electrical energy from sunlight.[27] A very important but poorly understood step in the photovoltaic process is the formation of free charges from an exciton. The properties of an exciton, which is a bound electron-hole pair, are significantly different in inorganic and organic photovoltaics. Inorganic semiconductors have a large dielectric constant and highly delocalized states, creating an environment where the exciton binding energy is on the order of kT or less.[13] An organic semiconductor, on the other hand, has a low dielectric and predominately localized states, making the exciton binding energy on the order of 40 kT.[23,24] In both photovoltaic materials the exciton binding energy must be overcome in order to harvest energy from the sun.

The classic inorganic PV is a p-n junction, which consists of two semiconductors, one doped with extra electrons and the other doped with extra holes. Represented in Figure 6-1a is the vacuum level, the highest occupied molecular orbital (HOMO), the lowest unoccupied molecular orbital (LUMO), and the fermi level of the p- and n-doped semiconductors. In this case, the HOMO and LUMO levels in the p- and n-type semiconductors are the same, but the fermi levels are not. As the two semiconductors are brought into electrical contact, charges transfer from one semiconductor the other in order to reach electrochemical equilibrium, finally yielding the band diagram in Figure 6-1b. The transferred charges create a dipolar electric field at the interface, which alters the vacuum level and is what drives the electrons and holes apart to the electrodes.

Organic photovoltaic (OPV) devices need a large driving force to overcome the large exciton binding energy and create separated electrons and holes. By using two organic materials that have different HOMOs and LUMOs, the driving force to break up an exciton is provided by the HOMO/HOMO or LUMO/LUMO difference of the two materials. A charge transfer (CT) state is formed after the exciton breakup, and due to the low dielectric of organic semiconductors, the binding energy of the CT state is still around 10 kT. Despite the large binding energy, the free carrier formation can be very efficient and fast in many OPVs.[37,38] One proposed mechanism for this is that some of the excess exciton energy might be used to create a "hot" CT state, where the carriers have a hyper-thermal distribution of energy[89] that helps them to overcome the dissociation barrier and behave as free carriers. Contradictory studies have shown that relaxed CT states can form free charges just as easily as "hot" CT states.[92] While the exact method of breaking up the charges is not known, it is understood that if the binding energy is not overcome, the ensuing charge recombination at the interface can

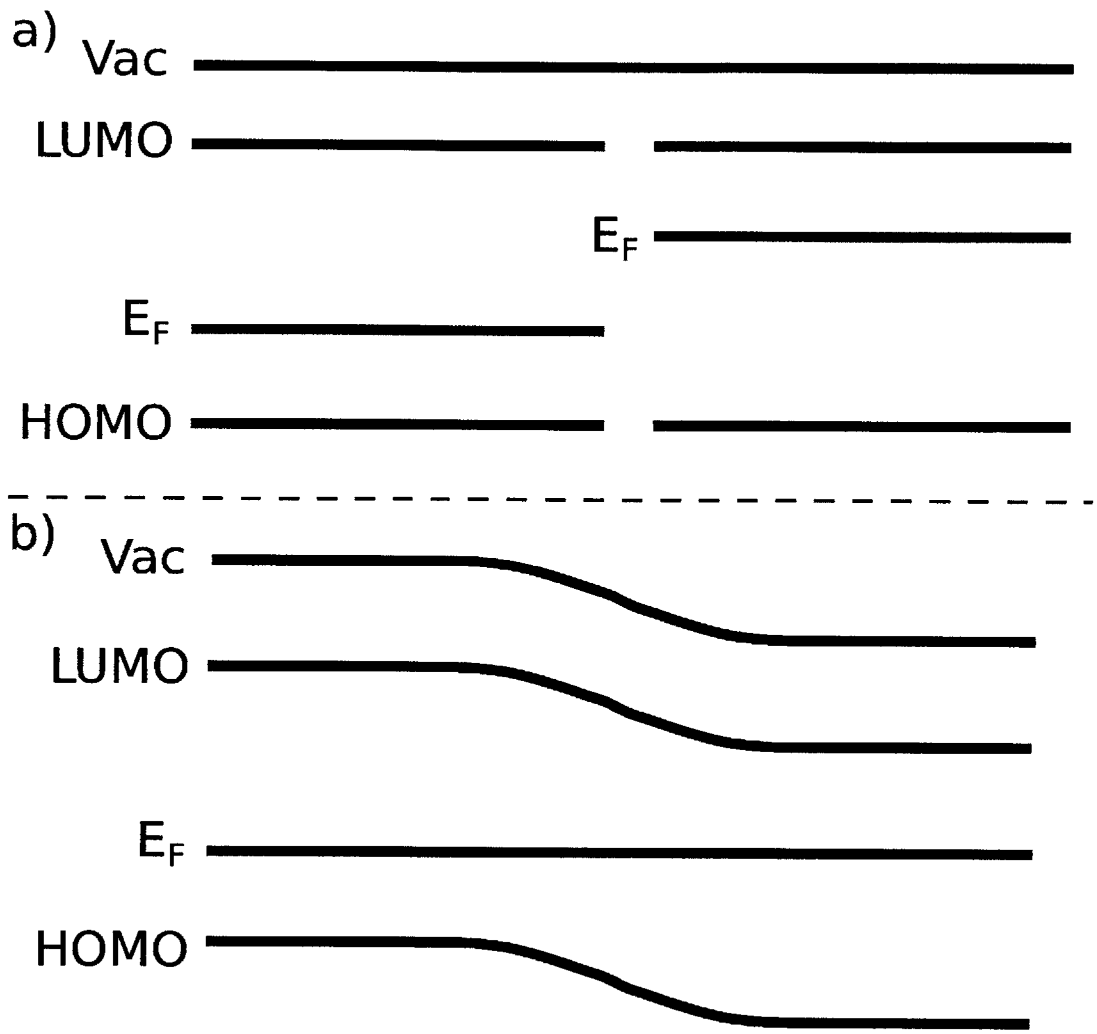

Figure 6-1: A basic band structure for a) an inorganic p-n junction not in electrical contact and b) an inorganic p-n junction in electrical contact.

decrease the open circuit voltage (V_{OC}) by 0.3-0.5 eV.[39] Therefore, knowing how the CT binding energy is overcome in OPVs is crucial to improving OPV performance.

Most OPV materials are selected solely based on bulk HOMO and LUMO levels, ignoring any changes that may occur at the organic/organic interface. The progression of PVs from inorganic to organic materials has driven the research on interfaces to mainly focus on fermi level alignment at first organic/metal interfaces,[394–398] and more recently organic/organic interfaces.[99,399–401] Using techniques such as ultraviolet photoelectron spectroscopy (UPS)[402] and inverse photoemission spectroscopy

(IPES)[3] researchers have measured charge transfer at the organic/metal interface that results from efforts of the materials to match the work function of the metal and the fermi level, or charge neutral level,[98,99] of the organic material.[395,403–405] The same charge transfer concepts have been applied to organic/organic interfaces,[99,397,401] with changes in the HOMO and LUMO levels typically measured around 0.0-0.2 eV.[99,406] It is not clear how these effects translate over to large scale manufactured devices where the fabrication process, such as spin casting, can be very different and lead to much more disordered OSC layers. The focus on charge transfer effects and the lack of such effects at the organic/organic interface has lead to a typical assumption that no changes occur in the HOMO and LUMO levels at the interface.

In the past few years the idea of non-charge-transfer effects at organic/organic interfaces has made its way into the literature. Experimental orientational dependent studies performed on organic/organic interfaces[400,407] showed that electrostatic multipoles can create an electric field that shifts the vacuum level. Theoretical work on the interface between planar organic molecules, like pentacene, with C_{60} have shown the orientation of the planar molecule can create HOMO and LUMO shifts on the order of 0.2 eV at the organic/organic interface.[103–106,408] These works indicate that significant stabilization or destabilization of the HOMO and LUMO levels can occur from non-charge-transfer effects.

In this chapter we us the combined quantum mechanics/molecular mechanics (QM/MM) model to obtain an atomistic picture of the metal-free phthalocyanine (H_2Pc)/3,4,9,10 perylenetetracarboxylic bisbenzimidazole (PTCBI) interface. Our calculated excitation energies reveal that thermal broadening accounts for only a fraction of the absorption width. Near the interface we find shifted values in the IP and EA, showing that band bending effects at the interface *must* be included to accurately estimate the binding energies of the interfacial CT states. Further, the CT binding energy shows sensitivity to the relative molecular orientations and thermal fluctuations, highlighting the influence of disorder on the energy landscape. Based on these findings we further study the role of the electrostatic environment on the HOMO and LUMO levels at the organic/organic interface. We show through simple models how a dielectric mismatch between the two organic materials, poor and inefficient packing at the interface, and molecular multipole moments can all contribute to significant changes in the HOMO and LUMO levels at the organic/organic interface. All three effects are found in realistic OPVs, with HOMO and LUMO interfacial shifts ranging from 0.2 to 1.0 eV. Due to the nature of the simulations we can isolate the contributions of different molecular properties to further understand how they alter the energies of localized electron and hole states. Importantly, the combination of band bending effects and fluctuations in CT binding energies make it possible for relaxed CT states to dissociate into free carriers *with no barrier*. This finding improves our understanding of exciton dissociation and carrier generation mechanisms in OPVs, which is a subject of much current interest.[88,89,92] Utilizing the environmental effects can help increase photovoltaic performance in future OPVs by driving apart the electron and hole at the interface, and thus increasing the V_{OC} and J_{SC}.

The chapter is organized as follows. First we introduce the QM and MM methods used, as well as the combined QM/MM method, to compute the relevant energies. We present our work on the organic/organic interface system composed of H_2Pc and PTCBI. This study is split into two parts, the first focusing on the accuracy of the QM/MM method for bulk values, and the second focusing on any changes in the energy levels at the organic/organic interface, including a detailed investigation of the charge transfer state. Next we discuss the different electrostatic effects that can alter the HOMO and LUMO levels at the organic/organic interface and present a number of different interfacial systems that display band bending due to these effects. Finally we summarize the implications of these results on the electronic processes that occur at the organic/organic interface.

6.2 Computational Details

The first organic/organic interface we choose to study is between two molecules that have been individually well characterized: H_2Pc and PTCBI. Both are planar organic molecules with extensive π-conjugation, and the combination of these materials is experimentally known to form a functional photovoltaic device.[409] PTCBI has been studied in many different devices with phthalocyanines and other OSCs;[410–413] its high electron affinity and broad absorption in the visible region make it a widely used acceptor material. Phthalocyanine molecules are widely used as a small molecule donor material, and there exists a gamut of studies on H_2Pc ranging from gas phase[414] to solid phase.[415,416]

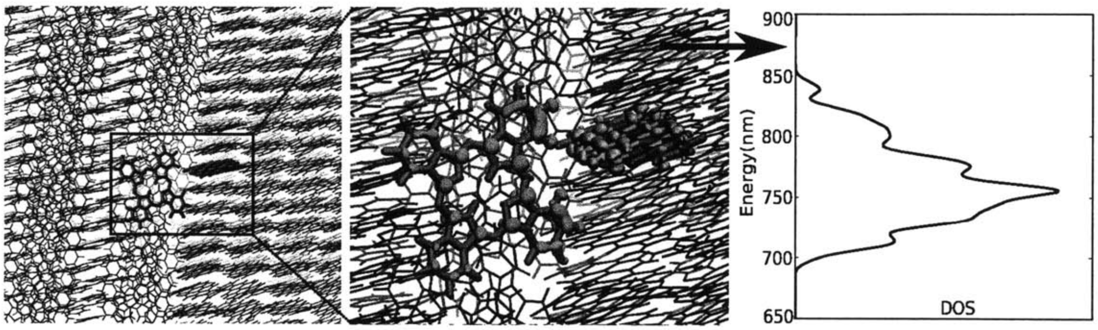

Figure 6-2: Illustration of the QM/MM method. Left: Disordered cell of the H_2Pc/PTCBI system described by MM. Center: Selection of a H_2Pc and PTCBI pair at the interface for calculation of the CT state energy. Right: Density-of-states plot obtained by repeating the calculation over different snapshots of a MM trajectory.

Our study can be divided into 1) calculations performed on bulk H_2Pc and PTCBI systems and 2) calculations performed on the H_2Pc/PTCBI interface; this allows us to benchmark our calculations by comparing to experimental measurements on single crystals and also examine effects of the interface by comparing bulk and interface calculations. Each study began with a pure NVT MM dynamics simulation, where the simulation cell contained several hundred molecules that are treated classically (Figure 6-2 left). Our simulation cells were ideal crystals in the sense that there were no site defects and the interface was constructed from perfectly cleaved crystal faces. Several snapshots were harvested from this MM dynamics trajectory. In a given snapshot, a select few molecules were chosen to be treated quantum mechanically while interacting with the MM environment (Figure 6-2 middle). QM/MM single-point calculations were then performed in order to obtain the relevant material properties, and repeated over many snapshots to obtain ensemble averaged values (Figure 6-2 right). We refer the reader to our previous work[101,189] and to Appendix B and C for information on the MM forcefields and the molecular geometries.

6.2.1 Interface Structure

For construction of the MM systems we started with a pure 14×7×5 (3×14×5) super-cell of the experimental crystal structure for a total of 490 (420) PTCBI (H_2Pc) molecules. The H_2Pc/PTCBI interface was constructed by aligning the (001) and (010) crystal faces of the H_2Pc and PTCBI super-cells along $\hat{z}$; periodic boundary conditions were applied along $\hat{x}$ and $\hat{y}$ (i.e. perpendicular to the interface), and the system was relaxed under constant pressure (1 bar and 300K) for 1 ns. All three systems were evolved under NVT dynamics for 5 ns at 300 K. The final 4 ns of the constant-volume dynamics were sampled at 40 ps intervals to obtain 100 snapshots for QM/MM calculations; the 40 ps time interval was chosen to minimize correlations between snapshots.

6.2.2 Density Functional Calculations

All of the QM/MM calculations were done using the CHARMM[417]-Q-Chem[262] interface,[418] and all pure MM calculations were run in Gromacs 4.0.[419] All quantum calculations were performed with Q-Chem 3.2 using the PBE0 functional and 6-31G* basis set. All of the singlet excited state calculations used linear-response time dependent density functional theory (TDDFT)[146] on one molecule. The charge transfer states were obtained using constrained DFT[153] on two molecules with an extra electron placed on PTCBI and one electron removed from H_2Pc. The PBE0 functional was chosen because it offered the best compromise between accurate prediction of the singlet energy and the band offset, as the singlet energies increased and the band offset decreased with respect to the fraction of exact Hartree-Fock exchange for various functionals tested (PBE0 contains 25% exact exchange).

6.3 H_2Pc/PTCBI Interface

We start by computing the band offset and Frenkel exciton energies of bulk H_2Pc and PTCBI, given in Table 6.2. To obtain the IP and EA values, we collect data from three different monomers in twenty distinct snapshots; the transport gap (TG) for a single material was given by $E_{\mathrm{IP}} - E_{\mathrm{EA}}$ and the bulk band offset by $E_{\mathrm{offset}} = E_{\mathrm{IP}}^{\mathrm{H_2Pc}} - E_{\mathrm{EA}}^{\mathrm{PTCBI}}$. Here we note that the TGs and band offset, the more critical quantities for device performance, are in good agreement with experimental values despite larger errors in the IPs and EAs themselves. This is because, as shown in Table 6.1, there are roughly equal shifts in the IP and EA when increasing the basis set (+0.2 eV with 6-311G*). The calculations in Table 6.1 are done using the COSMO solvation model in Turbomole[420] with a dielectric of 3. Also, when placing a molecule in the electrostatic environment of the crystal the IP and EA decrease by 0.3 eV.

Basis	H_2Pc (PTCBI) IP	H_2Pc (PTCBI) EA	H_2Pc (PTCBI) TG	Band Offset
3-21G	5.71 (6.20)	2.79 (3.37)	2.93 (2.83)	2.35
6-31G*	5.41 (5.98)	2.72 (3.26)	2.69 (2.72)	2.15
6-311G*	5.56 (6.15)	2.92 (3.47)	2.64 (2.68)	2.09

Table 6.1: Calculated transport properties for H_2Pc and PTCBI using PBE0 with the indicated basis set, all values are reported in eV.

6.3.1 Bulk Materials

Material	IP	EA	TG	Band Offset
H_2Pc	4.74 (5.2)	2.43 (3.0)	2.31 (2.2)	1.54 (1.6)
PTCBI	5.53 (6.2)	3.20 (3.6)	2.33 (2.6)	

Table 6.2: Calculated transport properties for H_2Pc and PTCBI. Experimental values, taken from Refs. 2, 3, and 4, are given in parentheses. All values are reported in eV; computed values have a statistical uncertainty of *le* 0.07 eV.

Turning our attention to optical properties, we note that most OSC materials have a broad absorption in the solid phase due to many different effects such as heterogeneous broadening, coupling between excited states (Davydov splitting), and vibronic transitions. The inclusion of all of these effects is beyond the scope of this study, and here we focus on heterogeneous broadening only. We computed the lowest few singlet excited state energies and their oscillator strengths for fifteen different molecules over fifty snapshots. We then plotted each state as a Gaussian weighted by its oscillator strength to get absorption spectra, which are plotted with the experimental spectra[421] in Figure 6-3. Both of the absorption features are in roughly the right spectral region, but we note that with only heterogeneous broadening the calculated lineshapes are not nearly as broad as the experimental results. It thus appears that Franck-Condon (FC) and/or Herzberg-Teller (HT) effects play a significant role in determining OSC absorption spectra, even in disordered environments[298,299]

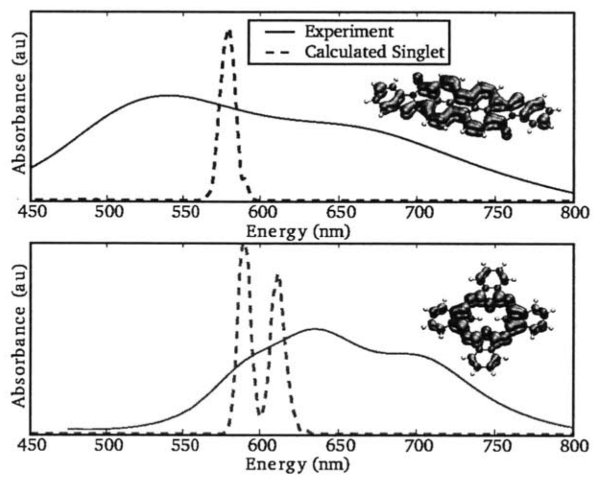

Figure 6-3: Calculated absorption spectrum (dashed) and experimental spectrum (solid) of PTCBI (top, blue) and H_2Pc (bottom, red). The calculated spectra contain 750 calculated energies sampled from 15 molecules each over 50 snapshots, each given a Gaussian distribution with width 1.7 nm. The inserted molecules show the attachment/detachment (blue/orange) densities of the lowest excited state of PTCBI and H_2Pc.

Looking at PTCBI in particular, our calculated spectrum is also missing a peak at around 660 nm. This peak is also absent with the higher-accuracy RI-CC2[422] method in Turbomole[420] with the larger TZVP basis, which predicts only one bright peak at ~525 nm. We suspect the missing peak is a HT effect; specifically, with either PBE0 or RI-CC2, there is a "dark" state in the 600-700 nm range with an oscillator strength that is essentially zero. This creates an ideal situation for the HT effect where the dark exciton could borrow intensity from the bright state via vibronic coupling.[299]

For H_2Pc our calculations underestimate the splitting of the Qx and Qy bands (given in order of increasing energy). This reflects a shortcoming of TDDFT for individual H_2Pc molecules, as the splitting of the two peaks and their relative heights arise primarily from the symmetry lowering brought about by the two hydrogens in the inner ring, with the Qx (Qy) transition dipole parallel (perpendicular) to the line connecting the two inner-hydrogens.

To better picture these excitons, the attachment-detachment plots[423] of the lowest singlet excited state both molecules are shown alongside the spectra in Figure 6-3. Both of the molecules have a strong transition dipole in the plane of the molecules; for PTCBI it points along the long molecular axis. The strength and alignment of the transition dipole moments suggest that exciton-exciton coupling in the solid phase could also have a significant effect on the lineshapes[424,425] of these crystalline materials, although we expect such effects to diminish in more realistic, disordered systems. In summary, our current implementation of the QM/MM model can reproduce the band offset accurately and obtain a qualitative picture of the excitonic levels, but obtaining a more accurate spectrum would require combining all of the above physical effects with the heterogeneous broadening presented here.

6.3.2 Organic-Organic Interface

Next, we examine the absorption spectra in the interface system. The absorption spectra at the interface are plotted in Figure 6-4 along with the bulk spectra reproduced from Figure 6-3. The absorption curve of PTCBI is red-shifted, and the splitting in H_2Pc is reduced for excitons closer to the interface; these changes indicate a shift towards gas phase values, likely due to the less dense packing at the interface. In contrast, the interface has a negligible effect on molecules located ≥ 2 nm (1-2 molecules) away; this agrees with our expectation that the highly localized exciton is not very susceptible to electrostatic changes.

The CT state, on the other hand, is more susceptible to changes in the electrostatic environment and is correspondingly more sensitive to the interface. We sampled five crystallographically distinct nearest-neighbor CT pairs at the interface

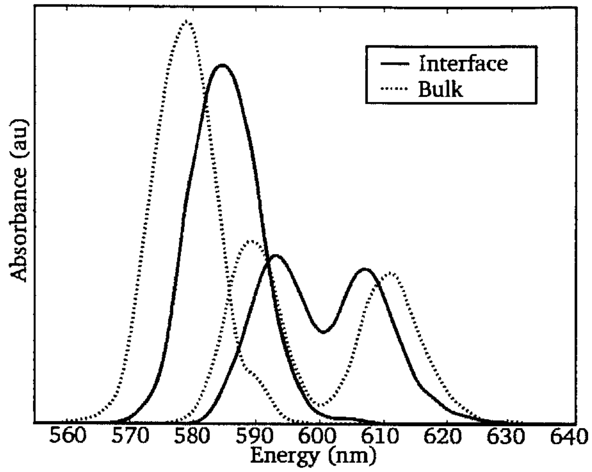

Figure 6-4: Calculated absorption spectrum of H_2Pc (red) and PTCBI (blue) at the organic-organic interface (solid) and in the bulk (dashed). Each curve was constructed from 750 different values sampled from 15 molecules each over 50 snapshots and given a Gaussian distribution with width 1.7nm.

over twenty snapshots and plotted their density of states alongside the absorption spectra in Figure 6-5. By comparing the energy levels, we see that a singlet exciton in either material is able to transfer its energy into an interfacial CT state, which can then separate into isolated charges; thus, our calculations correctly reproduce the experimental observation that PTCBI/H_2Pc forms a functional photovoltaic device.[409] Not surprisingly, the CT states have a broader energy distribution (FWHM ~220 meV) than excitonic states; this is in part due to the distribution of CT pairs, most notably the variation in the donor-acceptor distance between different pairs. By contrast, the dynamic fluctuations of the CT energy for a given pair are much smaller (FWHM ~60 meV).

We perform further analysis on the distance dependence of the CT binding energy (BE, given by $E_{BE} = (E_{IP}^{H_2Pc} - E_{EA}^{PTCBI}) - E_{CT}$). Using the procedure provided in Ref. 426, we fit the inverse of the BE to a linear combination of intermolecular distances; our results are shown in Figure 6-6. We choose to use a linear combination of intermolecular distances for the coordinate in Figure 6-6 in order to filter out the effects of relative molecular orientation as much as possible.[101] The BE has a clear R^{-1} decay as a function of distance, arising from the Coulomb interaction between

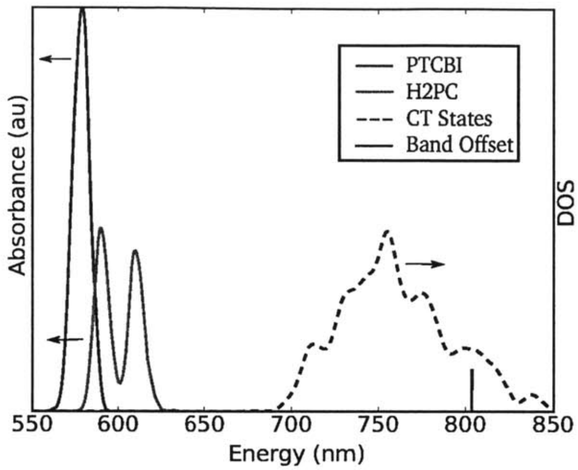

Figure 6-5: Full calculated spectra of all relevant energy states: bulk absorption (left axis) of H_2Pc (red) and PTCBI (blue), CT density of states (black, right axis), and the location of the average bulk band offset (brown). Each data point is given a Gaussians distribution with a width of 1.7 nm.

the electron on the acceptor and the hole on the donor; however, this trend is not observed when center-of-mass or closest contact distances were used, highlighting the important orientational dependence for these planar molecules. The average BE for the closest pairs is 0.2 eV, while averaging over all of the nearest neighbor pairs yields a BE of 0.15 eV for the CT states. The overall fit is good, with a correlation of 0.85 between the data and R^{-1}; there is also a clear scatter of 0.1 eV on top of the Coulombic decay which we attribute to thermal fluctuations. From moment to moment, the CT energy of a given dimer will fluctuate by a few kT. Thus, at any instant there can easily be a more distant CT pair that has a lower energy than a compact pair due to random fluctuations in molecular orientation. These variations are expected to aid the initial charge separation at the organic-organic interface.

Perhaps surprisingly, the average energy of the CT states (1.6 eV) is higher than the bulk band offset (1.5 eV), giving an apparent CT binding energy of $\approx$-0.1 eV; that is to say, the CT states seem to be unbound! We found that this can be explained by the significant contribution of interface effects to the band offset. In Figure 6-7 we plot the IP and EA of H_2Pc/PTCBI vs. the distance from the interface, each point corresponds to an average over four monomers each using twenty snapshots. The EA

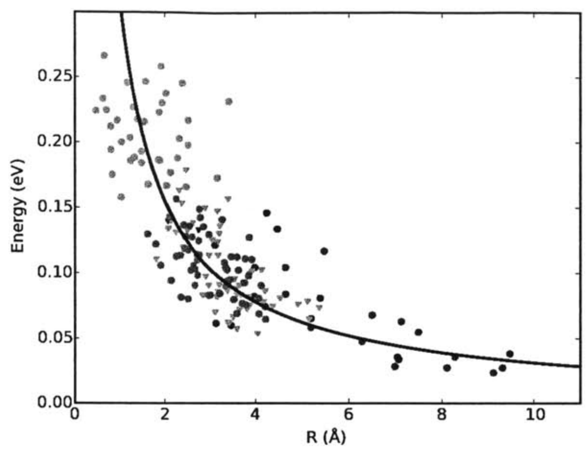

Figure 6-6: Plot of the distance dependence of the PTCBI/H_2Pc CT state binding energies. The coordinate R is a linear combination of intermolecular distances. Each different color/shape combination represents distinct dimer pairs in the simulation cell.

of PTCBI (IP of H_2Pc) decreases (increases) as one moves toward the interface by 0.1 (0.15) eV, such that the band offset at the interface is 0.25 eV larger the bulk value and giving an average CT binding energy of $\approx$0.15 eV. Thus the CT states are *locally* bound; the energy of the electron-hole pair at the interface is more stable than a single electron plus a single hole at the same site. At the same time, the CT states are *globally* unbound; the electron and hole gain energy by migrating away from the interface.

The 'gap bending' effect at the OSC donor-acceptor interface has been previously calculated in different systems and with different models.[99,105,408] In those cases, the effect was caused by an interfacial dipole that shifted the electron and hole levels asymmetrically. Our calculations did not find a significant dipole at the H_2Pc/PTCBI interface; instead, the gap bending appears to be due to differences in the polarizability and crystal packing. The interface has a stabilizing (destabilizing) effect on carriers in H_2Pc (PTCBI) because PTCBI has a higher dielectric constant than H_2Pc, and the relatively sparse packing introduces an overall destabilizing effect; our QM/MM simulations with a polarizable MM model were uniquely able to capture these effects.[189]

There is much discussion in the literature on understanding the origins of the high

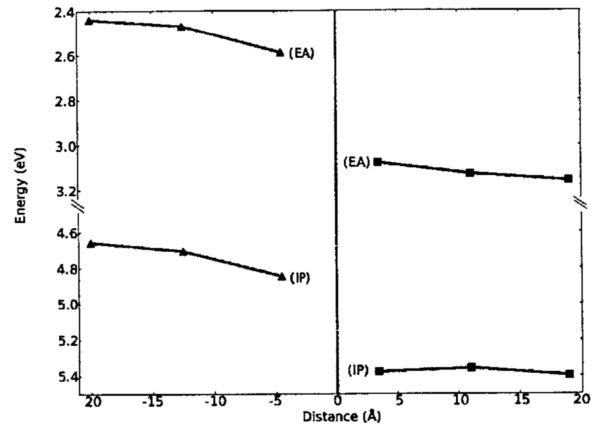

Figure 6-7: Plot of the average IP and EA of H_2Pc (red) and PTCBI (blue) crystal planes as a function of their distance from the interface. Each point has a standard deviation of about 50 meV.

internal quantum efficiency in OPVs and why the separation of a CT state appears to be essentially barrierless.[427] One prominent view is that the excess energy from exciton dissociation creates a "hot" CT state with sufficient kinetic energy to break free of the binding energy before thermal relaxation takes place.[88,89] On the other hand, there is also evidence that thermally relaxed CT states are separating into free charges.[92,428] Our work indicates the latter model to be more accurate, and suggests that thermally relaxed CT states can break up easily due to competition between the decreased dielectric screening at the interface and the Coulomb attraction, the first increasing and the second decreasing the CT energy. For our current H_2Pc/PTCBI model system, the decrease in dielectric screening is larger than the Coulomb attraction, and thus there is little to no energy barrier for CT separation. Future studies spanning a broad range of molecules and interfaces would be useful for testing the generality of these results.

6.4 Theory of charge carrier levels near interfaces

Controlling the amount of band bending at an organic/organic interface requires us to understand what environmental factors can shift the HOMO and LUMO levels in an OPV. In the typical example of an inorganic p-n junction, where there is a build up of negative charge on the p-type material, the holes and electrons in the neighboring n-type material are stabilized and destabilized, respectively. The result of the transferred charges is then manifested by the HOMO and LUMO in the n-type material shifting up at the interface, as seen in Figure 6-1b.

While charge transfer will not be considered in this study of the organic/organic interface, there are still many electrostatic effects that can alter the bands in OPVs. An environmental factor that has a significant impact on the energy of a charge and is always present in any material is the dielectric of the material.[429] The Born model[430] gives a simple picture of how the surrounding dielectric, ϵ, can change the energy of a molecule in a spherical cavity of radius a and charge q.

$$\Delta E = -\left(1 - \frac{1}{\epsilon}\right)\frac{q^2}{2a} \tag{6.1}$$

ΔE is the solvation energy, in atomic units, gained due to the dielectric surroundings stabilizing the charge. As the dielectric increases the hole(electron) is stabilized causing the HOMO(LUMO) band to go up(down). Overall this means the bands get pinched together as the dielectric increases.

Typically both OSC materials in an OPV will have different dielectrics, so there will be a lower dielectric (ϵ_{low}) material and a higher dielectric (ϵ_{high}) material, as shown in Figure 6-8a. A molecule at the organic/organic interface is solvated by both the high dielectric material and the low dielectric material. Therefore, when two OSCs are placed together the bands in the OSC with dielectric ϵ_{low} pinch together at the interface, while the bands in the OSC with ϵ_{high} pull apart at the interface. The band bending in the ϵ_{high} material also takes place over a shorter distance because of the larger dielectric screening of the charges. Combining everything, we arrive at the band picture in Figure 6-8a, with the lower dielectric material displaying pinched bands at the interface, and with the bands in the higher dielectric material being pulled apart over a shorter distances.

Efficient packing and disorder plays just as a significant role in the solvation of a charge. This is important in OPVs because the weak Van der Waals interactions

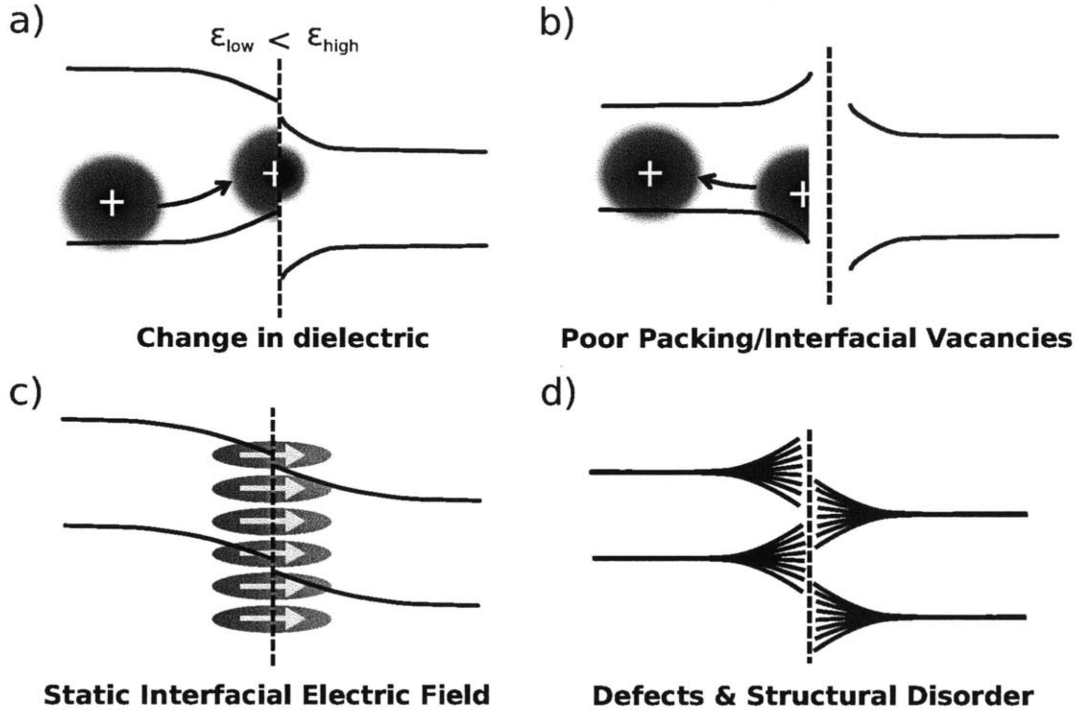

Figure 6-8: A schematic representation of four different environmental effects on the organic/organic band structure, a) a difference in dielectrics, b) poor molecular packing at the interface, c) a molecular multipole moment creating an electric field at the interface, and d) a rough depiction of general disorder at the interface.

holding them together and fabrication techniques, such as spin casting, can lead to significant disorder in the molecular packing.[6] By using a more detailed model for solvation that includes the molecular polarizability and packing density,[431] the authors in Ref 429 showed how poor packing lead to the observed changes in the HOMO and LUMO levels of their OPV. The poor packing can be even more severe at the organic/organic interface,[96,429,432] causing the dielectric of an organic material to decrease near the interface. A decreased dielectric caused by poor packing in one molecular layer at the interface destabilizes the charges in both organic materials, yielding the HOMO/LUMO diagram in Figure 6-8b. The changes in Figure 6-8b differ from Figure 6-8a because in the case of a dielectric mismatch only one of the materials feels a reduced dielectric at the interface, while when there is poor packing, both materials experience a reduced dielectric at the interface.

The nonzero multipole moments of OSCs can produce bigger changes than any dielectric effect, since in typical OSCs the range of dielectrics is only around 2-6. For example, pentacene contains a non-zero quadruple moment that causes significant shifts in the C_{60} HOMO and LUMO levels at the pentacene/C_{60} interface.[105,408] The quadruple moment locally will produce a positive electric field at the edges of the pentacene molecules and a negative electric field near the center of the pentacene molecules, the average of which produces a negative electric field destabilizing the electron in C_{60}. Any molecule will have a nonzero multipole moment, whether it be a dipole, quadruple, octupole, etc.., and these multipole moments contribute to the interfacial static electric field. If in a real system the molecules pack such that stray electric fields are not compensated near the interface, then a large, long range electric field could appear at the interface. The electric field will stabilize or destabilize any free charges and thus either pull up or down the HOMOs and LUMOs, as shown in Figure 6-8c. The amount of band bending that occurs will depend on the strength and type of the multipole moment. On average as one goes to higher order multipole moments the complexity of the local electric field increases and the strength decreases.

It is worth mentioning that substitutional defects, crystal defects, and other kinds of structural heterogeneity can also significantly impact the HOMO and LUMO levels at the organic/organic interface.[96] Their impact on the HOMO and LUMO levels near the interface is not easy to quantify. Static disorder can alter the localization length of the electron and hole, and potentially create trap states. In the end, one can envision scenarios where defects lead to a variety of different band bending motifs like those shown in Figure 6-8d. As shown in our previous work,[101] an exciton is not affected by these electrostatic effects due to it having no net charge. Though, simple structural disorder is expected to affect the energy available to uncharged carriers like excitons.[96] While these kinds of structural distortions can be significant, for simplicity this chapter will largely focus on purely electrostatic effects and their impact on the HOMO and LUMO levels of OPVs.

6.5 Modeling electrostatic effects on charge carrier levels

We now proceed to model the behavior of the electron and hole levels in some realistic organic/organic interface systems using density functional theory (DFT) calculations. Our aim here is to see to what extent realistic simulations reinforce the simple pictures outlined in the previous section. The HOMO and LUMO levels of a semiconductor are rigorously calculated as its ionization potential (IP) and electron affinity (EA), respectively. Any significant disorder in an OSC causes localization of the electronic states,[23] and so to a good approximation the HOMO and LUMO levels are just the IP and EA of single molecules. While this is not the case for more crystalline or polymeric materials, for thin film small molecule OPVs the amount of disorder will typically localize the states. Therefore, to model the HOMO and LUMO levels at an organic/organic interface we use a combined quantum mechanical and molecular mechanical (QM/MM) method, where the QM region is just a single molecule. Using this QM/MM model we achieve accurate energy calculations at specific locations relative to the complex environment at the organic/organic interface.

The first interface system studied is constructed with rubrene and C_{60},[383,401,429,433] and their calculated bulk HOMO/LUMO values are 5.2/1.9 and 6.1/3.5 eV, respectively. The rubrene/C_{60} interface chosen is the (0,1,0)/(0,1,0) interface. Both of these molecules have no significant multipole moment, but they do have different dielectric constants, with a ϵ of 2.7 and 3.8 for rubrene[434] and C_{60},[435] respectively. The calculated HOMO and LUMO levels of this interface system are plotted in Figure 6-9. Changes in the HOMO and LUMO levels occur in both layers, with rubrene's bands being pinched together and C_{60}'s bands being pulled apart at the interface. Figure 6-9 agrees very well with Figure 6-8a, and based on the bulk HOMO and LUMO values we see the dielectric effect persist for only a few molecular layers. Incidentally, setting a equal to 0.6 nm in Eq. 6.1 gives a difference in solvation energies between the two dielectrics of 0.13 eV, which is close to the actual changes of 0.1 eV and 0.15 eV in rubrene and C_{60}, respectively. The slope in the bands between the first

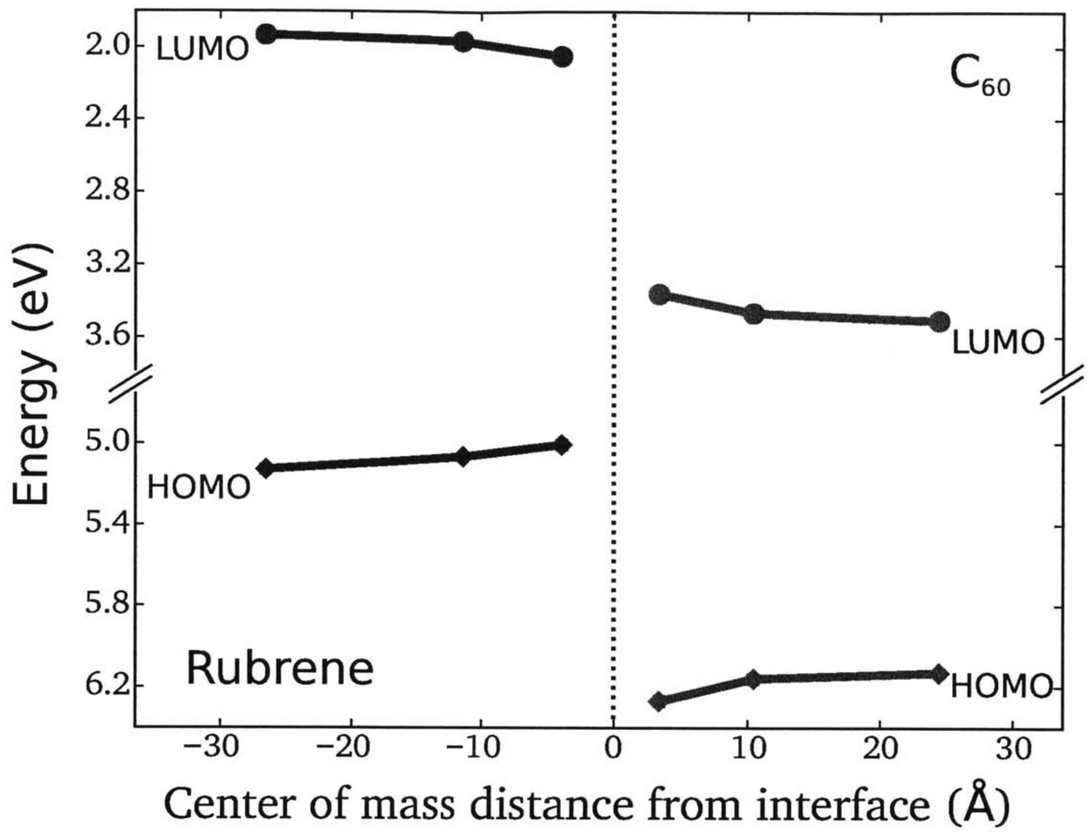

Figure 6-9: Rubrene/C_{60} interface band diagram showing how two different dielectrics at the organic/organic interface, with rubrene having the lower, can pinch or pull apart the bands.

and second layer is on average 0.05 and 0.10 eV/nm in rubrene and C_{60}, respectively, again in agreement with the fact that rubrene has the smaller dielectric and so the polarization effect persists over a longer distance. A minor difference in the dielectrics of only 1.1 providing a shift in the energy levels greater than 0.1 eV means that in most OPV devices this dielectric mismatch effect can significantly impact the HOMO and LUMO levels at the interface.

Next we turn to the effect of poor packing at the organic/organic interface, and model it by using the (1,0,0)/(0,1,0) copper phthalocyanine (CuPc)/PTCBI interface system.[436–438] Using Eq 6.1 with a equal to 0.6 nm, and the dielectrics of CuPc[439] and PTCBI[440] of 5.4 and 4.0, respectively, the change in solvation energy is 0.08 eV, which as shown above gives a crude estimate of the solvation effect. To further simulate the

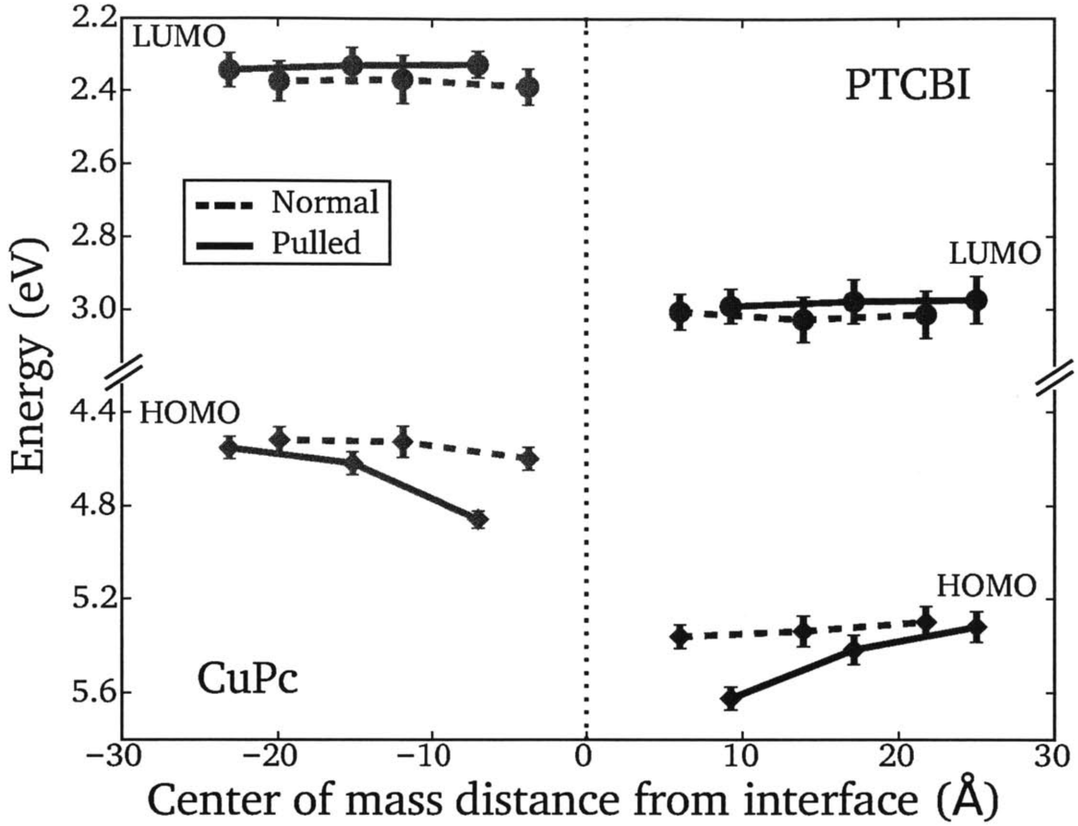

Figure 6-10: CuPc/PTCBI interface band diagram with a normal interface (dashed) and an interface system where the two layers are pulled apart by 0.6 nm (solid) to emphasis how the bands pull apart as the packing at the interface becomes worse.

effect of poor packing we compare two systems, a normal interface and an interface where a 0.6 nm gap is added between the two crystals. The bands for these two systems are shown in Figure 6-10. In the normal system there are shifts in the HOMO of CuPc and PTCBI and very little change in the LUMO. A much larger change in the HOMO is observed for both CuPc and PTCBI in the pulled apart system, as well as slight changes in the LUMOs. Thus we see that poor packing at the interface (here mimicked by the vacuum layer) can indeed lead to the expected shifts in the HOMO and LUMO levels of the two materials, as shown in Figure 6-8b. Similar types of shifts have been experimentally measured at the interface between CuPc and C_{60}.[429] An important distinction between the band bending seen in Figure 6-10 and in Figure 6-9 is that in Figure 6-10 the changes in the levels are mirrored about the interface, while tin Figure 6-9 the shifts are inverted about the interface. While the crystallinity of our simulations makes it difficult to model poor packing at the interface, comparison between the normal and pulled apart CuPc/PTCBI interfaces shows how poor packing at the interface, which creates a lower molecular density, causes the band gap to open up. The impact of poor packing at an organic/organic interface can be found in many different types of OPV systems, such as polymer/fullerene blends,[96] and can be relevant in all OPVs.

Interestingly, in Figure 6-10 the LUMO levels of both CuPc and PTCBI appear relatively constant, while the HOMO levels shift by as much as 0.2 eV. The differences in HOMO and LUMO level shifts have been observed in an experimental study on the CuPc/C_{60} interface.[429] The main reason behind this odd behavior is that excess positive and negative charges concentrate on different regions of a molecule, so a molecule's orientation to the interface determines the asymmetric solvation of the electron/hole densities. In most OSC materials, the excess positive charge from the hole will tend to be more localized on the less electronegative hydrogen atoms that surround the edges of the molecule, while the excess negative charge from the electron will tend to be located at the more electronegative carbon atoms in the middle of the molecule. The CuPc and PTCBI molecules at the organic/organic interface used to produce Figure 6-10 are facing in such a way that the edges of the molecules are the only part exposed to the interface. Thus, the HOMO levels are more susceptible to the environment at the organic/organic interface and so they shift more when the environment changes. Solvation effects from different dielectrics and poor packing will display this kind of dependence on the relative orientation of the molecules.

To model the effect of molecular multipoles on the organic/organic interface we chose a system composed of 4-(Dicyanomethylene)-2-methyl-6-(4-dimethylaminostyryl)-4H-pyran (DCM) and C_{60}. The calculated bulk HOMO and LUMO for DCM are 5.6 and 1.5 eV, respectively. The dipole of DCM is 14.8 debye and its dielectric constant is 2.28,[441] which gives a solvation effect with C_{60} of 0.23 eV. The unit cell of DCM has no net dipole, so a partially completed unit cell must used to get a net dipole at the interface. Therefore, one system is constructed with the (0,1,0)/(0,1,0) interface of DCM/C_{60}, and the other system is constructed with what we will call the $(0,\frac{1}{2},0)/(0,1,0)$ interface, both shown in Figure 6-11. To make the $(0,\frac{1}{2},0)/(0,1,0)$ interface, only half of a unit cell of DCM is used for the interface layer, the vacancies formed by removing DCM are filled with C_{60} to minimize any vacuum effect. In this modified cell there is no cancellation of dipoles between two DCM molecules at the interface, so we get the largest possible dipole effect with every dipole pointing in the same direction. Actual OPV devices will fall somewhere between these two extremes because there will be much more disorder in the orientation of the dipoles, and as such in the amount of band bending at the interface. In Figure 6-11b one can see the mixed interfacial layer highlighted in the $(1,\frac{1}{2},0)/(0,1,0)$ cell where both DCM and C_{60} exist. In this layer both the DCM and C_{60} molecules feel drastically different environments. One major difference is that when compared to the bulk C_{60} molecules the C_{60} molecules in the mixed interface layer end up on the other side of the dipole created by DCM. That plus the different dielectric environment in the mixed interfacial layer is why we chose not to include the HOMO and LUMO levels from that layer in our analysis in the rest of the section.

To make it more clear how the dipolar electric field alters the HOMO and LUMO levels, both the interface systems were also modeled with using the DCM dielectric constant. Using both types of dielectric environments we can investigate the normal interface energetics in one system and narrow out the contribution from the dipole of DCM in the other. The normal interface, plotted in Figure 6-12a, shows relatively no change in the $(0,1,0)/(0,1,0)$ interface because there is no net electric field at the interface. Though the difference in the dielectrics pushes apart the C_{60} bands and pulls together the DCM bands by 0.1 to 0.3 eV. On the other hand, there is a shift of 1.0 eV in the $(0,\frac{1}{2},0)/(0,1,0)$ system that continues well past the measured 3.0 nm. The shift due to the dipolar electric field is so significant that at the interface the LUMO of DCM is actually lower than that of C_{60}, which further shows the huge changes that can occur due to molecular multipoles.

A clearer picture of the dipole effect is shown in Figure 6-12b, where the dielectrics are matched to get rid of their effect on the bands. Again, there are somewhat small

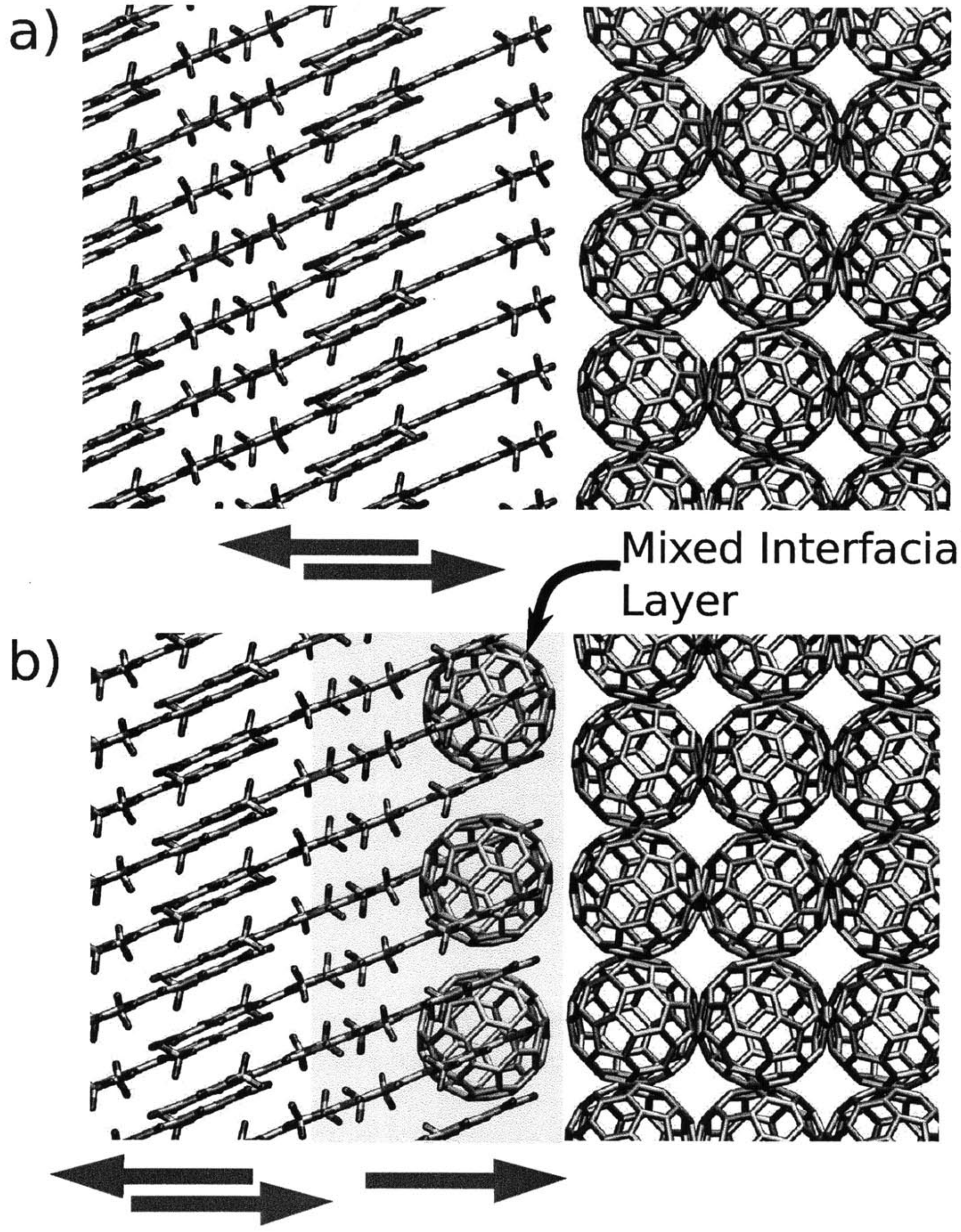

Figure 6-11: Pictures of the DCM/C_{60} interface for the a) (0,1,0)/(0,1,0) interface and b) (0,$\frac{1}{2}$,0)/(0,1,0) interface, where the arrows are used to depict the location and direction of the dipoles in the DCM layer.

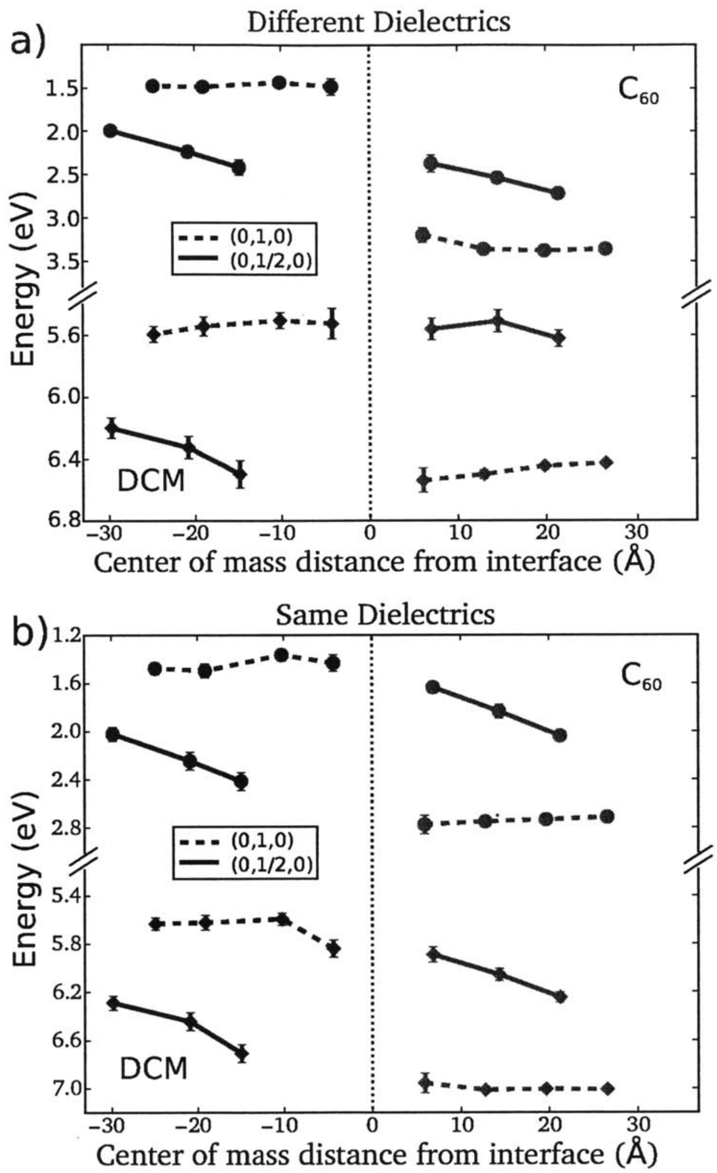

Figure 6-12: DCM/C_{60} band diagrams showing a 1 eV band bending effect due to the DCM dipole at the interface, with the (0,1,0)/(0,1,0) interface (dashed) and the $(0,\frac{1}{2},0)/(0,1,0)$ interface (solid) for a) different dielectrics and b) same dielectrics.

shifts in the HOMO and LUMO levels in the (0,1,0)/(0,1,0) interface system, though some changes occur in DCM due to its complex electrostatic environment within the unit cell. The clearest changes due to the dipole are seen in the $(0,\frac{1}{2},0)/(0,1,0)$ system, where again a 1.0 eV shift in all the bands is observed at the interface. In C_{60} the average slope of HOMO and LUMO is 0.2 eV/nm and 0.3 eV/nm, respectively, and in DCM the average slope is 0.3 eV/nm for both bands. The change from one molecular layer to the next is as large as a typical CT binding energy, immediately making CT separation very energetically favorable. The similar slopes and directions in both molecular layers agree with the assessment that the dipole of DCM is creating a long range dipolar electric field at the interface, and bending the bands in a fashion similar to Figure 6-8c. A study on the CuPc/F_{16}CuPc interface showed that only when the dipolar C-F bonds faced the interface did the HOMO and LUMO levels shift by 0.5 eV,[400] further emphasizing the large impact of multipole moments on the HOMO and LUMO levels in an OPV.

We can get a quantitative measure of the contributions of different effects in the DCM/C_{60} system by modifying the MM parameters to change the dipole of DCM or the dielectric of DCM and C_{60}. Figure 6-13 shows exactly what one would expect when the dielectric or dipole is increased by 25%. As the dielectric is increased for a material the HOMO and LUMO get pulled together, but less so at the interface since both materials are contributing to the dielectric in that region. The change in the HOMO and LUMO with respect to a 25% change in the dipole of DCM is plotted in Figure 6-13c. When the dipole of DCM is increased by 25% there is no significant change in the (0,1,0)/(0,1,0) system, but a large shift is observed in the HOMO and LUMO levels in the $(0,\frac{1}{2},0)/(0,1,0)$ system. The shifts in the $(0,\frac{1}{2},0)/(0,1,0)$ system have a linear dependence on the dipole of DCM such that multiplying each point in Figure 6-13c by the dipole of DCM (14.8 debye) yields the overall change observed in Figure 6-12b. This detailed analysis helps validate our expectations on how the electrostatic environment alters the HOMO and LUMO levels.

When considering how to use these electrostatic effects in an OPV one should note that the relative orientation and location of molecules can further impact the effects of the environment. The fact that the HOMOs and LUMOs shifted by different amounts in the CuPc/PTCBI system is not a fluke, it is due to how the molecules pack at the interface. The hole mainly resides on the less electronegative hydrogens of the molecules, which are exposed significantly more to the interface, while the electron

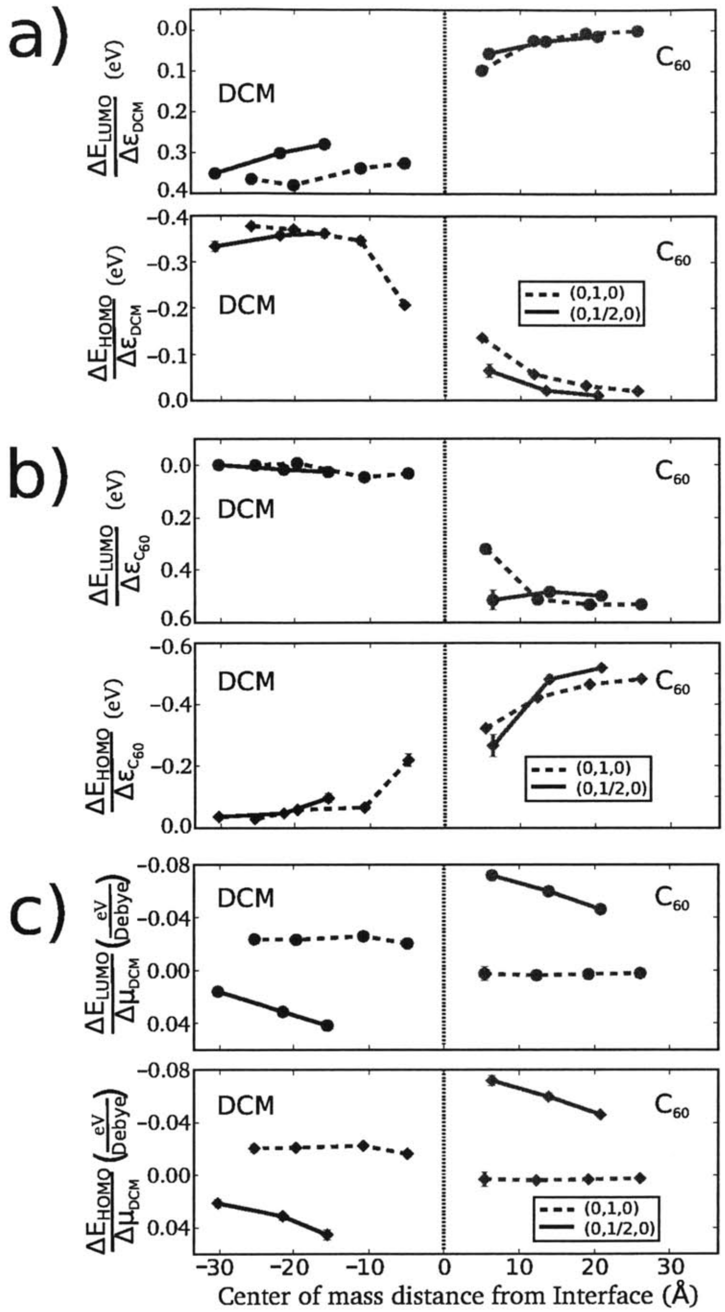

Figure 6-13: Changes in the bands when a) the dielectric of DCM is increased causing the C_{60} bands to be pinched, b) the dielectric of C_{60} is increased causing the DCM bands to be pinched, and c) the charges of DCM are increased creating band bending for the $(0,\frac{1}{2},0)/(0,1,0)$ interface (solid) and no bending in the $(0,1,0)/(0,1,0)$ interface (dashed).

resides more on π orbitals that are less exposed to the lower dielectric interface region. In the DCM/C_{60} interface system the electric field created by the dipole could be reversed if the DCM stack in the opposite direction. Other detailed studies have also pointed towards the significance of relative molecular orientations at the interface on the amount of band bending.[105,408] The shifts in the HOMO and LUMO at the interface for all the effects discussed can supply a driving force as large or larger than the charge transfer binding energy, and should be considered when designing OPVs.

6.6 Impact on charge separation efficiency in OPVs

A key step in the photovoltaic process is the separation of a bound charge transfer state into a free electron and hole. The lack of temperature dependence for charge separation in many OPVs suggests a barrier-less dissociation pathway. This is difficult to reconcile with the fact that the typical CT binding energy is around 0.2 eV. It could be that the 0.2 eV of excess energy needed during the exciton breakup process is going to creating a vibrationally excited charge transfer state.[88,89] The extra vibrational energy obtained assists in the formation of the free electron and hole. Further complicating matters, studies that directly excite a charge transfer state without any excess energy and found the relaxed charge transfer state is able to break up just as easily as one formed from the dissociation of an exciton.[92,428] At present there is no fully satisfying theory that explains all of these apparently conflicting experimental results.

Based on the results presented here, it is clear that the electric fields present at organic/organic interfaces could play a key role in resolving the situation. Reexamining Figure 6-8 we see that when the dielectric of two materials are different then the bands for the material with the higher dielectric will bend in such a way that the charges will be repelled from the interface. If there is poor packing at the interface then both materials will have a less favorable interfacial environment, that drives away both the electrons and holes. Finally, if there exists a molecular multipole, such as a dipole, oriented towards the acceptor then a large static electric field that favors charge separation is generated. All of the simulations used to calculate these effects are done on a single electron or hole, and as such lack the ability to determine the CT state binding energy. Calculating the binding energy provides the last crucial step in determining the ability of thermally relaxed CT states to separate at the interface. Though if the HOMO and LUMO level changes are on the order of the typical binding energy of a CT state, 0.1-0.3 eV, then in most cases the band bending will aid in charge separation. Then, if in the example given in the previous paragraph, the HOMO and LUMO levels of the OPV change at the interface increasing the band gap by at least 0.2 eV, then the exciton will need at least 0.2 eV more energy than the bulk band gap to break apart. Furthermore, the charges will be pulled away from the less favorable interface region, explaining both experimental observations.

Band bending effects can also just as easily decrease device performance in an OPV. It is known that the effect of film morphology is very important to bulk heterojunction OPV devices, and that higher efficiencies can be reached if the morphology of the OSCs are optimized.[442] As discussed in this article the morphology for small molecule bilayer photovoltaics can be just as important. Different substitutes of phthalocyanine have shown significantly different V_{OC}s, while still having similar HOMO and LUMO levels.[443] For example, the much larger dielectric in the lead phthalocyanine device could cause the electrons in the C_{60} layer to be more attracted to the interface, and thus increase charge recombination and lower the V_{OC}.

Controlling the changes in the HOMO and LUMO levels at an organic/organic interface, and thus the driving force for charge transfer separation, could open up a new route to increasing the efficiency of an OPV. Since the changes described here are all fairly short ranged the effective HOMOs and LUMOs can be modified at the organic/organic interface while keeping them unchanged in the bulk. Also, the changes provided here on localized states give an upper bound to the amount of band bending that will occur, since any delocalization of the electron and hole will reduce the impact of the electrostatic environment. Band bending at the organic/organic interface can increase the CT state energy to insure a driving force greater than the Coulombic binding energy is provided to minimize charge recombination. This helps both increase the J_{SC} and V_{OC} of an OPV, and so the environmental effects discussed in this chapter could prove to be key to improving device performance in OPVs.

6.7 Conclusion

In this chapter we used a QM/MM model to investigate many different organic/organic interfaces. For the the H_2Pc/PTCBI donor-acceptor interface we calculated thermal distributions of the exciton, IP, EA, and CT energies, in the bulk and near the interface. We found a strong dependence of the BE on the relative orientation of the molecules forming the CT pair. We addressed two effects on the CT state energy that depend on proximity to the interface: the electrostatic changes at the interface cause the band offset to increase by 0.25 eV, and the CT binding energy is strongest at the interface with a typical value of 0.15 eV. The competition between two effects create a situation where thermally relaxed CT states at the interface can easily separate into free carriers. In our model H_2Pc/PTCBI system, charge separation is downhill by about 0.1 eV. We addressed three molecular properties that yield significant changes to the HOMO and LUMO levels: 1) the bulk dielectric of an OSC, 2) the molecular packing structure, and 3) molecular multipole moments. By inspecting multiple bilayer OPVs we show that differences in dielectrics, poor packing at the organic/organic interface, and electric fields created by molecular multipole moments can shift the HOMO and LUMO levels at the interface by up to 1.0 eV. These effects can provide the driving force for charge separation of thermally relaxed CT states at the organic/organic interface.

Using the ideas from this chapter a few different approaches could be taken to create more efficient OPVs. Avoiding large differences in dielectrics between the donor and acceptor can help create a favorable environment at the organic/organic interface. Adding side groups that have significant multipole moments to OSC molecules could be one way to engineer shifts in the HOMO and LUMO levels at the interface. Having either one OSC layer with a significant multipole moment properly oriented, or a system with an interfacial layer of a molecule with a significant multipole, could increase charge separation and device performance.[444] These ideas can also be applied to OLEDs, but used to alter the bands in such a way that the charges are drawn to the interface. Future work needs to be done to better model the packing at an organic/organic interface to further investigate the effect of disorder, as well as including delocalization in the simulations. This article provides an initial framework for understanding how the electrostatic environment can generate band bending at organic/organic interfaces in ways that significantly impact device performance.

6.8 Acknowledgment

The force field creation described in this chapter was carried out with help from Lee-Ping Wang, who is an author in Ref. 101.

Chapter 7

Conclusion

As the demand for solar energy increases, so does the need for more efficient organic solar panels, which are currently limited to a maximum efficiency of 12%.[22] The device efficiency of an OPV, $\eta = \frac{J_{SC} \cdot V_{OC} \cdot FF}{P_{IN}}$, depends on the open circuit voltage (V_{OC}), the short circuit current (J_{SC}), the fill factor (FF)–which is a measure of the actual power relative to the theoretical power, and the input power (P_{IN}). Properties such as the charge carrier mobility, the solar absorption efficiency, and the charge carrier recombination rate modify the fill factor. The maximum achievable V_{OC} is equivalent to the band offset (E_{gap}), but this is rarely realized due to losses arising from, for example, charge recombination.[302,445–448] Recombination of the charge carriers is made up of two types, geminate recombination which is mainly due to the charge transfer states inability to overcome its binding energy, and non-geminate recombination which is caused by poor charge mobility and device morphology.[449–451] Charge recombination is a major cause of decreases in OPV efficiency, reducing both the V_{OC} and J_{SC}. Guided reduction of each loss mechanism requires a detailed understanding on the molecular level of the organic molecules and their environment in an OPV device.

Due to the disordered and widely varying environment present in OPVs, it is important to account for as many aspects of the environment as possible to obtain accurate results. The most common way this is done is by treating some or all of the system in a classical way by explicitly including the multipole moments and polarizability of the organic molecules. Current state-of-the-art simulations use either low cost semi-empirical methods or some sort of multi-scale method–which splits up the organic/organic interface into a system and surrounding. In the work presented here we have used different quantum techniques, often combined with a classical environment, to model the different processes in an OPV device in order to better understand the electronic processes in an OPV.

We have shown that the ΔSCF method is capable of achieving similar accuracy to the more widely used TDDFT method for computing excited state properties, which is around ±0.3 eV. The ΔSCF method is shown to be a theoretically sound way of computing excited state determinants, and due to its reliance on ground state methods it provides an easy way to sample the excited stat potential energy surface. Out of the ΔSCF method we created a new multi-reference perturbation theory method, called ΔSCF(2), in order to go beyond the ±0.3 eV accuracy of the excited states. After deriving low scaling formulas for computing the energies and couplings between different ΔSCF determinants we show that the ΔSCF(2) method can achieve similar accuracy to CASPT2. ΔSCF(2) has a rigorous definition of how to apply the second order perturbation expansion to the wavefunction and appears to require only a small number of ΔSCF states to achieve high accuracy excited states. It would be useful to expand the applications to excited states in radicals and incorporate the ΔSCF(2) method into a quantum chemistry package like Q-Chem.[262]

One important physical process that could greatly enhance the efficiency of many OPV devices is the use of singlet fission materials. The common consensus in singlet fission materials is that the fission process is very sensitive to the coupling between molecules, and thus on their crystal packing. Our recent experimental/theoretical work shows that this assumption is not entirely true. Using the ΔSCF method combined with constrained DFT with configuration interactions we computed the couplings between the singlet excited states, charge transfer states, and triplet-triplet states. Comparing these couplings and computed singlet fission rates with experimentally observed rates we find that the singlet fission process proceeds through either a direct non-adiabatic or adiabatic energy transfer step, with the crossover between the two at $\sim$ 20 meV. The coupling between the bright state and the triplet-triplet state determines the type of energy transfer mechanism. While the charge transfer states aid in increasing the coupling, and thus the fission rate, they are not required to achieve an overall fast singlet fission rate. This implies that a larger amount of potential singlet fission materials exist than what one might have previously thought, since the major requirement is just that the singlet excited state be twice the energy of the triplet state. Future studies should be done on screening for new singlet fission materials that can be solution processed and have different singlet excited state energies to increase the number of device architectures that one could use singlet fission materials in.

There is some concern with the triplet excitons produced by singlet fission being able to break up at the organic/organic interface. The wavefunction overlap dependence of the coupling makes it a concern that in disordered systems the triplet excitons will be trapped. Most OPV devices use singlet excitons which limit the device thickness to 10-15 nm because of the short singlet exciton diffusion length. Due to the shared dependence of the diffusion constant and the lifetime of the singlet exciton on the transition dipole the singlet excitons will not be able to diffusion much further than $\sim$ 100 nm. On the other hand, the triplet exciton, which has been shown to diffuse over 1 μm, is capable of a much longer diffusion length because the lifetime and diffusion constant are not coupled together in any way. Because our method of combining Kinetic Monte-Carlo with *ab initio* rate constants agrees well with experimental values we are able to probe the potential diffusion length in disordered environments. We show in tetracene that the semi-crystalline domains, and the lack of energy trap states, allow for triplet diffusion to remain very efficient, only decreasing by a factor of 10. Our results imply that triplet excitons are not trapped in disordered systems and the route to thicker OPV devices is to use materials where the primary energy carrier is a triplet exciton and not a singlet exciton, like in the case of singlet fission materials.

One poorly understood process in OPV systems is the ability of an OPV device to efficiently separate charges from the organic/organic interface. A number of different theories exist, from thermally excited charge transfer states to initially delocalized charge transfer states, but all of these theories assume a constant HOMO and LUMO level throughout the donor and acceptor layers. Our models on the organic/organic interface show that this is only qualitatively accurate at best, and that another potential way charges are being driven away from the organic/organic interface is because the HOMO and LUMO levels are changing at the interface due to a changing electrostatic environment. The H_2Pc/PTCBI interface system is a simple example where the charge transfer state is at a higher energy than the fully separated charges due to band bending at the organic/organic interface. The charge transfer state in the H_2Pc/PTCBI system has an average binding energy of 0.15 eV, but due to thermal fluctuation in the binding energy (~0.1 eV) and changes in the HOMO and LUMO levels (~0.2 eV) the charge transfer state is locally bound but globally unbound.

In order to better understand the band bending at the organic/organic interface we studied three main environmental effects, a dielectric mismatch, molecular multipole moments, and poor molecular packing. The dielectric of the surrounding medium can influence the HOMO and LUMO levels present in a material, since in any material, the presence of a large dielectric will act to lower the energy of the charges. At the interface both materials help solvate the charges, and as such the charges in the higher dielectric material will be destabilized and the charges in the lower dielectric material will be stabilized at the interface. In agreement with our study of band bending at the DCM/C_{60} interface, one experimental study on a CuPc/$CuPcF_{16}$ interface shows that when the molecules are stacked head to tail the dipolar nature of the C-H and C-F bonds shift the HOMO and LUMO levels of both materials.[400] The effect of molecular multipole moments can be very significant, for dipole moments we find that an ordered stacking at the interface could cause up to 1.0 eV shifts in the HOMO and LUMO levels. At the interface, both materials help solvate one another, and if one material is inefficiently packed at the interface, and therefore has a lower dielectric, then both materials will have a decreased effective dielectric constant. Our results and a recent experimental study on the CuPc/C_{60} interface[429] shows that the decreased interfacial dielectric will drive charges in both layers away from the organic/organic interface.

The results presented here suggest that the overall efficiency of OPV devices could be aided by a better consideration of the molecular properties and packing structure.

There is still a lot of improvements that can be made in the field of organic photovoltaics. The work presented here addresses a number of interesting physics in OPV devices on the molecular level. In the future it would be useful to apply the ΔSCF method to excited state dynamics calculations to further understand its capabilities and limitations in computing excited state properties in OPV systems. It would be useful to find a way to fix the intruder state problem in the second order perturbation expansion of the wavefunction in ΔSCF(2), which would then get rid of any empirical parameters to the method.

There are endless numbers of molecules that could preform singlet fission, and setting up an efficient way to screen them through computations can greatly speed up the process of discovery. Further work needs to be done on studying the effect of disorder at the organic/organic interface and delocalization of the charged states. Increased understanding of the electronic processes in organic photovoltaics can help create new design principles for more efficient devices.

Appendix A

Full equations and data for the ΔSCF(2) method

A.1 General Solutions to the ΔSCF(2) Equation

As a review, in Chapter 3 we solve the ΔSCF(2) equations by transforming into a corresponding orbital basis, which in this basis the occupied-occupied block in the overlap matrix is diagonal with matrix elements S_i. The Hamiltonian matrix element we want to evaluate is

$$\langle A^{(0)}|\hat{H}|B^{(1)}\rangle = \frac{1}{4}E_A\langle A^{(0)}|B_{ij}^{ab}\rangle t_{ij}^{ab} + \frac{1}{16}\langle kl\|cd\rangle\langle A_{kl}^{cd}|B_{ij}^{ab}\rangle t_{ij}^{ab} \tag{A.1}$$

In order to evaluate this expression we use the following definitions:

$$\langle \phi_i^A|\phi_j^B\rangle = S_i\delta_{ij} \tag{A.2}$$

$$\langle \phi_a^A|\phi_b^B\rangle = S_{ab} \tag{A.3}$$

$$\langle \phi_i^A|\phi_a^B\rangle = S_{ia} \tag{A.4}$$

$$\langle \phi_a^A|\phi_i^B\rangle = S_{ai} \tag{A.5}$$

$$S_{pr}^{ij} = \langle \phi_p^A | 1 - \sum_{k \neq i,j,s} \frac{|\phi_k^B\rangle\langle\phi_k^A|}{S_k} |\phi_r^B\rangle \tag{A.6}$$

$$S_{pr}^{i} = \langle \phi_p^A | 1 - \sum_{k \neq i,s} \frac{|\phi_k^B\rangle\langle\phi_k^A|}{S_k} |\phi_r^B\rangle \tag{A.7}$$

$$\langle A^{(0)} | B^{(0)} \rangle = \prod_k^N S_k \tag{A.8}$$

In the above equations and below, we use indices i, j, k, l for occupied orbitals, a, b, c, d for virtual orbitals, and p, q, r, s for either type of orbital, as well as index notation. The sums in S_{pr}^{ij} and S_{pr}^{i} have been slightly modified to not include any orbital s in the sum such that $S_s = 0$. We do this because the solution to Eq. 13 in the main text are unsuitable if there is an $S_s = 0$, since it leads to division by zero. Instead we can separate the evaluation of Eq. 13 into cases with different numbers vanishing S_s. If all S_s are non-zero, then we can use the solution in the main text, and if there are three or more s such that $S_s = 0$, then the total matrix element is zero. Therefore, all we need to derive are solutions to Eq. 13 from the main text that take into account the cases where one or two s give $S_s = 0$.

In general we can write the first term on the RHS of Eq. A.1 as:

$$\frac{1}{4} E_A \langle A^{(0)} | B_{ij}^{ab} \rangle t_{ij}^{ab} = \frac{1}{2} E_A S_{ai} S_{bj} \langle A^{(0)} | B^{(0)} \rangle_{ij} t_{ij}^{ab} \tag{A.9}$$

Where here we define $\langle A^{(0)} | B^{(0)} \rangle_{ij} = \prod_{k \neq i,j}^{N} S_k$. Eq. A.9 is a general solution that will work no matter how many $S_s = 0$, which means all we need are expressions for the second term on the RHS of Eq. A.1 for the cases of one and two $S_s = 0$.

A.2 No $S_s = 0$

For completeness, we first present the case where we have no $S_s = 0$, which is described in detail in the chapter 3. The solution is broken up into three parts reflecting different numbers of common indicies.

Case 1: $i = k$, $j = l$

$$\frac{1}{2}\frac{\left[\langle ij\|cd\rangle S^{ij}_{ac}\right]\left[t^{ab}_{ij}S^{ij}_{bd}\right]\langle A^{(0)}|B^{(0)}\rangle}{S_iS_j} \tag{A.10}$$

We place terms in brackets to indicate where they can be summed independently to reduce the scaling. Eq. A.10 scales as $N^2_{\text{occ}} \times N^3_{\text{virt}}$.

Case II $i = k$, $j \neq l$

$$\left[\frac{\langle il\|cd\rangle S_{ld}}{S_l}\right]\left[\frac{t^{ab}_{ij}S_{bj}}{S_j}\right]\frac{S^i_{ac}\langle A^{(0)}|B^{(0)}\rangle}{S_i} - \left[\frac{\langle ij\|cd\rangle S_{jd}}{S_j}\right]\left[\frac{t^{ab}_{ij}S_{bj}}{S_j}\right]\frac{S^i_{ac}\langle A^{(0)}|B^{(0)}\rangle}{S_i} \tag{A.11}$$

The second term of A.11 corrects for the inclusion of $j = l$ in the first term. While this expression is more complicated than restricting the implicit sum in the first term, it permits evaluation with a better scaling, namely $N^3_{\text{occ}}N^2_{\text{virt}}$.

Case III $i \neq k$, $j \neq l$

$$\frac{1}{4}\left[\frac{\langle kl\|cd\rangle S_{kc}S_{ld}}{S_kS_l}\right]\left[\frac{t^{ab}_{ij}S_{ai}S_{bj}}{S_iS_j}\right]\langle A^{(0)}|B^{(0)}\rangle - \left[\frac{\langle il\|cd\rangle S_{ic}S_{ld}}{S_iS_l}\right]\left[\frac{t^{ab}_{ij}S_{ai}S_{bj}}{S_iS_j}\right]\langle A^{(0)}|B^{(0)}\rangle$$

$$+\frac{1}{2}\left[\frac{\langle ij\|cd\rangle S_{ic}S_{jd}}{S_iS_j}\right]\left[\frac{t^{ab}_{ij}S_{ai}S_{bj}}{S_iS_j}\right]\langle A^{(0)}|B^{(0)}\rangle \tag{A.12}$$

Again, the second and third terms in this expression are correction factors which could be avoided if restrictions were placed on the sums in the first terms; but evaluation of the expression is more efficient in this form.

The key to solving Eq. A.10–A.12 is to break up the sum into two sums. The first sum will be over terms where $S_s \neq 0$, we will use the same notation as above for these terms. The second part of the sum will be over terms where $S_s = 0$; here we will place a bar over these terms to indicate this restriction. We can then solve for Eq. A.10–A.12 by breaking up the sums into these two different parts for the cases where there is one or two $S_s = 0$.

A.3 One $S_s = 0$

Here we assume that only one $S_s = 0$. Our solutions will use the following two definitions.

$$\bar{S}^{ij}_{rp} = \langle\phi^A_r| - {\sum_{k\neq i,j}}' \frac{|\phi^B_k\rangle\langle\phi^A_k|}{S_k}|\phi^B_p\rangle \tag{A.13}$$

$$\bar{S}^{i}_{rp} = \langle\phi^A_r| - {\sum_{k\neq i}}' \frac{|\phi^B_k\rangle\langle\phi^A_k|}{S_k}|\phi^B_p\rangle \tag{A.14}$$

Here, the primed sum only sums over the cases where $S_s = 0$. Now we can break up the second term in the RHS of Eq. A.1 in terms of the number of zeros in the overlap matrix eigenvalues. Again we need to break up our solution into three cases, based on the number of common indicies.

Case 1: $i = k$, $j = l$

$$\left(\left[\langle ij||cd\rangle S^{ij}_{ac}\right]\left[t^{ab}_{ij}\bar{S}^{ij}_{bd}\right] + \left[\langle ij||cd\rangle \bar{S}^{ij}_{ac}\right]\left[t^{ab}_{ij}S^{ij}_{bd}\right]\right)\frac{\langle A^{(0)}\bar{|}B^{(0)}\rangle_{ij}}{2} \tag{A.15}$$

$$\langle A^{(0)}\bar{|}B^{(0)}\rangle_{ij} = \prod_{k\neq i,j,p}^{N} S_k \tag{A.16}$$

Where in Eq. A.16 the index p indicates that $S_p = 0$, thus the product does not include any S_k that have a value of 0.

Case 2: $i = k$, $j \neq l$

$$\begin{aligned}
&\left(\left[\langle il||cd\rangle \bar{S}_{ld}\right]\left[\frac{t^{ab}_{ij}S_{bj}}{S_j}\right] + \left[\frac{\langle il||cd\rangle S_{ld}}{S_l}\right]\left[t^{ab}_{ij}\bar{S}_{bj}\right]\right) S^i_{ac}\langle A^{(0)}\bar{|}B^{(0)}\rangle_i \\
&+ \left[\frac{\langle il||cd\rangle S_{ld}}{S_l}\right]\left[\frac{t^{ab}_{ij}S_{bj}}{S_j}\right]\left(S^i_{ac}\langle A^{(0)}|B^{(0)}\rangle_i + \bar{S}^i_{ac}\langle A^{(0)}\bar{|}B^{(0)}\rangle_i\right) \\
&- \left[\frac{\langle ij||cd\rangle S_{jd}}{S_j}\right]\left[\frac{t^{ab}_{ij}S_{bj}}{S_j}\right]\left(S^i_{ac}\langle A^{(0)}|B^{(0)}\rangle + \bar{S}^i_{ac}\langle A^{(0)}\bar{|}B^{(0)}\rangle_i\right)
\end{aligned} \tag{A.17}$$

$$\langle A^{(0)}\bar{|}B^{(0)}\rangle_i = \prod_{k\neq i,p}^{N} S_k\ ;\ \langle A^{(0)}|B^{(0)}\rangle_i = \prod_{k\neq i}^{N} S_k \tag{A.18}$$

Here we again have to subract the terms where we included $j = l$ in our sums.

Case 3: $i \neq k$, $j \neq l$

$$\left(\left[\frac{\langle kl\|cd\rangle S_{kc}S_{ld}}{S_k S_l}\right]\left[\frac{t_{ij}^{ab}S_{ai}\bar{S}_{bj}}{S_i}\right]+\left[\frac{\langle kl\|cd\rangle S_{kc}\bar{S}_{ld}}{S_k}\right]\left[\frac{t_{ij}^{ab}S_{ai}S_{bj}}{S_i S_j}\right]\right)\frac{\langle A^{(0)}\bar{|}B^{(0)}\rangle}{2} \quad (A.19)$$
$$-\left(\left[\frac{\langle il\|cd\rangle S_{ic}S_{ld}}{S_i S_l}\right]\left[\frac{t_{ij}^{ab}S_{ai}\bar{S}_{bj}}{S_i}\right]+\left[\frac{\langle il\|cd\rangle S_{ic}\bar{S}_{ld}}{S_i}\right]\left[\frac{t_{ij}^{ab}S_{ai}S_{bj}}{S_i S_j}\right]\right)\langle A^{(0)}\bar{|}B^{(0)}\rangle$$

$$\langle A^{(0)}\bar{|}B^{(0)}\rangle = \prod_{k\neq p}^{N} S_p \quad (A.20)$$

These equations resolve the case where one $S_s = 0$. The equations are similar in form to the case where no $S_s = 0$, but with the sums broken into parts where we sum over s such that $S_s \neq 0$ and t such that $S_t = 0$.

A.4 Two $S_i = 0$

Finally, we do all of the three cases of common indicies but use the fact that we have exactly two S_p equal to 0. The equations are again a little more complicated in this case, but still have the same general form. **Case 1:** $i = k$, $j = l$

$$\frac{1}{2}\left(\left[\langle ij\|cd\rangle S_{ac}^{ij}\right]\left[t_{ij}^{ab}S_{bd}^{ij}\right]\langle A^{(0)}|B^{(0)}\rangle_{ij}+\left[\langle ij\|cd\rangle \bar{S}_{ac}^{ij}\right]\left[t_{ij}^{ab}S_{bd}^{ij}\right]\langle A^{(0)}\hat{|}B^{(0)}\rangle_{ij}\right) \quad (A.21)$$
$$+\frac{1}{2}\left(\left[\langle ij\|cd\rangle S_{ac}^{ij}\right]\left[t_{ij}^{ab}\bar{S}_{bd}^{ij}\right]\langle A^{(0)}\hat{|}B^{(0)}\rangle_{ij}+\left[\langle ij\|cd\rangle \bar{S}_{ac}^{ij}\right]\left[t_{ij}^{ab}\bar{S}_{bd}^{ij}\right]\langle A^{(0)}\bar{|}B^{(0)}\rangle_{ij}\right)$$

$$\langle A^{(0)}|B^{(0)}\rangle_{ij} = \prod_{k\neq i,j}^{N} S_k \; ; \; \langle A^{(0)}\bar{|}B^{(0)}\rangle_{ij} = \prod_{k\neq i,j,p}^{N} S_k \; ; \; \langle A^{(0)}\hat{|}B^{(0)}\rangle_{ij} = \prod_{k\neq i,j,p}^{N} S_k \quad (A.22)$$

In Eq. A.22 the $\langle A^{(0)}\hat{|}B^{(0)}\rangle_{ij}$ is a little more tricky because it does not include i and j in its products, as well as one of the S_p that equals zero. If for example $S_i \neq 0$ and $S_j \neq 0$, then $\langle A^{(0)}\hat{|}B^{(0)}\rangle_{ij} = 0$ because it includes one of the two S_p that equal 0, but if say $S_i = 0$ and $S_j \neq 0$ then $\langle A^{(0)}\hat{|}B^{(0)}\rangle_{ij} \neq 0$.

Case 2: $i = k$, $j \neq l$

$$
\begin{aligned}
&\left(\left[\langle il \| cd \rangle \bar{S}_{ld} \right] \left[\frac{t_{ij}^{ab} S_{bj}}{S_j} \right] + \left[\frac{\langle il \| cd \rangle S_{ld}}{S_l} \right] \left[t_{ij}^{ab} \bar{S}_{bj} \right] \right) \left(S_{ac}^{i} \langle A^{(0)} \hat{|} B^{(0)} \rangle_i + \bar{S}_{ac}^{i} \langle A^{(0)} \bar{|} B^{(0)} \rangle_i \right) \\
&+ \left[\langle il \| cd \rangle \bar{S}_{ld} \right] \left[t_{ij}^{ab} \bar{S}_{bj} \right] S_{ac}^{i} \langle A^{(0)} \bar{|} B^{(0)} \rangle_i + \left[\frac{\langle il \| cd \rangle S_{ld}}{S_l} \right] \left[\frac{t_{ij}^{ab} S_{bj}}{S_j} \right] \bar{S}_{ac}^{i} \langle A^{(0)} \hat{|} B^{(0)} \rangle_i \\
&- \left[\langle ij \| cd \rangle \bar{S}_{jd} \right] \left[t_{ij}^{ab} \bar{S}_{bj} \right] S_{ac}^{i} \langle A^{(0)} \bar{|} B^{(0)} \rangle_i - \left[\frac{\langle ij \| cd \rangle S_{jd}}{S_j} \right] \left[\frac{t_{ij}^{ab} S_{bj}}{S_j} \right] \bar{S}_{ac}^{i} \langle A^{(0)} \hat{|} B^{(0)} \rangle_i
\end{aligned}
\tag{A.23}
$$

Case 3: $i \neq k,\ j \neq l$

$$
\begin{aligned}
&\left(\left[\frac{\langle kl \| cd \rangle S_{kc} S_{ld}}{S_k S_l} \right] \left[t_{ij}^{ab} \bar{S}_{ai} \bar{S}_{bj} \right] + \left[\langle kl \| cd \rangle \bar{S}_{kc} \bar{S}_{ld} \right] \left[\frac{t_{ij}^{ab} S_{ai} S_{bj}}{S_i S_j} \right] \right) \frac{\langle A^{(0)} \bar{|} B^{(0)} \rangle}{4} \\
&+ \left[\frac{\langle kl \| cd \rangle S_{kc} \bar{S}_{ld}}{S_k} \right] \left[\frac{t_{ij}^{ab} S_{ai} \bar{S}_{bj}}{S_i} \right] \langle A^{(0)} \bar{|} B^{(0)} \rangle - \left[\frac{\langle il \| cd \rangle S_{ic} \bar{S}_{ld}}{S_i} \right] \left[\frac{t_{ij}^{ab} S_{ai} \bar{S}_{bj}}{S_i} \right] \langle A^{(0)} \bar{|} B^{(0)} \rangle \\
&- \left[\frac{\langle kj \| cd \rangle S_{kc} \bar{S}_{jd}}{S_k} \right] \left[\frac{t_{ij}^{ab} S_{ai} \bar{S}_{bj}}{S_i} \right] \langle A^{(0)} \bar{|} B^{(0)} \rangle + \left[\frac{\langle ij \| cd \rangle S_{ic} \bar{S}_{jd}}{S_i} \right] \left[\frac{t_{ij}^{ab} S_{ai} \bar{S}_{bj}}{S_i} \right] \langle A^{(0)} \bar{|} B^{(0)} \rangle
\end{aligned}
\tag{A.24}
$$

Now we have defined all of the equations used to calculate the second term on the RHS of Eq. A.1, taking fully into account the possibility of singular values in the overlap. These equations were used in order to compute the ΔSCF(2) energies in the text.

A.5 Numerical Results for the ΔSCF(2) Method

Below are two tables of ΔSCF(2) energies, which are the source data for Figures 3.1 and 3.3 in chapter 3.

Table A.1: Distance between the two hydrogens in H_2 is in Å and all energies are in Hartree.

Distance	S_0	T_0	S_1	S_2
0.50	-1.07774685	-0.55819124	-0.49405686	0.34769141
0.60	-1.13013860	-0.66509981	-0.58112701	0.14234507
0.70	-1.14783202	-0.73620109	-0.62922547	-0.01160873
0.80	-1.14795740	-0.78815843	-0.65617554	-0.13244142
0.90	-1.13914954	-0.82873262	-0.67120807	-0.23164291
1.00	-1.12594753	-0.86152737	-0.67937325	-0.31617528
1.10	-1.11083046	-0.88829046	-0.68358747	-0.38788287
1.20	-1.09524864	-0.91002386	-0.68561832	-0.44598684
1.30	-1.08011139	-0.92746919	-0.68654557	-0.49195243
1.40	-1.06597554	-0.94128409	-0.68698267	-0.52881312
1.50	-1.05314684	-0.95208306	-0.68721204	-0.55885545
1.60	-1.04176059	-0.96042957	-0.68729705	-0.58338905
1.70	-1.03184035	-0.96681970	-0.68718075	-0.60323551
1.80	-1.02333716	-0.97167276	-0.68676320	-0.61902623
1.90	-1.01615586	-0.97533158	-0.68595203	-0.63130959
2.00	-1.01017315	-0.97806991	-0.68468751	-0.64058216
2.10	-1.00525064	-0.98010312	-0.68294910	-0.64729733
2.20	-1.00124497	-0.98159935	-0.68075086	-0.65186701
2.30	-0.99801614	-0.98268934	-0.67813216	-0.65466102
2.40	-0.99543366	-0.98347468	-0.67514768	-0.65600609
2.50	-0.99338079	-0.98403414	-0.67185901	-0.65618567
2.60	-0.99175658	-0.98442857	-0.66832851	-0.65544130
2.70	-0.99047590	-0.98470474	-0.66461535	-0.65397548
2.80	-0.98946893	-0.98489822	-0.66077329	-0.65195566
2.90	-0.98867898	-0.98503572	-0.65684984	-0.64951874
3.00	-0.98806174	-0.98513694	-0.65288603	-0.64677573
3.10	-0.98757832	-0.98521606	-0.64891681	-0.64381554
3.20	-0.98720221	-0.98528296	-0.64497150	-0.64070972
3.30	-0.98691364	-0.98534420	-0.64107437	-0.63751532
3.40	-0.98669163	-0.98540385	-0.63724526	-0.63427688
3.50	-0.98652355	-0.98546416	-0.63350005	-0.63102993

Table A.2: Distance between hydrogen and flourine in FH is given in Å and the energies are in Hartree

Distance	$X^1\Sigma$	$^3\Pi$	$^1\Pi$	$^3\Sigma$	$^1\Sigma$
0.529178	-99.54589105	-99.00339860	-98.98515497	-98.79276499	-98.78012818
0.661472	-99.96260051	-99.45951833	-99.44035807	-99.27100552	-99.24773500
0.793767	-100.10303259	-99.65287508	-99.63187942	-99.49420494	-99.44657120
0.917065	-100.13616665	-99.74795798	-99.72574352	-99.62027524	-99.53873349
0.926061	-100.13669681	-99.75331009	-99.73107477	-99.62792272	-99.54366072
1.05836	-100.12891374	-99.81715071	-99.79601087	-99.72448570	-99.60070353
1.19065	-100.10620950	-99.86123848	-99.84326395	-99.79655796	-99.64092659
1.32294	-100.07979463	-99.89200363	-99.87790966	-99.84858260	-99.67258494
1.45524	-100.05456832	-99.91339550	-99.90290629	-99.88497334	-99.69811049
1.58753	-100.03261195	-99.92820279	-99.92064497	-99.90993507	-99.71791755
1.83413	-100.00245794	-99.94456736	-99.94066122	-99.93680687	-99.73978605
1.85212	-100.00080536	-99.94536471	-99.94164851	-99.93807490	-99.74065659
2.11671	-99.98381192	-99.95326201	-99.95151163	-99.95010361	-99.74415963
2.64589	-99.97409248	-99.95826133	-99.95791176	-99.95665044	-99.72183400
2.75119	-99.97363202	-99.95857577	-99.95832685	-99.95703433	-99.71589424

Appendix B

Forcefield for Organic Semiconductor Molecules

All of the forcields are created using the same procedure.[189] Starting from a crystal structure the monomer geometries are optimized in the gas phase using PBE0 and 6-31G*. The optimized geometries are then placed in maximal coincidence with the experimentally determined crystal structures. The bond lengths, angles, and diehedral angles are all chosen to match the optimized geometry structure. The force constants are all selected from an OPLS database, or UFF when not available. The point charges were minimized under the constraint that they reproduce the monomer dipole and quadrupole. Any polarizability parameters were chosen such that MM forcefield reproduced the experimental bulk dielectric constant.

B.1 Forcefields

1: tetracene

```
[ defaults ]
1    2    yes          0.5  0.5

[ atomtypes ]
CC       12.0107    0.0000    A     3.34748e-01    2.9288e-01
CB       12.0107    0.0000    A     3.34748e-01    2.9288e-01
CA       12.0107    0.0000    A     3.34748e-01    2.9288e-01
HA        1.0079    0.0000    A     2.28571e-01    1.2552e-01

[ bondtypes ]
   CA    CB     1     1.3635e-01    3.9246e+05
   CA    CC     1     1.4085e-01    3.9246e+05
   CA    HA     1     1.0881e-01    3.0711e+05
   CB    CB     1     1.4269e-01    3.9246e+05
```

```
  CB   HA    1    1.0867e-01    3.0711e+05
  CC   CC    1    1.4458e-01    3.9246e+05

[ angletypes ]
  CA   CB   CB    1    1.2050e+02    5.2718e+02
  CA   CB   HA    1    1.2016e+02    2.9288e+02
  CA   CC   CA    1    1.2220e+02    5.2718e+02
  CA   CC   CC    1    1.1890e+02    5.2718e+02
  CB   CA   CC    1    1.2098e+02    5.2718e+02
  CB   CA   HA    1    1.2064e+02    2.9288e+02
  CB   CB   HA    1    1.1934e+02    2.9288e+02
  CC   CA   CC    1    1.2181e+02    5.2718e+02
  CC   CA   HA    1    1.1885e+02    2.9288e+02

[ dihedraltypes ]
  CA   CB   CB   CA    3    3.0334e+01    0.0000e+00    -3.0334e+01    0.0000e+00    0.0000e+00    0.0000e+00
  CA   CB   CB   HA    3    3.0334e+01    0.0000e+00    -3.0334e+01    0.0000e+00    0.0000e+00    0.0000e+00
  CA   CC   CA   CB    3    3.0334e+01    0.0000e+00    -3.0334e+01    0.0000e+00    0.0000e+00    0.0000e+00
  CA   CC   CA   CC    3    3.0334e+01    0.0000e+00    -3.0334e+01    0.0000e+00    0.0000e+00    0.0000e+00
  CA   CC   CA   HA    3    3.0334e+01    0.0000e+00    -3.0334e+01    0.0000e+00    0.0000e+00    0.0000e+00
  CA   CC   CC   CA    3    3.0334e+01    0.0000e+00    -3.0334e+01    0.0000e+00    0.0000e+00    0.0000e+00
  CB   CA   CC   CC    3    3.0334e+01    0.0000e+00    -3.0334e+01    0.0000e+00    0.0000e+00    0.0000e+00
  CB   CB   CA   CC    3    3.0334e+01    0.0000e+00    -3.0334e+01    0.0000e+00    0.0000e+00    0.0000e+00
  CB   CB   CA   HA    3    3.0334e+01    0.0000e+00    -3.0334e+01    0.0000e+00    0.0000e+00    0.0000e+00
  CC   CA   CB   HA    3    3.0334e+01    0.0000e+00    -3.0334e+01    0.0000e+00    0.0000e+00    0.0000e+00
  CC   CA   CC   CC    3    3.0334e+01    0.0000e+00    -3.0334e+01    0.0000e+00    0.0000e+00    0.0000e+00
  CC   CC   CA   CC    3    3.0334e+01    0.0000e+00    -3.0334e+01    0.0000e+00    0.0000e+00    0.0000e+00
  CC   CC   CA   HA    3    3.0334e+01    0.0000e+00    -3.0334e+01    0.0000e+00    0.0000e+00    0.0000e+00
  HA   CA   CB   HA    3    3.0334e+01    0.0000e+00    -3.0334e+01    0.0000e+00    0.0000e+00    0.0000e+00
  HA   CB   CA   HA    3    3.0334e+01    0.0000e+00    -3.0334e+01    0.0000e+00    0.0000e+00    0.0000e+00
  HA   CB   CB   HA    3    3.0334e+01    0.0000e+00    -3.0334e+01    0.0000e+00    0.0000e+00    0.0000e+00


 [ moleculetype ]
TET           3

[ atoms ]
    1   CA    1       TET   CA1    1   -0.009545   12.0107
    2   CC    1       TET   CC2    2   -0.079715   12.0107
    3   CA    1       TET   CA3    3   -0.055745   12.0107
    4   CB    1       TET   CB4    4   -0.047835   12.0107
    5   CB    1       TET   CB5    5   -0.041887   12.0107
    6   CA    1       TET   CA6    6   -0.051389   12.0107
    7   CC    1       TET   CC7    7   -0.088261   12.0107
    8   CA    1       TET   CA8    8   -0.013825   12.0107
    9   CC    1       TET   CC9    9   -0.047905   12.0107
   10   HA    1       TET   HA10  10    0.107537    1.0079
   11   HA    1       TET   HA11  11    0.088507    1.0079
   12   HA    1       TET   HA12  12    0.042291    1.0079
   13   HA    1       TET   HA13  13    0.060753    1.0079
   14   HA    1       TET   HA14  14    0.075043    1.0079
   15   HA    1       TET   HA15  15    0.094225    1.0079
   16   CC    1       TET   CC16  16   -0.047528   12.0107
   17   CA    1       TET   CA17  17   -0.009545   12.0107
   18   CC    1       TET   CC18  18   -0.079715   12.0107
   19   CA    1       TET   CA19  19   -0.055745   12.0107
   20   CB    1       TET   CB20  20   -0.047835   12.0107
   21   CB    1       TET   CB21  21   -0.041887   12.0107
   22   CA    1       TET   CA22  22   -0.051389   12.0107
   23   CC    1       TET   CC23  23   -0.088261   12.0107
   24   CA    1       TET   CA24  24   -0.013825   12.0107
   25   HA    1       TET   HA25  25    0.068789    1.0079
   26   HA    1       TET   HA26  26    0.039306    1.0079
   27   HA    1       TET   HA27  27    0.090208    1.0079
   28   HA    1       TET   HA28  28    0.069030    1.0079
   29   HA    1       TET   HA29  29    0.051965    1.0079
   30   HA    1       TET   HA30  30    0.084183    1.0079

[ bonds ]
    1    2    1
    1    9    1
    1   10    1
    2    3    1
    2    7    1
    3    4    1
    3   11    1
    4    5    1
    4   12    1
    5    6    1
    5   13    1
    6    7    1
    6   14    1
    7    8    1
    8   15    1
    8   16    1
    9   16    1
    9   24    1
   16   17    1
   17   18    1
   17   30    1
   18   19    1
   18   23    1
```

```
   19   20    1
   19   29    1
   20   21    1
   20   28    1
   21   22    1
   21   27    1
   22   23    1
   22   26    1
   23   24    1
   24   25    1

[ angles ]
    1    2    3    1
    1    2    7    1
    1    9   16    1
    1    9   24    1
    2    1    9    1
    2    1   10    1
    2    3    4    1
    2    3   11    1
    2    7    6    1
    2    7    8    1
    3    2    7    1
    3    4    5    1
    3    4   12    1
    4    3   11    1
    4    5    6    1
    4    5   13    1
    5    4   12    1
    5    6    7    1
    5    6   14    1
    6    5   13    1
    6    7    8    1
    7    6   14    1
    7    8   15    1
    7    8   16    1
    8   16    9    1
    8   16   17    1
    9    1   10    1
    9   16   17    1
    9   24   23    1
    9   24   25    1
   15    8   16    1
   16    9   24    1
   16   17   18    1
   16   17   30    1
   17   18   19    1
   17   18   23    1
   18   17   30    1
   18   19   20    1
   18   19   29    1
   18   23   22    1
   18   23   24    1
   19   18   23    1
   19   20   21    1
   19   20   28    1
   20   19   29    1
   20   21   22    1
   20   21   27    1
   21   20   28    1
   21   22   23    1
   21   22   26    1
   22   21   27    1
   22   23   24    1
   23   22   26    1
   23   24   25    1

[ dihedrals ]
    1    2    3    4    3
    1    2    3   11    3
    1    2    7    6    3
    1    2    7    8    3
    1    9   16    8    3
    1    9   16   17    3
    1    9   24   23    3
    1    9   24   25    3
    2    1    9   16    3
    2    1    9   24    3
    2    3    4    5    3
    2    3    4   12    3
    2    7    6    5    3
    2    7    6   14    3
    2    7    8   15    3
    2    7    8   16    3
    3    2    1    9    3
    3    2    1   10    3
    3    2    7    6    3
    3    2    7    8    3
    3    4    5    6    3
    3    4    5   13    3
    4    3    2    7    3
    4    5    6    7    3
```

```
    4     5     6    14     3
    5     4     3    11     3
    5     6     7     8     3
    6     5     4    12     3
    6     7     8    15     3
    6     7     8    16     3
    7     2     1     9     3
    7     2     1    10     3
    7     2     3    11     3
    7     6     5    13     3
    7     8    16     9     3
    7     8    16    17     3
    8     7     6    14     3
    8    16     9    24     3
    8    16    17    18     3
    8    16    17    30     3
    9    16     8    15     3
    9    16    17    18     3
    9    16    17    30     3
    9    24    23    18     3
    9    24    23    22     3
   10     1     9    16     3
   10     1     9    24     3
   11     3     4    12     3
   12     4     5    13     3
   13     5     6    14     3
   15     8    16    17     3
   16     9    24    23     3
   16     9    24    25     3
   16    17    18    19     3
   16    17    18    23     3
   17    16     9    24     3
   17    18    19    20     3
   17    18    19    29     3
   17    18    23    22     3
   17    18    23    24     3
   18    19    20    21     3
   18    19    20    28     3
   18    23    22    21     3
   18    23    22    26     3
   18    23    24    25     3
   19    18    17    30     3
   19    18    23    22     3
   19    18    23    24     3
   19    20    21    22     3
   19    20    21    27     3
   20    19    18    23     3
   20    21    22    23     3
   20    21    22    26     3
   21    20    19    29     3
   21    22    23    24     3
   22    21    20    28     3
   22    23    24    25     3
   23    18    17    30     3
   23    18    19    29     3
   23    22    21    27     3
   24    23    22    26     3
   26    22    21    27     3
   27    21    20    28     3
   28    20    19    29     3

[ exclusions ]
   10    11
   10    25
   14    15
   15    30
   25    26
   29    30
```

2: H_2Pc

```
[ defaults ]
1    2    yes         0.5  0.5

[ atomtypes ]
CP       12.0107    0.0000    A    3.2390e-01    2.9288e-01
CQ       12.0107    0.0000    A    3.2978e-01    2.9288e-01
CR       12.0107    0.0000    A    2.8467e-01    2.9288e-01
HP        1.0079    0.0000    A    2.0793e-01    1.2552e-01
HQ        1.0079    0.0000    A    3.2390e-01    1.2552e-01
NP       14.0067    0.0000    A    2.6819e-01    7.1128e-01
NQ       14.0067    0.0000    A    3.2563e-01    7.1128e-01
NR       14.0067    0.0000    A    3.2563e-01    7.1128e-01

[ nonbond_params ]
   CP   CP    1    3.4154e-01    2.9288e-01
   CP   CQ    1    3.3338e-01    2.9288e-01
   CP   CR    1    3.2987e-01    2.9288e-01
   CP   HP    1    2.7796e-01    2.0920e-01
   CP   HQ    1    3.3038e-01    2.0920e-01
   CP   NP    1    3.8469e-01    5.0208e-01
```

```
   CP    NQ    1     3.4273e-01     5.0208e-01
   CP    NR    1     3.4012e-01     5.0208e-01
   CQ    CQ    1     3.6453e-01     2.9288e-01
   CQ    CR    1     3.3717e-01     2.9288e-01
   CQ    HP    1     2.8750e-01     2.0920e-01
   CQ    HQ    1     3.7386e-01     2.0920e-01
   CQ    NP    1     3.3591e-01     5.0208e-01
   CQ    NQ    1     3.7050e-01     5.0208e-01
   CQ    NR    1     3.6012e-01     5.0208e-01
   CR    CR    1     3.4328e-01     2.9288e-01
   CR    HP    1     2.5122e-01     2.0920e-01
   CR    HQ    1     4.0479e-01     2.0920e-01
   CR    NP    1     3.2194e-01     5.0208e-01
   CR    NQ    1     3.6210e-01     5.0208e-01
   CR    NR    1     3.4968e-01     5.0208e-01
   HP    HP    1     2.1209e-01     1.2552e-01
   HP    HQ    1     3.9044e-01     1.2552e-01
   HP    NP    1     2.4282e-01     4.1840e-01
   HP    NQ    1     3.4687e-01     4.1840e-01
   HP    NR    1     3.4200e-01     4.1840e-01
   HQ    HQ    1     4.0066e-01     1.2552e-01
   HQ    NP    1     3.3774e-01     4.1840e-01
   HQ    NQ    1     4.1022e-01     4.1840e-01
   HQ    NR    1     3.5034e-01     4.1840e-01
   NP    NP    1     4.5124e-01     7.1128e-01
   NP    NQ    1     3.7332e-01     7.1128e-01
   NP    NR    1     3.7748e-01     7.1128e-01
   NQ    NQ    1     4.4224e-01     7.1128e-01
   NQ    NR    1     3.3214e-01     7.1128e-01
   NR    NR    1     4.1467e-01     7.1128e-01

[ bondtypes ]
   CP    CQ    1     1.4628e-01     3.9246e+05
   CP    NP    1     1.3264e-01     3.5731e+05
   CP    NQ    1     1.3865e-01     3.5731e+05
   CP    NR    1     1.3805e-01     3.5731e+05
   CQ    CQ    1     1.4110e-01     3.9246e+05
   CQ    CR    1     1.3914e-01     3.9246e+05
   CR    CR    1     1.4008e-01     3.9246e+05
   CR    HP    1     1.0830e-01     2.8451e+05
   HQ    NQ    1     1.0203e-01     2.8451e+05

[ angletypes ]
   CP    CQ    CQ    1     1.0689e+02     5.8576e+02
   CP    CQ    CR    1     1.3191e+02     5.8576e+02
   CP    NP    CP    1     1.2483e+02     5.8576e+02
   CP    NQ    CP    1     1.1224e+02     5.8576e+02
   CP    NQ    HQ    1     1.2388e+02     2.9288e+02
   CP    NR    CP    1     1.0699e+02     5.8576e+02
   CQ    CP    NP    1     1.2430e+02     5.8576e+02
   CQ    CP    NQ    1     1.0614e+02     5.8576e+02
   CQ    CP    NR    1     1.1046e+02     5.8576e+02
   CQ    CQ    CR    1     1.2119e+02     5.8576e+02
   CQ    CR    CR    1     1.1768e+02     5.8576e+02
   CQ    CR    HP    1     1.2043e+02     2.9288e+02
   CR    CR    CR    1     1.2112e+02     5.8576e+02
   CR    CR    HP    1     1.2025e+02     2.9288e+02
   NP    CP    NQ    1     1.2765e+02     5.8576e+02
   NP    CP    NR    1     1.2714e+02     5.8576e+02

[ dihedraltypes ]
   CP    CQ    CQ    CP    3    3.0334e+01    0.0000e+00    -3.0334e+01    0.0000e+00    0.0000e+00    0.0000e+00
   CP    CQ    CQ    CR    3    3.0334e+01    0.0000e+00    -3.0334e+01    0.0000e+00    0.0000e+00    0.0000e+00
   CP    CQ    CR    CR    3    3.0334e+01    0.0000e+00    -3.0334e+01    0.0000e+00    0.0000e+00    0.0000e+00
   CP    CQ    CR    HP    3    3.0334e+01    0.0000e+00    -3.0334e+01    0.0000e+00    0.0000e+00    0.0000e+00
   CP    NP    CP    CQ    3    3.0334e+01    0.0000e+00    -3.0334e+01    0.0000e+00    0.0000e+00    0.0000e+00
   CP    NP    CP    NQ    3    3.0334e+01    0.0000e+00    -3.0334e+01    0.0000e+00    0.0000e+00    0.0000e+00
   CP    NP    CP    NR    3    3.0334e+01    0.0000e+00    -3.0334e+01    0.0000e+00    0.0000e+00    0.0000e+00
   CP    NQ    CP    CQ    3    3.0334e+01    0.0000e+00    -3.0334e+01    0.0000e+00    0.0000e+00    0.0000e+00
   CP    NQ    CP    NP    3    3.0334e+01    0.0000e+00    -3.0334e+01    0.0000e+00    0.0000e+00    0.0000e+00
   CP    NR    CP    CQ    3    3.0334e+01    0.0000e+00    -3.0334e+01    0.0000e+00    0.0000e+00    0.0000e+00
   CP    NR    CP    NP    3    3.0334e+01    0.0000e+00    -3.0334e+01    0.0000e+00    0.0000e+00    0.0000e+00
   CQ    CP    NQ    HQ    3    3.0334e+01    0.0000e+00    -3.0334e+01    0.0000e+00    0.0000e+00    0.0000e+00
   CQ    CQ    CP    NP    3    3.0334e+01    0.0000e+00    -3.0334e+01    0.0000e+00    0.0000e+00    0.0000e+00
   CQ    CQ    CP    NQ    3    3.0334e+01    0.0000e+00    -3.0334e+01    0.0000e+00    0.0000e+00    0.0000e+00
   CQ    CQ    CP    NR    3    3.0334e+01    0.0000e+00    -3.0334e+01    0.0000e+00    0.0000e+00    0.0000e+00
   CQ    CQ    CR    CR    3    3.0334e+01    0.0000e+00    -3.0334e+01    0.0000e+00    0.0000e+00    0.0000e+00
   CQ    CQ    CR    HP    3    3.0334e+01    0.0000e+00    -3.0334e+01    0.0000e+00    0.0000e+00    0.0000e+00
   CQ    CR    CR    CR    3    3.0334e+01    0.0000e+00    -3.0334e+01    0.0000e+00    0.0000e+00    0.0000e+00
   CQ    CR    CR    HP    3    3.0334e+01    0.0000e+00    -3.0334e+01    0.0000e+00    0.0000e+00    0.0000e+00
   CR    CQ    CP    NP    3    3.0334e+01    0.0000e+00    -3.0334e+01    0.0000e+00    0.0000e+00    0.0000e+00
   CR    CQ    CP    NQ    3    3.0334e+01    0.0000e+00    -3.0334e+01    0.0000e+00    0.0000e+00    0.0000e+00
   CR    CQ    CP    NR    3    3.0334e+01    0.0000e+00    -3.0334e+01    0.0000e+00    0.0000e+00    0.0000e+00
   CR    CQ    CQ    CR    3    3.0334e+01    0.0000e+00    -3.0334e+01    0.0000e+00    0.0000e+00    0.0000e+00
   CR    CR    CR    CR    3    3.0334e+01    0.0000e+00    -3.0334e+01    0.0000e+00    0.0000e+00    0.0000e+00
   CR    CR    CR    HP    3    3.0334e+01    0.0000e+00    -3.0334e+01    0.0000e+00    0.0000e+00    0.0000e+00
   HP    CR    CR    HP    3    3.0334e+01    0.0000e+00    -3.0334e+01    0.0000e+00    0.0000e+00    0.0000e+00
   HQ    NQ    CP    NP    3    3.0334e+01    0.0000e+00    -3.0334e+01    0.0000e+00    0.0000e+00    0.0000e+00

[ moleculetype ]
PHT          3
```

```
[ atoms ]
    1   NP    1       PHT    NP1    1   -0.018477   14.0067
    2   CP    1       PHT    CP2    2   -0.023938   12.0107
    3   CQ    1       PHT    CQ3    3   -0.015396   12.0107
    4   CR    1       PHT    CR4    4    0.018239   12.0107
    5   HP    1       PHT    HP5    5    0.000000    1.0079
    6   CR    1       PHT    CR6    6    0.053439   12.0107
    7   HP    1       PHT    HP7    7    0.000000    1.0079
    8   CR    1       PHT    CR8    8    0.053439   12.0107
    9   HP    1       PHT    HP9    9    0.000000    1.0079
   10   CR    1       PHT   CR10   10    0.018239   12.0107
   11   HP    1       PHT   HP11   11    0.000000    1.0079
   12   CQ    1       PHT   CQ12   12   -0.015396   12.0107
   13   CP    1       PHT   CP13   13   -0.023938   12.0107
   14   NQ    1       PHT   NQ14   14   -0.029079   14.0067
   15   HQ    1       PHT   HQ15   15    0.000000    1.0079
   16   NP    1       PHT   NP16   16   -0.018477   14.0067
   17   CP    1       PHT   CP17   17   -0.024117   12.0107
   18   CQ    1       PHT   CQ18   18   -0.015409   12.0107
   19   CR    1       PHT   CR19   19    0.012703   12.0107
   20   HP    1       PHT   HP20   20    0.000000    1.0079
   21   CR    1       PHT   CR21   21    0.042888   12.0107
   22   HP    1       PHT   HP22   22    0.000000    1.0079
   23   CR    1       PHT   CR23   23    0.042888   12.0107
   24   HP    1       PHT   HP24   24    0.000000    1.0079
   25   CR    1       PHT   CR25   25    0.012703   12.0107
   26   HP    1       PHT   HP26   26    0.000000    1.0079
   27   CQ    1       PHT   CQ27   27   -0.015409   12.0107
   28   CP    1       PHT   CP28   28   -0.024117   12.0107
   29   NR    1       PHT   NR29   29   -0.030785   14.0067
   30   NP    1       PHT   NP30   30   -0.018477   14.0067
   31   CP    1       PHT   CP31   31   -0.023938   12.0107
   32   CQ    1       PHT   CQ32   32   -0.015396   12.0107
   33   CR    1       PHT   CR33   33    0.018239   12.0107
   34   HP    1       PHT   HP34   34    0.000000    1.0079
   35   CR    1       PHT   CR35   35    0.053439   12.0107
   36   HP    1       PHT   HP36   36    0.000000    1.0079
   37   CR    1       PHT   CR37   37    0.053439   12.0107
   38   HP    1       PHT   HP38   38    0.000000    1.0079
   39   CR    1       PHT   CR39   39    0.018239   12.0107
   40   HP    1       PHT   HP40   40    0.000000    1.0079
   41   CQ    1       PHT   CQ41   41   -0.015396   12.0107
   42   CP    1       PHT   CP42   42   -0.023938   12.0107
   43   NQ    1       PHT   NQ43   43   -0.029079   14.0067
   44   HQ    1       PHT   HQ44   44    0.000000    1.0079
   45   NP    1       PHT   NP45   45   -0.018477   14.0067
   46   CP    1       PHT   CP46   46   -0.024117   12.0107
   47   CQ    1       PHT   CQ47   47   -0.015409   12.0107
   48   CR    1       PHT   CR48   48    0.012703   12.0107
   49   HP    1       PHT   HP49   49    0.000000    1.0079
   50   CR    1       PHT   CR50   50    0.042888   12.0107
   51   HP    1       PHT   HP51   51    0.000000    1.0079
   52   CR    1       PHT   CR52   52    0.042888   12.0107
   53   HP    1       PHT   HP53   53    0.000000    1.0079
   54   CR    1       PHT   CR54   54    0.012703   12.0107
   55   HP    1       PHT   HP55   55    0.000000    1.0079
   56   CQ    1       PHT   CQ56   56   -0.015409   12.0107
   57   CP    1       PHT   CP57   57   -0.024117   12.0107
   58   NR    1       PHT   NR58   58   -0.030785   14.0067

[ bonds ]
    1    2    1
    1   57    1
    2    3    1
    2   14    1
    3    4    1
    3   12    1
    4    5    1
    4    6    1
    6    7    1
    6    8    1
    8    9    1
    8   10    1
   10   11    1
   10   12    1
   12   13    1
   13   14    1
   13   16    1
   14   15    1
   16   17    1
   17   18    1
   17   29    1
   18   19    1
   18   27    1
   19   20    1
   19   21    1
   21   22    1
   21   23    1
   23   24    1
   23   25    1
   25   26    1
   25   27    1
```

```
    27    28     1
    28    29     1
    28    30     1
    30    31     1
    31    32     1
    31    43     1
    32    33     1
    32    41     1
    33    34     1
    33    35     1
    35    36     1
    35    37     1
    37    38     1
    37    39     1
    39    40     1
    39    41     1
    41    42     1
    42    43     1
    42    45     1
    43    44     1
    45    46     1
    46    47     1
    46    58     1
    47    48     1
    47    56     1
    48    49     1
    48    50     1
    50    51     1
    50    52     1
    52    53     1
    52    54     1
    54    55     1
    54    56     1
    56    57     1
    57    58     1

[ angles ]
     1     2     3     1
     1     2    14     1
     1    57    56     1
     1    57    58     1
     2     1    57     1
     2     3     4     1
     2     3    12     1
     2    14    13     1
     2    14    15     1
     3     2    14     1
     3     4     5     1
     3     4     6     1
     3    12    10     1
     3    12    13     1
     4     3    12     1
     4     6     7     1
     4     6     8     1
     5     4     6     1
     6     8     9     1
     6     8    10     1
     7     6     8     1
     8    10    11     1
     8    10    12     1
     9     8    10     1
    10    12    13     1
    11    10    12     1
    12    13    14     1
    12    13    16     1
    13    14    15     1
    13    16    17     1
    14    13    16     1
    16    17    18     1
    16    17    29     1
    17    18    19     1
    17    18    27     1
    17    29    28     1
    18    17    29     1
    18    19    20     1
    18    19    21     1
    18    27    25     1
    18    27    28     1
    19    18    27     1
    19    21    22     1
    19    21    23     1
    20    19    21     1
    21    23    24     1
    21    23    25     1
    22    21    23     1
    23    25    26     1
    23    25    27     1
    24    23    25     1
    25    27    28     1
    26    25    27     1
    27    28    29     1
    27    28    30     1
```

```
  28   30   31    1
  29   28   30    1
  30   31   32    1
  30   31   43    1
  31   32   33    1
  31   32   41    1
  31   43   42    1
  31   43   44    1
  32   31   43    1
  32   33   34    1
  32   33   35    1
  32   41   39    1
  32   41   42    1
  33   32   41    1
  33   35   36    1
  33   35   37    1
  34   33   35    1
  35   37   38    1
  35   37   39    1
  36   35   37    1
  37   39   40    1
  37   39   41    1
  38   37   39    1
  39   41   42    1
  40   39   41    1
  41   42   43    1
  41   42   45    1
  42   43   44    1
  42   45   46    1
  43   42   45    1
  45   46   47    1
  45   46   58    1
  46   47   48    1
  46   47   56    1
  46   58   57    1
  47   46   58    1
  47   48   49    1
  47   48   50    1
  47   56   54    1
  47   56   57    1
  48   47   56    1
  48   50   51    1
  48   50   52    1
  49   48   50    1
  50   52   53    1
  50   52   54    1
  51   50   52    1
  52   54   55    1
  52   54   56    1
  53   52   54    1
  54   56   57    1
  55   54   56    1
  56   57   58    1

[ dihedrals ]
    1    2    3    4    3
    1    2    3   12    3
    1    2   14   13    3
    1    2   14   15    3
    1   57   56   47    3
    1   57   56   54    3
    1   57   58   46    3
    2    1   57   56    3
    2    1   57   58    3
    2    3    4    5    3
    2    3    4    6    3
    2    3   12   10    3
    2    3   12   13    3
    2   14   13   12    3
    2   14   13   16    3
    3    2    1   57    3
    3    2   14   13    3
    3    2   14   15    3
    3    4    6    7    3
    3    4    6    8    3
    3   12   10    8    3
    3   12   10   11    3
    3   12   13   14    3
    3   12   13   16    3
    4    3    2   14    3
    4    3   12   10    3
    4    3   12   13    3
    4    6    8    9    3
    4    6    8   10    3
    5    4    3   12    3
    5    4    6    7    3
    5    4    6    8    3
    6    4    3   12    3
    6    8   10   11    3
    6    8   10   12    3
    7    6    8    9    3
    7    6    8   10    3
```

8	10	12	13	3
9	8	10	11	3
9	8	10	12	3
10	12	13	14	3
10	12	13	16	3
11	10	12	13	3
12	3	2	14	3
12	13	14	15	3
12	13	16	17	3
13	16	17	18	3
13	16	17	29	3
14	2	1	57	3
14	13	16	17	3
15	14	13	16	3
16	17	18	19	3
16	17	18	27	3
16	17	29	28	3
17	18	19	20	3
17	18	19	21	3
17	18	27	26	3
17	18	27	28	3
17	29	28	27	3
17	29	28	30	3
18	17	29	28	3
18	19	21	22	3
18	19	21	23	3
18	27	25	23	3
18	27	25	26	3
18	27	28	29	3
18	27	28	30	3
19	18	17	29	3
19	18	27	26	3
19	18	27	28	3
19	21	23	24	3
19	21	23	26	3
20	19	18	27	3
20	19	21	22	3
20	19	21	23	3
21	19	18	27	3
21	23	25	26	3
21	23	25	27	3
22	21	23	24	3
22	21	23	26	3
23	26	27	28	3
24	23	25	26	3
24	23	25	27	3
25	27	28	29	3
26	27	28	30	3
26	25	27	28	3
27	18	17	29	3
27	28	30	31	3
28	30	31	32	3
28	30	31	43	3
29	28	30	31	3
30	31	32	33	3
30	31	32	41	3
30	31	43	42	3
30	31	43	44	3
31	32	33	34	3
31	32	33	35	3
31	32	41	39	3
31	32	41	42	3
31	43	42	41	3
31	43	42	45	3
32	31	43	42	3
32	31	43	44	3
32	33	35	36	3
32	33	35	37	3
32	41	39	37	3
32	41	39	40	3
32	41	42	43	3
32	41	42	45	3
33	32	31	43	3
33	32	41	39	3
33	32	41	42	3
33	35	37	38	3
33	35	37	39	3
34	33	32	41	3
34	33	35	36	3
34	33	35	37	3
35	33	32	41	3
35	37	39	40	3
35	37	39	41	3
36	35	37	38	3
36	35	37	39	3
37	39	41	42	3
38	37	39	40	3
38	37	39	41	3
39	41	42	43	3
39	41	42	45	3
40	39	41	42	3
41	32	31	43	3

```
  41   42   43   44    3
  41   42   45   46    3
  42   45   46   47    3
  42   45   46   58    3
  43   42   45   46    3
  44   43   42   45    3
  45   46   47   48    3
  45   46   47   56    3
  45   46   58   57    3
  46   47   48   49    3
  46   47   48   50    3
  46   47   56   54    3
  46   47   56   57    3
  46   58   57   56    3
  47   46   58   57    3
  47   48   50   51    3
  47   48   50   52    3
  47   56   54   52    3
  47   56   54   55    3
  47   56   57   58    3
  48   47   46   58    3
  48   47   56   54    3
  48   47   56   57    3
  48   50   52   53    3
  48   50   52   54    3
  49   48   47   56    3
  49   48   50   51    3
  49   48   50   52    3
  50   48   47   56    3
  50   52   54   55    3
  50   52   54   56    3
  51   50   52   53    3
  51   50   52   54    3
  52   54   56   57    3
  53   52   54   55    3
  53   52   54   56    3
  54   56   57   58    3
  55   54   56   57    3
  56   47   46   58    3

[ exclusions ]
   14    58
   14    29
   14    43
   14    44
   15    17
   15    57
   15    58
   15    29
   15    28
   15    43
   15    44
   28    44
   29    43
   29    44
   29    58
   43    58
   44    46
   44    58
   44    57
```

3: Perylene-3,4,9,10-tetracarboxyl-bis-benzimidazole (PTCBI)

```
[ defaults ]
1    2     yes          0.5  0.5

[ atomtypes ]
C        12.0107    0.0000    A    3.4926e-01    4.3932e-01
CA       12.0107    0.0000    A    3.4211e-01    2.9288e-01
CB       12.0107    0.0000    A    3.2915e-01    2.9288e-01
CC       12.0107    0.0000    A    3.4136e-01    2.9288e-01
CD       12.0107    0.0000    A    3.4369e-01    2.9288e-01
CE       12.0107    0.0000    A    3.4136e-01    2.9288e-01
CF       12.0107    0.0000    A    3.4211e-01    2.9288e-01
CG       12.0107    0.0000    A    3.4525e-01    2.9288e-01
H         1.0079    0.0000    A    1.9630e-01    1.2552e-01
N        14.0067    0.0000    A    3.6771e-01    7.1128e-01
NA       14.0067    0.0000    A    3.4935e-01    7.1128e-01
O        15.9994    0.0000    A    3.0572e-01    8.7864e-01

[ nonbond_params ]
    C    C    1    4.5162e-01    4.3932e-01
    C   CA    1    3.5424e-01    3.6610e-01
    C   CB    1    3.2306e-01    3.6610e-01
    C   CC    1    4.6750e-01    3.6610e-01
    C   CD    1    3.4468e-01    3.6610e-01
    C   CE    1    3.9132e-01    3.6610e-01
    C   CF    1    4.0011e-01    3.6610e-01
    C   CG    1    3.8635e-01    3.6610e-01
    C    H    1    3.3016e-01    2.8242e-01
    C    N    1    4.0404e-01    5.7530e-01
```

```
   C    NA     1     4.6172e-01     5.7530e-01
   C     O     1     4.4611e-01     6.5898e-01
  CA    CA     1     3.3649e-01     2.9288e-01
  CA    CB     1     3.2537e-01     2.9288e-01
  CA    CC     1     3.5296e-01     2.9288e-01
  CA    CD     1     3.2657e-01     2.9288e-01
  CA    CE     1     3.3687e-01     2.9288e-01
  CA    CF     1     3.2582e-01     2.9288e-01
  CA    CG     1     3.2881e-01     2.9288e-01
  CA     H     1     3.3512e-01     2.0920e-01
  CA     N     1     3.3822e-01     5.0208e-01
  CA    NA     1     3.3271e-01     5.0208e-01
  CA     O     1     3.9216e-01     5.8576e-01
  CB    CB     1     3.1348e-01     2.9288e-01
  CB    CC     1     3.2252e-01     2.9288e-01
  CB    CD     1     3.2922e-01     2.9288e-01
  CB    CE     1     3.5162e-01     2.9288e-01
  CB    CF     1     3.6835e-01     2.9288e-01
  CB    CG     1     3.4934e-01     2.9288e-01
  CB     H     1     2.5890e-01     2.0920e-01
  CB     N     1     3.3184e-01     5.0208e-01
  CB    NA     1     3.2970e-01     5.0208e-01
  CB     O     1     3.1568e-01     5.8576e-01
  CC    CC     1     4.5162e-01     2.9288e-01
  CC    CD     1     3.8763e-01     2.9288e-01
  CC    CE     1     3.2511e-01     2.9288e-01
  CC    CF     1     3.3711e-01     2.9288e-01
  CC    CG     1     3.4064e-01     2.9288e-01
  CC     H     1     3.4111e-01     2.0920e-01
  CC     N     1     4.5428e-01     5.0208e-01
  CC    NA     1     3.9089e-01     5.0208e-01
  CC     O     1     5.4782e-01     5.8576e-01
  CD    CD     1     4.5162e-01     2.9288e-01
  CD    CE     1     4.0437e-01     2.9288e-01
  CD    CF     1     3.4391e-01     2.9288e-01
  CD    CG     1     4.3751e-01     2.9288e-01
  CD     H     1     3.2938e-01     2.0920e-01
  CD     N     1     3.7083e-01     5.0208e-01
  CD    NA     1     4.6889e-01     5.0208e-01
  CD     O     1     3.9655e-01     5.8576e-01
  CE    CE     1     3.3666e-01     2.9288e-01
  CE    CF     1     3.5255e-01     2.9288e-01
  CE    CG     1     4.0819e-01     2.9288e-01
  CE     H     1     4.0248e-01     2.0920e-01
  CE     N     1     3.5197e-01     5.0208e-01
  CE    NA     1     3.6322e-01     5.0208e-01
  CE     O     1     4.6513e-01     5.8576e-01
  CF    CF     1     4.1542e-01     2.9288e-01
  CF    CG     1     3.4480e-01     2.9288e-01
  CF     H     1     4.0108e-01     2.0920e-01
  CF     N     1     3.3839e-01     5.0208e-01
  CF    NA     1     3.4327e-01     5.0208e-01
  CF     O     1     4.5411e-01     5.8576e-01
  CG    CG     1     4.5162e-01     2.9288e-01
  CG     H     1     3.0737e-01     2.0920e-01
  CG     N     1     3.6671e-01     5.0208e-01
  CG    NA     1     3.9745e-01     5.0208e-01
  CG     O     1     4.1527e-01     5.8576e-01
   H     H     1     1.8695e-01     1.2552e-01
   H     N     1     3.7041e-01     4.1840e-01
   H    NA     1     2.7731e-01     4.1840e-01
   H     O     1     2.3906e-01     5.0208e-01
   N     N     1     4.5162e-01     7.1128e-01
   N    NA     1     4.4718e-01     7.1128e-01
   N     O     1     4.6133e-01     7.9496e-01
  NA    NA     1     4.5162e-01     7.1128e-01
  NA     O     1     4.4464e-01     7.9496e-01
   O     O     1     4.5162e-01     8.7864e-01

[ bondtypes ]
   C    CA     1     1.4788e-01     3.3472e+05
   C     N     1     1.4021e-01     4.1003e+05
   C     O     1     1.2394e-01     4.7698e+05
  CA    CA     1     1.4702e-01     3.9246e+05
  CA    CB     1     1.3916e-01     3.9246e+05
  CA    CC     1     1.4402e-01     3.9246e+05
  CA    CE     1     1.4338e-01     3.9246e+05
  CA    CF     1     1.4233e-01     3.9246e+05
  CB    CB     1     1.3978e-01     3.9246e+05
  CB    CD     1     1.3904e-01     3.9246e+05
  CB    CG     1     1.3960e-01     3.9246e+05
  CB     H     1     1.0818e-01     3.0711e+05
  CC     N     1     1.4173e-01     3.5731e+05
  CC    NA     1     1.3199e-01     3.5731e+05
  CD    CG     1     1.4191e-01     3.9246e+05
  CD     N     1     1.4020e-01     3.5731e+05
  CE    CF     1     1.4305e-01     3.9246e+05
  CG    NA     1     1.4111e-01     3.5731e+05

[ angletypes ]
   C    CA    CB     1     1.1772e+02     7.1128e+02
   C    CA    CF     1     1.2242e+02     7.1128e+02
```

```
  C    N   CC   1   1.2556e+02   4.1840e+02
  C    N   CD   1   1.2786e+02   4.1840e+02
 CA    C    N   1   1.1388e+02   5.8576e+02
 CA    C    O   1   1.2452e+02   6.6944e+02
 CA   CA   CB   1   1.2207e+02   5.2718e+02
 CA   CA   CE   1   1.1923e+02   5.2718e+02
 CA   CB   CB   1   1.2119e+02   5.2718e+02
 CA   CB    H   1   1.1927e+02   2.9288e+02
 CA   CC    N   1   1.1921e+02   5.8576e+02
 CA   CC   NA   1   1.2851e+02   5.8576e+02
 CA   CE   CA   1   1.2155e+02   5.2718e+02
 CA   CE   CF   1   1.1923e+02   5.2718e+02
 CA   CF   CA   1   1.2049e+02   5.2718e+02
 CA   CF   CE   1   1.1976e+02   5.2718e+02
 CB   CA   CC   1   1.2155e+02   5.2718e+02
 CB   CA   CE   1   1.1871e+02   5.2718e+02
 CB   CA   CF   1   1.1993e+02   5.2718e+02
 CB   CB   CB   1   1.2146e+02   5.2718e+02
 CB   CB   CD   1   1.1665e+02   5.2718e+02
 CB   CB   CG   1   1.1791e+02   5.2718e+02
 CB   CB    H   1   1.2001e+02   2.9288e+02
 CB   CD   CG   1   1.2253e+02   5.2718e+02
 CB   CD    N   1   1.3228e+02   5.8576e+02
 CB   CG   CD   1   1.1998e+02   5.2718e+02
 CB   CG   NA   1   1.2983e+02   5.8576e+02
 CC   CA   CF   1   1.1844e+02   5.2718e+02
 CC    N   CD   1   1.0668e+02   5.8576e+02
 CC   NA   CG   1   1.0576e+02   5.8576e+02
 CD   CB    H   1   1.2041e+02   2.9288e+02
 CD   CG   NA   1   1.1019e+02   5.8576e+02
 CG   CB    H   1   1.2014e+02   2.9288e+02
 CG   CD    N   1   1.0519e+02   5.8576e+02
  N    C    O   1   1.2159e+02   6.6944e+02
  N   CC   NA   1   1.1228e+02   5.8576e+02

[ dihedraltypes ]
  C   CA   CB   CB   3   3.0334e+01   0.0000e+00   -3.0334e+01   0.0000e+00   0.0000e+00   0.0000e+00
  C   CA   CB    H   3   3.0334e+01   0.0000e+00   -3.0334e+01   0.0000e+00   0.0000e+00   0.0000e+00
  C   CA   CF   CA   3   3.0334e+01   0.0000e+00   -3.0334e+01   0.0000e+00   0.0000e+00   0.0000e+00
  C   CA   CF   CE   3   3.0334e+01   0.0000e+00   -3.0334e+01   0.0000e+00   0.0000e+00   0.0000e+00
  C    N   CC   CA   3   3.0334e+01   0.0000e+00   -3.0334e+01   0.0000e+00   0.0000e+00   0.0000e+00
  C    N   CC   NA   3   3.0334e+01   0.0000e+00   -3.0334e+01   0.0000e+00   0.0000e+00   0.0000e+00
  C    N   CD   CB   3   3.0334e+01   0.0000e+00   -3.0334e+01   0.0000e+00   0.0000e+00   0.0000e+00
  C    N   CD   CG   3   3.0334e+01   0.0000e+00   -3.0334e+01   0.0000e+00   0.0000e+00   0.0000e+00
 CA    C    N   CC   3   3.0334e+01   0.0000e+00   -3.0334e+01   0.0000e+00   0.0000e+00   0.0000e+00
 CA    C    N   CD   3   3.0334e+01   0.0000e+00   -3.0334e+01   0.0000e+00   0.0000e+00   0.0000e+00
 CA   CA   CB   CB   3   3.0334e+01   0.0000e+00   -3.0334e+01   0.0000e+00   0.0000e+00   0.0000e+00
 CA   CA   CB    H   3   3.0334e+01   0.0000e+00   -3.0334e+01   0.0000e+00   0.0000e+00   0.0000e+00
 CA   CA   CE   CA   3   3.0334e+01   0.0000e+00   -3.0334e+01   0.0000e+00   0.0000e+00   0.0000e+00
 CA   CA   CE   CF   3   3.0334e+01   0.0000e+00   -3.0334e+01   0.0000e+00   0.0000e+00   0.0000e+00
 CA   CB   CB   CA   3   3.0334e+01   0.0000e+00   -3.0334e+01   0.0000e+00   0.0000e+00   0.0000e+00
 CA   CB   CB    H   3   3.0334e+01   0.0000e+00   -3.0334e+01   0.0000e+00   0.0000e+00   0.0000e+00
 CA   CC    N   CD   3   3.0334e+01   0.0000e+00   -3.0334e+01   0.0000e+00   0.0000e+00   0.0000e+00
 CA   CC   NA   CG   3   3.0334e+01   0.0000e+00   -3.0334e+01   0.0000e+00   0.0000e+00   0.0000e+00
 CA   CE   CA   CA   3   3.0334e+01   0.0000e+00   -3.0334e+01   0.0000e+00   0.0000e+00   0.0000e+00
 CA   CE   CA   CB   3   3.0334e+01   0.0000e+00   -3.0334e+01   0.0000e+00   0.0000e+00   0.0000e+00
 CA   CE   CF   CA   3   3.0334e+01   0.0000e+00   -3.0334e+01   0.0000e+00   0.0000e+00   0.0000e+00
 CA   CF   CA   CB   3   3.0334e+01   0.0000e+00   -3.0334e+01   0.0000e+00   0.0000e+00   0.0000e+00
 CA   CF   CA   CC   3   3.0334e+01   0.0000e+00   -3.0334e+01   0.0000e+00   0.0000e+00   0.0000e+00
 CA   CF   CE   CA   3   3.0334e+01   0.0000e+00   -3.0334e+01   0.0000e+00   0.0000e+00   0.0000e+00
 CB   CA    C    N   3   3.0334e+01   0.0000e+00   -3.0334e+01   0.0000e+00   0.0000e+00   0.0000e+00
 CB   CA    C    O   3   3.0334e+01   0.0000e+00   -3.0334e+01   0.0000e+00   0.0000e+00   0.0000e+00
 CB   CA   CA   CB   3   3.0334e+01   0.0000e+00   -3.0334e+01   0.0000e+00   0.0000e+00   0.0000e+00
 CB   CA   CA   CE   3   3.0334e+01   0.0000e+00   -3.0334e+01   0.0000e+00   0.0000e+00   0.0000e+00
 CB   CA   CC    N   3   3.0334e+01   0.0000e+00   -3.0334e+01   0.0000e+00   0.0000e+00   0.0000e+00
 CB   CA   CC   NA   3   3.0334e+01   0.0000e+00   -3.0334e+01   0.0000e+00   0.0000e+00   0.0000e+00
 CB   CA   CE   CF   3   3.0334e+01   0.0000e+00   -3.0334e+01   0.0000e+00   0.0000e+00   0.0000e+00
 CB   CA   CF   CE   3   3.0334e+01   0.0000e+00   -3.0334e+01   0.0000e+00   0.0000e+00   0.0000e+00
 CB   CB   CA   CC   3   3.0334e+01   0.0000e+00   -3.0334e+01   0.0000e+00   0.0000e+00   0.0000e+00
 CB   CB   CA   CE   3   3.0334e+01   0.0000e+00   -3.0334e+01   0.0000e+00   0.0000e+00   0.0000e+00
 CB   CB   CA   CF   3   3.0334e+01   0.0000e+00   -3.0334e+01   0.0000e+00   0.0000e+00   0.0000e+00
 CB   CB   CB   CB   3   3.0334e+01   0.0000e+00   -3.0334e+01   0.0000e+00   0.0000e+00   0.0000e+00
 CB   CB   CB   CD   3   3.0334e+01   0.0000e+00   -3.0334e+01   0.0000e+00   0.0000e+00   0.0000e+00
 CB   CB   CB   CG   3   3.0334e+01   0.0000e+00   -3.0334e+01   0.0000e+00   0.0000e+00   0.0000e+00
 CB   CB   CB    H   3   3.0334e+01   0.0000e+00   -3.0334e+01   0.0000e+00   0.0000e+00   0.0000e+00
 CB   CB   CD   CG   3   3.0334e+01   0.0000e+00   -3.0334e+01   0.0000e+00   0.0000e+00   0.0000e+00
 CB   CB   CD    N   3   3.0334e+01   0.0000e+00   -3.0334e+01   0.0000e+00   0.0000e+00   0.0000e+00
 CB   CB   CG   CD   3   3.0334e+01   0.0000e+00   -3.0334e+01   0.0000e+00   0.0000e+00   0.0000e+00
 CB   CB   CG   NA   3   3.0334e+01   0.0000e+00   -3.0334e+01   0.0000e+00   0.0000e+00   0.0000e+00
 CB   CD   CG   NA   3   3.0334e+01   0.0000e+00   -3.0334e+01   0.0000e+00   0.0000e+00   0.0000e+00
 CB   CD    N   CC   3   3.0334e+01   0.0000e+00   -3.0334e+01   0.0000e+00   0.0000e+00   0.0000e+00
 CB   CG   CD   CB   3   3.0334e+01   0.0000e+00   -3.0334e+01   0.0000e+00   0.0000e+00   0.0000e+00
 CB   CG   CD    N   3   3.0334e+01   0.0000e+00   -3.0334e+01   0.0000e+00   0.0000e+00   0.0000e+00
 CB   CG   NA   CC   3   3.0334e+01   0.0000e+00   -3.0334e+01   0.0000e+00   0.0000e+00   0.0000e+00
 CC   CA   CB    H   3   3.0334e+01   0.0000e+00   -3.0334e+01   0.0000e+00   0.0000e+00   0.0000e+00
 CC   CA   CF   CE   3   3.0334e+01   0.0000e+00   -3.0334e+01   0.0000e+00   0.0000e+00   0.0000e+00
 CC    N    C    O   3   3.0334e+01   0.0000e+00   -3.0334e+01   0.0000e+00   0.0000e+00   0.0000e+00
 CC    N   CD   CG   3   3.0334e+01   0.0000e+00   -3.0334e+01   0.0000e+00   0.0000e+00   0.0000e+00
 CC   NA   CG   CD   3   3.0334e+01   0.0000e+00   -3.0334e+01   0.0000e+00   0.0000e+00   0.0000e+00
 CD   CB   CB    H   3   3.0334e+01   0.0000e+00   -3.0334e+01   0.0000e+00   0.0000e+00   0.0000e+00
 CD   CG   CB    H   3   3.0334e+01   0.0000e+00   -3.0334e+01   0.0000e+00   0.0000e+00   0.0000e+00
 CD    N    C    O   3   3.0334e+01   0.0000e+00   -3.0334e+01   0.0000e+00   0.0000e+00   0.0000e+00
```

```
  CD    N    CC   NA    3    3.0334e+01    0.0000e+00   -3.0334e+01    0.0000e+00    0.0000e+00    0.0000e+00
  CE    CA   CA   CE    3    3.0334e+01    0.0000e+00   -3.0334e+01    0.0000e+00    0.0000e+00    0.0000e+00
  CE    CA   CB   H     3    3.0334e+01    0.0000e+00   -3.0334e+01    0.0000e+00    0.0000e+00    0.0000e+00
  CF    CA   C    N     3    3.0334e+01    0.0000e+00   -3.0334e+01    0.0000e+00    0.0000e+00    0.0000e+00
  CF    CA   C    O     3    3.0334e+01    0.0000e+00   -3.0334e+01    0.0000e+00    0.0000e+00    0.0000e+00
  CF    CA   CB   H     3    3.0334e+01    0.0000e+00   -3.0334e+01    0.0000e+00    0.0000e+00    0.0000e+00
  CF    CA   CC   N     3    3.0334e+01    0.0000e+00   -3.0334e+01    0.0000e+00    0.0000e+00    0.0000e+00
  CF    CA   CC   NA    3    3.0334e+01    0.0000e+00   -3.0334e+01    0.0000e+00    0.0000e+00    0.0000e+00
  CG    CB   CB   H     3    3.0334e+01    0.0000e+00   -3.0334e+01    0.0000e+00    0.0000e+00    0.0000e+00
  CG    CD   CB   H     3    3.0334e+01    0.0000e+00   -3.0334e+01    0.0000e+00    0.0000e+00    0.0000e+00
  CG    NA   CC   N     3    3.0334e+01    0.0000e+00   -3.0334e+01    0.0000e+00    0.0000e+00    0.0000e+00
   H    CB   CB   H     3    3.0334e+01    0.0000e+00   -3.0334e+01    0.0000e+00    0.0000e+00    0.0000e+00
   H    CB   CD   N     3    3.0334e+01    0.0000e+00   -3.0334e+01    0.0000e+00    0.0000e+00    0.0000e+00
   H    CB   CG   NA    3    3.0334e+01    0.0000e+00   -3.0334e+01    0.0000e+00    0.0000e+00    0.0000e+00
   N    CD   CG   NA    3    3.0334e+01    0.0000e+00   -3.0334e+01    0.0000e+00    0.0000e+00    0.0000e+00

[ moleculetype ]
PTC          3

[ atoms ]
    1    O     1        PTC    O1     1    0.038815   15.9994
    2    N     1        PTC    N2     2   -0.067127   14.0067
    3    NA    1        PTC    NA3    3   -0.040789   14.0067
    4    C     1        PTC    C4     4    0.012292   12.0107
    5    CA    1        PTC    CA5    5    0.026565   12.0107
    6    CB    1        PTC    CB6    6    0.126670   12.0107
    7    CB    1        PTC    CB7    7    0.078423   12.0107
    8    CA    1        PTC    CA8    8    0.005038   12.0107
    9    CE    1        PTC    CE9    9   -0.024213   12.0107
   10    CA    1        PTC    CA10   10  -0.017825   12.0107
   11    CB    1        PTC    CB11   11   0.023182   12.0107
   12    CB    1        PTC    CB12   12  -0.008199   12.0107
   13    CA    1        PTC    CA13   13  -0.047943   12.0107
   14    CC    1        PTC    CC14   14  -0.108662   12.0107
   15    CF    1        PTC    CF15   15  -0.030133   12.0107
   16    CG    1        PTC    CG16   16  -0.025484   12.0107
   17    CB    1        PTC    CB17   17   0.118987   12.0107
   18    CB    1        PTC    CB18   18   0.114672   12.0107
   19    CB    1        PTC    CB19   19  -0.061704   12.0107
   20    CB    1        PTC    CB20   20  -0.059438   12.0107
   21    CD    1        PTC    CD21   21  -0.053127   12.0107
   22    H     1        PTC    H22    22   0.000000    1.0079
   23    H     1        PTC    H23    23   0.000000    1.0079
   24    H     1        PTC    H24    24   0.000000    1.0079
   25    H     1        PTC    H25    25   0.000000    1.0079
   26    H     1        PTC    H26    26   0.000000    1.0079
   27    H     1        PTC    H27    27   0.000000    1.0079
   28    H     1        PTC    H28    28   0.000000    1.0079
   29    H     1        PTC    H29    29   0.000000    1.0079
   30    O     1        PTC    O30    30   0.038815   15.9994
   31    N     1        PTC    N31    31  -0.067127   14.0067
   32    NA    1        PTC    NA32   32  -0.040789   14.0067
   33    C     1        PTC    C33    33   0.012292   12.0107
   34    CA    1        PTC    CA34   34   0.026565   12.0107
   35    CB    1        PTC    CB35   35   0.126670   12.0107
   36    CB    1        PTC    CB36   36   0.078423   12.0107
   37    CA    1        PTC    CA37   37   0.005038   12.0107
   38    CE    1        PTC    CE38   38  -0.024213   12.0107
   39    CA    1        PTC    CA39   39  -0.017825   12.0107
   40    CB    1        PTC    CB40   40   0.023182   12.0107
   41    CB    1        PTC    CB41   41  -0.008199   12.0107
   42    CA    1        PTC    CA42   42  -0.047943   12.0107
   43    CC    1        PTC    CC43   43  -0.108662   12.0107
   44    CF    1        PTC    CF44   44  -0.030133   12.0107
   45    CG    1        PTC    CG45   45  -0.025484   12.0107
   46    CB    1        PTC    CB46   46   0.118987   12.0107
   47    CB    1        PTC    CB47   47   0.114672   12.0107
   48    CB    1        PTC    CB48   48  -0.061704   12.0107
   49    CB    1        PTC    CB49   49  -0.059438   12.0107
   50    CD    1        PTC    CD50   50  -0.053127   12.0107
   51    H     1        PTC    H51    51   0.000000    1.0079
   52    H     1        PTC    H52    52   0.000000    1.0079
   53    H     1        PTC    H53    53   0.000000    1.0079
   54    H     1        PTC    H54    54   0.000000    1.0079
   55    H     1        PTC    H55    55   0.000000    1.0079
   56    H     1        PTC    H56    56   0.000000    1.0079
   57    H     1        PTC    H57    57   0.000000    1.0079
   58    H     1        PTC    H58    58   0.000000    1.0079

[ bonds ]
    1    4    1
    2    4    1
    2   14    1
    2   21    1
    3   14    1
    3   16    1
    4    5    1
    5    6    1
    5   15    1
    6    7    1
    6   22    1
```

```
    7    8    1
    7   23    1
    8    9    1
    8   39    1
    9   10    1
    9   15    1
   10   11    1
   10   37    1
   11   12    1
   11   24    1
   12   13    1
   12   25    1
   13   14    1
   13   15    1
   16   17    1
   16   21    1
   17   18    1
   17   26    1
   18   19    1
   18   27    1
   19   20    1
   19   28    1
   20   21    1
   20   29    1
   30   33    1
   31   33    1
   31   43    1
   31   50    1
   32   43    1
   32   45    1
   33   34    1
   34   35    1
   34   44    1
   35   36    1
   35   51    1
   36   37    1
   36   52    1
   37   38    1
   38   39    1
   38   44    1
   39   40    1
   40   41    1
   40   53    1
   41   42    1
   41   54    1
   42   43    1
   42   44    1
   45   46    1
   45   50    1
   46   47    1
   46   55    1
   47   48    1
   47   56    1
   48   49    1
   48   57    1
   49   50    1
   49   58    1

[ angles ]
    1    4    2    1
    1    4    5    1
    2    4    5    1
    2   14    3    1
    2   14   13    1
    2   21   16    1
    2   21   20    1
    3   14   13    1
    3   16   17    1
    3   16   21    1
    4    2   14    1
    4    2   21    1
    4    5    6    1
    4    5   15    1
    5    6    7    1
    5    6   22    1
    5   15    9    1
    5   15   13    1
    6    5   15    1
    6    7    8    1
    6    7   23    1
    7    6   22    1
    7    8    9    1
    7    8   39    1
    8    7   23    1
    8    9   10    1
    8    9   15    1
    8   39   38    1
    8   39   40    1
    9    8   39    1
    9   10   11    1
    9   10   37    1
    9   15   13    1
```

```
    10    9   15    1
    10   11   12    1
    10   11   24    1
    10   37   36    1
    10   37   38    1
    11   10   37    1
    11   12   13    1
    11   12   25    1
    12   11   24    1
    12   13   14    1
    12   13   15    1
    13   12   25    1
    14    2   21    1
    14    3   16    1
    14   13   15    1
    16   17   18    1
    16   17   26    1
    16   21   20    1
    17   16   21    1
    17   18   19    1
    17   18   27    1
    18   17   26    1
    18   19   20    1
    18   19   28    1
    19   18   27    1
    19   20   21    1
    19   20   29    1
    20   19   28    1
    21   20   29    1
    30   33   31    1
    30   33   34    1
    31   33   34    1
    31   43   32    1
    31   43   42    1
    31   50   45    1
    31   50   49    1
    32   43   42    1
    32   45   46    1
    32   45   50    1
    33   31   43    1
    33   31   50    1
    33   34   35    1
    33   34   44    1
    34   35   36    1
    34   35   51    1
    34   44   38    1
    34   44   42    1
    35   34   44    1
    35   36   37    1
    35   36   52    1
    36   35   51    1
    36   37   38    1
    37   36   52    1
    37   38   39    1
    37   38   44    1
    38   39   40    1
    38   44   42    1
    39   38   44    1
    39   40   41    1
    39   40   53    1
    40   41   42    1
    40   41   54    1
    41   40   53    1
    41   42   43    1
    41   42   44    1
    42   41   54    1
    43   31   50    1
    43   32   45    1
    43   42   44    1
    45   46   47    1
    45   46   55    1
    45   50   49    1
    46   45   50    1
    46   47   48    1
    46   47   56    1
    47   46   55    1
    47   48   49    1
    47   48   57    1
    48   47   56    1
    48   49   50    1
    48   49   58    1
    49   48   57    1
    50   49   58    1

[ dihedrals ]
     1    4    2   14    3
     1    4    2   21    3
     1    4    5    6    3
     1    4    5   15    3
     2    4    5    6    3
     2    4    5   15    3
     2   14    3   16    3
```

2	14	13	12	3
2	14	13	15	3
2	21	16	3	3
2	21	16	17	3
2	21	20	19	3
2	21	20	29	3
3	14	2	4	3
3	14	2	21	3
3	14	13	12	3
3	14	13	15	3
3	16	17	18	3
3	16	17	26	3
3	16	21	20	3
4	2	14	13	3
4	2	21	16	3
4	2	21	20	3
4	5	6	7	3
4	5	6	22	3
4	5	15	9	3
4	5	15	13	3
5	4	2	14	3
5	4	2	21	3
5	6	7	8	3
5	6	7	23	3
5	15	9	8	3
5	15	9	10	3
5	15	13	12	3
5	15	13	14	3
6	5	15	9	3
6	5	15	13	3
6	7	8	9	3
6	7	8	39	3
7	6	5	15	3
7	8	9	10	3
7	8	9	15	3
7	8	39	38	3
7	8	39	40	3
8	7	6	22	3
8	9	10	11	3
8	9	10	37	3
8	9	15	13	3
8	39	38	37	3
8	39	38	44	3
8	39	40	41	3
8	39	40	53	3
9	8	7	23	3
9	8	39	38	3
9	8	39	40	3
9	10	11	12	3
9	10	11	24	3
9	10	37	36	3
9	10	37	38	3
9	15	13	12	3
9	15	13	14	3
10	9	8	39	3
10	9	15	13	3
10	11	12	13	3
10	11	12	25	3
10	37	36	35	3
10	37	36	52	3
10	37	38	39	3
10	37	38	44	3
11	10	9	15	3
11	10	37	36	3
11	10	37	38	3
11	12	13	14	3
11	12	13	15	3
12	11	10	37	3
13	12	11	24	3
13	14	2	21	3
13	14	3	16	3
14	2	21	16	3
14	2	21	20	3
14	3	16	17	3
14	3	16	21	3
14	13	12	25	3
15	5	6	22	3
15	9	8	39	3
15	9	10	37	3
15	13	12	25	3
16	17	18	19	3
16	17	18	27	3
16	21	20	19	3
16	21	20	29	3
17	16	21	20	3
17	18	19	20	3
17	18	19	28	3
18	17	16	21	3
18	19	20	21	3
18	19	20	29	3
19	18	17	26	3
20	19	18	27	3

21	16	17	26	3
21	20	19	28	3
22	6	7	23	3
23	7	8	39	3
24	11	10	37	3
24	11	12	25	3
26	17	18	27	3
27	18	19	28	3
28	19	20	29	3
30	33	31	43	3
30	33	31	50	3
30	33	34	35	3
30	33	34	44	3
31	33	34	35	3
31	33	34	44	3
31	43	32	45	3
31	43	42	41	3
31	43	42	44	3
31	50	45	32	3
31	50	45	46	3
31	50	49	48	3
31	50	49	58	3
32	43	31	33	3
32	43	31	50	3
32	43	42	41	3
32	43	42	44	3
32	45	46	47	3
32	45	46	55	3
32	45	50	49	3
33	31	43	42	3
33	31	50	45	3
33	31	50	49	3
33	34	35	36	3
33	34	35	51	3
33	34	44	38	3
33	34	44	42	3
34	33	31	43	3
34	33	31	50	3
34	35	36	37	3
34	35	36	52	3
34	44	38	37	3
34	44	38	39	3
34	44	42	41	3
34	44	42	43	3
35	34	44	38	3
35	34	44	42	3
35	36	37	38	3
36	35	34	44	3
36	37	38	39	3
36	37	38	44	3
37	36	35	51	3
37	38	39	40	3
37	38	44	42	3
38	37	36	52	3
38	39	40	41	3
38	39	40	53	3
38	44	42	41	3
38	44	42	43	3
39	38	44	42	3
39	40	41	42	3
39	40	41	54	3
40	39	38	44	3
40	41	42	43	3
40	41	42	44	3
42	41	40	53	3
42	43	31	50	3
42	43	32	45	3
43	31	50	45	3
43	31	50	49	3
43	32	45	46	3
43	32	45	50	3
43	42	41	54	3
44	34	35	51	3
44	42	41	54	3
45	46	47	48	3
45	46	47	56	3
45	50	49	48	3
45	50	49	58	3
46	45	50	49	3
46	47	48	49	3
46	47	48	57	3
47	46	45	50	3
47	48	49	50	3
47	48	49	58	3
48	47	46	55	3
49	48	47	56	3
50	45	46	55	3
50	49	48	57	3
51	35	36	52	3
53	40	41	54	3
55	46	47	56	3
56	47	48	57	3

```
  57   48   49   58    3

[ exclusions ]
    1     3
    1     7
    1    13
    1    16
    1    20
    1    22
    1    19
    1    29
    2    18
    3     5
    3    19
    3    25
    4     8
    4    12
    4    19
    4    29
    5    39
    5    11
    5    16
    5    20
    6    40
    6    10
    6    14
    7    37
    7    41
    7    13
    7    53
    8    42
    8    12
    8    36
    9    44
   10    34
   10    40
   10    14
   11    35
   11    39
   11    52
   12    36
   12    16
   12    21
   13    37
   14    18
   14    19
   15    38
   15    16
   15    21
   23    40
   23    53
   24    36
   24    52
   30    32
   30    36
   30    42
   30    45
   30    49
   30    51
   30    48
   30    58
   31    47
   32    34
   32    48
   32    54
   33    37
   33    41
   33    48
   33    58
   34    45
   34    49
   34    40
   35    43
   35    39
   36    42
   37    41
   39    43
   41    45
   41    50
   43    47
   43    48
   44    45
   44    50
```

4: Copper Phthalocyanine (CuPc)

```
[ defaults ]
1    2    yes          0.5  0.5

[ atomtypes ]
CK        12.0107     0.0000     A     2.85169e-01  2.9288e-01
```

```
CJ       12.0107    0.0000    A     3.47568e-01  2.9288e-01
CI       12.0107    0.0000    A     3.32e-01     2.9288e-01
NK       14.0067    0.0000    A     3.60453e-01  7.1128e-01
NI       14.0067    0.0000    A     2.65164e-01  7.1128e-01
NJ       14.0067    0.0000    A     3.60453e-01  7.1128e-01
CUC      63.5460    0.0000    A     4.17487e-01  4.7698e+00
HG        1.0079    0.0000    A     1.99046e-01  1.2552e-01

[ bondtypes ]
   CI   CJ    1    1.4571e-01    3.9246e+05
   CI   NI    1    1.3247e-01    4.0417e+05
   CI   NJ    1    1.3752e-01    4.2007e+05
   CI   NK    1    1.3751e-01    4.2007e+05
   CJ   CJ    1    1.4056e-01    3.9246e+05
   CJ   CK    1    1.3955e-01    3.9246e+05
   CK   CK    1    1.3986e-01    3.9246e+05
   CK   HG    1    1.0861e-01    3.0711e+05
  CUC   NJ    1    1.9537e-01    2.2416e+05
  CUC   NK    1    1.9538e-01    2.2416e+05

[ angletypes ]
   CI   CJ   CJ    1    1.0640e+02    5.2718e+02
   CI   CJ   CK    1    1.3240e+02    5.2718e+02
   CI   NI   CI    1    1.2291e+02    5.8576e+02
   CI   NJ   CI    1    1.0823e+02    5.8576e+02
   CI   NJ  CUC    1    1.2589e+02    5.4924e+02
   CI   NK   CI    1    1.0823e+02    5.8576e+02
   CI   NK  CUC    1    1.2588e+02    5.4924e+02
   CJ   CI   NI    1    1.2285e+02    5.8576e+02
   CJ   CI   NJ    1    1.0949e+02    5.8576e+02
   CJ   CI   NK    1    1.0949e+02    5.8576e+02
   CJ   CJ   CK    1    1.2121e+02    5.2718e+02
   CJ   CK   CK    1    1.1761e+02    5.2718e+02
   CJ   CK   HG    1    1.2071e+02    2.9288e+02
   CK   CK   CK    1    1.2118e+02    5.2718e+02
   CK   CK   HG    1    1.2017e+02    2.9288e+02
   NI   CI   NJ    1    1.2766e+02    5.8576e+02
   NI   CI   NK    1    1.2766e+02    5.8576e+02
   NJ  CUC   NJ    1    1.8000e+02    2.9334e+02
   NJ  CUC   NK    1    9.0000e+01    1.2445e+03
   NK  CUC   NK    1    1.8000e+02    2.9334e+02

[ dihedraltypes ]
   CI   CJ   CJ   CI    3   3.0334e+01   0.0000e+00  -3.0334e+01   0.0000e+00   0.0000e+00   0.0000e+00
   CI   CJ   CJ   CK    3   3.0334e+01   0.0000e+00  -3.0334e+01   0.0000e+00   0.0000e+00   0.0000e+00
   CI   CJ   CK   CK    3   3.0334e+01   0.0000e+00  -3.0334e+01   0.0000e+00   0.0000e+00   0.0000e+00
   CI   CJ   CK   HG    3   3.0334e+01   0.0000e+00  -3.0334e+01   0.0000e+00   0.0000e+00   0.0000e+00
   CI   NI   CI   CJ    3   3.0334e+01   0.0000e+00  -3.0334e+01   0.0000e+00   0.0000e+00   0.0000e+00
   CI   NI   CI   NJ    3   3.0334e+01   0.0000e+00  -3.0334e+01   0.0000e+00   0.0000e+00   0.0000e+00
   CI   NI   CI   NK    3   3.0334e+01   0.0000e+00  -3.0334e+01   0.0000e+00   0.0000e+00   0.0000e+00
   CI   NJ   CI   CJ    3   3.0334e+01   0.0000e+00  -3.0334e+01   0.0000e+00   0.0000e+00   0.0000e+00
   CI   NJ   CI   NI    3   3.0334e+01   0.0000e+00  -3.0334e+01   0.0000e+00   0.0000e+00   0.0000e+00
   CI   NJ  CUC   NJ    3   0.0000e+00   0.0000e+00   0.0000e+00   0.0000e+00   0.0000e+00   0.0000e+00
   CI   NJ  CUC   NK    3   3.0334e+01   0.0000e+00  -3.0334e+01   0.0000e+00   0.0000e+00   0.0000e+00
   CI   NK   CI   CJ    3   3.0334e+01   0.0000e+00  -3.0334e+01   0.0000e+00   0.0000e+00   0.0000e+00
   CI   NK   CI   NI    3   3.0334e+01   0.0000e+00  -3.0334e+01   0.0000e+00   0.0000e+00   0.0000e+00
   CI   NK  CUC   NJ    3   3.0334e+01   0.0000e+00  -3.0334e+01   0.0000e+00   0.0000e+00   0.0000e+00
   CI   NK  CUC   NK    3   0.0000e+00   0.0000e+00   0.0000e+00   0.0000e+00   0.0000e+00   0.0000e+00
   CJ   CI   NJ  CUC    3   3.0334e+01   0.0000e+00  -3.0334e+01   0.0000e+00   0.0000e+00   0.0000e+00
   CJ   CI   NK  CUC    3   3.0334e+01   0.0000e+00  -3.0334e+01   0.0000e+00   0.0000e+00   0.0000e+00
   CJ   CJ   CI   NI    3   3.0334e+01   0.0000e+00  -3.0334e+01   0.0000e+00   0.0000e+00   0.0000e+00
   CJ   CJ   CI   NJ    3   3.0334e+01   0.0000e+00  -3.0334e+01   0.0000e+00   0.0000e+00   0.0000e+00
   CJ   CJ   CI   NK    3   3.0334e+01   0.0000e+00  -3.0334e+01   0.0000e+00   0.0000e+00   0.0000e+00
   CJ   CJ   CK   CK    3   3.0334e+01   0.0000e+00  -3.0334e+01   0.0000e+00   0.0000e+00   0.0000e+00
   CJ   CJ   CK   HG    3   3.0334e+01   0.0000e+00  -3.0334e+01   0.0000e+00   0.0000e+00   0.0000e+00
   CJ   CK   CK   CK    3   3.0334e+01   0.0000e+00  -3.0334e+01   0.0000e+00   0.0000e+00   0.0000e+00
   CJ   CK   CK   HG    3   3.0334e+01   0.0000e+00  -3.0334e+01   0.0000e+00   0.0000e+00   0.0000e+00
   CK   CJ   CI   NI    3   3.0334e+01   0.0000e+00  -3.0334e+01   0.0000e+00   0.0000e+00   0.0000e+00
   CK   CJ   CI   NJ    3   3.0334e+01   0.0000e+00  -3.0334e+01   0.0000e+00   0.0000e+00   0.0000e+00
   CK   CJ   CI   NK    3   3.0334e+01   0.0000e+00  -3.0334e+01   0.0000e+00   0.0000e+00   0.0000e+00
   CK   CJ   CJ   CK    3   3.0334e+01   0.0000e+00  -3.0334e+01   0.0000e+00   0.0000e+00   0.0000e+00
   CK   CK   CK   CK    3   3.0334e+01   0.0000e+00  -3.0334e+01   0.0000e+00   0.0000e+00   0.0000e+00
   CK   CK   CK   HG    3   3.0334e+01   0.0000e+00  -3.0334e+01   0.0000e+00   0.0000e+00   0.0000e+00
  CUC   NJ   CI   NI    3   3.0334e+01   0.0000e+00  -3.0334e+01   0.0000e+00   0.0000e+00   0.0000e+00
  CUC   NK   CI   NI    3   3.0334e+01   0.0000e+00  -3.0334e+01   0.0000e+00   0.0000e+00   0.0000e+00
   HG   CK   CK   HG    3   3.0334e+01   0.0000e+00  -3.0334e+01   0.0000e+00   0.0000e+00   0.0000e+00


[ moleculetype ]
CPC           3

[ atoms ]
    1  CUC    1        CPC   CUC1    1   -0.013384   63.5460
    2   CI    1        CPC    CI2    2   -0.007730   12.0107
    3   CJ    1        CPC    CJ3    3   -0.018180   12.0107
    4   CK    1        CPC    CK4    4   -0.009246   12.0107
    5   CK    1        CPC    CK5    5    0.014221   12.0107
    6   CK    1        CPC    CK6    6    0.008501   12.0107
    7   CK    1        CPC    CK7    7   -0.012161   12.0107
    8   CJ    1        CPC    CJ8    8   -0.010863   12.0107
    9   CI    1        CPC    CI9    9   -0.011716   12.0107
   10   CJ    1        CPC   CJ10   10   -0.005538   12.0107
```

```
  11   CK    1      CPC   CK11   11    0.001164   12.0107
  12   CK    1      CPC   CK12   12    0.013859   12.0107
  13   CK    1      CPC   CK13   13    0.011036   12.0107
  14   CK    1      CPC   CK14   14   -0.004397   12.0107
  15   CJ    1      CPC   CJ15   15   -0.006667   12.0107
  16   CI    1      CPC   CI16   16   -0.010383   12.0107
  17   CI    1      CPC   CI17   17   -0.014056   12.0107
  18   HG    1      CPC   HG18   18   -0.003059    1.0079
  19   HG    1      CPC   HG19   19    0.046604    1.0079
  20   HG    1      CPC   HG20   20    0.026872    1.0079
  21   HG    1      CPC   HG21   21    0.000153    1.0079
  22   HG    1      CPC   HG22   22    0.030795    1.0079
  23   HG    1      CPC   HG23   23    0.025030    1.0079
  24   HG    1      CPC   HG24   24   -0.006728    1.0079
  25   NI    1      CPC   NI25   25   -0.009014   14.0067
  26   NJ    1      CPC   NJ26   26   -0.010154   14.0067
  27   NI    1      CPC   NI27   27   -0.012146   14.0067
  28   NK    1      CPC   NK28   28   -0.014490   14.0067
  29   NJ    1      CPC   NJ29   29   -0.010154   14.0067
  30   NK    1      CPC   NK30   30   -0.014490   14.0067
  31   NI    1      CPC   NI31   31   -0.012146   14.0067
  32   CI    1      CPC   CI32   32   -0.014056   12.0107
  33   CI    1      CPC   CI33   33   -0.011716   12.0107
  34   CI    1      CPC   CI34   34   -0.007730   12.0107
  35   CI    1      CPC   CI35   35   -0.010383   12.0107
  36   CJ    1      CPC   CJ36   36   -0.018180   12.0107
  37   CJ    1      CPC   CJ37   37   -0.010863   12.0107
  38   NI    1      CPC   NI38   38   -0.009014   14.0067
  39   CJ    1      CPC   CJ39   39   -0.005538   12.0107
  40   CJ    1      CPC   CJ40   40   -0.006667   12.0107
  41   CK    1      CPC   CK41   41   -0.009246   12.0107
  42   CK    1      CPC   CK42   42   -0.012161   12.0107
  43   CK    1      CPC   CK43   43    0.001164   12.0107
  44   CK    1      CPC   CK44   44   -0.004397   12.0107
  45   CK    1      CPC   CK45   45    0.014221   12.0107
  46   HG    1      CPC   HG46   46   -0.003059    1.0079
  47   CK    1      CPC   CK47   47    0.008501   12.0107
  48   CK    1      CPC   CK48   48    0.013859   12.0107
  49   HG    1      CPC   HG49   49    0.000153    1.0079
  50   CK    1      CPC   CK50   50    0.011036   12.0107
  51   HG    1      CPC   HG51   51   -0.006728    1.0079
  52   HG    1      CPC   HG52   52    0.046604    1.0079
  53   HG    1      CPC   HG53   53    0.026872    1.0079
  54   HG    1      CPC   HG54   54    0.030795    1.0079
  55   HG    1      CPC   HG55   55    0.025030    1.0079
  56   HG    1      CPC   HG56   56   -0.005015    1.0079
  57   HG    1      CPC   HG57   57   -0.005015    1.0079

[ bonds ]
    1   26    1
    1   28    1
    1   29    1
    1   30    1
    2   10    1
    2   25    1
    2   26    1
    3    4    1
    3    8    1
    3   17    1
    4    5    1
    4   18    1
    5    6    1
    5   19    1
    6    7    1
    6   20    1
    7    8    1
    7   56    1
    8    9    1
    9   25    1
    9   30    1
   10   11    1
   10   15    1
   11   12    1
   11   21    1
   12   13    1
   12   22    1
   13   14    1
   13   23    1
   14   15    1
   14   24    1
   15   16    1
   16   26    1
   16   27    1
   17   30    1
   17   31    1
   27   32    1
   28   32    1
   28   33    1
   29   34    1
   29   35    1
   31   35    1
   32   36    1
```

```
   33   37    1
   33   38    1
   34   38    1
   34   39    1
   35   40    1
   36   37    1
   36   41    1
   37   42    1
   39   40    1
   39   43    1
   40   44    1
   41   45    1
   41   46    1
   42   47    1
   42   57    1
   43   48    1
   43   49    1
   44   50    1
   44   51    1
   45   47    1
   45   52    1
   47   53    1
   48   50    1
   48   54    1
   50   55    1

[ angles ]
    1   26    2    1
    1   26   16    1
    1   28   32    1
    1   28   33    1
    1   29   34    1
    1   29   35    1
    1   30    9    1
    1   30   17    1
    2   10   11    1
    2   10   15    1
    2   25    9    1
    2   26   16    1
    3    4    5    1
    3    4   18    1
    3    8    7    1
    3    8    9    1
    3   17   30    1
    3   17   31    1
    4    3    8    1
    4    3   17    1
    4    5    6    1
    4    5   19    1
    5    4   18    1
    5    6    7    1
    5    6   20    1
    6    5   19    1
    6    7    8    1
    6    7   56    1
    7    6   20    1
    7    8    9    1
    8    3   17    1
    8    7   56    1
    8    9   25    1
    8    9   30    1
    9   30   17    1
   10    2   25    1
   10    2   26    1
   10   11   12    1
   10   11   21    1
   10   15   14    1
   10   15   16    1
   11   10   15    1
   11   12   13    1
   11   12   22    1
   12   11   21    1
   12   13   14    1
   12   13   23    1
   13   12   22    1
   13   14   15    1
   13   14   24    1
   14   13   23    1
   14   15   16    1
   15   14   24    1
   15   16   26    1
   15   16   27    1
   16   27   32    1
   17   31   35    1
   25    2   26    1
   25    9   30    1
   26    1   28    1
   26    1   29    1
   26    1   30    1
   26   16   27    1
   27   32   28    1
   27   32   36    1
```

```
  28    1   29    1
  28    1   30    1
  28   32   36    1
  28   33   37    1
  28   33   38    1
  29    1   30    1
  29   34   38    1
  29   34   39    1
  29   35   31    1
  29   35   40    1
  30   17   31    1
  31   35   40    1
  32   28   33    1
  32   36   37    1
  32   36   41    1
  33   37   36    1
  33   37   42    1
  33   38   34    1
  34   29   35    1
  34   39   40    1
  34   39   43    1
  35   40   39    1
  35   40   44    1
  36   37   42    1
  36   41   45    1
  36   41   46    1
  37   33   38    1
  37   36   41    1
  37   42   47    1
  37   42   57    1
  38   34   39    1
  39   40   44    1
  39   43   48    1
  39   43   49    1
  40   39   43    1
  40   44   50    1
  40   44   51    1
  41   45   47    1
  41   45   52    1
  42   47   45    1
  42   47   53    1
  43   48   50    1
  43   48   54    1
  44   50   48    1
  44   50   55    1
  45   41   46    1
  45   47   53    1
  47   42   57    1
  47   45   52    1
  48   43   49    1
  48   50   55    1
  50   44   51    1
  50   48   54    1

[ dihedrals ]
    1   26    2   10    3
    1   26    2   25    3
    1   26   16   15    3
    1   26   16   27    3
    1   28   32   27    3
    1   28   32   36    3
    1   28   33   37    3
    1   28   33   38    3
    1   29   34   38    3
    1   29   34   39    3
    1   29   35   31    3
    1   29   35   40    3
    1   30    9    8    3
    1   30    9   25    3
    1   30   17    3    3
    1   30   17   31    3
    2   10   11   12    3
    2   10   11   21    3
    2   10   15   14    3
    2   10   15   16    3
    2   25    9    8    3
    2   25    9   30    3
    2   26    1   28    3
    2   26    1   29    3
    2   26    1   30    3
    2   26   16   15    3
    2   26   16   27    3
    3    4    5    6    3
    3    4    5   19    3
    3    8    7    6    3
    3    8    7   56    3
    3    8    9   25    3
    3    8    9   30    3
    3   17   30    9    3
    3   17   31   35    3
    4    3    8    7    3
    4    3    8    9    3
```

4	3	17	30	3
4	3	17	31	3
4	5	6	7	3
4	5	6	20	3
5	4	3	8	3
5	4	3	17	3
5	6	7	8	3
5	6	7	56	3
6	5	4	18	3
6	7	8	9	3
7	6	5	19	3
7	8	3	17	3
7	8	9	25	3
7	8	9	30	3
8	3	4	18	3
8	3	17	30	3
8	3	17	31	3
8	7	6	20	3
8	9	30	17	3
9	8	3	17	3
9	8	7	56	3
9	25	2	10	3
9	25	2	26	3
9	30	1	26	3
9	30	1	28	3
9	30	1	29	3
9	30	17	31	3
10	2	26	16	3
10	11	12	13	3
10	11	12	22	3
10	15	14	13	3
10	15	14	24	3
10	15	16	26	3
10	15	16	27	3
11	10	2	25	3
11	10	2	26	3
11	10	15	14	3
11	10	15	16	3
11	12	13	14	3
11	12	13	23	3
12	11	10	15	3
12	13	14	15	3
12	13	14	24	3
13	12	11	21	3
13	14	15	16	3
14	13	12	22	3
14	15	16	26	3
14	15	16	27	3
15	10	2	25	3
15	10	2	26	3
15	10	11	21	3
15	14	13	23	3
15	16	27	32	3
16	15	14	24	3
16	26	1	28	3
16	26	1	29	3
16	26	1	30	3
16	26	2	25	3
16	27	32	28	3
16	27	32	36	3
17	3	4	18	3
17	30	1	26	3
17	30	1	28	3
17	30	1	29	3
17	30	9	25	3
17	31	35	29	3
17	31	35	40	3
18	4	5	19	3
19	5	6	20	3
20	6	7	56	3
21	11	12	22	3
22	12	13	23	3
23	13	14	24	3
26	1	28	32	3
26	1	28	33	3
26	1	29	34	3
26	1	29	35	3
26	16	27	32	3
27	32	28	33	3
27	32	36	37	3
27	32	36	41	3
28	1	29	34	3
28	1	29	35	3
28	32	36	37	3
28	32	36	41	3
28	33	37	36	3
28	33	37	42	3
28	33	38	34	3
29	1	28	32	3
29	1	28	33	3
29	34	38	33	3
29	34	39	40	3

```
  29    34    39    43    3
  29    35    40    39    3
  29    35    40    44    3
  30     1    28    32    3
  30     1    28    33    3
  30     1    29    34    3
  30     1    29    35    3
  30    17    31    35    3
  31    35    29    34    3
  31    35    40    39    3
  31    35    40    44    3
  32    28    33    37    3
  32    28    33    38    3
  32    36    37    33    3
  32    36    37    42    3
  32    36    41    45    3
  32    36    41    46    3
  33    28    32    36    3
  33    37    36    41    3
  33    37    42    47    3
  33    37    42    57    3
  33    38    34    39    3
  34    29    35    40    3
  34    38    33    37    3
  34    39    40    35    3
  34    39    40    44    3
  34    39    43    48    3
  34    39    43    49    3
  35    29    34    38    3
  35    29    34    39    3
  35    40    39    43    3
  35    40    44    50    3
  35    40    44    51    3
  36    37    33    38    3
  36    37    42    47    3
  36    37    42    57    3
  36    41    45    47    3
  36    41    45    52    3
  37    36    41    45    3
  37    36    41    46    3
  37    42    47    45    3
  37    42    47    53    3
  38    33    37    42    3
  38    34    39    40    3
  38    34    39    43    3
  39    40    44    50    3
  39    40    44    51    3
  39    43    48    50    3
  39    43    48    54    3
  40    39    43    48    3
  40    39    43    49    3
  40    44    50    48    3
  40    44    50    55    3
  41    36    37    42    3
  41    45    47    42    3
  41    45    47    53    3
  42    47    45    52    3
  43    39    40    44    3
  43    48    50    44    3
  43    48    50    55    3
  44    50    48    54    3
  45    47    42    57    3
  46    41    45    47    3
  46    41    45    52    3
  48    50    44    51    3
  49    43    48    50    3
  49    43    48    54    3
  51    44    50    55    3
  52    45    47    53    3
  53    47    42    57    3
  54    48    50    55    3
```

5: Rubrene

```
[ defaults ]
1    2    yes          0.5  0.5

[ atomtypes ]
CC       12.0107    0.0000    A    3.53757e-01  2.9288e-01
CB       12.0107    0.0000    A    3.47833e-01  2.9288e-01
CA       12.0107    0.0000    A    3.49563e-01  2.9288e-01
CF       12.0107    0.0000    A    3.53757e-01  2.9288e-01
CE       12.0107    0.0000    A    3.20704e-01  2.9288e-01
CD       12.0107    0.0000    A    4.48460e-01  2.9288e-01
HB        1.0079    0.0000    A    1.80914e-01  1.2552e-01
HA        1.0079    0.0000    A    2.08183e-01  1.2552e-01

[ nonbond_params ]
   CA   CA    1    3.74012e-01    2.9288e-01
   CA   CB    1    3.59165e-01    2.9288e-01
   CA   CC    1    4.39452e-01    2.9288e-01
```

```
   CA    CD    1    5.05397e-01    2.9288e-01
   CA    CE    1    4.63994e-01    2.9288e-01
   CA    CF    1    3.67637e-01    2.9288e-01
   CA    HA    1    3.05612e-01    2.0920e-01
   CA    HB    1    3.70345e-01    2.0920e-01
   CB    CB    1    3.73965e-01    2.9288e-01
   CB    CC    1    3.79880e-01    2.9288e-01
   CB    CD    1    4.36696e-01    2.9288e-01
   CB    CE    1    3.53127e-01    2.9288e-01
   CB    CF    1    3.77568e-01    2.9288e-01
   CB    HA    1    2.87294e-01    2.0920e-01
   CB    HB    1    2.72305e-01    2.0920e-01
   CC    CC    1    5.14660e-01    2.9288e-01
   CC    CD    1    5.53402e-01    2.9288e-01
   CC    CE    1    5.07467e-01    2.9288e-01
   CC    CF    1    3.64374e-01    2.9288e-01
   CC    HA    1    3.50682e-01    2.0920e-01
   CC    HB    1    4.31420e-01    2.0920e-01
   CD    CD    1    5.57832e-01    2.9288e-01
   CD    CE    1    4.56961e-01    2.9288e-01
   CD    CF    1    4.13141e-01    2.9288e-01
   CD    HA    1    3.52319e-01    2.0920e-01
   CD    HB    1    3.73702e-01    2.0920e-01
   CE    CE    1    3.47721e-01    2.9288e-01
   CE    CF    1    3.50081e-01    2.9288e-01
   CE    HA    1    2.97300e-01    2.0920e-01
   CE    HB    1    2.58332e-01    2.0920e-01
   CF    CF    1    4.13008e-01    2.9288e-01
   CF    HA    1    3.26168e-01    2.0920e-01
   CF    HB    1    2.79950e-01    2.0920e-01
   HA    HA    1    3.09261e-01    1.2552e-01
   HA    HB    1    2.00379e-01    1.2552e-01
   HB    HB    1    1.86339e-01    1.2552e-01

[ bondtypes ]
   CA    CA    1    1.4554e-01    3.9246e+05
   CA    CB    1    1.4389e-01    3.9246e+05
   CA    CC    1    1.4196e-01    3.9246e+05
   CB    CF    1    1.3658e-01    3.9246e+05
   CB    HA    1    1.0823e-01    3.0711e+05
   CC    CD    1    1.5020e-01    3.9246e+05
   CD    CE    1    1.4026e-01    3.9246e+05
   CE    CE    1    1.3954e-01    3.9246e+05
   CE    HB    1    1.0868e-01    3.0711e+05
   CF    CF    1    1.4237e-01    3.9246e+05
   CF    HA    1    1.0868e-01    3.0711e+05

[ angletypes ]
   CA    CA    CB    1    1.1798e+02    5.2718e+02
   CA    CA    CC    1    1.1949e+02    5.2718e+02
   CA    CB    CF    1    1.2182e+02    5.2718e+02
   CA    CB    HA    1    1.1867e+02    2.9288e+02
   CA    CC    CA    1    1.2051e+02    5.2718e+02
   CA    CC    CD    1    1.1946e+02    5.2718e+02
   CB    CA    CC    1    1.2182e+02    5.2718e+02
   CB    CF    CF    1    1.2017e+02    5.2718e+02
   CB    CF    HA    1    1.1996e+02    2.9288e+02
   CC    CA    CC    1    1.2217e+02    5.2718e+02
   CC    CD    CE    1    1.2065e+02    5.2718e+02
   CD    CE    CE    1    1.2084e+02    5.2718e+02
   CD    CE    HB    1    1.1929e+02    2.9288e+02
   CE    CD    CE    1    1.1840e+02    5.2718e+02
   CE    CE    CE    1    1.1997e+02    5.2718e+02
   CE    CE    HB    1    1.1998e+02    2.9288e+02
   CF    CB    HA    1    1.1950e+02    2.9288e+02
   CF    CF    HA    1    1.1986e+02    2.9288e+02

[ dihedraltypes ]
   CA    CA    CB    CF    3    3.0334e+01    0.0000e+00    -3.0334e+01    0.0000e+00    0.0000e+00    0.0000e+00
   CA    CA    CB    HA    3    3.0334e+01    0.0000e+00    -3.0334e+01    0.0000e+00    0.0000e+00    0.0000e+00
   CA    CA    CC    CA    3    3.0334e+01    0.0000e+00    -3.0334e+01    0.0000e+00    0.0000e+00    0.0000e+00
   CA    CA    CC    CD    3    3.0334e+01    0.0000e+00    -3.0334e+01    0.0000e+00    0.0000e+00    0.0000e+00
   CA    CB    CF    CF    3    3.0334e+01    0.0000e+00    -3.0334e+01    0.0000e+00    0.0000e+00    0.0000e+00
   CA    CB    CF    HA    3    3.0334e+01    0.0000e+00    -3.0334e+01    0.0000e+00    0.0000e+00    0.0000e+00
   CA    CC    CA    CA    3    3.0334e+01    0.0000e+00    -3.0334e+01    0.0000e+00    0.0000e+00    0.0000e+00
   CA    CC    CA    CB    3    3.0334e+01    0.0000e+00    -3.0334e+01    0.0000e+00    0.0000e+00    0.0000e+00
   CA    CC    CA    CC    3    3.0334e+01    0.0000e+00    -3.0334e+01    0.0000e+00    0.0000e+00    0.0000e+00
   CA    CC    CD    CE    1    1.6132e+02    -2.7332e+00   2
   CB    CA    CA    CB    3    3.0334e+01    0.0000e+00    -3.0334e+01    0.0000e+00    0.0000e+00    0.0000e+00
   CB    CA    CA    CC    3    3.0334e+01    0.0000e+00    -3.0334e+01    0.0000e+00    0.0000e+00    0.0000e+00
   CB    CA    CC    CD    3    3.0334e+01    0.0000e+00    -3.0334e+01    0.0000e+00    0.0000e+00    0.0000e+00
   CB    CF    CF    CB    3    3.0334e+01    0.0000e+00    -3.0334e+01    0.0000e+00    0.0000e+00    0.0000e+00
   CB    CF    CF    HA    3    3.0334e+01    0.0000e+00    -3.0334e+01    0.0000e+00    0.0000e+00    0.0000e+00
   CC    CA    CA    CC    3    3.0334e+01    0.0000e+00    -3.0334e+01    0.0000e+00    0.0000e+00    0.0000e+00
   CC    CA    CB    CF    3    3.0334e+01    0.0000e+00    -3.0334e+01    0.0000e+00    0.0000e+00    0.0000e+00
   CC    CA    CB    HA    3    3.0334e+01    0.0000e+00    -3.0334e+01    0.0000e+00    0.0000e+00    0.0000e+00
   CC    CA    CC    CD    3    3.0334e+01    0.0000e+00    -3.0334e+01    0.0000e+00    0.0000e+00    0.0000e+00
   CC    CD    CE    CE    3    3.0334e+01    0.0000e+00    -3.0334e+01    0.0000e+00    0.0000e+00    0.0000e+00
   CC    CD    CE    HB    3    3.0334e+01    0.0000e+00    -3.0334e+01    0.0000e+00    0.0000e+00    0.0000e+00
   CD    CE    CE    CE    3    3.0334e+01    0.0000e+00    -3.0334e+01    0.0000e+00    0.0000e+00    0.0000e+00
   CD    CE    CE    HB    3    3.0334e+01    0.0000e+00    -3.0334e+01    0.0000e+00    0.0000e+00    0.0000e+00
   CE    CD    CE    CE    3    3.0334e+01    0.0000e+00    -3.0334e+01    0.0000e+00    0.0000e+00    0.0000e+00
```

```
  CE   CD   CE   HB    3    3.0334e+01    0.0000e+00   -3.0334e+01    0.0000e+00    0.0000e+00    0.0000e+00
  CE   CE   CD   CE    3    3.0334e+01    0.0000e+00   -3.0334e+01    0.0000e+00    0.0000e+00    0.0000e+00
  CE   CE   CE   CE    3    3.0334e+01    0.0000e+00   -3.0334e+01    0.0000e+00    0.0000e+00    0.0000e+00
  CE   CE   CE   HB    3    3.0334e+01    0.0000e+00   -3.0334e+01    0.0000e+00    0.0000e+00    0.0000e+00
  CF   CF   CB   HA    3    3.0334e+01    0.0000e+00   -3.0334e+01    0.0000e+00    0.0000e+00    0.0000e+00
  HA   CB   CF   HA    3    3.0334e+01    0.0000e+00   -3.0334e+01    0.0000e+00    0.0000e+00    0.0000e+00
  HA   CF   CF   HA    3    3.0334e+01    0.0000e+00   -3.0334e+01    0.0000e+00    0.0000e+00    0.0000e+00
  HB   CE   CE   HB    3    3.0334e+01    0.0000e+00   -3.0334e+01    0.0000e+00    0.0000e+00    0.0000e+00

[ moleculetype ]
RUB          3

[ atoms ]
    1   CA    1     RUB   CA1    1   -0.001082   12.0107
    2   CC    1     RUB   CC2    2   -0.002186   12.0107
    3   CA    1     RUB   CA3    3   -0.005771   12.0107
    4   CB    1     RUB   CB4    4   -0.007521   12.0107
    5   CF    1     RUB   CF5    5   -0.012987   12.0107
    6   CD    1     RUB   CD6    6    0.001735   12.0107
    7   CE    1     RUB   CE7    7   -0.014849   12.0107
    8   CE    1     RUB   CE8    8   -0.015622   12.0107
    9   CE    1     RUB   CE9    9    0.008234   12.0107
   10   CE    1     RUB   CE10  10    0.022677   12.0107
   11   CE    1     RUB   CE11  11    0.026831   12.0107
   12   HA    1     RUB   HA12  12    0.000000    1.0079
   13   HA    1     RUB   HA13  13    0.000000    1.0079
   14   HB    1     RUB   HB14  14    0.000000    1.0079
   15   HB    1     RUB   HB15  15    0.000000    1.0079
   16   HB    1     RUB   HB16  16    0.000000    1.0079
   17   HB    1     RUB   HB17  17    0.000000    1.0079
   18   HB    1     RUB   HB18  18    0.000000    1.0079
   19   CC    1     RUB   CC19  19   -0.002186   12.0107
   20   CA    1     RUB   CA20  20   -0.005771   12.0107
   21   CB    1     RUB   CB21  21   -0.007521   12.0107
   22   CF    1     RUB   CF22  22   -0.012987   12.0107
   23   CD    1     RUB   CD23  23    0.001735   12.0107
   24   CE    1     RUB   CE24  24   -0.014849   12.0107
   25   CE    1     RUB   CE25  25   -0.015622   12.0107
   26   CE    1     RUB   CE26  26    0.008234   12.0107
   27   CE    1     RUB   CE27  27    0.022677   12.0107
   28   CE    1     RUB   CE28  28    0.026831   12.0107
   29   HA    1     RUB   HA29  29    0.000000    1.0079
   30   HA    1     RUB   HA30  30    0.000000    1.0079
   31   HB    1     RUB   HB31  31    0.000000    1.0079
   32   HB    1     RUB   HB32  32    0.000000    1.0079
   33   HB    1     RUB   HB33  33    0.000000    1.0079
   34   HB    1     RUB   HB34  34    0.000000    1.0079
   35   HB    1     RUB   HB35  35    0.000000    1.0079
   36   CA    1     RUB   CA36  36   -0.001082   12.0107
   37   CC    1     RUB   CC37  37   -0.002186   12.0107
   38   CA    1     RUB   CA38  38   -0.005771   12.0107
   39   CB    1     RUB   CB39  39   -0.007521   12.0107
   40   CF    1     RUB   CF40  40   -0.012987   12.0107
   41   CD    1     RUB   CD41  41    0.001735   12.0107
   42   CE    1     RUB   CE42  42   -0.014849   12.0107
   43   CE    1     RUB   CE43  43   -0.015622   12.0107
   44   CE    1     RUB   CE44  44    0.008234   12.0107
   45   CE    1     RUB   CE45  45    0.022677   12.0107
   46   CE    1     RUB   CE46  46    0.026831   12.0107
   47   HA    1     RUB   HA47  47    0.000000    1.0079
   48   HA    1     RUB   HA48  48    0.000000    1.0079
   49   HB    1     RUB   HB49  49    0.000000    1.0079
   50   HB    1     RUB   HB50  50    0.000000    1.0079
   51   HB    1     RUB   HB51  51    0.000000    1.0079
   52   HB    1     RUB   HB52  52    0.000000    1.0079
   53   HB    1     RUB   HB53  53    0.000000    1.0079
   54   CC    1     RUB   CC54  54   -0.002186   12.0107
   55   CA    1     RUB   CA55  55   -0.005771   12.0107
   56   CB    1     RUB   CB56  56   -0.007521   12.0107
   57   CF    1     RUB   CF57  57   -0.012987   12.0107
   58   CD    1     RUB   CD58  58    0.001735   12.0107
   59   CE    1     RUB   CE59  59   -0.014849   12.0107
   60   CE    1     RUB   CE60  60   -0.015622   12.0107
   61   CE    1     RUB   CE61  61    0.008234   12.0107
   62   CE    1     RUB   CE62  62    0.022677   12.0107
   63   CE    1     RUB   CE63  63    0.026831   12.0107
   64   HA    1     RUB   HA64  64    0.000000    1.0079
   65   HA    1     RUB   HA65  65    0.000000    1.0079
   66   HB    1     RUB   HB66  66    0.000000    1.0079
   67   HB    1     RUB   HB67  67    0.000000    1.0079
   68   HB    1     RUB   HB68  68    0.000000    1.0079
   69   HB    1     RUB   HB69  69    0.000000    1.0079
   70   HB    1     RUB   HB70  70    0.000000    1.0079

[ bonds ]
    1    2    1
    1   19    1
    1   36    1
    2    3    1
    2    6    1
    3    4    1
    3   55    1
```

```
   4    5    1
   4   12    1
   5   13    1
   5   57    1
   6    7    1
   6   11    1
   7    8    1
   7   14    1
   8    9    1
   8   15    1
   9   10    1
   9   16    1
  10   11    1
  10   17    1
  11   18    1
  19   20    1
  19   23    1
  20   21    1
  20   38    1
  21   22    1
  21   29    1
  22   30    1
  22   40    1
  23   24    1
  23   28    1
  24   25    1
  24   31    1
  25   26    1
  25   32    1
  26   27    1
  26   33    1
  27   28    1
  27   34    1
  28   35    1
  36   37    1
  36   54    1
  37   38    1
  37   41    1
  38   39    1
  39   40    1
  39   47    1
  40   48    1
  41   42    1
  41   46    1
  42   43    1
  42   49    1
  43   44    1
  43   50    1
  44   45    1
  44   51    1
  45   46    1
  45   52    1
  46   53    1
  54   55    1
  54   58    1
  55   56    1
  56   57    1
  56   64    1
  57   65    1
  58   59    1
  58   63    1
  59   60    1
  59   66    1
  60   61    1
  60   67    1
  61   62    1
  61   68    1
  62   63    1
  62   69    1
  63   70    1

[ angles ]
   1    2    3    1
   1    2    6    1
   1   19   20    1
   1   19   23    1
   1   36   37    1
   1   36   54    1
   2    1   19    1
   2    1   36    1
   2    3    4    1
   2    3   55    1
   2    6    7    1
   2    6   11    1
   3    2    6    1
   3    4    5    1
   3    4   12    1
   3   55   54    1
   3   55   56    1
   4    3   55    1
   4    5   13    1
   4    5   57    1
```

5	4	12	1
5	57	56	1
5	57	65	1
6	7	8	1
6	7	14	1
6	11	10	1
6	11	18	1
7	6	11	1
7	8	9	1
7	8	15	1
8	7	14	1
8	9	10	1
8	9	16	1
9	8	15	1
9	10	11	1
9	10	17	1
10	9	16	1
10	11	18	1
11	10	17	1
13	5	57	1
19	1	36	1
19	20	21	1
19	20	38	1
19	23	24	1
19	23	28	1
20	19	23	1
20	21	22	1
20	21	29	1
20	38	37	1
20	38	39	1
21	20	38	1
21	22	30	1
21	22	40	1
22	21	29	1
22	40	39	1
22	40	48	1
23	24	25	1
23	24	31	1
23	28	27	1
23	28	35	1
24	23	28	1
24	25	26	1
24	25	32	1
25	24	31	1
25	26	27	1
25	26	33	1
26	25	32	1
26	27	28	1
26	27	34	1
27	26	33	1
27	28	35	1
28	27	34	1
30	22	40	1
36	37	38	1
36	37	41	1
36	54	55	1
36	54	58	1
37	36	54	1
37	38	39	1
37	41	42	1
37	41	46	1
38	37	41	1
38	39	40	1
38	39	47	1
39	40	48	1
40	39	47	1
41	42	43	1
41	42	49	1
41	46	45	1
41	46	53	1
42	41	46	1
42	43	44	1
42	43	50	1
43	42	49	1
43	44	45	1
43	44	51	1
44	43	50	1
44	45	46	1
44	45	52	1
45	44	51	1
45	46	53	1
46	45	52	1
54	55	56	1
54	58	59	1
54	58	63	1
55	54	58	1
55	56	57	1
55	56	64	1
56	57	65	1
57	56	64	1
58	59	60	1
58	59	66	1

```
    58    63    62     1
    58    63    70     1
    59    58    63     1
    59    60    61     1
    59    60    67     1
    60    59    66     1
    60    61    62     1
    60    61    68     1
    61    60    67     1
    61    62    63     1
    61    62    69     1
    62    61    68     1
    62    63    70     1
    63    62    69     1

[ dihedrals ]
     1     2     3     4     3
     1     2     3    55     3
     1     2     6     7     1
     1     2     6    11     1
     1    19    20    21     3
     1    19    20    38     3
     1    19    23    24     1
     1    19    23    28     1
     1    36    37    38     3
     1    36    37    41     3
     1    36    54    55     3
     1    36    54    58     3
     2     1    19    20     3
     2     1    19    23     3
     2     1    36    37     3
     2     1    36    54     3
     2     3     4     5     3
     2     3     4    12     3
     2     3    55    54     3
     2     3    55    56     3
     2     6     7     8     3
     2     6     7    14     3
     2     6    11    10     3
     2     6    11    18     3
     3     2     1    19     3
     3     2     1    36     3
     3     2     6     7     1
     3     2     6    11     1
     3     4     5    13     3
     3     4     5    57     3
     3    55    54    36     3
     3    55    54    58     3
     3    55    56    57     3
     3    55    56    64     3
     4     3     2     6     3
     4     3    55    54     3
     4     3    55    56     3
     4     5    57    56     3
     4     5    57    65     3
     5     4     3    55     3
     5    57    56    55     3
     5    57    56    64     3
     6     2     1    19     3
     6     2     1    36     3
     6     2     3    55     3
     6     7     8     9     3
     6     7     8    15     3
     6    11    10     9     3
     6    11    10    17     3
     7     6    11    10     3
     7     6    11    18     3
     7     8     9    10     3
     7     8     9    16     3
     8     7     6    11     3
     8     9    10    11     3
     8     9    10    17     3
     9     8     7    14     3
     9    10    11    18     3
    10     9     8    15     3
    11     6     7    14     3
    11    10     9    16     3
    12     4     3    55     3
    12     4     5    13     3
    12     4     5    57     3
    13     5    57    56     3
    13     5    57    65     3
    14     7     8    15     3
    15     8     9    16     3
    16     9    10    17     3
    17    10    11    18     3
    19     1    36    37     3
    19     1    36    54     3
    19    20    21    22     3
    19    20    21    29     3
    19    20    38    37     3
    19    20    38    39     3
```

19	23	24	25	3
19	23	24	31	3
19	23	28	27	3
19	23	28	35	3
20	19	1	36	3
20	19	23	24	1
20	19	23	28	1
20	21	22	30	3
20	21	22	40	3
20	38	37	36	3
20	38	37	41	3
20	38	39	40	3
20	38	39	47	3
21	20	19	23	3
21	20	38	37	3
21	20	38	39	3
21	22	40	39	3
21	22	40	48	3
22	21	20	38	3
22	40	39	38	3
22	40	39	47	3
23	19	1	36	3
23	19	20	38	3
23	24	25	26	3
23	24	25	32	3
23	28	27	26	3
23	28	27	34	3
24	23	28	27	3
24	23	28	35	3
24	25	26	27	3
24	25	26	33	3
25	24	23	28	3
25	26	27	28	3
25	26	27	34	3
26	25	24	31	3
26	27	28	35	3
27	26	25	32	3
28	23	24	31	3
28	27	26	33	3
29	21	20	38	3
29	21	22	30	3
29	21	22	40	3
30	22	40	39	3
30	22	40	48	3
31	24	25	32	3
32	25	26	33	3
33	26	27	34	3
34	27	28	35	3
36	37	38	39	3
36	37	41	42	1
36	37	41	46	1
36	54	55	56	3
36	54	58	59	1
36	54	58	63	1
37	36	54	55	3
37	36	54	58	3
37	38	39	40	3
37	38	39	47	3
37	41	42	43	3
37	41	42	49	3
37	41	46	45	3
37	41	46	53	3
38	37	36	54	3
38	37	41	42	1
38	37	41	46	1
38	39	40	48	3
39	38	37	41	3
41	37	36	54	3
41	42	43	44	3
41	42	43	50	3
41	46	45	44	3
41	46	45	52	3
42	41	46	45	3
42	41	46	53	3
42	43	44	45	3
42	43	44	51	3
43	42	41	46	3
43	44	45	46	3
43	44	45	52	3
44	43	42	49	3
44	45	46	53	3
45	44	43	50	3
46	41	42	49	3
46	45	44	51	3
47	39	40	48	3
49	42	43	50	3
50	43	44	51	3
51	44	45	52	3
52	45	46	53	3
54	55	56	57	3
54	55	56	64	3
54	58	59	60	3

```
  54   58   59   66    3
  54   58   63   62    3
  54   58   63   70    3
  55   54   58   59    1
  55   54   58   63    1
  55   56   57   65    3
  56   55   54   58    3
  58   59   60   61    3
  58   59   60   67    3
  58   63   62   61    3
  58   63   62   69    3
  59   58   63   62    3
  59   58   63   70    3
  59   60   61   62    3
  59   60   61   68    3
  60   59   58   63    3
  60   61   62   63    3
  60   61   62   69    3
  61   60   59   66    3
  61   62   63   70    3
  62   61   60   67    3
  63   58   59   66    3
  63   62   61   68    3
  64   56   57   65    3
  66   59   60   67    3
  67   60   61   68    3
  68   61   62   69    3
  69   62   63   70    3

[ exclusions ]
   1    35
   1     8
   1    10
   1    14
   1    59
   1    18
   1    42
   1    25
   1    27
   1    31
   2    38
   2     9
   2    41
   2    24
   2    58
   2    28
   2    35
   2    63
   2    59
   2    25
   2    27
   2    31
   2    26
   3    37
   3     8
   3    10
   3    14
   3    18
   3    23
   3    59
   3    63
   3    41
   3    24
   4     7
   4    11
   5     6
   6    37
   6    12
   6    16
   6    20
   6    54
   6    23
   6    38
   6    24
   6    58
   6    28
   6    35
   6    25
   6    27
   6    31
   6    26
   7    19
   7    36
   7    55
   7    20
   7    54
   7    23
   7    28
   8    19
   8    23
   8    28
   9    19
```

9	23
10	19
10	23
11	55
11	19
11	12
11	54
11	23
11	24
11	28
11	25
14	19
14	23
18	19
18	23
19	41
19	55
19	26
19	58
19	46
19	42
20	42
20	46
20	35
20	54
20	25
20	27
20	31
20	58
21	24
21	28
22	23
23	33
23	37
23	54
23	29
23	41
23	55
24	36
24	38
24	37
28	38
28	29
28	37
36	66
36	43
36	70
36	60
36	45
36	49
36	62
36	53
37	44
37	59
37	63
37	66
37	70
37	60
37	62
37	61
38	43
38	45
38	49
38	53
38	58
38	59
39	42
39	46
40	41
41	51
41	47
41	55
41	58
41	59
41	63
41	66
41	70
41	60
41	62
41	61
42	54
42	55
42	58
42	63
43	54
43	58
43	63
44	54
44	58
45	54
45	58
46	54

```
   46     47
   46     58
   46     59
   46     63
   46     60
   49     54
   49     58
   53     54
   53     58
   54     61
   55     66
   55     70
   55     60
   55     62
   56     59
   56     63
   57     58
   58     64
   58     68
   63     64
```

6: Buckminsterfullerene (C_{60})

```
[ defaults ]
1    2    yes          0.5  0.5

[ atomtypes ]
CO       12.0107    0.0000    A     2.8978e-01  2.9288e-01
CS       12.0107    0.0000    A     2.8978e-01  2.9288e-01
CR       12.0107    0.0000    A     2.8978e-01  2.9288e-01
CP       12.0107    0.0000    A     2.8978e-01  2.9288e-01
CV       12.0107    0.0000    A     2.8978e-01  2.9288e-01
CU       12.0107    0.0000    A     2.8978e-01  2.9288e-01

[ nonbond_params ]
   CO    CO     1     4.63750e-01     2.9288e-01
   CO    CP     1     4.14705e-01     2.9288e-01
   CO    CR     1     3.97350e-01     2.9288e-01
   CO    CS     1     4.14705e-01     2.9288e-01
   CO    CU     1     2.98470e-01     2.9288e-01
   CO    CV     1     3.12374e-01     2.9288e-01
   CP    CP     1     4.63750e-01     2.9288e-01
   CP    CR     1     3.12374e-01     2.9288e-01
   CP    CS     1     4.14705e-01     2.9288e-01
   CP    CU     1     3.97350e-01     2.9288e-01
   CP    CV     1     2.98470e-01     2.9288e-01
   CR    CR     1     4.87202e-01     2.9288e-01
   CR    CS     1     2.98470e-01     2.9288e-01
   CR    CU     1     3.98085e-01     2.9288e-01
   CR    CV     1     3.98085e-01     2.9288e-01
   CS    CS     1     4.63750e-01     2.9288e-01
   CS    CU     1     3.12374e-01     2.9288e-01
   CS    CV     1     3.97350e-01     2.9288e-01
   CU    CU     1     4.87202e-01     2.9288e-01
   CU    CV     1     3.98085e-01     2.9288e-01
   CV    CV     1     4.87202e-01     2.9288e-01

[ bondtypes ]
   CO    CO     1     1.4533e-01     3.0126e+05
   CO    CP     1     1.3955e-01     3.0126e+05
   CO    CR     1     1.3958e-01     3.0126e+05
   CO    CS     1     1.3955e-01     3.0126e+05
   CO    CU     1     1.3952e-01     3.0126e+05
   CO    CV     1     1.3952e-01     3.0126e+05
   CP    CP     1     1.4533e-01     3.0126e+05
   CP    CR     1     1.3952e-01     3.0126e+05
   CP    CS     1     1.3955e-01     3.0126e+05
   CP    CU     1     1.3958e-01     3.0126e+05
   CP    CV     1     1.3952e-01     3.0126e+05
   CR    CR     1     1.4534e-01     3.0126e+05
   CR    CS     1     1.3952e-01     3.0126e+05
   CR    CU     1     1.3955e-01     3.0126e+05
   CR    CV     1     1.3955e-01     3.0126e+05
   CS    CS     1     1.4533e-01     3.0126e+05
   CS    CU     1     1.3952e-01     3.0126e+05
   CS    CV     1     1.3958e-01     3.0126e+05
   CU    CU     1     1.4534e-01     3.0126e+05
   CU    CV     1     1.3955e-01     3.0126e+05
   CV    CV     1     1.4534e-01     3.0126e+05

[ angletypes ]
   CO    CO    CO     1     1.0800e+02     6.1547e+02
   CO    CO    CP     1     1.2001e+02     6.1547e+02
   CO    CO    CR     1     1.1997e+02     6.1547e+02
   CO    CO    CS     1     1.2000e+02     6.1547e+02
   CO    CO    CU     1     1.2001e+02     6.1547e+02
   CO    CO    CV     1     1.2001e+02     6.1547e+02
   CO    CP    CP     1     1.2000e+02     6.1547e+02
   CO    CR    CR     1     1.2001e+02     6.1547e+02
   CO    CS    CS     1     1.2001e+02     6.1547e+02
   CO    CU    CU     1     1.1999e+02     6.1547e+02
```

CO	CV	CV	1	1.1999e+02	6.1547e+02
CP	CP	CP	1	1.0800e+02	6.1547e+02
CP	CP	CR	1	1.2001e+02	6.1547e+02
CP	CP	CS	1	1.2001e+02	6.1547e+02
CP	CP	CU	1	1.1997e+02	6.1547e+02
CP	CP	CV	1	1.2001e+02	6.1547e+02
CP	CR	CR	1	1.1999e+02	6.1547e+02
CP	CS	CS	1	1.2000e+02	6.1547e+02
CP	CU	CU	1	1.2001e+02	6.1547e+02
CP	CV	CV	1	1.1999e+02	6.1547e+02
CR	CR	CR	1	1.0800e+02	6.1547e+02
CR	CR	CS	1	1.1999e+02	6.1547e+02
CR	CR	CU	1	1.2000e+02	6.1547e+02
CR	CR	CV	1	1.2000e+02	6.1547e+02
CR	CS	CS	1	1.2001e+02	6.1547e+02
CR	CU	CU	1	1.2000e+02	6.1547e+02
CR	CV	CV	1	1.2000e+02	6.1547e+02
CS	CS	CS	1	1.0800e+02	6.1547e+02
CS	CS	CU	1	1.2001e+02	6.1547e+02
CS	CS	CV	1	1.1997e+02	6.1547e+02
CS	CU	CU	1	1.1999e+02	6.1547e+02
CS	CV	CV	1	1.2001e+02	6.1547e+02
CU	CU	CU	1	1.0800e+02	6.1547e+02
CU	CU	CV	1	1.2000e+02	6.1547e+02
CU	CV	CV	1	1.2000e+02	6.1547e+02
CV	CV	CV	1	1.0800e+02	6.1547e+02

[dihedraltypes]

CO	CO	CO	CO	3	3.0334e+01	0.0000e+00	-3.0334e+01	0.0000e+00	0.0000e+00	0.0000e+00
CO	CO	CO	CP	3	3.0334e+01	0.0000e+00	-3.0334e+01	0.0000e+00	0.0000e+00	0.0000e+00
CO	CO	CO	CR	3	3.0334e+01	0.0000e+00	-3.0334e+01	0.0000e+00	0.0000e+00	0.0000e+00
CO	CO	CO	CS	3	3.0334e+01	0.0000e+00	-3.0334e+01	0.0000e+00	0.0000e+00	0.0000e+00
CO	CO	CO	CU	3	3.0334e+01	0.0000e+00	-3.0334e+01	0.0000e+00	0.0000e+00	0.0000e+00
CO	CO	CO	CV	3	3.0334e+01	0.0000e+00	-3.0334e+01	0.0000e+00	0.0000e+00	0.0000e+00
CO	CO	CP	CP	3	3.0334e+01	0.0000e+00	-3.0334e+01	0.0000e+00	0.0000e+00	0.0000e+00
CO	CO	CR	CR	3	3.0334e+01	0.0000e+00	-3.0334e+01	0.0000e+00	0.0000e+00	0.0000e+00
CO	CO	CS	CS	3	3.0334e+01	0.0000e+00	-3.0334e+01	0.0000e+00	0.0000e+00	0.0000e+00
CO	CO	CU	CU	3	3.0334e+01	0.0000e+00	-3.0334e+01	0.0000e+00	0.0000e+00	0.0000e+00
CO	CO	CV	CV	3	3.0334e+01	0.0000e+00	-3.0334e+01	0.0000e+00	0.0000e+00	0.0000e+00
CO	CP	CP	CP	3	3.0334e+01	0.0000e+00	-3.0334e+01	0.0000e+00	0.0000e+00	0.0000e+00
CO	CP	CP	CR	3	3.0334e+01	0.0000e+00	-3.0334e+01	0.0000e+00	0.0000e+00	0.0000e+00
CO	CP	CP	CU	3	3.0334e+01	0.0000e+00	-3.0334e+01	0.0000e+00	0.0000e+00	0.0000e+00
CO	CR	CR	CP	3	3.0334e+01	0.0000e+00	-3.0334e+01	0.0000e+00	0.0000e+00	0.0000e+00
CO	CR	CR	CR	3	3.0334e+01	0.0000e+00	-3.0334e+01	0.0000e+00	0.0000e+00	0.0000e+00
CO	CR	CR	CS	3	3.0334e+01	0.0000e+00	-3.0334e+01	0.0000e+00	0.0000e+00	0.0000e+00
CO	CS	CS	CR	3	3.0334e+01	0.0000e+00	-3.0334e+01	0.0000e+00	0.0000e+00	0.0000e+00
CO	CS	CS	CS	3	3.0334e+01	0.0000e+00	-3.0334e+01	0.0000e+00	0.0000e+00	0.0000e+00
CO	CS	CS	CV	3	3.0334e+01	0.0000e+00	-3.0334e+01	0.0000e+00	0.0000e+00	0.0000e+00
CO	CU	CU	CP	3	3.0334e+01	0.0000e+00	-3.0334e+01	0.0000e+00	0.0000e+00	0.0000e+00
CO	CU	CU	CU	3	3.0334e+01	0.0000e+00	-3.0334e+01	0.0000e+00	0.0000e+00	0.0000e+00
CO	CU	CU	CV	3	3.0334e+01	0.0000e+00	-3.0334e+01	0.0000e+00	0.0000e+00	0.0000e+00
CO	CV	CV	CS	3	3.0334e+01	0.0000e+00	-3.0334e+01	0.0000e+00	0.0000e+00	0.0000e+00
CO	CV	CV	CU	3	3.0334e+01	0.0000e+00	-3.0334e+01	0.0000e+00	0.0000e+00	0.0000e+00
CO	CV	CV	CV	3	3.0334e+01	0.0000e+00	-3.0334e+01	0.0000e+00	0.0000e+00	0.0000e+00
CP	CO	CO	CR	3	3.0334e+01	0.0000e+00	-3.0334e+01	0.0000e+00	0.0000e+00	0.0000e+00
CP	CO	CO	CU	3	3.0334e+01	0.0000e+00	-3.0334e+01	0.0000e+00	0.0000e+00	0.0000e+00
CP	CP	CP	CP	3	3.0334e+01	0.0000e+00	-3.0334e+01	0.0000e+00	0.0000e+00	0.0000e+00
CP	CP	CP	CR	3	3.0334e+01	0.0000e+00	-3.0334e+01	0.0000e+00	0.0000e+00	0.0000e+00
CP	CP	CP	CS	3	3.0334e+01	0.0000e+00	-3.0334e+01	0.0000e+00	0.0000e+00	0.0000e+00
CP	CP	CP	CU	3	3.0334e+01	0.0000e+00	-3.0334e+01	0.0000e+00	0.0000e+00	0.0000e+00
CP	CP	CP	CV	3	3.0334e+01	0.0000e+00	-3.0334e+01	0.0000e+00	0.0000e+00	0.0000e+00
CP	CP	CR	CR	3	3.0334e+01	0.0000e+00	-3.0334e+01	0.0000e+00	0.0000e+00	0.0000e+00
CP	CP	CS	CS	3	3.0334e+01	0.0000e+00	-3.0334e+01	0.0000e+00	0.0000e+00	0.0000e+00
CP	CP	CU	CU	3	3.0334e+01	0.0000e+00	-3.0334e+01	0.0000e+00	0.0000e+00	0.0000e+00
CP	CP	CV	CV	3	3.0334e+01	0.0000e+00	-3.0334e+01	0.0000e+00	0.0000e+00	0.0000e+00
CP	CR	CR	CR	3	3.0334e+01	0.0000e+00	-3.0334e+01	0.0000e+00	0.0000e+00	0.0000e+00
CP	CR	CR	CV	3	3.0334e+01	0.0000e+00	-3.0334e+01	0.0000e+00	0.0000e+00	0.0000e+00
CP	CS	CS	CS	3	3.0334e+01	0.0000e+00	-3.0334e+01	0.0000e+00	0.0000e+00	0.0000e+00
CP	CS	CS	CU	3	3.0334e+01	0.0000e+00	-3.0334e+01	0.0000e+00	0.0000e+00	0.0000e+00
CP	CS	CS	CV	3	3.0334e+01	0.0000e+00	-3.0334e+01	0.0000e+00	0.0000e+00	0.0000e+00
CP	CU	CU	CS	3	3.0334e+01	0.0000e+00	-3.0334e+01	0.0000e+00	0.0000e+00	0.0000e+00
CP	CU	CU	CU	3	3.0334e+01	0.0000e+00	-3.0334e+01	0.0000e+00	0.0000e+00	0.0000e+00
CP	CV	CV	CR	3	3.0334e+01	0.0000e+00	-3.0334e+01	0.0000e+00	0.0000e+00	0.0000e+00
CP	CV	CV	CS	3	3.0334e+01	0.0000e+00	-3.0334e+01	0.0000e+00	0.0000e+00	0.0000e+00
CP	CV	CV	CV	3	3.0334e+01	0.0000e+00	-3.0334e+01	0.0000e+00	0.0000e+00	0.0000e+00
CR	CO	CO	CS	3	3.0334e+01	0.0000e+00	-3.0334e+01	0.0000e+00	0.0000e+00	0.0000e+00
CR	CP	CP	CV	3	3.0334e+01	0.0000e+00	-3.0334e+01	0.0000e+00	0.0000e+00	0.0000e+00
CR	CR	CR	CR	3	3.0334e+01	0.0000e+00	-3.0334e+01	0.0000e+00	0.0000e+00	0.0000e+00
CR	CR	CR	CS	3	3.0334e+01	0.0000e+00	-3.0334e+01	0.0000e+00	0.0000e+00	0.0000e+00
CR	CR	CR	CU	3	3.0334e+01	0.0000e+00	-3.0334e+01	0.0000e+00	0.0000e+00	0.0000e+00
CR	CR	CR	CV	3	3.0334e+01	0.0000e+00	-3.0334e+01	0.0000e+00	0.0000e+00	0.0000e+00
CR	CR	CS	CS	3	3.0334e+01	0.0000e+00	-3.0334e+01	0.0000e+00	0.0000e+00	0.0000e+00
CR	CR	CU	CU	3	3.0334e+01	0.0000e+00	-3.0334e+01	0.0000e+00	0.0000e+00	0.0000e+00
CR	CR	CV	CV	3	3.0334e+01	0.0000e+00	-3.0334e+01	0.0000e+00	0.0000e+00	0.0000e+00
CR	CS	CS	CS	3	3.0334e+01	0.0000e+00	-3.0334e+01	0.0000e+00	0.0000e+00	0.0000e+00
CR	CS	CS	CU	3	3.0334e+01	0.0000e+00	-3.0334e+01	0.0000e+00	0.0000e+00	0.0000e+00
CR	CU	CU	CS	3	3.0334e+01	0.0000e+00	-3.0334e+01	0.0000e+00	0.0000e+00	0.0000e+00
CR	CU	CU	CU	3	3.0334e+01	0.0000e+00	-3.0334e+01	0.0000e+00	0.0000e+00	0.0000e+00
CR	CU	CU	CV	3	3.0334e+01	0.0000e+00	-3.0334e+01	0.0000e+00	0.0000e+00	0.0000e+00
CR	CV	CV	CU	3	3.0334e+01	0.0000e+00	-3.0334e+01	0.0000e+00	0.0000e+00	0.0000e+00
CR	CV	CV	CV	3	3.0334e+01	0.0000e+00	-3.0334e+01	0.0000e+00	0.0000e+00	0.0000e+00
CS	CO	CO	CV	3	3.0334e+01	0.0000e+00	-3.0334e+01	0.0000e+00	0.0000e+00	0.0000e+00

```
  CS    CP    CP    CU    3    3.0334e+01    0.0000e+00    -3.0334e+01    0.0000e+00    0.0000e+00    0.0000e+00
  CS    CP    CP    CV    3    3.0334e+01    0.0000e+00    -3.0334e+01    0.0000e+00    0.0000e+00    0.0000e+00
  CS    CR    CR    CU    3    3.0334e+01    0.0000e+00    -3.0334e+01    0.0000e+00    0.0000e+00    0.0000e+00
  CS    CS    CS    CS    3    3.0334e+01    0.0000e+00    -3.0334e+01    0.0000e+00    0.0000e+00    0.0000e+00
  CS    CS    CS    CU    3    3.0334e+01    0.0000e+00    -3.0334e+01    0.0000e+00    0.0000e+00    0.0000e+00
  CS    CS    CS    CV    3    3.0334e+01    0.0000e+00    -3.0334e+01    0.0000e+00    0.0000e+00    0.0000e+00
  CS    CS    CU    CU    3    3.0334e+01    0.0000e+00    -3.0334e+01    0.0000e+00    0.0000e+00    0.0000e+00
  CS    CS    CV    CV    3    3.0334e+01    0.0000e+00    -3.0334e+01    0.0000e+00    0.0000e+00    0.0000e+00
  CS    CU    CU    CU    3    3.0334e+01    0.0000e+00    -3.0334e+01    0.0000e+00    0.0000e+00    0.0000e+00
  CS    CV    CV    CV    3    3.0334e+01    0.0000e+00    -3.0334e+01    0.0000e+00    0.0000e+00    0.0000e+00
  CU    CO    CO    CV    3    3.0334e+01    0.0000e+00    -3.0334e+01    0.0000e+00    0.0000e+00    0.0000e+00
  CU    CR    CR    CV    3    3.0334e+01    0.0000e+00    -3.0334e+01    0.0000e+00    0.0000e+00    0.0000e+00
  CU    CU    CU    CU    3    3.0334e+01    0.0000e+00    -3.0334e+01    0.0000e+00    0.0000e+00    0.0000e+00
  CU    CU    CU    CV    3    3.0334e+01    0.0000e+00    -3.0334e+01    0.0000e+00    0.0000e+00    0.0000e+00
  CU    CU    CV    CV    3    3.0334e+01    0.0000e+00    -3.0334e+01    0.0000e+00    0.0000e+00    0.0000e+00
  CU    CV    CV    CV    3    3.0334e+01    0.0000e+00    -3.0334e+01    0.0000e+00    0.0000e+00    0.0000e+00
  CV    CV    CV    CV    3    3.0334e+01    0.0000e+00    -3.0334e+01    0.0000e+00    0.0000e+00    0.0000e+00

[ moleculetype ]
BUK           3

[ atoms ]
    1   CU    1      BUK   CU1    1     0.000015   12.0107
    2   CS    1      BUK   CS2    2     0.000013   12.0107
    3   CU    1      BUK   CU3    3     0.000015   12.0107
    4   CU    1      BUK   CU4    4     0.000015   12.0107
    5   CS    1      BUK   CS5    5     0.000013   12.0107
    6   CS    1      BUK   CS6    6     0.000013   12.0107
    7   CR    1      BUK   CR7    7    -0.000032   12.0107
    8   CU    1      BUK   CU8    8     0.000015   12.0107
    9   CS    1      BUK   CS9    9     0.000013   12.0107
   10   CP    1      BUK   CP10   10    0.000028   12.0107
   11   CV    1      BUK   CV11   11    0.000005   12.0107
   12   CO    1      BUK   CO12   12   -0.000031   12.0107
   13   CV    1      BUK   CV13   13    0.000005   12.0107
   14   CV    1      BUK   CV14   14    0.000005   12.0107
   15   CO    1      BUK   CO15   15   -0.000031   12.0107
   16   CO    1      BUK   CO16   16   -0.000031   12.0107
   17   CU    1      BUK   CU17   17    0.000015   12.0107
   18   CV    1      BUK   CV18   18    0.000005   12.0107
   19   CO    1      BUK   CO19   19   -0.000031   12.0107
   20   CS    1      BUK   CS20   20    0.000014   12.0107
   21   CR    1      BUK   CR21   21   -0.000030   12.0107
   22   CP    1      BUK   CP22   22    0.000024   12.0107
   23   CR    1      BUK   CR23   23   -0.000031   12.0107
   24   CR    1      BUK   CR24   24   -0.000031   12.0107
   25   CP    1      BUK   CP25   25    0.000024   12.0107
   26   CP    1      BUK   CP26   26    0.000024   12.0107
   27   CV    1      BUK   CV27   27    0.000005   12.0107
   28   CR    1      BUK   CR28   28   -0.000031   12.0107
   29   CP    1      BUK   CP29   29    0.000024   12.0107
   30   CO    1      BUK   CO30   30   -0.000028   12.0107
   31   CV    1      BUK   CV31   31    0.000002   12.0107
   32   CO    1      BUK   CO32   32    0.000002   12.0107
   33   CV    1      BUK   CV33   33   -0.000028   12.0107
   34   CV    1      BUK   CV34   34    0.000002   12.0107
   35   CO    1      BUK   CO35   35   -0.000028   12.0107
   36   CO    1      BUK   CO36   36   -0.000028   12.0107
   37   CU    1      BUK   CU37   37    0.000015   12.0107
   38   CV    1      BUK   CV38   38    0.000002   12.0107
   39   CO    1      BUK   CO39   39   -0.000028   12.0107
   40   CS    1      BUK   CS40   40    0.000013   12.0107
   41   CR    1      BUK   CR41   41   -0.000026   12.0107
   42   CP    1      BUK   CP42   42    0.000028   12.0107
   43   CR    1      BUK   CR43   43   -0.000026   12.0107
   44   CR    1      BUK   CR44   44   -0.000026   12.0107
   45   CP    1      BUK   CP45   45    0.000028   12.0107
   46   CP    1      BUK   CP46   46    0.000028   12.0107
   47   CV    1      BUK   CV47   47    0.000002   12.0107
   48   CR    1      BUK   CR48   48   -0.000026   12.0107
   49   CP    1      BUK   CP49   49    0.000028   12.0107
   50   CO    1      BUK   CO50   50   -0.000031   12.0107
   51   CU    1      BUK   CU51   51    0.000015   12.0107
   52   CS    1      BUK   CS52   52    0.000014   12.0107
   53   CU    1      BUK   CU53   53    0.000015   12.0107
   54   CU    1      BUK   CU54   54    0.000015   12.0107
   55   CS    1      BUK   CS55   55    0.000014   12.0107
   56   CS    1      BUK   CS56   56    0.000014   12.0107
   57   CR    1      BUK   CR57   57   -0.000026   12.0107
   58   CU    1      BUK   CU58   58    0.000015   12.0107
   59   CS    1      BUK   CS59   59    0.000014   12.0107
   60   CP    1      BUK   CP60   60    0.000024   12.0107

[ bonds ]
    1    2    1
    1    3    1
    1    4    1
    2    5    1
    2    6    1
    3    7    1
    3   17    1
    4    8    1
```

```
   4   10    1
   5    9    1
   5   28    1
   6   40    1
   6   49    1
   7   23    1
   7   28    1
   8   15    1
   8   17    1
   9   36    1
   9   40    1
  10   46    1
  10   49    1
  11   12    1
  11   13    1
  11   14    1
  12   15    1
  12   16    1
  13   17    1
  13   27    1
  14   18    1
  14   20    1
  15   19    1
  16   50    1
  16   59    1
  18   25    1
  18   27    1
  19   46    1
  19   50    1
  20   56    1
  20   59    1
  21   22    1
  21   23    1
  21   24    1
  22   25    1
  22   26    1
  23   27    1
  24   28    1
  24   30    1
  25   29    1
  26   39    1
  26   60    1
  29   56    1
  29   60    1
  30   36    1
  30   39    1
  31   32    1
  31   33    1
  31   34    1
  32   35    1
  32   36    1
  33   37    1
  33   47    1
  34   38    1
  34   40    1
  35   39    1
  35   58    1
  37   53    1
  37   58    1
  38   45    1
  38   47    1
  41   42    1
  41   43    1
  41   44    1
  42   45    1
  42   46    1
  43   47    1
  43   57    1
  44   48    1
  44   50    1
  45   49    1
  48   55    1
  48   57    1
  51   52    1
  51   53    1
  51   54    1
  52   55    1
  52   56    1
  53   57    1
  54   58    1
  54   60    1
  55   59    1

[ angles ]
    1    2    5    1
    1    2    6    1
    1    3    7    1
    1    3   17    1
    1    4    8    1
    1    4   10    1
    2    1    3    1
    2    1    4    1
```

2	5	9	1
2	5	28	1
2	6	40	1
2	6	49	1
3	1	4	1
3	7	23	1
3	7	28	1
3	17	8	1
3	17	13	1
4	8	15	1
4	8	17	1
4	10	46	1
4	10	49	1
5	2	6	1
5	9	36	1
5	9	40	1
5	28	7	1
5	28	24	1
6	40	9	1
6	40	34	1
6	49	10	1
6	49	45	1
7	3	17	1
7	23	21	1
7	23	27	1
7	28	24	1
8	4	10	1
8	15	12	1
8	15	19	1
8	17	13	1
9	5	28	1
9	36	30	1
9	36	32	1
9	40	34	1
10	46	19	1
10	46	42	1
10	49	45	1
11	12	15	1
11	12	16	1
11	13	17	1
11	13	27	1
11	14	18	1
11	14	20	1
12	11	13	1
12	11	14	1
12	15	19	1
12	16	50	1
12	16	59	1
13	11	14	1
13	27	18	1
13	27	23	1
14	18	25	1
14	18	27	1
14	20	56	1
14	20	59	1
15	8	17	1
15	12	16	1
15	19	46	1
15	19	50	1
16	50	19	1
16	50	44	1
16	59	20	1
16	59	55	1
17	13	27	1
18	14	20	1
18	25	22	1
18	25	29	1
18	27	23	1
19	46	42	1
19	60	44	1
20	56	29	1
20	56	52	1
20	59	55	1
21	22	25	1
21	22	26	1
21	23	27	1
21	24	28	1
21	24	30	1
22	21	23	1
22	21	24	1
22	25	29	1
22	26	39	1
22	26	60	1
23	7	28	1
23	21	24	1
24	30	36	1
24	30	39	1
25	18	27	1
25	22	26	1
25	29	56	1
25	29	60	1
26	39	30	1

```
  26   39   35    1
  26   60   29    1
  26   60   54    1
  28   24   30    1
  29   56   52    1
  29   60   54    1
  30   36   32    1
  30   39   35    1
  31   32   35    1
  31   32   36    1
  31   33   37    1
  31   33   47    1
  31   34   38    1
  31   34   40    1
  32   31   33    1
  32   31   34    1
  32   35   39    1
  32   35   58    1
  33   31   34    1
  33   37   53    1
  33   37   58    1
  33   47   38    1
  33   47   43    1
  34   38   45    1
  34   38   47    1
  35   32   36    1
  35   58   37    1
  35   58   54    1
  36    9   40    1
  36   30   39    1
  37   33   47    1
  37   53   51    1
  37   53   57    1
  37   58   54    1
  38   34   40    1
  38   45   42    1
  38   45   49    1
  38   47   43    1
  39   26   60    1
  39   35   58    1
  40    6   49    1
  41   42   45    1
  41   42   46    1
  41   43   47    1
  41   43   57    1
  41   44   48    1
  41   44   50    1
  42   41   43    1
  42   41   44    1
  42   45   49    1
  43   41   44    1
  43   57   48    1
  43   57   53    1
  44   48   55    1
  44   48   57    1
  45   38   47    1
  45   42   46    1
  46   10   49    1
  46   19   50    1
  47   43   57    1
  48   44   50    1
  48   55   52    1
  48   55   59    1
  48   57   53    1
  50   16   59    1
  51   52   55    1
  51   52   56    1
  51   53   57    1
  51   54   58    1
  51   54   60    1
  52   51   53    1
  52   51   54    1
  52   55   59    1
  53   37   58    1
  53   51   54    1
  55   48   57    1
  55   52   56    1
  56   20   59    1
  56   29   60    1
  58   54   60    1

[ dihedrals ]
    1    2    5    9    3
    1    2    5   28    3
    1    2    6   40    3
    1    2    6   49    3
    1    3    7   23    3
    1    3    7   28    3
    1    3   17    8    3
    1    3   17   13    3
    1    4    8   15    3
    1    4    8   17    3
```

1	4	10	46	3
1	4	10	49	3
2	1	3	7	3
2	1	3	17	3
2	1	4	8	3
2	1	4	10	3
2	5	9	36	3
2	5	9	40	3
2	5	28	7	3
2	5	28	24	3
2	6	40	9	3
2	6	40	34	3
2	6	49	10	3
2	6	49	45	3
3	1	2	5	3
3	1	2	6	3
3	1	4	8	3
3	1	4	10	3
3	7	23	21	3
3	7	23	27	3
3	7	28	5	3
3	7	28	24	3
3	17	8	4	3
3	17	8	15	3
3	17	13	11	3
3	17	13	27	3
4	1	2	5	3
4	1	2	6	3
4	1	3	7	3
4	1	3	17	3
4	8	15	12	3
4	8	15	19	3
4	8	17	13	3
4	10	46	19	3
4	10	46	42	3
4	10	49	6	3
4	10	49	45	3
5	2	6	40	3
5	2	6	49	3
5	9	36	30	3
5	9	36	32	3
5	9	40	6	3
5	9	40	34	3
5	28	7	23	3
5	28	24	21	3
5	28	24	30	3
6	2	5	9	3
6	2	5	28	3
6	40	9	36	3
6	40	34	31	3
6	40	34	38	3
6	49	10	46	3
6	49	45	38	3
6	49	45	42	3
7	3	17	8	3
7	3	17	13	3
7	23	21	22	3
7	23	21	24	3
7	23	27	13	3
7	23	27	18	3
7	28	5	9	3
7	28	24	21	3
7	28	24	30	3
8	4	10	46	3
8	4	10	49	3
8	15	12	11	3
8	15	12	16	3
8	15	19	46	3
8	15	19	50	3
8	17	13	11	3
8	17	13	27	3
9	5	28	24	3
9	36	30	24	3
9	36	30	39	3
9	36	32	31	3
9	36	32	35	3
9	40	6	49	3
9	40	34	31	3
9	40	34	38	3
10	4	8	15	3
10	4	8	17	3
10	46	19	15	3
10	46	19	50	3
10	46	42	41	3
10	46	42	45	3
10	49	6	40	3
10	49	45	38	3
10	49	45	42	3
11	12	15	19	3
11	12	16	50	3
11	12	16	59	3
11	13	27	18	3

11	13	27	23	3
11	14	18	25	3
11	14	18	27	3
11	14	20	56	3
11	14	20	59	3
12	11	13	17	3
12	11	13	27	3
12	11	14	18	3
12	11	14	20	3
12	15	8	17	3
12	15	19	46	3
12	15	19	50	3
12	16	50	19	3
12	16	50	44	3
12	16	59	20	3
12	16	59	55	3
13	11	12	15	3
13	11	12	16	3
13	11	14	18	3
13	11	14	20	3
13	17	8	15	3
13	27	18	14	3
13	27	18	25	3
13	27	23	21	3
14	11	12	15	3
14	11	12	16	3
14	11	13	17	3
14	11	13	27	3
14	18	25	22	3
14	18	25	29	3
14	18	27	23	3
14	20	56	29	3
14	20	56	52	3
14	20	59	16	3
14	20	59	55	3
15	12	16	50	3
15	12	16	59	3
15	19	46	42	3
15	19	50	16	3
15	19	50	44	3
16	12	15	19	3
16	50	19	46	3
16	50	44	41	3
16	50	44	48	3
16	59	20	56	3
16	59	55	48	3
16	59	55	52	3
17	3	7	23	3
17	3	7	28	3
17	8	15	19	3
17	13	27	18	3
17	13	27	23	3
18	14	20	56	3
18	14	20	59	3
18	25	22	21	3
18	25	22	26	3
18	25	29	56	3
18	25	29	60	3
18	27	23	21	3
19	46	10	49	3
19	46	42	41	3
19	46	42	45	3
19	50	16	59	3
19	50	44	41	3
19	50	44	48	3
20	14	18	25	3
20	14	18	27	3
20	56	29	25	3
20	56	29	60	3
20	56	52	51	3
20	56	52	55	3
20	59	16	50	3
20	59	55	48	3
20	59	55	52	3
21	22	25	29	3
21	22	26	39	3
21	22	26	60	3
21	23	7	28	3
21	24	30	36	3
21	24	30	39	3
22	21	23	27	3
22	21	24	28	3
22	21	24	30	3
22	25	18	27	3
22	25	29	56	3
22	25	29	60	3
22	26	39	30	3
22	26	39	35	3
22	26	60	29	3
22	26	60	54	3
23	7	28	24	3
23	21	22	25	3

23	21	22	26	3
23	21	24	28	3
23	21	24	30	3
23	27	18	25	3
24	21	22	25	3
24	21	22	26	3
24	21	23	27	3
24	30	36	32	3
24	30	39	26	3
24	30	39	35	3
25	22	26	39	3
25	22	26	60	3
25	29	56	52	3
25	29	60	26	3
25	29	60	54	3
26	22	25	29	3
26	39	30	36	3
26	39	35	32	3
26	39	35	58	3
26	60	29	56	3
26	60	54	51	3
26	60	54	58	3
27	18	25	29	3
27	23	7	28	3
28	5	9	36	3
28	5	9	40	3
28	24	30	36	3
28	24	30	39	3
29	56	20	59	3
29	56	52	51	3
29	56	52	55	3
29	60	26	39	3
29	60	54	51	3
29	60	54	58	3
30	36	9	40	3
30	36	32	31	3
30	36	32	35	3
30	39	26	60	3
30	39	35	32	3
30	39	35	58	3
31	32	35	39	3
31	32	35	58	3
31	33	37	53	3
31	33	37	58	3
31	33	47	38	3
31	33	47	43	3
31	34	38	45	3
31	34	38	47	3
32	31	33	37	3
32	31	33	47	3
32	31	34	38	3
32	31	34	40	3
32	35	58	37	3
32	35	58	54	3
32	36	9	40	3
32	36	30	39	3
33	31	32	35	3
33	31	32	36	3
33	31	34	38	3
33	31	34	40	3
33	37	53	51	3
33	37	53	57	3
33	37	58	35	3
33	37	58	54	3
33	47	38	34	3
33	47	38	45	3
33	47	43	41	3
33	47	43	57	3
34	31	32	35	3
34	31	32	36	3
34	31	33	37	3
34	31	33	47	3
34	38	45	42	3
34	38	45	49	3
34	38	47	43	3
34	40	6	49	3
34	40	9	36	3
35	39	26	60	3
35	39	30	36	3
35	58	37	53	3
35	58	54	51	3
35	58	54	60	3
36	32	35	39	3
36	32	35	58	3
37	33	47	38	3
37	33	47	43	3
37	53	51	52	3
37	53	51	54	3
37	53	57	43	3
37	53	57	48	3
37	58	35	39	3
37	58	54	51	3

```
   37   58   54   60    3
   38   45   42   41    3
   38   45   42   46    3
   38   47   43   41    3
   38   47   43   57    3
   39   26   60   54    3
   39   35   58   54    3
   40    6   49   45    3
   40   34   38   45    3
   40   34   38   47    3
   41   42   45   49    3
   41   43   57   48    3
   41   43   57   53    3
   41   44   48   55    3
   41   44   48   57    3
   42   41   43   47    3
   42   41   43   57    3
   42   41   44   48    3
   42   41   44   50    3
   42   45   38   47    3
   42   46   10   49    3
   42   46   19   50    3
   43   41   42   45    3
   43   41   42   46    3
   43   41   44   48    3
   43   41   44   50    3
   43   47   38   45    3
   43   57   48   44    3
   43   57   48   55    3
   43   57   53   51    3
   44   41   42   45    3
   44   41   42   46    3
   44   41   43   47    3
   44   41   43   57    3
   44   48   55   52    3
   44   48   55   59    3
   44   48   57   53    3
   44   50   16   59    3
   44   50   19   46    3
   45   49   10   46    3
   46   42   45   49    3
   47   33   37   53    3
   47   33   37   58    3
   47   38   45   49    3
   47   43   57   48    3
   47   43   57   53    3
   48   55   52   51    3
   48   55   52   56    3
   48   57   53   51    3
   50   16   59   55    3
   50   44   48   55    3
   50   44   48   57    3
   51   52   55   59    3
   51   53   37   58    3
   52   51   53   57    3
   52   51   54   58    3
   52   51   54   60    3
   52   55   48   57    3
   52   56   20   59    3
   52   56   29   60    3
   53   37   58   54    3
   53   51   52   55    3
   53   51   52   56    3
   53   51   54   58    3
   53   51   54   60    3
   53   57   48   55    3
   54   51   52   55    3
   54   51   52   56    3
   54   51   53   57    3
   54   60   29   56    3
   55   59   20   56    3
   56   52   55   59    3
   57   48   55   59    3
   57   53   37   58    3

[ exclusions ]
    1    45
    1    24
    1    27
    2    38
    2    46
    2    30
    3    49
    3    18
    4    11
    4    28
    5    39
    5    10
    5    31
    6    32
    6    47
    7    36
```

```
    7    11
    8    42
    8    14
    8    23
    9    33
    9    45
   10    12
   11    55
   12    48
   12    56
   13    59
   13    28
   14    21
   15    41
   15    49
   15    20
   16    42
   16    57
   17    46
   17    21
   18    52
   18    24
   19    43
   19    55
   20    22
   21    35
   22    36
   22    58
   23    39
   25    51
   25    59
   25    30
   26    37
   26    52
   27    56
   28    32
   29    35
   29    53
   31    54
   31    57
   32    60
   33    48
   34    41
   34    58
   35    40
   37    41
   38    44
   38    53
   40    42
   43    58
   44    51
   45    50
   47    51
   48    54
   50    52
   55    60
```

7: 4-(Dicyanomethylene)-2-methyl-6-(4-dimethylaminostyryl)4H-pyran (DCM)

```
[ defaults ]
1    2    yes          0.5  0.5

[ atomtypes ]
CK       12.0107     0.0000     A     3.19824e-01  2.9288e-01
CJ       12.0107     0.0000     A     3.11789e-01  2.9288e-01
CI       12.0107     0.0000     A     3.28748e-01  2.9288e-01
CH       12.0107     0.0000     A     3.3228e-01   2.7614e-01
NE       14.0067     0.0000     A     3.3228e-01   7.1128e-01
CL       12.0107     0.0000     A     3.4921e-01   2.9288e-01
CC       12.0107     0.0000     A     3.19824e-01  2.9288e-01
CB       12.0107     0.0000     A     3.13222e-01  6.2760e-01
NC       14.0067     0.0000     A     2.28979e-01  7.1128e-01
CG       12.0107     0.0000     A     3.31752e-01  3.1798e-01
CF       12.0107     0.0000     A     3.15599e-01  2.9288e-01
CE       12.0107     0.0000     A     3.34489e-01  2.7614e-01
CD       12.0107     0.0000     A     3.34489e-01  2.7614e-01
HJ        1.0079     0.0000     A     1.87536e-01  1.2552e-01
HI        1.0079     0.0000     A     1.92787e-01  1.2552e-01
OD       15.9994     0.0000     A     3.11789e-01  5.8576e-01

[ nonbond_params ]
   CB    CB     1     3.68442e-01     6.2760e-01
   CB    CC     1     3.34647e-01     4.6024e-01
   CB    CD     1     3.81572e-01     4.5187e-01
   CB    CE     1     3.7645e-01      4.5187e-01
   CB    CF     1     4.33241e-01     4.6024e-01
   CB    CG     1     4.27665e-01     4.7279e-01
   CB    CH     1     5.60536e-01     4.5187e-01
   CB    CI     1     3.61868e-01     4.6024e-01
   CB    CJ     1     3.21886e-01     4.6024e-01
   CB    CK     1     3.41766e-01     4.6024e-01
```

CB	CL	1	4.51632e-01	4.6024e-01
CB	HI	1	3.10152e-01	3.7656e-01
CB	HJ	1	3.02154e-01	3.7656e-01
CB	NC	1	3.43542e-01	6.6944e-01
CB	NE	1	4.50485e-01	6.6944e-01
CB	OD	1	4.3374e-01	6.0668e-01
CC	CC	1	3.67822e-01	2.9288e-01
CC	CD	1	4.74628e-01	2.8451e-01
CC	CE	1	4.43329e-01	2.8451e-01
CC	CF	1	5.39288e-01	2.9288e-01
CC	CG	1	4.95599e-01	3.0543e-01
CC	CH	1	6.43671e-01	2.8451e-01
CC	CI	1	3.67314e-01	2.9288e-01
CC	CJ	1	3.29625e-01	2.9288e-01
CC	CK	1	3.29413e-01	2.9288e-01
CC	CL	1	4.02247e-01	2.9288e-01
CC	HI	1	3.54905e-01	2.0920e-01
CC	HJ	1	3.90837e-01	2.0920e-01
CC	NC	1	3.47305e-01	5.0208e-01
CC	NE	1	5.2528e-01	5.0208e-01
CC	OD	1	4.02173e-01	4.3932e-01
CD	CD	1	3.54655e-01	2.7614e-01
CD	CE	1	3.44521e-01	2.7614e-01
CD	CF	1	3.45917e-01	2.8451e-01
CD	CG	1	3.89903e-01	2.9706e-01
CD	CH	1	3.58428e-01	2.7614e-01
CD	CI	1	4.4185e-01	2.8451e-01
CD	CJ	1	5.15793e-01	2.8451e-01
CD	CK	1	3.89977e-01	2.8451e-01
CD	CL	1	4.75775e-01	2.8451e-01
CD	HI	1	3.24688e-01	2.0083e-01
CD	HJ	1	2.71281e-01	2.0083e-01
CD	NC	1	3.3005e-01	4.9371e-01
CD	NE	1	3.75506e-01	4.9371e-01
CD	OD	1	4.20619e-01	4.3095e-01
CE	CE	1	4.49801e-01	2.7614e-01
CE	CF	1	4.03301e-01	2.8451e-01
CE	CG	1	3.74591e-01	2.9706e-01
CE	CH	1	5.61045e-01	2.7614e-01
CE	CI	1	4.64734e-01	2.8451e-01
CE	CJ	1	3.61443e-01	2.8451e-01
CE	CK	1	4.13952e-01	2.8451e-01
CE	CL	1	4.11438e-01	2.8451e-01
CE	HI	1	3.04068e-01	2.0083e-01
CE	HJ	1	3.02173e-01	2.0083e-01
CE	NC	1	3.26733e-01	4.9371e-01
CE	NE	1	4.80315e-01	4.9371e-01
CE	OD	1	4.97347e-01	4.3095e-01
CF	CF	1	3.3571e-01	2.9288e-01
CF	CG	1	3.92186e-01	3.0543e-01
CF	CH	1	3.33888e-01	2.8451e-01
CF	CI	1	4.59732e-01	2.9288e-01
CF	CJ	1	5.48137e-01	2.9288e-01
CF	CK	1	3.38382e-01	2.9288e-01
CF	CL	1	5.05844e-01	2.9288e-01
CF	HI	1	2.61821e-01	2.0920e-01
CF	HJ	1	2.7804e-01	2.0920e-01
CF	NC	1	3.64558e-01	5.0208e-01
CF	NE	1	3.42571e-01	5.0208e-01
CF	OD	1	4.53038e-01	4.3932e-01
CG	CG	1	4.18927e-01	3.1798e-01
CG	CH	1	4.48942e-01	2.9706e-01
CG	CI	1	3.41711e-01	3.0543e-01
CG	CJ	1	3.7055e-01	3.0543e-01
CG	CK	1	4.12686e-01	3.0543e-01
CG	CL	1	3.83217e-01	3.0543e-01
CG	HI	1	3.46029e-01	2.2175e-01
CG	HJ	1	2.86306e-01	2.2175e-01
CG	NC	1	3.18114e-01	5.1463e-01
CG	NE	1	4.59593e-01	5.1463e-01
CG	OD	1	3.43495e-01	4.5187e-01
CH	CH	1	3.5767e-01	2.7614e-01
CH	CI	1	6.27194e-01	2.8451e-01
CH	CJ	1	6.83495e-01	2.8451e-01
CH	CK	1	3.72483e-01	2.8451e-01
CH	CL	1	6.06925e-01	2.8451e-01
CH	HI	1	3.64752e-01	2.0083e-01
CH	HJ	1	2.93962e-01	2.0083e-01
CH	NC	1	4.74739e-01	4.9371e-01
CH	NE	1	3.42247e-01	4.9371e-01
CH	OD	1	5.9362e-01	4.3095e-01
CI	CI	1	4.72658e-01	2.9288e-01
CI	CJ	1	3.29875e-01	2.9288e-01
CI	CK	1	3.51614e-01	2.9288e-01
CI	CL	1	3.59575e-01	2.9288e-01
CI	HI	1	3.18825e-01	2.0920e-01
CI	HJ	1	3.64947e-01	2.0920e-01
CI	NC	1	3.92094e-01	5.0208e-01
CI	NE	1	5.79898e-01	5.0208e-01
CI	OD	1	3.99972e-01	4.3932e-01
CJ	CJ	1	3.4884e-01	2.9288e-01
CJ	CK	1	3.50929e-01	2.9288e-01

```
    CJ    CL    1    3.4343e-01     2.9288e-01
    CJ    HI    1    3.55608e-01    2.0920e-01
    CJ    HJ    1    2.99667e-01    2.0920e-01
    CJ    NC    1    3.557e-01      5.0208e-01
    CJ    NE    1    6.33907e-01    5.0208e-01
    CJ    OD    1    3.21147e-01    4.3932e-01
    CK    CK    1    3.58224e-01    2.9288e-01
    CK    CL    1    3.46121e-01    2.9288e-01
    CK    HI    1    3.29505e-01    2.0920e-01
    CK    HJ    1    3.00887e-01    2.0920e-01
    CK    NC    1    3.88386e-01    5.0208e-01
    CK    NE    1    4.00499e-01    5.0208e-01
    CK    OD    1    3.46759e-01    4.3932e-01
    CL    CL    1    3.79242e-01    2.9288e-01
    CL    HI    1    3.50939e-01    2.0920e-01
    CL    HJ    1    3.37911e-01    2.0920e-01
    CL    NC    1    3.83097e-01    5.0208e-01
    CL    NE    1    5.79251e-01    5.0208e-01
    CL    OD    1    3.40417e-01    4.3932e-01
    HI    HI    1    1.98567e-01    1.2552e-01
    HI    HJ    1    2.13786e-01    1.2552e-01
    HI    NC    1    2.17208e-01    4.1840e-01
    HI    NE    1    3.40961e-01    4.1840e-01
    HI    OD    1    3.43874e-01    3.5564e-01
    HJ    HJ    1    1.93157e-01    1.2552e-01
    HJ    NC    1    2.32732e-01    4.1840e-01
    HJ    NE    1    3.15599e-01    4.1840e-01
    HJ    OD    1    3.70559e-01    3.5564e-01
    NC    NC    1    3.78557e-01    7.1128e-01
    NC    NE    1    3.9375e-01     7.1128e-01
    NC    OD    1    4.68525e-01    6.4852e-01
    NE    NE    1    3.44235e-01    7.1128e-01
    NE    OD    1    5.5276e-01     6.4852e-01
    OD    OD    1    3.7999e-01     5.8576e-01

[ bondtypes ]
    CB    CC    1    1.4225e-01    3.3472e+05
    CB    NC    1    1.1664e-01    5.4392e+05
    CC    CK    1    1.3973e-01    3.9246e+05
    CD    HJ    1    1.0961e-01    2.8451e+05
    CD    NE    1    1.4546e-01    2.8200e+05
    CE    CI    1    1.4934e-01    2.6527e+05
    CE    HJ    1    1.0951e-01    2.8451e+05
    CF    CF    1    1.3839e-01    3.9246e+05
    CF    CH    1    1.4183e-01    2.6527e+05
    CF    CK    1    1.4101e-01    3.9246e+05
    CF    HI    1    1.0852e-01    3.0711e+05
    CG    CG    1    1.3572e-01    3.2217e+05
    CG    CK    1    1.4494e-01    3.2217e+05
    CG    CL    1    1.4392e-01    4.5940e+05
    CG    HI    1    1.0873e-01    3.0711e+05
    CH    NE    1    1.3771e-01    2.8200e+05
    CI    CJ    1    1.3517e-01    4.5689e+05
    CI    OD    1    1.3650e-01    2.8451e+05
    CJ    CK    1    1.4360e-01    3.9246e+05
    CJ    CL    1    1.3682e-01    4.5689e+05
    CJ    HI    1    1.0839e-01    3.0711e+05
    CL    OD    1    1.3710e-01    2.8451e+05

[ angletypes ]
    CB    CC    CB    1    1.1825e+02    5.8576e+02
    CB    CC    CK    1    1.2088e+02    5.8576e+02
    CC    CB    NC    1    1.7802e+02    1.2552e+03
    CC    CK    CJ    1    1.2236e+02    5.2718e+02
    CD    NE    CD    1    1.1936e+02    4.1840e+02
    CD    NE    CH    1    1.2006e+02    4.1840e+02
    CE    CI    CJ    1    1.2638e+02    5.8576e+02
    CE    CI    OD    1    1.1175e+02    5.8576e+02
    CF    CF    CH    1    1.2100e+02    5.8576e+02
    CF    CF    CK    1    1.2214e+02    5.2718e+02
    CF    CF    HI    1    1.1857e+02    2.9288e+02
    CF    CH    CF    1    1.1714e+02    3.3472e+02
    CF    CH    NE    1    1.2143e+02    6.6944e+02
    CF    CK    CF    1    1.1660e+02    5.2718e+02
    CF    CK    CG    1    1.2170e+02    5.8576e+02
    CG    CG    CK    1    1.2741e+02    5.8576e+02
    CG    CG    CL    1    1.2472e+02    2.9288e+02
    CG    CG    HI    1    1.1921e+02    2.9288e+02
    CG    CL    CJ    1    1.2452e+02    5.8576e+02
    CG    CL    OD    1    1.1487e+02    5.8576e+02
    CH    CF    HI    1    1.2030e+02    2.9288e+02
    CI    CE    HJ    1    1.1055e+02    2.9288e+02
    CI    CJ    CK    1    1.2082e+02    5.8576e+02
    CI    CJ    HI    1    1.1918e+02    2.9288e+02
    CI    OD    CL    1    1.1994e+02    5.8576e+02
    CJ    CI    OD    1    1.2186e+02    5.8576e+02
    CJ    CK    CJ    1    1.1529e+02    5.2718e+02
    CJ    CL    OD    1    1.2061e+02    5.8576e+02
    CK    CF    HI    1    1.1942e+02    2.9288e+02
    CK    CG    HI    1    1.1522e+02    2.9288e+02
    CK    CJ    CL    1    1.2148e+02    5.8576e+02
    CK    CJ    HI    1    1.1997e+02    2.9288e+02
```

```
   CL    CG    HI     1     1.1424e+02     2.9288e+02
   CL    CJ    HI     1     1.1858e+02     2.9288e+02
   HJ    CD    HJ     1     1.0801e+02     2.7614e+02
   HJ    CD    NE     1     1.1089e+02     2.9288e+02
   HJ    CE    HJ     1     1.0837e+02     2.7614e+02

[ dihedraltypes ]
   CB    CC    CB    NC    3    0.0000e+00    0.0000e+00     0.0000e+00    0.0000e+00    0.0000e+00    0.0000e+00
   CB    CC    CK    CJ    3    3.0334e+01    0.0000e+00    -3.0334e+01    0.0000e+00    0.0000e+00    0.0000e+00
   CC    CK    CJ    CI    3    3.0334e+01    0.0000e+00    -3.0334e+01    0.0000e+00    0.0000e+00    0.0000e+00
   CC    CK    CJ    CL    3    3.0334e+01    0.0000e+00    -3.0334e+01    0.0000e+00    0.0000e+00    0.0000e+00
   CC    CK    CJ    HI    3    3.0334e+01    0.0000e+00    -3.0334e+01    0.0000e+00    0.0000e+00    0.0000e+00
   CD    NE    CD    HJ    3    0.0000e+00    0.0000e+00     0.0000e+00    0.0000e+00    0.0000e+00    0.0000e+00
   CD    NE    CH    CF    3    3.0334e+01    0.0000e+00    -3.0334e+01    0.0000e+00    0.0000e+00    0.0000e+00
   CE    CI    CJ    CK    3    3.0334e+01    0.0000e+00    -3.0334e+01    0.0000e+00    0.0000e+00    0.0000e+00
   CE    CI    CJ    HI    3    3.0334e+01    0.0000e+00    -3.0334e+01    0.0000e+00    0.0000e+00    0.0000e+00
   CE    CI    OD    CL    3    3.0334e+01    0.0000e+00    -3.0334e+01    0.0000e+00    0.0000e+00    0.0000e+00
   CF    CF    CH    CF    3    3.0334e+01    0.0000e+00    -3.0334e+01    0.0000e+00    0.0000e+00    0.0000e+00
   CF    CF    CH    NE    3    3.0334e+01    0.0000e+00    -3.0334e+01    0.0000e+00    0.0000e+00    0.0000e+00
   CF    CF    CK    CF    3    3.0334e+01    0.0000e+00    -3.0334e+01    0.0000e+00    0.0000e+00    0.0000e+00
   CF    CF    CK    CG    3    3.0334e+01    0.0000e+00    -3.0334e+01    0.0000e+00    0.0000e+00    0.0000e+00
   CF    CH    CF    CF    3    3.0334e+01    0.0000e+00    -3.0334e+01    0.0000e+00    0.0000e+00    0.0000e+00
   CF    CH    CF    HI    3    3.0334e+01    0.0000e+00    -3.0334e+01    0.0000e+00    0.0000e+00    0.0000e+00
   CF    CK    CF    CF    3    3.0334e+01    0.0000e+00    -3.0334e+01    0.0000e+00    0.0000e+00    0.0000e+00
   CF    CK    CF    HI    3    3.0334e+01    0.0000e+00    -3.0334e+01    0.0000e+00    0.0000e+00    0.0000e+00
   CF    CK    CG    CG    3    3.0334e+01    0.0000e+00    -3.0334e+01    0.0000e+00    0.0000e+00    0.0000e+00
   CF    CK    CG    HI    3    3.0334e+01    0.0000e+00    -3.0334e+01    0.0000e+00    0.0000e+00    0.0000e+00
   CG    CG    CL    CJ    3    3.0334e+01    0.0000e+00    -3.0334e+01    0.0000e+00    0.0000e+00    0.0000e+00
   CG    CG    CL    OD    3    3.0334e+01    0.0000e+00    -3.0334e+01    0.0000e+00    0.0000e+00    0.0000e+00
   CG    CK    CF    HI    3    3.0334e+01    0.0000e+00    -3.0334e+01    0.0000e+00    0.0000e+00    0.0000e+00
   CG    CL    CJ    CK    3    3.0334e+01    0.0000e+00    -3.0334e+01    0.0000e+00    0.0000e+00    0.0000e+00
   CG    CL    CJ    HI    3    3.0334e+01    0.0000e+00    -3.0334e+01    0.0000e+00    0.0000e+00    0.0000e+00
   CG    CL    OD    CI    3    3.0334e+01    0.0000e+00    -3.0334e+01    0.0000e+00    0.0000e+00    0.0000e+00
   CH    CF    CF    CK    3    3.0334e+01    0.0000e+00    -3.0334e+01    0.0000e+00    0.0000e+00    0.0000e+00
   CH    CF    CF    HI    3    3.0334e+01    0.0000e+00    -3.0334e+01    0.0000e+00    0.0000e+00    0.0000e+00
   CH    NE    CD    HJ    3    0.0000e+00    0.0000e+00     0.0000e+00    0.0000e+00    0.0000e+00    0.0000e+00
   CI    CJ    CK    CJ    3    3.0334e+01    0.0000e+00    -3.0334e+01    0.0000e+00    0.0000e+00    0.0000e+00
   CI    OD    CL    CJ    3    3.0334e+01    0.0000e+00    -3.0334e+01    0.0000e+00    0.0000e+00    0.0000e+00
   CJ    CI    CE    HJ    3    0.0000e+00    0.0000e+00     0.0000e+00    0.0000e+00    0.0000e+00    0.0000e+00
   CJ    CI    OD    CL    3    3.0334e+01    0.0000e+00    -3.0334e+01    0.0000e+00    0.0000e+00    0.0000e+00
   CJ    CK    CJ    CL    3    3.0334e+01    0.0000e+00    -3.0334e+01    0.0000e+00    0.0000e+00    0.0000e+00
   CJ    CK    CJ    HI    3    3.0334e+01    0.0000e+00    -3.0334e+01    0.0000e+00    0.0000e+00    0.0000e+00
   CJ    CL    CG    HI    3    3.0334e+01    0.0000e+00    -3.0334e+01    0.0000e+00    0.0000e+00    0.0000e+00
   CK    CC    CB    NC    3    0.0000e+00    0.0000e+00     0.0000e+00    0.0000e+00    0.0000e+00    0.0000e+00
   CK    CF    CF    HI    3    3.0334e+01    0.0000e+00    -3.0334e+01    0.0000e+00    0.0000e+00    0.0000e+00
   CK    CG    CG    CL    3    3.0334e+01    0.0000e+00    -3.0334e+01    0.0000e+00    0.0000e+00    0.0000e+00
   CK    CG    CG    HI    3    3.0334e+01    0.0000e+00    -3.0334e+01    0.0000e+00    0.0000e+00    0.0000e+00
   CK    CJ    CI    OD    3    3.0334e+01    0.0000e+00    -3.0334e+01    0.0000e+00    0.0000e+00    0.0000e+00
   CK    CJ    CL    OD    3    3.0334e+01    0.0000e+00    -3.0334e+01    0.0000e+00    0.0000e+00    0.0000e+00
   CL    CG    CG    HI    3    3.0334e+01    0.0000e+00    -3.0334e+01    0.0000e+00    0.0000e+00    0.0000e+00
   HI    CF    CF    HI    3    3.0334e+01    0.0000e+00    -3.0334e+01    0.0000e+00    0.0000e+00    0.0000e+00
   HI    CF    CH    NE    3    3.0334e+01    0.0000e+00    -3.0334e+01    0.0000e+00    0.0000e+00    0.0000e+00
   HI    CG    CG    HI    3    3.0334e+01    0.0000e+00    -3.0334e+01    0.0000e+00    0.0000e+00    0.0000e+00
   HI    CG    CL    OD    3    3.0334e+01    0.0000e+00    -3.0334e+01    0.0000e+00    0.0000e+00    0.0000e+00
   HI    CJ    CI    OD    3    3.0334e+01    0.0000e+00    -3.0334e+01    0.0000e+00    0.0000e+00    0.0000e+00
   HI    CJ    CL    OD    3    3.0334e+01    0.0000e+00    -3.0334e+01    0.0000e+00    0.0000e+00    0.0000e+00
   HJ    CE    CI    OD    3    0.0000e+00    0.0000e+00     0.0000e+00    0.0000e+00    0.0000e+00    0.0000e+00

[ moleculetype ]
DCM           3

[ atoms ]
    1    OD    1        DCM    OD1     1     0.003491    15.9994
    2    NE    1        DCM    NE2     2     0.002743    14.0067
    3    NC    1        DCM    NC3     3    -0.024259    14.0067
    4    NC    1        DCM    NC4     4    -0.037830    14.0067
    5    CI    1        DCM    CI5     5     0.005876    12.0107
    6    CJ    1        DCM    CJ6     6     0.000830    12.0107
    7    HI    1        DCM    HI7     7     0.001279     1.0079
    8    CK    1        DCM    CK8     8    -0.011636    12.0107
    9    CJ    1        DCM    CJ9     9    -0.006995    12.0107
   10    HI    1        DCM    HI10    10    -0.004114     1.0079
   11    CL    1        DCM    CL11    11    -0.001190    12.0107
   12    CG    1        DCM    CG12    12    -0.000421    12.0107
   13    HI    1        DCM    HI13    13    -0.000039     1.0079
   14    CG    1        DCM    CG14    14     0.000427    12.0107
   15    HI    1        DCM    HI15    15     0.001874     1.0079
   16    CK    1        DCM    CK16    16     0.000305    12.0107
   17    CF    1        DCM    CF17    17    -0.000360    12.0107
   18    HI    1        DCM    HI18    18     0.001519     1.0079
   19    CF    1        DCM    CF19    19    -0.003321    12.0107
   20    HI    1        DCM    HI20    20    -0.002542     1.0079
   21    CH    1        DCM    CH21    21     0.001386    12.0107
   22    CF    1        DCM    CF22    22     0.006795    12.0107
   23    HI    1        DCM    HI23    23     0.016271     1.0079
   24    CF    1        DCM    CF24    24     0.002819    12.0107
   25    HI    1        DCM    HI25    25     0.006042     1.0079
   26    CD    1        DCM    CD26    26    -0.012777    12.0107
   27    HJ    1        DCM    HJ27    27    -0.006004     1.0079
   28    HJ    1        DCM    HJ28    28     0.019242     1.0079
   29    HJ    1        DCM    HJ29    29    -0.036685     1.0079
   30    CD    1        DCM    CD30    30     0.039435    12.0107
```

```
   31   HJ    1        DCM   HJ31   31    0.010587    1.0079
   32   HJ    1        DCM   HJ32   32    0.029610    1.0079
   33   HJ    1        DCM   HJ33   33    0.006991    1.0079
   34   CE    1        DCM   CE34   34    0.020737   12.0107
   35   HJ    1        DCM   HJ35   35    0.025928    1.0079
   36   HJ    1        DCM   HJ36   36    0.029825    1.0079
   37   HJ    1        DCM   HJ37   37    0.022658    1.0079
   38   CC    1        DCM   CC38   38   -0.028288   12.0107
   39   CB    1        DCM   CB39   39   -0.035298   12.0107
   40   CB    1        DCM   CB40   40   -0.044911   12.0107

[ bonds ]
    1    5    1
    1   11    1
    2   21    1
    2   26    1
    2   30    1
    3   39    1
    4   40    1
    5    6    1
    5   34    1
    6    7    1
    6    8    1
    8    9    1
    8   38    1
    9   10    1
    9   11    1
   11   12    1
   12   13    1
   12   14    1
   14   15    1
   14   16    1
   16   17    1
   16   24    1
   17   18    1
   17   19    1
   19   20    1
   19   21    1
   21   22    1
   22   23    1
   22   24    1
   24   25    1
   26   27    1
   26   28    1
   26   29    1
   30   31    1
   30   32    1
   30   33    1
   34   35    1
   34   36    1
   34   37    1
   38   39    1
   38   40    1

[ angles ]
    1    5    6    1
    1    5   34    1
    1   11    9    1
    1   11   12    1
    2   21   19    1
    2   21   22    1
    2   26   27    1
    2   26   28    1
    2   26   29    1
    2   30   31    1
    2   30   32    1
    2   30   33    1
    3   39   38    1
    4   40   38    1
    5    1   11    1
    5    6    7    1
    5    6    8    1
    5   34   35    1
    5   34   36    1
    5   34   37    1
    6    5   34    1
    6    8    9    1
    6    8   38    1
    7    6    8    1
    8    9   10    1
    8    9   11    1
    8   38   39    1
    8   38   40    1
    9    8   38    1
    9   11   12    1
   10    9   11    1
   11   12   13    1
   11   12   14    1
   12   14   15    1
   12   14   16    1
   13   12   14    1
   14   16   17    1
```

```
   14    16    24     1
   15    14    16     1
   16    17    18     1
   16    17    19     1
   16    24    22     1
   16    24    25     1
   17    16    24     1
   17    19    20     1
   17    19    21     1
   18    17    19     1
   19    21    22     1
   20    19    21     1
   21     2    26     1
   21     2    30     1
   21    22    23     1
   21    22    24     1
   22    24    25     1
   23    22    24     1
   26     2    30     1
   27    26    28     1
   27    26    29     1
   28    26    29     1
   31    30    32     1
   31    30    33     1
   32    30    33     1
   35    34    36     1
   35    34    37     1
   36    34    37     1
   39    38    40     1

[ dihedrals ]
    1     5     6     7     3
    1     5     6     8     3
    1     5    34    35     3
    1     5    34    36     3
    1     5    34    37     3
    1    11     9     8     3
    1    11     9    10     3
    1    11    12    13     3
    1    11    12    14     3
    2    21    19    17     3
    2    21    19    20     3
    2    21    22    23     3
    2    21    22    24     3
    3    39    38     8     3
    3    39    38    40     3
    4    40    38     8     3
    4    40    38    39     3
    5     1    11     9     3
    5     1    11    12     3
    5     6     8     9     3
    5     6     8    38     3
    6     5     1    11     3
    6     5    34    35     3
    6     5    34    36     3
    6     5    34    37     3
    6     8     9    10     3
    6     8     9    11     3
    6     8    38    39     3
    6     8    38    40     3
    7     6     5    34     3
    7     6     8     9     3
    7     6     8    38     3
    8     6     5    34     3
    8     9    11    12     3
    9     8    38    39     3
    9     8    38    40     3
    9    11    12    13     3
    9    11    12    14     3
   10     9     8    38     3
   10     9    11    12     3
   11     1     5    34     3
   11     9     8    38     3
   11    12    14    15     3
   11    12    14    16     3
   12    14    16    17     3
   12    14    16    24     3
   13    12    14    15     3
   13    12    14    16     3
   14    16    17    18     3
   14    16    17    19     3
   14    16    24    22     3
   14    16    24    25     3
   15    14    16    17     3
   15    14    16    24     3
   16    17    19    20    `3
   16    17    19    21     3
   16    24    22    21     3
   16    24    22    23     3
   17    16    24    22     3
   17    16    24    25     3
   17    19    21    22     3
```

```
   18   17   16   24    3
   18   17   19   20    3
   18   17   19   21    3
   19   17   16   24    3
   19   21    2   26    3
   19   21    2   30    3
   19   21   22   23    3
   19   21   22   24    3
   20   19   21   22    3
   21    2   26   27    3
   21    2   26   28    3
   21    2   26   29    3
   21    2   30   31    3
   21    2   30   32    3
   21    2   30   33    3
   21   22   24   25    3
   22   21    2   26    3
   22   21    2   30    3
   23   22   24   25    3
   26    2   30   31    3
   26    2   30   32    3
   26    2   30   33    3
   27   26    2   30    3
   28   26    2   30    3
   29   26    2   30    3

[ exclusions ]
    1    38
    1    15
    2    16
    3     6
    4     9
    7    39
    9    24
   10    40
   11    40
   11    17
   11    24
   12    38
   12    25
   13    24
   14    21
   19    28
   19    29
   20    26
   20    29
   22    32
   22    33
   23    30
   23    32
```

B.2 Polarizability Parameters

The CHARMM Drude[452] model was used to model the polarizability of the molecular mechanics region of the cells. The choice of which atoms in a molecule to attach a Drude atom and polarizability parameters were done to match the experimental bulk dielectric constant.[440,453] For H_2Pc and PTCBI, a total of 8 atoms on each molecule had a Drude atom attached. For H_2Pc the chosen atoms are CR8, CP13, CP17, CR21, CR37, CP42, CP46, and CR50, with the alpha parameter set to 6.20 and thole set to 1.4. For PTCBI the chosen atoms are CA5, CA10, CB17, CB19, CA34, CA39, CB46, and CB48, with alpha set to 6.2 and thole set to 1.5. For CuPc the chosen atoms are CUC1, CI2, CK5, CK11, CI17, CI32, CI34, CK45, CK48, with alpha set to 5.50 and thole set to 1.7. For rubrene the chosen atoms are CD6, CC19, CB21, CE28, CD41, CB56, CE63, with alpha set to 6.20 and thole set to 1.3 For C_{60} the drude site is located at the center of mass of the C_{60} molecule. We use two different polarizable forcefield for C_{60}, one with an alpha parameter of 92 and a thole parameter of 1.5 that reproduces the bulk dielectric of C_{60}. The other alpha and thole parameters are 29 and 1.5, respectively, and are used for the simulations where the dielectric of C_{60} is matched to the dielectric of DCM. For DCM the chosen atoms are OD1, NE2, CK16, CF19, CB39, CB40, with alpha set to 4.00 and thole set to 1.4.

Appendix C

Optimized geometries of key structures

C.1 Test set of large organic dyes

All geometries are optimized at the B3LYP/6-31G* level in the gas phase. The geometries are provided in .xyz format. All coordinates are specified in Å. The geometry for H_2Pc is given in the organic semiconductor crystal geometries section below. The geometry for anthracene is given in the crystal diffusion geometries section below.

1: β-carotene

```
96
beta-carotene
C        12.745662      -0.445000       0.701009
C        14.041652       0.396507       0.629154
C        13.778523       1.897929       0.708324
C        12.915735       2.321017      -0.479297
C        11.742468       1.399574      -0.741787
C        11.630196       0.169005      -0.179960
C        10.439094      -0.680888      -0.364302
C         9.148869      -0.282707      -0.247826
C         7.972372      -1.119059      -0.420817
C         6.740902      -0.546373      -0.251680
C         5.449240      -1.158543      -0.372973
C         4.283616      -0.475280      -0.179269
C         2.947185      -1.007309      -0.286088
C         1.886951      -0.163011      -0.061397
C         0.490913      -0.461292      -0.120562
C        10.755529       1.987546      -1.723955
```

C	13.102178	-1.874152	0.226580
C	12.250384	-0.529161	2.164423
C	8.169985	-2.571767	-0.780451
C	2.780483	-2.465140	-0.645739
H	14.554973	0.182279	-0.319794
H	14.719882	0.073345	1.430309
H	13.265698	2.143773	1.647179
H	14.722762	2.456344	0.712260
H	12.534639	3.342823	-0.333063
H	13.533249	2.375759	-1.391502
H	10.626799	-1.734158	-0.559650
H	8.948649	0.755148	0.015647
H	6.726710	0.513693	0.006058
H	5.400044	-2.212738	-0.631502
H	4.355597	0.581984	0.079809
H	2.131007	0.869468	0.192862
H	0.182044	-1.474305	-0.372187
H	10.076483	1.243603	-2.144590
H	10.146153	2.776458	-1.259889
H	11.299300	2.468301	-2.549302
H	13.331463	-1.893456	-0.845586
H	13.988645	-2.228985	0.766098
H	12.299578	-2.593707	0.418643
H	11.308674	-1.084945	2.226756
H	12.990344	-1.039787	2.793978
H	12.073395	0.465653	2.587547
H	8.756821	-3.089381	-0.010416
H	7.227016	-3.109378	-0.893469
H	8.726185	-2.668928	-1.721466
H	3.297365	-3.107554	0.078324
H	3.217168	-2.677224	-1.630067
H	1.734714	-2.774933	-0.673402
C	-12.745662	0.445000	-0.701009
C	-14.041652	-0.396507	-0.629154
C	-13.778523	-1.897929	-0.708324
C	-12.915735	-2.321017	0.479297
C	-11.742468	-1.399574	0.741787
C	-11.630196	-0.169005	0.179960
C	-10.439094	0.680888	0.364302
C	-9.148869	0.282707	0.247826
C	-7.972372	1.119059	0.420817
C	-6.740902	0.546373	0.251680
C	-5.449240	1.158543	0.372973
C	-4.283616	0.475280	0.179269
C	-2.947185	1.007309	0.286088
C	-1.886951	0.163011	0.061397
C	-0.490913	0.461292	0.120562
C	-10.755529	-1.987546	1.723955
C	-13.102178	1.874152	-0.226580
C	-12.250384	0.529161	-2.164423
C	-8.169985	2.571767	0.780451
C	-2.780483	2.465140	0.645739
H	-14.554973	-0.182279	0.319794
H	-14.719882	-0.073345	-1.430309

H	-13.265698	-2.143773	-1.647179
H	-14.722762	-2.456344	-0.712260
H	-12.534639	-3.342823	0.333063
H	-13.533249	-2.375759	1.391502
H	-10.626799	1.734158	0.559650
H	-8.948649	-0.755148	-0.015647
H	-6.726710	-0.513693	-0.006058
H	-5.400044	2.212738	0.631502
H	-4.355597	-0.581984	-0.079809
H	-2.131007	-0.869468	-0.192862
H	-0.182044	1.474305	0.372187
H	-10.076483	-1.243603	2.144590
H	-10.146153	-2.776458	1.259889
H	-11.299300	-2.468301	2.549302
H	-13.331463	1.893456	0.845586
H	-13.988645	2.228985	-0.766098
H	-12.299578	2.593707	-0.418643
H	-11.308674	1.084945	-2.226756
H	-12.990344	1.039787	-2.793978
H	-12.073395	-0.465653	-2.587547
H	-8.756821	3.089381	0.010416
H	-7.227016	3.109378	0.893469
H	-8.726185	2.668928	1.721466
H	-3.297365	3.107554	-0.078324
H	-3.217168	2.677224	1.630067
H	-1.734714	2.774933	0.673402

2: zinc phthalocyanine

57
ZnPc

Zn	0.000000	0.000000	0.000000
N	2.906374	1.727951	0.000086
N	0.490205	1.928681	0.000066
N	-1.727957	2.906371	-0.000023
N	-1.928695	0.490211	-0.000107
C	1.771642	2.421274	0.000077
C	1.714336	3.880351	0.000041
C	2.708259	4.859110	-0.000003
C	2.305381	6.193802	-0.000062
C	0.940874	6.541820	-0.000059
C	-0.053634	5.564562	-0.000007
C	0.347809	4.228406	0.000029
C	-0.400001	2.973987	0.000030
C	-2.421297	1.771647	-0.000070
C	-3.880385	1.714334	-0.000045
C	-4.859201	2.708209	0.000001
C	-6.193878	2.305268	0.000071
C	-6.541847	0.940750	0.000098
C	-5.564544	-0.053709	0.000032
C	-4.228412	0.347798	-0.000044
C	-2.973993	-0.399996	-0.000092
N	-0.490205	-1.928681	-0.000066
N	1.928695	-0.490211	0.000107
C	2.973993	0.399996	0.000092

N	-2.906374	-1.727951	-0.000086
C	-1.771642	-2.421274	-0.000077
C	0.400001	-2.973987	-0.000030
C	2.421297	-1.771647	0.000070
C	4.228412	-0.347798	0.000044
C	-1.714336	-3.880351	-0.000041
N	1.727957	-2.906371	0.000023
C	-0.347809	-4.228406	-0.000029
C	3.880385	-1.714334	0.000045
C	5.564544	0.053709	-0.000032
C	-2.708259	-4.859110	0.000003
C	0.053634	-5.564562	0.000007
C	4.859201	-2.708209	-0.000001
C	6.541847	-0.940750	-0.000098
C	-2.305381	-6.193802	0.000062
C	-0.940874	-6.541820	0.000059
C	6.193878	-2.305268	-0.000071
H	5.827925	1.106935	-0.000054
H	7.591846	-0.659481	-0.000191
H	6.981000	-3.054942	-0.000122
H	4.581682	-3.757757	0.000014
H	3.757783	4.581505	0.000000
H	3.055091	6.980889	-0.000125
H	0.659647	7.591830	-0.000109
H	-1.106842	5.828019	0.000000
H	-4.581682	3.757757	-0.000014
H	-6.981000	3.054942	0.000122
H	-7.591846	0.659481	0.000191
H	-5.827925	-1.106935	0.000054
H	-3.757783	-4.581505	0.000000
H	-3.055091	-6.980889	0.000125
H	-0.659647	-7.591830	0.000109
H	1.106842	-5.828019	0.000000

3: N,N'-diphenyl-N,N'-bis(3-methylphenyl)-1,1′-biphenyl-4-4′-diamine (TPD)

72
TPD

N	5.099263	0.251313	0.116701
N	-4.905755	0.085956	-0.211313
C	3.681498	0.224920	0.071445
C	3.004510	-0.106021	-1.113701
H	3.575168	-0.346900	-2.004877
C	1.615093	-0.142109	-1.149769
H	1.124091	-0.431559	-2.074625
C	0.837206	0.172834	-0.021457
C	1.527396	0.513680	1.155114
H	0.967674	0.784673	2.045745
C	2.916755	0.528131	1.209703
H	3.418007	0.787682	2.136750
C	-0.643469	0.148095	-0.070924
C	-1.344691	0.487516	-1.241412
H	-0.794152	0.793998	-2.126228
C	-2.733609	0.455762	-1.296926
H	-3.243079	0.715593	-2.219381

C	-3.487941	0.105634	-0.165087
C	-2.800286	-0.224749	1.014062
H	-3.362189	-0.501506	1.900322
C	-1.410372	-0.214514	1.050494
H	-0.910181	-0.505248	1.969989
C	-5.611710	1.089977	-0.928631
C	-5.214619	2.435116	-0.855490
H	-4.362487	2.706134	-0.240192
C	-5.906172	3.412729	-1.568201
H	-5.583931	4.448604	-1.499377
C	-7.013121	3.073857	-2.349110
H	-7.553787	3.839628	-2.898093
C	-7.416428	1.738587	-2.416121
C	-6.719699	0.751207	-1.722427
H	-7.028887	-0.287086	-1.790250
C	-5.627059	-0.935748	0.467288
C	-6.775009	-0.618332	1.209205
H	-7.097313	0.417755	1.263661
C	-7.506838	-1.605974	1.875310
C	-7.058668	-2.932244	1.815740
H	-7.607901	-3.710955	2.339471
C	-5.912005	-3.255145	1.089539
H	-5.573138	-4.287059	1.043577
C	-5.199983	-2.271031	0.407840
H	-4.314440	-2.526674	-0.165096
C	-8.762521	-1.245275	2.636120
H	-8.919226	-1.912017	3.490847
H	-9.650608	-1.324620	1.994717
H	-8.724419	-0.216788	3.010409
C	5.773571	1.264909	0.850125
C	6.897925	0.949735	1.630534
H	7.243828	-0.078153	1.676172
C	7.564471	1.947109	2.339522
H	8.433465	1.684103	2.937322
C	7.114551	3.268481	2.301487
H	7.631978	4.041844	2.862091
C	5.991472	3.583622	1.533678
H	5.633063	4.608828	1.486906
C	5.329719	2.596760	0.805751
H	4.465470	2.850406	0.200024
C	5.853702	-0.736774	-0.576407
C	5.474372	-2.085045	-0.526401
H	4.600060	-2.365029	0.055061
C	6.196232	-3.069824	-1.210958
C	7.327868	-2.689232	-1.941096
H	7.902914	-3.442196	-2.474281
C	7.719897	-1.349456	-1.986744
H	8.597148	-1.061942	-2.560698
C	6.988445	-0.371939	-1.319285
H	7.285920	0.670670	-1.366861
C	5.759049	-4.515753	-1.142256
H	4.765564	-4.655292	-1.586819
H	5.697611	-4.866584	-0.104840
H	6.457368	-5.168809	-1.674927

H	-8.271934	1.457555	-3.025073

4: 2,9-dimethyl-1,3,8,10-tetraazaperopyrene

60
RiehmGade

C	5.533782	0.018361	-0.018383
C	3.576010	1.217551	-0.012843
C	2.827083	0.016273	-0.009645
C	3.577442	-1.187494	-0.011537
C	2.861482	2.459484	-0.011193
C	1.403649	0.016404	-0.004683
C	0.712098	1.265638	-0.002766
C	1.496962	2.471175	-0.006297
C	0.710913	-1.233305	-0.001832
C	1.496566	-2.440318	-0.003620
C	2.859832	-2.430041	-0.008319
H	3.436755	-3.349277	-0.009484
H	0.990052	-3.398640	-0.000895
H	3.439224	3.378191	-0.013975
H	0.991210	3.429927	-0.005230
N	4.919262	-1.179441	-0.015960
N	4.923461	1.210860	-0.017289
C	7.065265	-0.016892	-0.023671
C	7.542462	-0.777935	1.234777
C	7.533708	-0.778768	-1.284910
C	7.662104	1.399010	-0.026173
H	7.250961	-0.249068	2.150118
H	7.114278	-1.783770	1.269202
H	8.635700	-0.863509	1.228925
H	7.235606	-0.250646	-2.198555
H	8.626968	-0.864140	-1.286757
H	7.105579	-1.784767	-1.315514
H	8.756673	1.333740	-0.030462
H	7.346280	1.966796	-0.906583
H	7.353206	1.967059	0.856529
C	-0.710922	-1.233306	0.002733
C	-1.403662	0.016402	0.005056
C	-1.496572	-2.440320	0.004988
C	-2.827096	0.016270	0.009989
C	-0.712114	1.265637	0.002583
C	-2.859838	-2.430045	0.009642
H	-0.990057	-3.398641	0.002656
C	-3.576025	1.217548	0.012617
C	-3.577452	-1.187499	0.012334
C	-1.496981	2.471174	0.005536
H	-3.436760	-3.349282	0.011172
C	-2.861501	2.459482	0.010404
N	-4.923476	1.210856	0.017056
N	-4.919272	-1.179448	0.016745
H	-0.991231	3.429926	0.004006
H	-3.439245	3.378188	0.012722
C	-5.533793	0.018355	0.018988
C	-7.065280	-0.016901	0.022840
C	-7.541255	-0.778820	-1.235542

C	-7.534934	-0.777900	1.284156
C	-7.662123	1.399002	0.023765
H	-7.248965	-0.250523	-2.150958
H	-7.112925	-1.784633	-1.268904
H	-8.634487	-0.864520	-1.230646
H	-7.237512	-0.249266	2.197729
H	-8.628212	-0.863049	1.285119
H	-7.107028	-1.783962	1.315760
H	-8.756694	1.333733	0.027086
H	-7.347116	1.967428	0.904055
H	-7.352407	1.966414	-0.859063

5: 10-(4-dimethylamino-phenyl ethynyl)-anthracene-9-carbonitrile (DMAPEAC)

45
DMAPEAC

C	3.626515	-3.668541	-0.000382
C	2.205880	-3.671714	-0.000115
C	4.317776	-2.484552	-0.000418
C	3.630350	-1.233409	-0.000187
C	2.192778	-1.234562	0.000070
C	1.513209	-2.488280	0.000098
C	4.322835	0.002930	-0.000202
C	3.628770	1.238386	0.000067
C	2.191187	1.237757	0.000346
C	1.482295	0.001142	0.000307
C	4.314623	2.490392	0.000071
C	3.621885	3.673520	0.000337
C	2.201251	3.674916	0.000623
C	1.510053	2.490616	0.000624
C	5.750850	0.003833	-0.000496
N	6.916462	0.004535	-0.000736
C	0.067080	0.000158	0.000487
C	-1.153535	0.000060	0.000508
C	-2.570762	-0.000855	0.000327
C	-3.303220	-1.206633	-0.000832
C	-3.304867	1.203904	0.001233
C	-4.689552	1.208533	0.001020
C	-5.425554	-0.002821	-0.000109
C	-4.687893	-1.213167	-0.001097
N	-6.804290	-0.003735	-0.000192
C	-7.533381	-1.260560	-0.002039
C	-7.534981	1.252153	-0.000578
H	4.167378	-4.610804	-0.000560
H	1.669120	-4.616241	-0.000080
H	5.403414	-2.481497	-0.000616
H	0.428474	-2.483656	0.000302
H	5.400265	2.488718	-0.000141
H	4.161566	4.616460	0.000335
H	1.663301	4.618766	0.000844
H	0.425328	2.484615	0.000841
H	-2.766941	-2.151022	-0.001593
H	-2.769909	2.149043	0.002114
H	-5.205813	2.160718	0.001751
H	-5.202829	-2.166064	-0.002110

H	-7.306972	-1.864596	-0.892185
H	-8.604544	-1.053708	-0.001066
H	-7.306013	-1.867464	0.885863
H	-7.309373	1.857799	0.888646
H	-8.605877	1.043938	-0.001176
H	-7.308342	1.858018	-0.889409

6: ambipolar tri(p-phenylene vinylene)

```
78
OPV1a
```

C	8.063131	-0.528291	0.043519
C	7.601632	0.786181	0.068644
C	6.225566	1.023372	0.074751
C	5.287765	-0.021551	0.056063
C	5.793354	-1.340000	0.031885
C	7.155799	-1.593850	0.025508
H	5.110091	-2.183064	0.018546
H	7.536065	-2.610378	0.006952
O	9.404091	-0.887016	0.034831
H	8.281084	1.631637	0.083568
H	5.872681	2.051348	0.094005
C	3.861161	0.305731	0.062594
C	2.827260	-0.562535	0.035592
C	1.402326	-0.236284	0.041409
C	0.897123	1.078119	0.074065
C	0.463310	-1.288261	0.012821
C	-0.902425	-1.048182	0.016413
C	-1.407615	0.266215	0.048695
C	-0.468589	1.318196	0.077633
C	-2.832508	0.592553	0.053814
H	-1.583431	-1.893661	-0.005413
H	0.822658	-2.314561	-0.012156
H	-0.827953	2.344484	0.102830
H	1.578097	1.923603	0.096490
H	3.038971	-1.630550	0.005056
H	3.649286	1.373205	0.092052
C	-3.866550	-0.275381	0.022146
H	-3.044149	1.660484	0.087493
C	-5.293071	0.052421	0.027610
H	-3.654991	-1.342798	-0.011345
C	-5.798196	1.370917	0.058584
C	-6.231220	-0.991997	0.000631
C	-7.607219	-0.754310	0.004945
C	-8.068252	0.560171	0.036957
C	-7.160546	1.625250	0.063373
H	-5.878649	-2.019965	-0.024020
H	-8.286999	-1.599348	-0.017031
H	-5.114688	2.213644	0.078742
H	-7.540515	2.641779	0.087244
O	-9.409074	0.919436	0.044396
C	-10.369322	-0.106920	0.031472
C	-11.693267	0.664564	0.053400
H	-10.261252	-0.759218	0.909794
H	-10.272288	-0.727010	-0.871124

```
N      -12.962576     -0.180071      0.051802
H      -11.746580      1.315027     -0.822686
H      -11.731264      1.289193      0.948839
C      -13.030934     -1.058712      1.277230
H      -12.949462     -0.430964      2.166112
H      -12.217906     -1.783363      1.253923
H      -13.988857     -1.580958      1.277533
C      -13.043592     -1.034094     -1.190164
H      -12.969855     -0.388901     -2.067137
H      -14.001932     -1.555596     -1.191951
H      -12.231110     -1.759770     -1.188779
C      -14.145254      0.761091      0.068008
H      -14.094872      1.375374      0.967825
H      -15.063448      0.171734      0.068460
H      -14.106862      1.392538     -0.820484
C       10.363831      0.139809      0.046543
C       11.688214     -0.631020      0.028648
H       10.264962      0.762308      0.947292
H       10.256820      0.789690     -0.833698
N       12.957154      0.214372      0.031864
H       11.728769     -1.256921     -0.865780
H       11.739884     -1.280096      0.905852
C       13.035583      1.069213      1.273385
H       12.960913      0.424505      2.150641
H       12.222529      1.794230      1.270317
H       13.993529      1.591421      1.276373
C       14.140317     -0.726170      0.018478
H       14.092189     -1.340983     -0.881112
H       14.100411     -1.357152      0.907229
H       15.058235     -0.136374      0.019559
C       13.027110      1.092229     -1.194037
H       12.213658      1.816451     -1.172555
H       12.947532      0.463863     -2.082656
H       13.984750      1.615000     -1.193076
```

7: 1,1-didemethylretinal chromophore

```
57
retinal B
C        7.090168     -0.361093      0.172283
C        8.363423      0.445587      0.053805
C        8.163928      1.895802     -0.392077
C        7.004169      2.516471      0.385416
C        5.706066      1.752595      0.102384
C        5.854535      0.237317      0.164181
C        7.341717     -1.843118      0.277931
C        4.651393     -0.556410      0.174417
C        3.370221     -0.076572      0.071409
C        2.190082     -0.886509      0.056362
C        2.316418     -2.386047      0.171766
C        0.963008     -0.241997     -0.069861
C       -0.308436     -0.841376     -0.115597
C       -1.488584     -0.124324     -0.252384
C       -2.782969     -0.685257     -0.315714
C       -2.954817     -2.184624     -0.230880
```

C	-3.873629	0.187747	-0.464267
C	-5.208818	-0.185118	-0.564688
N	-6.223211	0.662463	-0.718823
C	-7.639879	0.293775	-0.807153
C	-8.465766	0.825512	0.370137
C	-9.948770	0.446371	0.246762
C	-10.790477	0.976731	1.411416
H	9.048198	-0.083394	-0.624119
H	8.864761	0.420594	1.035846
H	7.944549	1.926494	-1.467988
H	9.089838	2.461778	-0.241797
H	6.873329	3.572560	0.124963
H	7.226273	2.480404	1.460693
H	5.322558	2.033413	-0.890137
H	4.937106	2.065163	0.819991
H	8.186474	-2.023823	0.953884
H	7.639588	-2.248304	-0.699338
H	6.497037	-2.428973	0.643024
H	4.774749	-1.631354	0.242653
H	3.213407	0.994684	-0.017883
H	2.898822	-2.789018	-0.664885
H	1.354434	-2.898915	0.179943
H	2.841969	-2.658968	1.093712
H	0.987529	0.844406	-0.146083
H	-0.373356	-1.923059	-0.043992
H	-1.414568	0.959754	-0.322874
H	-2.435056	-2.678413	-1.059419
H	-3.996200	-2.505831	-0.262472
H	-2.525052	-2.568579	0.700596
H	-3.651519	1.252802	-0.514633
H	-5.505480	-1.229005	-0.527814
H	-7.689272	-0.798766	-0.855553
H	-8.035401	0.678134	-1.755633
H	-8.369382	1.919504	0.418207
H	-8.052447	0.431292	1.307680
H	-10.039143	-0.647338	0.194123
H	-10.344963	0.834171	-0.701695
H	-10.440830	0.575843	2.370027
H	-11.841426	0.693701	1.295046
H	-10.744019	2.070556	1.469297
H	-6.011691	1.655268	-0.748403

8: 5,6-dihydroretinal chromophore

65
retinal D

C	6.174197	-1.218460	0.100274
C	7.629792	-0.878688	0.487796
C	8.081940	0.525885	0.040141
C	6.972317	1.587578	0.238180
C	5.940769	1.130298	1.277320
C	5.192682	-0.168628	0.803194
C	4.985807	2.256218	1.695400
C	6.045567	-1.229658	-1.439596
C	5.819521	-2.624891	0.616970

C	4.017520	0.161087	-0.060970
C	2.734210	-0.184599	0.206476
C	1.585594	0.155258	-0.601951
C	1.790853	0.929354	-1.878511
C	0.339858	-0.244557	-0.149340
C	-0.906485	0.011591	-0.763477
C	-2.114833	-0.400999	-0.233565
C	-3.388709	-0.146947	-0.800395
C	-3.491197	0.627826	-2.093470
C	-4.514010	-0.632694	-0.122351
C	-5.840641	-0.463844	-0.514403
N	-6.885025	-0.945440	0.148446
C	-8.296069	-0.744818	-0.202362
C	-9.039843	0.114552	0.827407
C	-10.527032	0.272426	0.480368
C	-11.278905	1.134151	1.499526
H	8.299495	-1.637899	0.064269
H	7.729214	-0.967287	1.577103
H	8.398547	0.505852	-1.008557
H	8.971449	0.803046	0.617503
H	6.462573	1.799720	-0.712953
H	7.410915	2.541274	0.554763
H	6.495555	0.837134	2.178687
H	4.803269	-0.650448	1.709149
H	5.550057	3.079835	2.146880
H	4.249766	1.912332	2.432071
H	4.433570	2.667213	0.841194
H	6.254474	-0.255823	-1.894844
H	5.045424	-1.544297	-1.759415
H	6.761947	-1.944715	-1.860159
H	4.770726	-2.873215	0.409836
H	5.977295	-2.704232	1.699374
H	6.442552	-3.386222	0.132960
H	4.226982	0.734162	-0.961684
H	2.529768	-0.752759	1.113141
H	2.260425	1.897896	-1.670419
H	0.863976	1.121464	-2.419336
H	2.462247	0.384748	-2.552208
H	0.310931	-0.802556	0.785627
H	-0.916384	0.569286	-1.695410
H	-2.093866	-0.960295	0.700404
H	-3.043845	1.621291	-1.981564
H	-4.516150	0.767221	-2.437527
H	-2.947119	0.110982	-2.891578
H	-4.337467	-1.189538	0.796676
H	-6.096350	0.088960	-1.413420
H	-8.766306	-1.731638	-0.290437
H	-8.323579	-0.280833	-1.193207
H	-8.559017	1.099767	0.887532
H	-8.941375	-0.344591	1.821442
H	-10.993413	-0.720460	0.420609
H	-10.622186	0.717938	-0.519529
H	-11.228554	0.697480	2.503805
H	-12.335464	1.226158	1.228914

H	-10.858519	2.145218	1.552183
H	-6.703818	-1.460827	1.005266

9: rhodamine-6G

64			
C	2.858536	-1.842571	0.253880
C	3.945990	-0.956615	0.118093
C	3.716252	0.391105	-0.354986
C	2.435502	0.772403	-0.660118
C	1.313892	-0.099546	-0.533819
C	1.583944	-1.415316	-0.064969
C	-0.016304	0.270498	-0.819106
C	-1.036091	-0.696635	-0.682377
O	0.583511	-2.322371	0.084110
C	-0.701567	-1.995036	-0.216167
C	-1.657485	-2.970039	-0.031470
C	-3.020751	-2.717642	-0.305245
C	-3.396781	-1.418300	-0.818338
C	-2.408801	-0.470791	-0.972966
N	-3.884188	-3.761290	-0.116919
C	-5.314327	-3.749869	0.226460
C	-5.603794	-3.215459	1.632560
H	-3.417921	-4.596122	0.217096
N	5.203722	-1.348566	0.423003
C	5.583726	-2.672691	0.912407
C	7.088244	-2.744020	1.152514
H	5.949712	-0.680037	0.295742
C	-0.329643	1.626627	-1.367826
C	-0.320198	1.785079	-2.759554
C	-0.608644	3.021212	-3.339691
C	-0.909988	4.117870	-2.532173
C	-0.920001	3.974718	-1.146915
C	-0.632703	2.738560	-0.551572
C	-0.647631	2.578903	0.935468
O	-0.454731	1.517598	1.502514
O	-0.892580	3.731403	1.575036
C	-0.928792	3.667340	3.027141
C	-1.161967	5.073893	3.540177
H	2.994869	-2.858408	0.601796
C	4.872065	1.348478	-0.499263
H	2.257883	1.782956	-1.013199
H	-1.344925	-3.937264	0.350149
C	-4.800456	-1.066138	-1.256615
H	-2.688674	0.503302	-1.359981
H	-5.642675	-4.790170	0.142522
H	-5.873250	-3.193591	-0.524514
H	-5.088185	-3.808858	2.395370
H	-6.678913	-3.260139	1.837772
H	-5.278627	-2.174697	1.737485
H	5.280163	-3.431555	0.178430
H	5.039574	-2.882661	1.843014
H	7.646283	-2.560041	0.227530
H	7.361020	-3.738987	1.514811
H	7.405745	-2.014327	1.905714

H	-0.085368	0.932509	-3.390414
H	-0.597039	3.122862	-4.420916
H	-1.136263	5.081352	-2.978632
H	-1.152062	4.819624	-0.509291
H	0.019408	3.248151	3.376558
H	-1.727695	2.979203	3.320227
H	-0.354772	5.744863	3.230109
H	-1.196969	5.063098	4.634606
H	-2.110638	5.476411	3.171471
H	-5.513407	-1.042642	-0.425204
H	-5.179195	-1.772345	-2.004223
H	-4.805317	-0.073687	-1.715003
H	5.386550	1.513894	0.457132
H	4.525475	2.322304	-0.853937
H	5.618935	0.986835	-1.219570

10: (*Z*)-2-(3-((*E*)-4-(diphenylamino)styryl)-5,5-dimethylcyclohex-2-enylidene)-2-cyanoacetic acid

63
TAAS1

N	4.741370	-0.117929	-0.000764
C	5.691248	0.942882	-0.093737
C	5.228225	-1.457812	0.085270
C	3.361692	0.146468	0.044229
C	6.814353	0.952944	0.745779
C	7.757554	1.973701	0.642815
C	7.587500	3.003688	-0.284611
C	6.466881	2.997834	-1.118304
C	5.527508	1.971464	-1.034198
C	6.197845	-1.910634	-0.820924
C	6.692266	-3.210289	-0.725774
C	6.218825	-4.077336	0.261208
C	5.249941	-3.629103	1.161613
C	4.761683	-2.325653	1.083555
C	2.432130	-0.787852	-0.463199
C	1.071533	-0.540007	-0.407193
C	0.559855	0.655368	0.142714
C	1.500007	1.588841	0.625045
C	2.864471	1.345635	0.590606
C	-0.855500	0.966550	0.234316
C	-1.902435	0.139887	-0.029083
C	-3.297989	0.485170	0.098917
C	-4.244130	-0.489691	-0.089520
C	-3.720902	1.886616	0.477079
C	-5.161674	2.231055	0.041607
C	-6.109998	1.099774	0.495913
C	-5.653750	-0.281972	0.084063
C	-5.595038	3.544005	0.714385
C	-5.235509	2.405741	-1.489454
C	-6.536506	-1.339364	-0.084530
C	-6.041628	-2.620440	-0.475828
C	-8.015489	-1.259202	0.124914
N	-5.713555	-3.692974	-0.800447
O	-8.601367	-0.284016	0.546141

O	-8.724125	-2.375937	-0.178068
H	6.941316	0.158116	1.473861
H	8.623080	1.968488	1.299890
H	8.321129	3.801282	-0.358910
H	6.328421	3.788139	-1.851301
H	4.665908	1.958403	-1.694553
H	6.559638	-1.239606	-1.593918
H	7.443056	-3.548861	-1.434797
H	6.602061	-5.091428	0.329307
H	4.880328	-4.291231	1.940047
H	4.020955	-1.973276	1.794865
H	2.792305	-1.706775	-0.912693
H	0.392985	-1.278819	-0.823563
H	1.143390	2.519644	1.060380
H	3.553249	2.079261	0.994923
H	-1.070676	1.977067	0.577083
H	-1.704549	-0.887671	-0.329643
H	-3.909264	-1.488264	-0.358674
H	-3.026502	2.619079	0.049083
H	-3.639746	1.992050	1.570326
H	-7.125634	1.281336	0.143991
H	-6.184302	1.105645	1.594738
H	-5.559529	3.466045	1.807894
H	-6.620520	3.808999	0.431546
H	-4.941336	4.372083	0.413867
H	-4.920628	1.502798	-2.022208
H	-4.590654	3.230462	-1.816651
H	-6.260231	2.638843	-1.801547
H	-8.143325	-3.087027	-0.503878

11: 5,5′,6,6′-tetrachloro-1,1′-diethyl-3,3′-di(4-sulfobutyl)-benzimidazolocarbocyanine (TDBC)

78
TDBC

C	3.659824	-2.199905	-3.717044
C	5.031426	-2.258027	-3.982076
C	5.915292	-1.307329	-3.441027
C	5.448205	-0.270128	-2.627782
C	4.083364	-0.214077	-2.374044
C	3.201551	-1.172766	-2.901154
Cl	5.611969	-3.555601	-5.005786
Cl	7.636109	-1.382707	-3.762468
N	1.923009	-0.857738	-2.452170
C	2.003860	0.255770	-1.653885
N	3.319449	0.671796	-1.626470
C	0.695943	-1.390492	-3.096418
C	0.523387	-0.870658	-4.522478
C	3.861593	1.534591	-0.562739
C	4.130743	0.738530	0.721194
C	4.318018	1.636189	1.951068
C	4.394384	0.857983	3.268633
S	2.824701	0.026038	3.748319
O	2.646687	-1.079600	2.746263
O	3.074967	-0.450295	5.130227

O	1.782189	1.087549	3.621922
C	0.965780	0.901275	-0.955737
C	-0.061608	0.250218	-0.284409
C	-1.157396	0.889925	0.293988
C	-2.067068	0.308660	1.185770
N	-1.835076	-0.673523	2.119967
N	-3.393065	0.688759	1.290274
C	-3.020468	-0.938634	2.791611
C	-4.007117	-0.086119	2.262451
C	-0.511380	-1.145583	2.579758
C	-0.165616	-2.561867	2.128602
C	-4.099082	1.428872	0.232902
C	-4.372657	0.541202	-0.988176
C	-4.704344	1.341653	-2.257255
C	-4.560117	0.515673	-3.539931
S	-2.821008	0.065375	-3.934129
O	-2.067514	1.348280	-3.819054
O	-2.427567	-0.943682	-2.891374
O	-2.891482	-0.504514	-5.304652
C	-3.310512	-1.822827	3.822967
C	-4.623861	-1.853894	4.304395
C	-5.613751	-1.017401	3.761392
C	-5.313891	-0.118252	2.732197
Cl	-4.994714	-2.976466	5.597475
H	-6.089816	0.521322	2.329932
H	2.993031	-2.940673	-4.140366
H	6.143711	0.450538	-2.215229
H	-0.178027	-1.102870	-2.513593
H	0.774511	-2.482413	-3.060286
H	0.361832	0.210963	-4.508889
H	-0.383528	-1.308084	-4.948791
H	1.378832	-1.108716	-5.164831
H	3.131466	2.324383	-0.377908
H	4.760427	2.018604	-0.960023
H	5.011356	0.097367	0.577755
H	3.287759	0.069157	0.913833
H	3.470219	2.328842	2.026651
H	5.227234	2.247692	1.840505
H	4.624245	1.537165	4.095410
H	5.165201	0.079614	3.242925
H	1.053633	1.977853	-0.848935
H	0.004120	-0.831015	-0.191473
H	-1.381839	1.901006	-0.028925
H	-0.515907	-1.079265	3.671971
H	0.239746	-0.430419	2.245403
H	-0.850072	-3.310859	2.544415
H	0.853193	-2.766053	2.468715
H	-0.193863	-2.656542	1.037370
H	-3.479408	2.284314	-0.047288
H	-5.012291	1.837229	0.678479
H	-5.181000	-0.165330	-0.754221
H	-3.478170	-0.054439	-1.194452
H	-4.017080	2.192966	-2.340897
H	-5.723525	1.753146	-2.200577

H	-4.912021	1.087626	-4.403916
H	-5.127468	-0.420313	-3.494977
H	-2.559836	-2.477299	4.248132
Cl	-7.266381	-1.066524	4.346446

12: chlorin

```
40
chlorin
C      0.930549     -4.219503      0.000273
C     -0.442208     -4.263680      0.000068
C     -0.932371     -2.915277     -0.000015
N      0.165868     -2.101802      0.000192
C      1.330040     -2.845137      0.000280
C      2.615911     -2.321331      0.000272
C      2.982035     -0.965842      0.000083
N      2.110050      0.083572     -0.000116
C      4.360086     -0.503473     -0.000086
C      4.303028      0.856014     -0.000240
C      2.891152      1.201909     -0.000194
C      2.415157      2.522675     -0.000246
C      1.091258      2.941394     -0.000134
C     -2.274506     -2.508319     -0.000343
C     -2.783081     -1.215743     -0.000404
C     -4.285684     -0.944747     -0.001558
N     -2.049587     -0.080830      0.000071
C     -4.350670      0.592492      0.001543
C     -2.875661      0.989099      0.000520
N     -0.010442      2.108125      0.000036
C     -1.169580      2.831960      0.000227
C     -0.788243      4.214740      0.000189
C      0.583724      4.279910     -0.000037
C     -2.474844      2.318918      0.000510
H      1.618533     -5.054854      0.000373
H     -1.076371     -5.140402     -0.000031
H      0.153363     -1.088153      0.000147
H      3.423860     -3.048139      0.000351
H      5.236411     -1.140500     -0.000050
H      5.123244      1.563889     -0.000357
H      3.161989      3.312153     -0.000345
H     -3.000569     -3.316761     -0.000667
H     -4.766687     -1.390626      0.876800
H     -4.763934     -1.386471     -0.883571
H     -4.864148      0.992608      0.883486
H     -4.867110      0.996497     -0.876835
H      0.053159      1.096498      0.000093
H     -1.489711      5.038599      0.000327
H      1.203774      5.166884     -0.000123
H     -3.263320      3.066731      0.000806
```

13: free-base porphyrin (porphin)

```
38
porphin
C      4.260039     -0.682826      0.000028
```

C	4.259003	0.689328	0.000043
C	2.894326	1.132289	0.000038
N	2.116259	0.001641	0.000000
C	2.896026	-1.127843	0.000036
C	2.423407	-2.439201	0.000036
C	1.086754	-2.854952	0.000016
N	0.001518	-2.029789	-0.000012
C	0.681409	-4.257724	-0.000024
C	-0.674911	-4.258786	0.000020
C	-1.082444	-2.856653	-0.000009
C	-2.419723	-2.442935	-0.000004
C	-2.894314	-1.132287	0.000001
C	2.419730	2.442931	0.000042
C	1.082441	2.856639	0.000011
C	0.674924	4.258781	-0.000130
N	-0.001516	2.029789	-0.000085
C	-0.681397	4.257729	0.000075
C	-1.086757	2.854965	-0.000017
N	-2.116248	-0.001641	-0.000003
C	-2.896014	1.127841	0.000009
C	-4.260027	0.682827	0.000044
C	-4.258991	-0.689328	0.000018
C	-2.423400	2.439205	0.000015
H	5.116594	-1.344007	0.000029
H	5.114567	1.351790	0.000055
H	1.100839	0.000898	-0.000036
H	3.182106	-3.216806	0.000039
H	1.356413	-5.105042	-0.000039
H	-1.348591	-5.107156	0.000039
H	-3.177266	-3.221668	0.000007
H	3.177262	3.221674	0.000042
H	1.348612	5.107144	-0.000207
H	-1.356392	5.105054	0.000160
H	-1.100827	-0.000898	-0.000016
H	-5.116574	1.344017	0.000073
H	-5.114548	-1.351800	0.000028
H	-3.182110	3.216801	0.000061

14: pentacene

36
pentacene

C	4.941789	-1.410408	0.000240
C	6.117814	-0.716617	0.000127
C	6.117814	0.716617	-0.000127
C	4.941789	1.410408	-0.000240
C	3.678571	0.727467	-0.000115
C	3.678571	-0.727467	0.000115
C	2.467682	-1.407697	0.000171
C	1.226431	-0.728336	0.000048
C	1.226431	0.728336	-0.000048
C	2.467682	1.407697	-0.000171
C	0.000000	1.408315	0.000000
C	-1.226431	0.728336	0.000048
C	-1.226431	-0.728336	-0.000048

```
C        0.000000     -1.408315      0.000000
H        4.939421     -2.498043      0.000427
H        7.066072     -1.247456      0.000230
H        7.066072      1.247456     -0.000230
H        4.939421      2.498043     -0.000427
H        2.467469     -2.496005      0.000300
H        2.467469      2.496005     -0.000300
H        0.000000      2.496525      0.000000
C       -2.467682      1.407697      0.000171
C       -2.467682     -1.407697     -0.000171
H        0.000000     -2.496525      0.000000
C       -3.678571      0.727467      0.000115
C       -3.678571     -0.727467     -0.000115
C       -4.941789     -1.410408     -0.000240
C       -6.117814     -0.716617     -0.000127
C       -6.117814      0.716617      0.000127
C       -4.941789      1.410408      0.000240
H       -2.467469      2.496005      0.000300
H       -2.467469     -2.496005     -0.000300
H       -4.939421     -2.498043     -0.000427
H       -7.066072     -1.247456     -0.000230
H       -7.066072      1.247456      0.000230
H       -4.939421      2.498043      0.000427
```

C.2 Crystal Diffusion Geometries

All geometries are optimized at the PBE0/6-31G* level in the gas phase. The monomer geometries are put in maximal coincidence with the experimentally determined crystal structure[454–459] to create the final optimized unit cell (RMSD ¡ 0.01 nm). The geometries are given in `.gro` format. All coordinates are specified in nm.

1: tetracene

```
tetracene
60
    1TET     C1    1  -0.0569927   0.3768245  -0.1657946
    1TET     C2    2   0.0362213   0.4344985  -0.2517048
    1TET     C3    3   0.0133923   0.4462232  -0.3927829
    1TET     C4    4   0.1067039   0.5033039  -0.4747739
    1TET     C5    5   0.2297956   0.5528336  -0.4212768
    1TET     C6    6   0.2558842   0.5437985  -0.2873891
    1TET     C7    7   0.1611146   0.4847539  -0.1974250
    1TET     C8    8   0.1849920   0.4741962  -0.0606233
    1TET     C9    9  -0.0337130   0.3656865  -0.0271485
    1TET    H10   10  -0.1506328   0.3391428  -0.2064700
    1TET    H11   11  -0.0802489   0.4085207  -0.4332543
    1TET    H12   12   0.0879569   0.5114725  -0.5815002
```

```
    1TET    H13   13   0.3026163   0.5978464  -0.4882052
    1TET    H14   14   0.3493917   0.5814036  -0.2465221
    1TET    H15   15   0.2786198   0.5118689  -0.0199127
    1TET    C16   16   0.0912233   0.4159607   0.0271485
    1TET    C17   17   0.1145030   0.4048227   0.1657946
    1TET    C18   18   0.0212891   0.3471487   0.2517048
    1TET    C19   19   0.0441180   0.3354240   0.3927829
    1TET    C20   20  -0.0491936   0.2783433   0.4747739
    1TET    C21   21  -0.1722853   0.2288136   0.4212768
    1TET    C22   22  -0.1983739   0.2378487   0.2873891
    1TET    C23   23  -0.1036043   0.2968933   0.1974250
    1TET    C24   24  -0.1274817   0.3074510   0.0606233
    1TET    H25   25  -0.2211095   0.2697783   0.0199127
    1TET    H26   26  -0.2918814   0.2002435   0.2465221
    1TET    H27   27  -0.2451060   0.1838008   0.4882052
    1TET    H28   28  -0.0304466   0.2701746   0.5815002
    1TET    H29   29   0.1377592   0.3731265   0.4332543
    1TET    H30   30   0.2081431   0.4425043   0.2064700
    2TET     C1    1  -0.3962827   0.1000413  -0.1276476
    2TET     C2    2  -0.3073754   0.1007321  -0.2348423
    2TET     C3    3  -0.3368875   0.1672213  -0.3584136
    2TET     C4    4  -0.2477063   0.1662548  -0.4620166
    2TET     C5    5  -0.1223419   0.0985168  -0.4492871
    2TET     C6    6  -0.0899167   0.0337765  -0.3333326
    2TET     C7    7  -0.1801756   0.0320033  -0.2219267
    2TET     C8    8  -0.1498285  -0.0331234  -0.1026210
    2TET     C9    9  -0.3664472   0.0343755  -0.0064593
    2TET    H10   10  -0.4916502   0.1515635  -0.1373112
    2TET    H11   11  -0.4322371   0.2186681  -0.3678874
    2TET    H12   12  -0.2715092   0.2170999  -0.5550589
    2TET    H13   13  -0.0528869   0.0989708  -0.5328587
    2TET    H14   14   0.0053399  -0.0177642  -0.3234510
    2TET    H15   15  -0.0544699  -0.0846539  -0.0929208
    2TET    C16   16  -0.2392028  -0.0343755   0.0064593
    2TET    C17   17  -0.2093673  -0.1000413   0.1276476
    2TET    C18   18  -0.2982746  -0.1007321   0.2348423
    2TET    C19   19  -0.2687625  -0.1672213   0.3584136
    2TET    C20   20  -0.3579437  -0.1662548   0.4620166
    2TET    C21   21  -0.4833081  -0.0985168   0.4492871
    2TET    C22   22  -0.5157333  -0.0337765   0.3333326
    2TET    C23   23  -0.4254744  -0.0320033   0.2219267
    2TET    C24   24  -0.4558215   0.0331234   0.1026210
    2TET    H25   25  -0.5511801   0.0846539   0.0929208
    2TET    H26   26  -0.6109899   0.0177642   0.3234510
    2TET    H27   27  -0.5527631  -0.0989708   0.5328587
    2TET    H28   28  -0.3341408  -0.2170999   0.5550589
    2TET    H29   29  -0.1734129  -0.2186681   0.3678874
    2TET    H30   30  -0.1139998  -0.1515635   0.1373112
0.62873  0.77725  1.41718  0.00000  0.00000  0.07201  0.00000  0.06032  0.33720
```

2: anthracene

```
anthracene
   48
    1ANT     C1    1  -0.1584124   0.0174255   0.3346886
```

```
    1ANT     C2    2  -0.0782055   0.0934368   0.2570651
    1ANT     C3    3  -0.0379675   0.0490318   0.1272037
    1ANT     C4    4   0.0439453   0.1252234   0.0441730
    1ANT     C5    5  -0.0828967  -0.0792561   0.0821142
    1ANT     C6    6  -0.1676551  -0.1558082   0.1678942
    1ANT     C7    7  -0.2042577  -0.1091799   0.2896908
    1ANT     H8    8  -0.1831731   0.0474695   0.4261507
    1ANT     H9    9  -0.0432485   0.1802640   0.2859333
    1ANT    H10   10   0.0763705   0.2133124   0.0742327
    1ANT    H11   11  -0.1977085  -0.2439573   0.1338021
    1ANT    H12   12  -0.2648754  -0.1634394   0.3510015
    1ANT    C13   13   0.0828967   0.0792561  -0.0821142
    1ANT    C14   14  -0.0439453  -0.1252234  -0.0441730
    1ANT    C15   15   0.0379675  -0.0490318  -0.1272037
    1ANT    C16   16   0.1676551   0.1558082  -0.1678942
    1ANT    H17   17  -0.0763705  -0.2133124  -0.0742327
    1ANT    C18   18   0.0782055  -0.0934368  -0.2570651
    1ANT    C19   19   0.2042577   0.1091799  -0.2896908
    1ANT    H20   20   0.1977085   0.2439573  -0.1338021
    1ANT    C21   21   0.1584124  -0.0174255  -0.3346886
    1ANT    H22   22   0.0432485  -0.1802640  -0.2859333
    1ANT    H23   23   0.2648754   0.1634394  -0.3510015
    1ANT    H24   24   0.1831731  -0.0474695  -0.4261507
    2ANT     C1   25   0.5846824   0.3178655  -0.3346886
    2ANT     C2   26   0.5044755   0.3938768  -0.2570651
    2ANT     C3   27   0.4642375   0.3494718  -0.1272037
    2ANT     C4   28   0.3823247   0.4256634  -0.0441730
    2ANT     C5   29   0.5091667   0.2211839  -0.0821142
    2ANT     C6   30   0.5939251   0.1446318  -0.1678942
    2ANT     C7   31   0.6305277   0.1912601  -0.2896908
    2ANT     H8   32   0.6094431   0.3479095  -0.4261507
    2ANT     H9   33   0.4695185   0.4807040  -0.2859333
    2ANT    H10   34   0.3498995   0.5137524  -0.0742327
    2ANT    H11   35   0.6239785   0.0564827  -0.1338021
    2ANT    H12   36   0.6911454   0.1370006  -0.3510015
    2ANT    C13   37   0.3433733   0.3796961   0.0821142
    2ANT    C14   38   0.4702153   0.1752166   0.0441730
    2ANT    C15   39   0.3883025   0.2514082   0.1272037
    2ANT    C16   40   0.2586149   0.4562482   0.1678942
    2ANT    H17   41   0.5026405   0.0871276   0.0742327
    2ANT    C18   42   0.3480645   0.2070032   0.2570651
    2ANT    C19   43   0.2220123   0.4096199   0.2896908
    2ANT    H20   44   0.2285615   0.5443973   0.1338021
    2ANT    C21   45   0.2678576   0.2830145   0.3346886
    2ANT    H22   46   0.3830215   0.1201760   0.2859333
    2ANT    H23   47   0.1613946   0.4638794   0.3510015
    2ANT    H24   48   0.2430969   0.2529705   0.4261507
  0.85254   0.60088   0.91645   0.00000   0.00000   0.00000   0.00000  -0.63593   0.00000
```

3: napthalene

```
napthalene
36
    1NAP     C1    1  -0.0825431   0.0105798   0.2393944
    1NAP     C2    2  -0.0083015   0.0958803   0.1609037
```

```
    1NAP     C3    3   0.0233745   0.0623692   0.0264960
    1NAP     C4    4   0.0997791   0.1481184  -0.0571951
    1NAP     C5    5  -0.1287940  -0.1126658   0.1870008
    1NAP     H6    6  -0.1059558   0.0374702   0.3420570
    1NAP     H7    7   0.0272776   0.1905418   0.2009654
    1NAP     H8    8   0.1351432   0.2426933  -0.0167236
    1NAP     H9    9  -0.1873828  -0.1791907   0.2498725
    1NAP    C10   10   0.0825431  -0.0105798  -0.2393944
    1NAP    C11   11   0.0083015  -0.0958803  -0.1609037
    1NAP    C12   12  -0.0233745  -0.0623692  -0.0264960
    1NAP    C13   13  -0.0997791  -0.1481184   0.0571951
    1NAP    C14   14   0.1287940   0.1126658  -0.1870008
    1NAP    H15   15   0.1059558  -0.0374702  -0.3420570
    1NAP    H16   16  -0.0272776  -0.1905418  -0.2009654
    1NAP    H17   17  -0.1351432  -0.2426933   0.0167236
    1NAP    H18   18   0.1873828   0.1791907  -0.2498725
    2NAP     C1   19   0.4953432   0.3097297  -0.2393944
    2NAP     C2   20   0.4211017   0.3950304  -0.1609037
    2NAP     C3   21   0.3894257   0.3615192  -0.0264960
    2NAP     C4   22   0.3130212   0.4472686   0.0571951
    2NAP     C5   23   0.5415938   0.1864840  -0.1870008
    2NAP     H6   24   0.5187561   0.3366201  -0.3420570
    2NAP     H7   25   0.3855229   0.4896919  -0.2009653
    2NAP     H8   26   0.2776573   0.5418436   0.0167236
    2NAP     H9   27   0.6001824   0.1199589  -0.2498725
    2NAP    C10   28   0.3302568   0.2885703   0.2393944
    2NAP    C11   29   0.4044983   0.2032696   0.1609037
    2NAP    C12   30   0.4361743   0.2367808   0.0264960
    2NAP    C13   31   0.5125788   0.1510314  -0.0571951
    2NAP    C14   32   0.2840062   0.4118160   0.1870008
    2NAP    H15   33   0.3068439   0.2616799   0.3420570
    2NAP    H16   34   0.4400771   0.1086081   0.2009653
    2NAP    H17   35   0.5479427   0.0564564  -0.0167236
    2NAP    H18   36   0.2254176   0.4783411   0.2498725
 0.82560  0.59830  0.72994  0.00000  0.00000  0.00000  0.00000 -0.46914  0.00000
```

4: rubrene

```
rubrene
280
    1RUB    CA1    1  -0.0000000   0.0000000   0.0736803
    1RUB    CC2    2   0.1031875   0.0710312   0.1428734
    1RUB    CA3    3   0.2122921   0.1252862   0.0723126
    1RUB    CB4    4   0.3219815   0.1894317   0.1398294
    1RUB    CF5    5   0.4256660   0.2459259   0.0711859
    1RUB    CD6    6   0.0927311   0.1091879   0.2877733
    1RUB    CE7    7   0.0143537   0.2205015   0.3217589
    1RUB    CE8    8   0.0089834   0.2669825   0.4531970
    1RUB    CE9    9   0.0828546   0.2033171   0.5529963
    1RUB   CE10   10   0.1625361   0.0934665   0.5201261
    1RUB   CE11   11   0.1678661   0.0472573   0.3886357
    1RUB   HA12   12   0.3222872   0.1915023   0.2480435
    1RUB   HA13   13   0.5079652   0.2918653   0.1253013
    1RUB   HB14   14  -0.0422618   0.2711352   0.2440056
    1RUB   HB15   15  -0.0523996   0.3534047   0.4773379
```

1RUB	HB16	16	0.0789485	0.2392962	0.6554794
1RUB	HB17	17	0.2207234	0.0433720	0.5970536
1RUB	HB18	18	0.2299149	-0.0383798	0.3639738
1RUB	CC19	19	-0.1031875	-0.0710312	0.1428734
1RUB	CA20	20	-0.2122921	-0.1252862	0.0723126
1RUB	CB21	21	-0.3219815	-0.1894317	0.1398294
1RUB	CF22	22	-0.4256660	-0.2459259	0.0711859
1RUB	CD23	23	-0.0927311	-0.1091879	0.2877733
1RUB	CE24	24	-0.0143537	-0.2205015	0.3217589
1RUB	CE25	25	-0.0089834	-0.2669825	0.4531970
1RUB	CE26	26	-0.0828546	-0.2033171	0.5529963
1RUB	CE27	27	-0.1625361	-0.0934664	0.5201261
1RUB	CE28	28	-0.1678661	-0.0472573	0.3886357
1RUB	HA29	29	-0.3222872	-0.1915023	0.2480435
1RUB	HA30	30	-0.5079652	-0.2918653	0.1253013
1RUB	HB31	31	0.0422618	-0.2711352	0.2440056
1RUB	HB32	32	0.0523996	-0.3534047	0.4773379
1RUB	HB33	33	-0.0789485	-0.2392962	0.6554794
1RUB	HB34	34	-0.2207234	-0.0433720	0.5970536
1RUB	HB35	35	-0.2299149	0.0383798	0.3639738
1RUB	CA36	36	0.0000000	-0.0000000	-0.0736803
1RUB	CC37	37	-0.1031875	-0.0710312	-0.1428734
1RUB	CA38	38	-0.2122921	-0.1252862	-0.0723126
1RUB	CB39	39	-0.3219815	-0.1894317	-0.1398294
1RUB	CF40	40	-0.4256660	-0.2459259	-0.0711859
1RUB	CD41	41	-0.0927311	-0.1091879	-0.2877733
1RUB	CE42	42	-0.0143537	-0.2205015	-0.3217589
1RUB	CE43	43	-0.0089834	-0.2669825	-0.4531970
1RUB	CE44	44	-0.0828546	-0.2033171	-0.5529963
1RUB	CE45	45	-0.1625361	-0.0934665	-0.5201261
1RUB	CE46	46	-0.1678661	-0.0472573	-0.3886357
1RUB	HA47	47	-0.3222872	-0.1915023	-0.2480435
1RUB	HA48	48	-0.5079652	-0.2918653	-0.1253013
1RUB	HB49	49	0.0422618	-0.2711352	-0.2440056
1RUB	HB50	50	0.0523996	-0.3534047	-0.4773379
1RUB	HB51	51	-0.0789485	-0.2392962	-0.6554794
1RUB	HB52	52	-0.2207234	-0.0433720	-0.5970536
1RUB	HB53	53	-0.2299149	0.0383798	-0.3639738
1RUB	CC54	54	0.1031875	0.0710312	-0.1428734
1RUB	CA55	55	0.2122921	0.1252862	-0.0723126
1RUB	CB56	56	0.3219815	0.1894317	-0.1398294
1RUB	CF57	57	0.4256660	0.2459259	-0.0711859
1RUB	CD58	58	0.0927311	0.1091879	-0.2877733
1RUB	CE59	59	0.0143537	0.2205015	-0.3217589
1RUB	CE60	60	0.0089834	0.2669825	-0.4531970
1RUB	CE61	61	0.0828546	0.2033171	-0.5529963
1RUB	CE62	62	0.1625361	0.0934664	-0.5201261
1RUB	CE63	63	0.1678661	0.0472573	-0.3886357
1RUB	HA64	64	0.3222872	0.1915023	-0.2480435
1RUB	HA65	65	0.5079652	0.2918653	-0.1253013
1RUB	HB66	66	-0.0422618	0.2711352	-0.2440056
1RUB	HB67	67	-0.0523996	0.3534047	-0.4773379
1RUB	HB68	68	0.0789485	0.2392962	-0.6554794
1RUB	HB69	69	0.2207234	0.0433720	-0.5970536

1RUB	HB70	70	0.2299149	-0.0383798	-0.3639738
2RUB	CA1	71	0.3592000	0.7216500	0.0736803
2RUB	CC2	72	0.2560125	0.7926812	0.1428730
2RUB	CA3	73	0.1469079	0.8469362	0.0723126
2RUB	CB4	74	0.0372185	0.9110817	0.1398290
2RUB	CF5	75	-0.0664660	0.9675759	0.0711859
2RUB	CD6	76	0.2664689	0.8308379	0.2877730
2RUB	CE7	77	0.3448463	0.9421515	0.3217590
2RUB	CE8	78	0.3502165	0.9886325	0.4531970
2RUB	CE9	79	0.2763454	0.9249671	0.5529960
2RUB	CE10	80	0.1966639	0.8151165	0.5201260
2RUB	CE11	81	0.1913339	0.7689073	0.3886360
2RUB	HA12	82	0.0369128	0.9131523	0.2480440
2RUB	HA13	83	-0.1487652	1.0135153	0.1253010
2RUB	HB14	84	0.4014617	0.9927852	0.2440060
2RUB	HB15	85	0.4115995	1.0750547	0.4773380
2RUB	HB16	86	0.2802515	0.9609462	0.6554790
2RUB	HB17	87	0.1384766	0.7650220	0.5970540
2RUB	HB18	88	0.1292851	0.6832702	0.3639740
2RUB	CC19	89	0.4623875	0.6506188	0.1428730
2RUB	CA20	90	0.5714921	0.5963638	0.0723126
2RUB	CB21	91	0.6811815	0.5322183	0.1398290
2RUB	CF22	92	0.7848660	0.4757240	0.0711859
2RUB	CD23	93	0.4519311	0.6124621	0.2877730
2RUB	CE24	94	0.3735537	0.5011485	0.3217590
2RUB	CE25	95	0.3681834	0.4546675	0.4531970
2RUB	CE26	96	0.4420546	0.5183330	0.5529960
2RUB	CE27	97	0.5217361	0.6281836	0.5201260
2RUB	CE28	98	0.5270661	0.6743927	0.3886360
2RUB	HA29	99	0.6814871	0.5301477	0.2480440
2RUB	HA30	100	0.8671652	0.4297847	0.1253010
2RUB	HB31	101	0.3169382	0.4505148	0.2440060
2RUB	HB32	102	0.3068004	0.3682453	0.4773380
2RUB	HB33	103	0.4381485	0.4823539	0.6554790
2RUB	HB34	104	0.5799234	0.6782780	0.5970540
2RUB	HB35	105	0.5891149	0.7600298	0.3639740
2RUB	CA36	106	0.3592000	0.7216500	-0.0736803
2RUB	CC37	107	0.4623875	0.6506188	-0.1428730
2RUB	CA38	108	0.5714921	0.5963638	-0.0723126
2RUB	CB39	109	0.6811815	0.5322183	-0.1398290
2RUB	CF40	110	0.7848660	0.4757240	-0.0711859
2RUB	CD41	111	0.4519311	0.6124621	-0.2877730
2RUB	CE42	112	0.3735537	0.5011484	-0.3217590
2RUB	CE43	113	0.3681835	0.4546675	-0.4531970
2RUB	CE44	114	0.4420546	0.5183329	-0.5529960
2RUB	CE45	115	0.5217361	0.6281835	-0.5201260
2RUB	CE46	116	0.5270661	0.6743926	-0.3886360
2RUB	HA47	117	0.6814872	0.5301477	-0.2480440
2RUB	HA48	118	0.8671652	0.4297847	-0.1253010
2RUB	HB49	119	0.3169383	0.4505147	-0.2440060
2RUB	HB50	120	0.3068005	0.3682453	-0.4773380
2RUB	HB51	121	0.4381485	0.4823538	-0.6554790
2RUB	HB52	122	0.5799234	0.6782780	-0.5970540
2RUB	HB53	123	0.5891149	0.7600297	-0.3639740

2RUB	CC54	124	0.2560125	0.7926812	-0.1428730
2RUB	CA55	125	0.1469079	0.8469362	-0.0723126
2RUB	CB56	126	0.0372185	0.9110817	-0.1398290
2RUB	CF57	127	-0.0664660	0.9675759	-0.0711859
2RUB	CD58	128	0.2664689	0.8308378	-0.2877730
2RUB	CE59	129	0.3448463	0.9421515	-0.3217590
2RUB	CE60	130	0.3502166	0.9886325	-0.4531970
2RUB	CE61	131	0.2763454	0.9249670	-0.5529960
2RUB	CE62	132	0.1966639	0.8151164	-0.5201260
2RUB	CE63	133	0.1913339	0.7689073	-0.3886360
2RUB	HA64	134	0.0369129	0.9131523	-0.2480440
2RUB	HA65	135	-0.1487652	1.0135153	-0.1253010
2RUB	HB66	136	0.4014618	0.9927852	-0.2440060
2RUB	HB67	137	0.4115996	1.0750546	-0.4773380
2RUB	HB68	138	0.2802515	0.9609461	-0.6554790
2RUB	HB69	139	0.1384766	0.7650219	-0.5970540
2RUB	HB70	140	0.1292851	0.6832702	-0.3639740
3RUB	CA1	141	0.3592000	0.0000000	1.4185303
3RUB	CC2	142	0.4623875	0.0710312	1.4877234
3RUB	CA3	143	0.5714921	0.1252862	1.4171626
3RUB	CB4	144	0.6811815	0.1894317	1.4846794
3RUB	CF5	145	0.7848660	0.2459260	1.4160359
3RUB	CD6	146	0.4519311	0.1091879	1.6326233
3RUB	CE7	147	0.3735537	0.2205016	1.6666089
3RUB	CE8	148	0.3681834	0.2669825	1.7980470
3RUB	CE9	149	0.4420546	0.2033171	1.8978463
3RUB	CE10	150	0.5217361	0.0934665	1.8649761
3RUB	CE11	151	0.5270661	0.0472574	1.7334857
3RUB	HA12	152	0.6814872	0.1915023	1.5928935
3RUB	HA13	153	0.8671652	0.2918653	1.4701513
3RUB	HB14	154	0.3169382	0.2711352	1.5888556
3RUB	HB15	155	0.3068004	0.3534047	1.8221879
3RUB	HB16	156	0.4381485	0.2392962	2.0003294
3RUB	HB17	157	0.5799234	0.0433720	1.9419036
3RUB	HB18	158	0.5891149	-0.0383798	1.7088238
3RUB	CC19	159	0.2560125	-0.0710312	1.4877234
3RUB	CA20	160	0.1469079	-0.1252862	1.4171626
3RUB	CB21	161	0.0372185	-0.1894317	1.4846794
3RUB	CF22	162	-0.0664660	-0.2459259	1.4160359
3RUB	CD23	163	0.2664689	-0.1091879	1.6326233
3RUB	CE24	164	0.3448463	-0.2205015	1.6666089
3RUB	CE25	165	0.3502166	-0.2669825	1.7980470
3RUB	CE26	166	0.2763454	-0.2033170	1.8978463
3RUB	CE27	167	0.1966639	-0.0934664	1.8649761
3RUB	CE28	168	0.1913339	-0.0472573	1.7334857
3RUB	HA29	169	0.0369128	-0.1915023	1.5928935
3RUB	HA30	170	-0.1487652	-0.2918653	1.4701513
3RUB	HB31	171	0.4014618	-0.2711352	1.5888556
3RUB	HB32	172	0.4115996	-0.3534047	1.8221879
3RUB	HB33	173	0.2802515	-0.2392961	2.0003294
3RUB	HB34	174	0.1384766	-0.0433720	1.9419036
3RUB	HB35	175	0.1292851	0.0383798	1.7088238
3RUB	CA36	176	0.3592000	0.0000000	1.2711697
3RUB	CC37	177	0.2560125	-0.0710312	1.2019766

3RUB	CA38	178	0.1469079	-0.1252862	1.2725374
3RUB	CB39	179	0.0372185	-0.1894317	1.2050206
3RUB	CF40	180	-0.0664660	-0.2459259	1.2736641
3RUB	CD41	181	0.2664689	-0.1091879	1.0570767
3RUB	CE42	182	0.3448463	-0.2205015	1.0230911
3RUB	CE43	183	0.3502166	-0.2669825	0.8916530
3RUB	CE44	184	0.2763454	-0.2033171	0.7918537
3RUB	CE45	185	0.1966639	-0.0934664	0.8247239
3RUB	CE46	186	0.1913339	-0.0472573	0.9562143
3RUB	HA47	187	0.0369128	-0.1915023	1.0968065
3RUB	HA48	188	-0.1487652	-0.2918653	1.2195487
3RUB	HB49	189	0.4014618	-0.2711352	1.1008444
3RUB	HB50	190	0.4115996	-0.3534047	0.8675121
3RUB	HB51	191	0.2802515	-0.2392962	0.6893706
3RUB	HB52	192	0.1384766	-0.0433720	0.7477964
3RUB	HB53	193	0.1292851	0.0383798	0.9808762
3RUB	CC54	194	0.4623875	0.0710312	1.2019766
3RUB	CA55	195	0.5714921	0.1252862	1.2725374
3RUB	CB56	196	0.6811815	0.1894317	1.2050206
3RUB	CF57	197	0.7848660	0.2459260	1.2736641
3RUB	CD58	198	0.4519311	0.1091879	1.0570767
3RUB	CE59	199	0.3735537	0.2205016	1.0230911
3RUB	CE60	200	0.3681834	0.2669825	0.8916530
3RUB	CE61	201	0.4420546	0.2033171	0.7918537
3RUB	CE62	202	0.5217361	0.0934665	0.8247239
3RUB	CE63	203	0.5270661	0.0472573	0.9562143
3RUB	HA64	204	0.6814872	0.1915023	1.0968065
3RUB	HA65	205	0.8671652	0.2918653	1.2195487
3RUB	HB66	206	0.3169382	0.2711352	1.1008444
3RUB	HB67	207	0.3068004	0.3534047	0.8675121
3RUB	HB68	208	0.4381485	0.2392962	0.6893706
3RUB	HB69	209	0.5799234	0.0433720	0.7477964
3RUB	HB70	210	0.5891149	-0.0383798	0.9808762
4RUB	CA1	211	0.0000000	0.7216500	1.4185303
4RUB	CC2	212	-0.1031875	0.7926812	1.4877230
4RUB	CA3	213	-0.2122921	0.8469362	1.4171626
4RUB	CB4	214	-0.3219815	0.9110817	1.4846790
4RUB	CF5	215	-0.4256660	0.9675760	1.4160359
4RUB	CD6	216	-0.0927311	0.8308379	1.6326230
4RUB	CE7	217	-0.0143537	0.9421515	1.6666090
4RUB	CE8	218	-0.0089834	0.9886325	1.7980470
4RUB	CE9	219	-0.0828546	0.9249671	1.8978460
4RUB	CE10	220	-0.1625361	0.8151165	1.8649760
4RUB	CE11	221	-0.1678661	0.7689073	1.7334860
4RUB	HA12	222	-0.3222871	0.9131523	1.5928940
4RUB	HA13	223	-0.5079652	1.0135153	1.4701510
4RUB	HB14	224	0.0422618	0.9927852	1.5888560
4RUB	HB15	225	0.0523996	1.0750547	1.8221880
4RUB	HB16	226	-0.0789485	0.9609462	2.0003290
4RUB	HB17	227	-0.2207234	0.7650220	1.9419040
4RUB	HB18	228	-0.2299149	0.6832702	1.7088240
4RUB	CC19	229	0.1031875	0.6506188	1.4877230
4RUB	CA20	230	0.2122921	0.5963638	1.4171626
4RUB	CB21	231	0.3219815	0.5322183	1.4846790

```
    4RUB   CF22  232    0.4256660   0.4757241   1.4160359
    4RUB   CD23  233    0.0927311   0.6124621   1.6326230
    4RUB   CE24  234    0.0143537   0.5011485   1.6666090
    4RUB   CE25  235    0.0089834   0.4546675   1.7980470
    4RUB   CE26  236    0.0828546   0.5183329   1.8978460
    4RUB   CE27  237    0.1625361   0.6281836   1.8649760
    4RUB   CE28  238    0.1678661   0.6743927   1.7334860
    4RUB   HA29  239    0.3222872   0.5301477   1.5928940
    4RUB   HA30  240    0.5079652   0.4297847   1.4701510
    4RUB   HB31  241   -0.0422618   0.4505148   1.5888560
    4RUB   HB32  242   -0.0523996   0.3682453   1.8221880
    4RUB   HB33  243    0.0789485   0.4823538   2.0003290
    4RUB   HB34  244    0.2207234   0.6782780   1.9419040
    4RUB   HB35  245    0.2299149   0.7600298   1.7088240
    4RUB   CA36  246   -0.0000000   0.7216500   1.2711697
    4RUB   CC37  247    0.1031875   0.6506188   1.2019770
    4RUB   CA38  248    0.2122921   0.5963638   1.2725374
    4RUB   CB39  249    0.3219815   0.5322183   1.2050210
    4RUB   CF40  250    0.4256660   0.4757241   1.2736641
    4RUB   CD41  251    0.0927311   0.6124621   1.0570770
    4RUB   CE42  252    0.0143537   0.5011485   1.0230910
    4RUB   CE43  253    0.0089834   0.4546675   0.8916530
    4RUB   CE44  254    0.0828546   0.5183329   0.7918540
    4RUB   CE45  255    0.1625361   0.6281835   0.8247240
    4RUB   CE46  256    0.1678661   0.6743927   0.9562140
    4RUB   HA47  257    0.3222871   0.5301477   1.0968060
    4RUB   HA48  258    0.5079652   0.4297847   1.2195490
    4RUB   HB49  259   -0.0422618   0.4505148   1.1008440
    4RUB   HB50  260   -0.0523996   0.3682453   0.8675120
    4RUB   HB51  261    0.0789485   0.4823538   0.6893710
    4RUB   HB52  262    0.2207234   0.6782780   0.7477960
    4RUB   HB53  263    0.2299149   0.7600298   0.9808760
    4RUB   CC54  264   -0.1031875   0.7926812   1.2019770
    4RUB   CA55  265   -0.2122921   0.8469362   1.2725374
    4RUB   CB56  266   -0.3219815   0.9110817   1.2050210
    4RUB   CF57  267   -0.4256660   0.9675760   1.2736641
    4RUB   CD58  268   -0.0927311   0.8308379   1.0570770
    4RUB   CE59  269   -0.0143537   0.9421515   1.0230910
    4RUB   CE60  270   -0.0089834   0.9886325   0.8916530
    4RUB   CE61  271   -0.0828546   0.9249671   0.7918540
    4RUB   CE62  272   -0.1625361   0.8151165   0.8247240
    4RUB   CE63  273   -0.1678661   0.7689073   0.9562140
    4RUB   HA64  274   -0.3222872   0.9131523   1.0968060
    4RUB   HA65  275   -0.5079652   1.0135153   1.2195490
    4RUB   HB66  276    0.0422618   0.9927852   1.1008440
    4RUB   HB67  277    0.0523996   1.0750547   0.8675120
    4RUB   HB68  278   -0.0789485   0.9609462   0.6893710
    4RUB   HB69  279   -0.2207234   0.7650220   0.7477960
    4RUB   HB70  280   -0.2299149   0.6832702   0.9808760
0.71840  1.44330  2.68970  0.00000  0.00000  0.00000  0.00000  0.00000  0.00000
```

5: dibromo-napthalene

```
dibromo napthalene
144
```

1DBN	Br1	1	0.0323125	0.2353462	3.0040654
1DBN	Br2	2	0.2035831	0.6829435	2.5467700
1DBN	C3	3	0.0855804	0.3590143	2.8668996
1DBN	C4	4	0.0526073	0.4911871	2.8845613
1DBN	C5	5	0.0887847	0.5865641	2.7869044
1DBN	C6	6	0.1567147	0.5470446	2.6742425
1DBN	C7	7	0.2627712	0.3666584	2.5362649
1DBN	C8	8	0.2955172	0.2341470	2.5192703
1DBN	C9	9	0.2598137	0.1388523	2.6172167
1DBN	C10	10	0.1917884	0.1777323	2.7302730
1DBN	C11	11	0.1560414	0.3135031	2.7516231
1DBN	C12	12	0.1927993	0.4109763	2.6516348
1DBN	H13	13	-0.0010829	0.5232137	2.9731378
1DBN	H14	14	0.0625661	0.6907145	2.8017185
1DBN	H15	15	0.2902298	0.4395735	2.4609023
1DBN	H16	16	0.3490819	0.2027616	2.4301258
1DBN	H17	17	0.2861344	0.0343821	2.6032745
1DBN	H18	18	0.1644028	0.1043945	2.8052314
2DBN	Br1	19	0.2425383	1.0591380	1.0848928
2DBN	Br2	20	0.0714301	1.5067488	1.5422358
2DBN	C3	21	0.1893187	1.1828102	1.2220736
2DBN	C4	22	0.2222914	1.3149814	1.2043995
2DBN	C5	23	0.1861487	1.4103613	1.3020664
2DBN	C6	24	0.1182528	1.3708462	1.4147504
2DBN	C7	25	0.0122330	1.1904661	1.5527643
2DBN	C8	26	-0.0205129	1.0579563	1.5697712
2DBN	C9	27	0.0151559	0.9626588	1.4718149
2DBN	C10	28	0.0831468	1.0015344	1.3587365
2DBN	C11	29	0.1188925	1.1373034	1.3373731
2DBN	C12	30	0.0821701	1.2347796	1.4373716
2DBN	H13	31	0.2759548	1.3470047	1.1158056
2DBN	H14	32	0.2123667	1.5145105	1.2872425
2DBN	H15	33	-0.0151989	1.2633835	1.6281346
2DBN	H16	34	-0.0740506	1.0265743	1.6589331
2DBN	H17	35	-0.0111646	0.8581898	1.4857669
2DBN	H18	36	0.1105058	0.9281944	1.2837705
3DBN	Br1	37	0.2849261	1.4119983	-0.2788733
3DBN	Br2	38	0.1172448	0.9650209	0.1803547
3DBN	C3	39	0.2327890	1.2885257	-0.1410982
3DBN	C4	40	0.2654533	1.1562991	-0.1589300
3DBN	C5	41	0.2293857	1.0609392	-0.0612159
3DBN	C6	42	0.1614800	1.1004603	0.0514601
3DBN	C7	43	0.0549773	1.2807651	0.1892003
3DBN	C8	44	0.0226527	1.4133501	0.2064259
3DBN	C9	45	0.0592209	1.5087988	0.1089497
3DBN	C10	46	0.1272308	1.4699187	-0.0041159
3DBN	C11	47	0.1624486	1.3340555	-0.0257554
3DBN	C12	48	0.1253273	1.2365162	0.0740340
3DBN	H13	49	0.3189510	1.1242406	-0.2476114
3DBN	H14	50	0.2557375	0.9568124	-0.0759602
3DBN	H15	51	0.0267262	1.2077091	0.2641324
3DBN	H16	52	-0.0312035	1.4446824	0.2954134
3DBN	H17	53	0.0335494	1.6133828	0.1232455
3DBN	H18	54	0.1550765	1.5433390	-0.0788236

4DBN	Br1	55	0.0775906	0.5881981	1.6418715
4DBN	Br2	56	0.2452657	0.1412212	1.1826409
4DBN	C3	57	0.1297259	0.4647256	1.5040957
4DBN	C4	58	0.0970608	0.3324992	1.5219273
4DBN	C5	59	0.1331271	0.2371394	1.4242125
4DBN	C6	60	0.2010322	0.2766605	1.3115362
4DBN	C7	61	0.3075351	0.4569650	1.1737959
4DBN	C8	62	0.3398605	0.5895499	1.1565705
4DBN	C9	63	0.3032936	0.6849985	1.2540473
4DBN	C10	64	0.2352842	0.6461184	1.3671132
4DBN	C11	65	0.2000657	0.5102554	1.3887526
4DBN	C12	66	0.2371857	0.4127161	1.2889625
4DBN	H13	67	0.0435636	0.3004408	1.6106090
4DBN	H14	68	0.1067748	0.1330127	1.4389568
4DBN	H15	69	0.3357852	0.3839091	1.0988634
4DBN	H16	70	0.3937162	0.6208821	1.0675827
4DBN	H17	71	0.3289656	0.7895823	1.2397516
4DBN	H18	72	0.2074396	0.7195387	1.4418213
5DBN	Br1	73	-0.0796665	0.7483765	0.3841966
5DBN	Br2	74	0.0962490	0.3094958	0.8481293
5DBN	C3	75	-0.0250943	0.6273371	0.5231824
5DBN	C4	76	-0.0569904	0.4946309	0.5076739
5DBN	C5	77	-0.0198228	0.4011120	0.6067457
5DBN	C6	78	0.0479923	0.4429704	0.7186294
5DBN	C7	79	0.1527986	0.6263915	0.8535270
5DBN	C8	80	0.1844635	0.7594238	0.8683636
5DBN	C9	81	0.1477699	0.8528598	0.7690027
5DBN	C10	82	0.0798534	0.8116337	0.6567147
5DBN	C11	83	0.0452065	0.6752488	0.6375807
5DBN	C12	84	0.0829767	0.5796755	0.7390155
5DBN	H13	85	-0.1105823	0.4607632	0.4197249
5DBN	H14	86	-0.0451946	0.2965252	0.5936289
5DBN	H15	87	0.1810156	0.5549063	0.9299717
5DBN	H16	88	0.2379364	0.7926583	0.9568909
5DBN	H17	89	0.1732393	0.9577535	0.7812424
5DBN	H18	90	0.0517067	0.8835485	0.5806674
6DBN	Br1	91	0.4421818	1.5721795	0.9787976
6DBN	Br2	92	0.2662644	1.1332937	0.5148704
6DBN	C3	93	0.3876089	1.4511386	0.8398133
6DBN	C4	94	0.4195063	1.3184328	0.8553225
6DBN	C5	95	0.3823383	1.2249128	0.7562519
6DBN	C6	96	0.3145215	1.2667698	0.6443687
6DBN	C7	97	0.2097121	1.4501888	0.5094709
6DBN	C8	98	0.1780459	1.5832208	0.4946336
6DBN	C9	99	0.2147399	1.6766578	0.5939934
6DBN	C10	100	0.2826581	1.6354332	0.7062808
6DBN	C11	101	0.3173064	1.4990488	0.7254155
6DBN	C12	102	0.2795358	1.4034744	0.6239819
6DBN	H13	103	0.4730996	1.2845662	0.9432711
6DBN	H14	104	0.4077111	1.1203263	0.7693692
6DBN	H15	105	0.1814948	1.3787028	0.4330271
6DBN	H16	106	0.1245716	1.6164542	0.4061067
6DBN	H17	107	0.1892695	1.7815513	0.5817531
6DBN	H18	108	0.3108052	1.7073489	0.7823272

```
    7DBN     Br1  109   0.3969924   0.8994676   2.3425531
    7DBN     Br2  110   0.2245075   1.3377493   1.8767697
    7DBN      C3  111   0.3435040   1.0203177   2.2029825
    7DBN      C4  112   0.3750905   1.1530781   2.2186593
    7DBN      C5  113   0.3379987   1.2465845   2.1195473
    7DBN      C6  114   0.2701755   1.2047284   2.0076676
    7DBN      C7  115   0.1648894   1.0213926   1.8730279
    7DBN      C8  116   0.1336471   0.8882862   1.8579619
    7DBN      C9  117   0.1712397   0.7946916   1.9568363
    7DBN     C10  118   0.2391734   0.8359138   2.0691153
    7DBN     C11  119   0.2732910   0.9723915   2.0885364
    7DBN     C12  120   0.2351224   1.0680355   1.9873176
    7DBN     H13  121   0.4285151   1.1869746   2.3066990
    7DBN     H14  122   0.3635031   1.3511479   2.1325932
    7DBN     H15  123   0.1358535   1.0930222   1.7970264
    7DBN     H16  124   0.0798571   0.8551080   1.7696058
    7DBN     H17  125   0.1464203   0.6896837   1.9442444
    7DBN     H18  126   0.2678064   0.7639129   2.1448992
    8DBN     Br1  127  -0.1220508   0.0756673   1.7464373
    8DBN     Br2  128   0.0504322   0.5139495   2.2122210
    8DBN      C3  129  -0.0685630   0.1965175   1.8860081
    8DBN      C4  130  -0.1001497   0.3292779   1.8703311
    8DBN      C5  131  -0.0630583   0.4227843   1.9694432
    8DBN      C6  132   0.0047648   0.3809284   2.0813230
    8DBN      C7  133   0.1100512   0.1975930   2.2159628
    8DBN      C8  134   0.1412939   0.0644866   2.2310289
    8DBN      C9  135   0.1037017  -0.0291081   2.1321544
    8DBN     C10  136   0.0357681   0.0121139   2.0198753
    8DBN     C11  137   0.0016501   0.1485915   2.0004542
    8DBN     C12  138   0.0398182   0.2442356   2.1016731
    8DBN     H13  139  -0.1535744   0.3631742   1.7822914
    8DBN     H14  140  -0.0885631   0.5273477   1.9563973
    8DBN     H15  141   0.1390868   0.2692227   2.2919644
    8DBN     H16  142   0.1950839   0.0313086   2.3193851
    8DBN     H17  143   0.1285214  -0.1341159   2.1447463
    8DBN     H18  144   0.0071353  -0.0598870   1.9440914
 0.40630   1.64760   2.72599   0.00000   0.00000   0.00000   0.00000  -0.08757   0.00000
```

6: stilbene

```
stilbene
104
    1STL      C1     1   0.0148685   0.0529199   0.0390671
    1STL      C2     2   0.1378454   0.0743797   0.1159054
    1STL      C3     3   0.1516113   0.1936190   0.1894237
    1STL      C4     4   0.2661191   0.2198341   0.2643700
    1STL      C5     5   0.3702161   0.1269892   0.2677964
    1STL      C6     6   0.3583245   0.0078896   0.1954857
    1STL      C7     7   0.2440010  -0.0181560   0.1206632
    1STL      H8     8  -0.0580758   0.1332518   0.0485122
    1STL      H9     9   0.0708444   0.2664729   0.1870988
    1STL     H10    10   0.2739941   0.3128315   0.3200757
    1STL     H11    11   0.4596949   0.1469285   0.3261357
    1STL     H12    12   0.4387807  -0.0651787   0.1976322
    1STL     H13    13   0.2370337  -0.1114927   0.0655785
```

1STL	C14	14	-0.0148685	-0.0529198	-0.0390671
1STL	C15	15	-0.1378454	-0.0743797	-0.1159054
1STL	H16	16	0.0580758	-0.1332518	-0.0485122
1STL	C17	17	-0.1516113	-0.1936190	-0.1894237
1STL	C18	18	-0.2440010	0.0181560	-0.1206632
1STL	C19	19	-0.2661191	-0.2198342	-0.2643699
1STL	H20	20	-0.0708445	-0.2664729	-0.1870988
1STL	C21	21	-0.3583244	-0.0078895	-0.1954857
1STL	H22	22	-0.2370337	0.1114927	-0.0655785
1STL	C23	23	-0.3702161	-0.1269892	-0.2677964
1STL	H24	24	-0.2739941	-0.3128315	-0.3200756
1STL	H25	25	-0.4387807	0.0651787	-0.1976322
1STL	H26	26	-0.4596949	-0.1469284	-0.3261357
2STL	C1	27	0.6042320	0.3389180	-0.0390699
2STL	C2	28	0.4812502	0.3603810	-0.1158993
2STL	C3	29	0.4674868	0.4796157	-0.1894255
2STL	C4	30	0.3529746	0.5058335	-0.2643640
2STL	C5	31	0.2488704	0.4129959	-0.2677746
2STL	C6	32	0.2607595	0.2939009	-0.1954558
2STL	C7	33	0.3750875	0.2678527	-0.1206411
2STL	H8	34	0.6771814	0.4192439	-0.0485272
2STL	H9	35	0.5482592	0.5524639	-0.1871130
2STL	H10	36	0.3451016	0.5988272	-0.3200762
2STL	H11	37	0.1593881	0.4329373	-0.3261078
2STL	H12	38	0.1802977	0.2208384	-0.1975900
2STL	H13	39	0.3820526	0.1745197	-0.0655499
2STL	C14	40	0.6339680	0.2330820	0.0390699
2STL	C15	41	0.7569498	0.2116190	0.1158994
2STL	H16	42	0.5610186	0.1527561	0.0485273
2STL	C17	43	0.7707132	0.0923843	0.1894255
2STL	C18	44	0.8631125	0.3041473	0.1206411
2STL	C19	45	0.8852254	0.0661665	0.2643640
2STL	H20	46	0.6899409	0.0195362	0.1871130
2STL	C21	47	0.9774405	0.2780991	0.1954558
2STL	H22	48	0.8561474	0.3974803	0.0655499
2STL	C23	49	0.9893296	0.1590041	0.2677746
2STL	H24	50	0.8930984	-0.0268272	0.3200761
2STL	H25	51	1.0579023	0.3511616	0.1975900
2STL	H26	52	1.0788119	0.1390627	0.3261078
3STL	C1	53	-0.3023292	-0.0451362	0.6828964
3STL	C2	54	-0.1752430	-0.0394220	0.6100651
3STL	C3	55	-0.1418816	-0.1456875	0.5240005
3STL	C4	56	-0.0225285	-0.1460778	0.4520914
3STL	C5	57	0.0668677	-0.0396596	0.4644040
3STL	C6	58	0.0354168	0.0668814	0.5493441
3STL	C7	59	-0.0837254	0.0671464	0.6211196
3STL	H8	60	-0.3623681	-0.1332735	0.6607502
3STL	H9	61	-0.2111122	-0.2290177	0.5140218
3STL	H10	62	0.0006119	-0.2295612	0.3864507
3STL	H11	63	0.1600457	-0.0394558	0.4084994
3STL	H12	64	0.1043034	0.1503565	0.5595096
3STL	H13	65	-0.1059992	0.1511675	0.6862267
3STL	C14	66	-0.3496554	0.0451361	0.7712278
3STL	C15	67	-0.4767416	0.0394220	0.8440591

```
   3STL    H16    68  -0.2896165   0.1332735   0.7933740
   3STL    C17    69  -0.5101031   0.1456874   0.9301237
   3STL    C18    70  -0.5682592  -0.0671464   0.8330046
   3STL    C19    71  -0.6294561   0.1460779   1.0020327
   3STL    H20    72  -0.4408725   0.2290177   0.9401023
   3STL    C21    73  -0.6874014  -0.0668814   0.9047800
   3STL    H22    74  -0.5459854  -0.1511675   0.7678975
   3STL    C23    75  -0.7188524   0.0396596   0.9897201
   3STL    H24    76  -0.6525965   0.2295612   1.0676733
   3STL    H25    77  -0.7562880  -0.1503565   0.8946146
   3STL    H26    78  -0.8120303   0.0394558   1.0456248
   4STL     C1    79   0.2701888   0.2412137   0.7719702
   4STL     C2    80   0.1440536   0.2471994   0.8464151
   4STL     C3    81   0.1122062   0.1416604   0.9339349
   4STL     C4    82  -0.0061870   0.1415594   1.0074144
   4STL     C5    83  -0.0961149   0.2475466   0.9952566
   4STL     C6    84  -0.0661639   0.3533656   0.9088838
   4STL     C7    85   0.0520207   0.3533418   0.8355418
   4STL     H8    86   0.3308266   0.1535014   0.7941715
   4STL     H9    87   0.1818576   0.0586682   0.9438024
   4STL    H10    88  -0.0281643   0.0586380   1.0741580
   4STL    H11    89  -0.1885484   0.2479740   1.0523824
   4STL    H12    90  -0.1354743   0.4365019   0.8988235
   4STL    H13    91   0.0731365   0.4368030   0.7693379
   4STL    C14    92   0.3160266   0.3307862   0.6821539
   4STL    C15    93   0.4421618   0.3248006   0.6077090
   4STL    H16    94   0.2553887   0.4184986   0.6599526
   4STL    C17    95   0.4740092   0.4303396   0.5201893
   4STL    C18    96   0.5341947   0.2186582   0.6185823
   4STL    C19    97   0.5924024   0.4304407   0.4467098
   4STL    H20    98   0.4043579   0.5133317   0.5103217
   4STL    C21    99   0.6523793   0.2186344   0.5452404
   4STL    H22   100   0.5130789   0.1351970   0.6847862
   4STL    C23   101   0.6823302   0.3244534   0.4588675
   4STL    H24   102   0.6143797   0.5133620   0.3799662
   4STL    H25   103   0.7216896   0.1354980   0.5553007
   4STL    H26   104   0.7747638   0.3240260   0.4017417
1.23820  0.57200  1.45412  0.00000  0.00000  0.00000  0.00000 -0.65198  0.00000
```

C.3 Vfit Molecular Geometries

The geometries presented here are for all of the molecules used to determine α in the modified singlet coupling. All geometries are optimized at the PBE0/6-31G* level in the gas phase. The geometries are given in **.xyz** format. All coordinates are specified in Å. The geometry for DCM are given in the organic semiconductor crystal geometries section below.

1: cyanine-3

```
42
cyanine-3
C          4.405920   -0.068155    0.482201
C          4.799239    0.049548   -0.887456
C          6.170910    0.123506   -1.225907
C          7.096901    0.077182   -0.214246
C          6.687630   -0.037844    1.138190
C          5.358468   -0.110712    1.507480
C          2.536029   -0.040210   -0.749335
C          3.623770    0.058421   -1.638913
H          6.473444    0.213450   -2.264828
H          8.156772    0.131198   -0.441235
H          7.448234   -0.065824    1.913105
H          5.082765   -0.187412    2.553990
H          3.529289    0.140970   -2.714261
C          1.203573   -0.015455   -1.179620
C          0.001682    0.000846   -0.476865
H         -0.001916    0.000627    0.604224
C         -1.195701    0.018064   -1.187305
C         -2.530893    0.041998   -0.765568
C         -3.612938   -0.051921   -1.662639
C         -4.408888    0.067618    0.453685
C         -4.793342   -0.043631   -0.919023
H         -3.511594   -0.130309   -2.737676
C         -5.368124    0.107312    1.472840
C         -6.162904   -0.113628   -1.266774
C         -6.694930    0.038322    1.094553
H         -5.099194    0.179380    2.521427
C         -7.095444   -0.070087   -0.261059
H         -6.458758   -0.198655   -2.308033
H         -7.460572    0.064364    1.864554
H         -8.153878   -0.121254   -0.495308
H         -1.102734   -0.007523   -2.272317
H          1.117627    0.011891   -2.265172
N          3.040254   -0.124419    0.545952
N         -3.043558    0.121464    0.526731
C          2.280569   -0.322419    1.759184
H          1.729604    0.581868    2.039591
H          1.588818   -1.161329    1.642525
H          2.965456   -0.569235    2.570377
C         -2.291511    0.309703    1.746258
H         -1.738568   -0.595365    2.019996
H         -1.602568    1.152760    1.643090
H         -2.981987    0.544905    2.556165
```

2: cyanine-5

```
46
cyanine-5
C         -0.893624    6.020856   -0.021827
C          0.493874    5.679602   -0.015412
C          1.482544    6.671020   -0.018794
C          1.060850    7.986543   -0.028131
```

```
C          -0.310046    8.343760   -0.034352
C          -1.286713    7.378779   -0.031474
C          -1.599155    4.815065   -0.016009
C          -0.665746    3.763513   -0.006906
H           2.541603    6.435801   -0.014965
H           1.807178    8.775686   -0.031087
H          -0.581669    9.394535   -0.041642
H          -2.340048    7.642717   -0.036360
H          -2.673360    4.681006   -0.018855
C          -1.044882    2.411378   -0.002031
C          -0.302874    1.239602    0.000692
H          -2.126958    2.285101   -0.001527
H           0.781850    1.256306   -0.001189
C          -0.941886   -0.001043    0.004357
C          -0.297599   -1.238968    0.005963
H          -2.033011   -0.003372    0.005906
H           0.787200   -1.250962    0.004611
C          -1.034781   -2.413792    0.009385
C          -0.650408   -3.764451    0.011368
C          -1.579827   -4.819551    0.016995
C           0.516491   -5.676133    0.013085
C          -0.869705   -6.022650    0.018246
H          -2.654529   -4.689543    0.020089
C           1.508874   -6.663845    0.012770
C          -1.257694   -7.382066    0.022993
C           1.092120   -7.980986    0.017437
H           2.567034   -6.424587    0.009219
C          -0.277410   -8.343372    0.022471
H          -2.310023   -7.650003    0.026875
H           1.841411   -8.767321    0.017354
H          -0.545074   -9.395183    0.026003
H          -2.117348   -2.291841    0.011222
N           0.611965    4.315249   -0.006251
N           0.629376   -4.311322    0.008936
C           1.864170    3.594562    0.007453
H           1.947679    2.973146    0.904538
H           1.968273    2.972565   -0.887173
H           2.685464    4.310507    0.017220
C           1.878779   -3.585722    0.001137
H           1.964837   -2.964512   -0.895889
H           1.975499   -2.962791    0.895904
H           2.702971   -4.298391   -0.003257
```

3: thiat

```
58
thiat
C          4.84796271     0.22808262    -1.44209242
C          4.86934623     0.16093390    -0.04384965
C          6.09691359     0.10502710     0.62384914
C          7.25092668     0.12619137    -0.14456111
C          7.23674468     0.19791715    -1.53511851
C          6.00940651     0.24882306    -2.19792311
H          6.16899197     0.04047278     1.69908536
H          5.97373966     0.30248864    -3.27812906
```

N	3.58770799	0.15716634	0.53884339
C	2.52781717	0.18067287	-0.33464524
C	1.19632904	0.15302356	0.05933471
C	0.00076859	0.14259000	-0.68802516
C	-1.19519097	0.14450862	0.05867329
H	1.05679678	0.13100209	1.13419039
H	-1.05715671	0.11351492	1.13363362
C	-2.52634879	0.17758041	-0.33685557
C	-4.86802014	0.16374551	-0.04591458
C	-4.84792174	0.23812297	-1.44357614
C	-6.09426324	0.10496524	0.62414147
C	-6.01059486	0.26413101	-2.19763027
C	-7.24921443	0.13291519	-0.14229444
H	-6.16338897	0.03187218	1.69889841
C	-7.23693838	0.21238437	-1.53233319
H	-5.97686519	0.32179251	-3.27765323
N	-3.58635687	0.15392810	0.53645416
Cl	8.85167015	0.05241216	0.71290225
Cl	-8.84897702	0.05619102	0.71759602
C	3.42092988	0.06878816	2.01989567
H	2.55394405	0.66978046	2.30312211
H	4.29730584	0.53983793	2.46946819
C	3.27987326	-1.38786609	2.50498069
H	2.40757384	-1.84679346	2.02682049
H	4.16325358	-1.95539371	2.19178557
C	-3.42030386	0.04888768	2.01630421
H	-2.54514385	0.63449688	2.30564020
H	-4.29020183	0.52593759	2.47186412
C	-3.29663744	-1.41577415	2.48407210
H	-2.43439189	-1.87971970	1.99286228
H	-4.19085643	-1.96591479	2.17105667
S	-3.14146759	0.28766297	-2.05420662
S	3.14244412	0.27775538	-2.05303355
C	0.00114926	0.14258992	-2.20301292
H	-0.86904586	-0.40084088	-2.57777685
H	0.87063403	-0.40392116	-2.57534821
C	0.00448115	1.59234744	-2.76707940
H	0.01073084	1.56604744	-3.86090043
H	-0.88582157	2.13416213	-2.43686476
H	0.89146424	2.13314707	-2.42695330
C	-3.14305300	-1.48239620	4.01851987
H	-3.99840915	-1.01330052	4.51739852
H	-2.23108193	-0.97063158	4.34670242
C	3.13818017	-1.43734248	4.04128901
H	4.00705828	-0.98195549	4.52930357
H	2.23924686	-0.90594336	4.37425517
H	-8.16658562	0.23022109	-2.08341671
H	8.16560526	0.21133110	-2.08768164
H	3.06480200	-2.47425773	4.38179455
H	-3.08711619	-2.52313643	4.35024105

4: thiophene

```
32
thiophene
```

```
C          -0.767003   -7.760632   -0.003573
C           0.589882   -7.926676   -0.000338
C           1.287173   -6.693637    0.002231
C           0.459129   -5.589791    0.001351
S          -1.207385   -6.096929   -0.003566
H          -1.535832   -8.522123   -0.006355
H           1.071837   -8.898238   -0.000790
H           2.368916   -6.605653    0.003874
C           0.868310   -4.211517    0.002248
C           0.065456   -3.119494    0.000298
H           1.948275   -4.061887    0.004605
H          -1.017703   -3.249809   -0.002201
C           0.552471   -1.773968    0.001348
C          -0.243249   -0.672211   -0.000084
H           1.635082   -1.638304    0.003386
H          -1.325738   -0.808486   -0.002146
C           0.243228    0.672183    0.000898
C          -0.552491    1.773942    0.000038
H           1.325718    0.808458    0.002413
H          -1.635104    1.638279   -0.001497
C          -0.065473    3.119466    0.000886
C          -0.868325    4.211492    0.000477
H           1.017689    3.249778    0.001915
H          -1.948292    4.061867   -0.000635
C          -0.459137    5.589765    0.001059
C          -1.287174    6.693614   -0.000301
S           1.207387    6.096895    0.001022
C          -0.589873    7.926651   -0.000701
H          -2.368918    6.605636   -0.001766
C           0.767015    7.760600   -0.000045
H          -1.071820    8.898215   -0.002415
H           1.535852    8.522087   -0.000539
```

C.4 Organic Semiconductor Crystal Geometries

All of the geometries in this section are used in the organic/organic interface simulations. All geometries are optimized at the PBE0/6-31G* level in the gas phase. The geometries are given in .gro format. All coordinates are specified in nm. The geometry for rubrene is given in the crystal diffusion geometries section above.

1: metal-free phthalocyanine (H_2Pc)

```
H2PC unit cell
116
    1PHT    NP1    1   0.3220009   0.2501039   1.1091898
    1PHT    CP2    2   0.2883024   0.1656519   1.0138908
    1PHT    CQ3    3   0.1717723   0.0784112   1.0148667
```

1PHT	CR4	4	0.0713198	0.0613601	1.1098562
1PHT	HP5	5	0.0723858	0.1189561	1.2014910
1PHT	CR6	6	-0.0289601	-0.0314961	1.0823329
1PHT	HP7	7	-0.1085890	-0.0472107	1.1540854
1PHT	CR8	8	-0.0288096	-0.1057445	0.9623790
1PHT	HP9	9	-0.1084077	-0.1770432	0.9444459
1PHT	CR10	10	0.0716175	-0.0888459	0.8671871
1PHT	HP11	11	0.0731136	-0.1450511	0.7747007
1PHT	CQ12	12	0.1720461	0.0040055	0.8945142
1PHT	CP13	13	0.2889503	0.0446950	0.8180187
1PHT	NQ14	14	0.3537011	0.1408151	0.8942961
1PHT	HQ15	15	0.4396600	0.1867991	0.8641777
1PHT	NP16	16	0.3255532	-0.0009748	0.6999452
1PHT	CP17	17	0.4341551	0.0396643	0.6336643
1PHT	CQ18	18	0.4708106	-0.0143920	0.5020046
1PHT	CR19	19	0.4120244	-0.1097752	0.4200207
1PHT	HP20	20	0.3208281	-0.1597776	0.4500783
1PHT	CR21	21	0.4749002	-0.1382780	0.2981830
1PHT	HP22	22	0.4317814	-0.2121985	0.2317211
1PHT	CR23	23	0.5932793	-0.0725384	0.2605008
1PHT	HP24	24	0.6394657	-0.0969090	0.1655376
1PHT	CR25	25	0.6521330	0.0235598	0.3435940
1PHT	HP26	26	0.7432847	0.0749664	0.3158559
1PHT	CQ27	27	0.5893202	0.0514625	0.4643654
1PHT	CP28	28	0.6210878	0.1436398	0.5744752
1PHT	NR29	29	0.5262305	0.1342392	0.6742719
1PHT	NP30	30	0.7282942	0.2231473	0.5725804
1PHT	CP31	31	0.7619939	0.3075975	0.6678803
1PHT	CQ32	32	0.8785281	0.3948330	0.6669079
1PHT	CR33	33	0.9789836	0.4118801	0.5719211
1PHT	HP34	34	0.9779176	0.3542846	0.4802859
1PHT	CR35	35	1.0792670	0.5047318	0.5994473
1PHT	HP36	36	1.1588985	0.5204428	0.5276970
1PHT	CR37	37	1.0791167	0.5789796	0.7194014
1PHT	HP38	38	1.1587175	0.6502747	0.7373370
1PHT	CR39	39	0.9786863	0.5620851	0.8145908
1PHT	HP40	40	0.9771904	0.6182898	0.9070774
1PHT	CQ41	41	0.8782545	0.4692383	0.7872606
1PHT	CP42	42	0.7613460	0.4285540	0.8637527
1PHT	NQ43	43	0.6965904	0.3324408	0.7874712
1PHT	HQ44	44	0.6106242	0.2864661	0.8175836
1PHT	NP45	45	0.7247421	0.4742255	0.9818252
1PHT	CP46	46	0.6161390	0.4335874	1.0481054
1PHT	CQ47	47	0.5794809	0.4876477	1.1797627
1PHT	CR48	48	0.6382649	0.5830342	1.2617443
1PHT	HP49	49	0.7294613	0.6330364	1.2316865
1PHT	CR50	50	0.5753867	0.6115407	1.3835799
1PHT	HP51	51	0.6185036	0.6854639	1.4500400
1PHT	CR52	52	0.4570073	0.5458016	1.4212621
1PHT	HP53	53	0.4108190	0.5701752	1.5162235
1PHT	CR54	54	0.3981558	0.4497001	1.3381711
1PHT	HP55	55	0.3070038	0.3982939	1.3659092
1PHT	CQ56	56	0.4609711	0.4217935	1.2174019
1PHT	CP57	57	0.4292062	0.3296124	1.1072947

1PHT	NR58	58	0.5240694	0.3390057	1.0075021
2PHT	NP1	59	0.2031465	0.4867283	-0.2683047
2PHT	CP2	60	0.2368454	0.4022768	-0.1730055
2PHT	CQ3	61	0.3533756	0.3150362	-0.1739814
2PHT	CR4	62	0.4538279	0.2979849	-0.2689710
2PHT	HP5	63	0.4527617	0.3555806	-0.3606061
2PHT	CR6	64	0.5541080	0.2051290	-0.2414477
2PHT	HP7	65	0.6337368	0.1894143	-0.3132003
2PHT	CR8	66	0.5539579	0.1308810	-0.1214935
2PHT	HP9	67	0.6335561	0.0595825	-0.1035603
2PHT	CR10	68	0.4535309	0.1477797	-0.0263014
2PHT	HP11	69	0.4520351	0.0915749	0.0661851
2PHT	CQ12	70	0.3531021	0.2406309	-0.0536287
2PHT	CP13	71	0.2361980	0.2813205	0.0228669
2PHT	NQ14	72	0.1714469	0.3774401	-0.0534107
2PHT	HQ15	73	0.0854880	0.4234241	-0.0232923
2PHT	NP16	74	0.1995954	0.2356510	0.1409406
2PHT	CP17	75	0.0909936	0.2762901	0.2072217
2PHT	CQ18	76	0.0543385	0.2222341	0.3388816
2PHT	CR19	77	0.1131249	0.1268513	0.4208656
2PHT	HP20	78	0.2043212	0.0768490	0.3908080
2PHT	CR21	79	0.0502495	0.0983488	0.5427036
2PHT	HP22	80	0.0933684	0.0244285	0.6091656
2PHT	CR23	81	-0.0681297	0.1640883	0.5803858
2PHT	HP24	82	-0.1143159	0.1397179	0.6753491
2PHT	CR25	83	-0.1269837	0.2601862	0.4972924
2PHT	HP26	84	-0.2181355	0.3115927	0.5250305
2PHT	CQ27	85	-0.0641712	0.2880885	0.3765208
2PHT	CP28	86	-0.0959392	0.3802654	0.2664108
2PHT	NR29	87	-0.0010820	0.3708647	0.1666139
2PHT	NP30	88	-0.2031457	0.4597728	0.2683055
2PHT	CP31	89	-0.2368458	0.5442226	0.1730054
2PHT	CQ32	90	-0.3533801	0.6314579	0.1739777
2PHT	CR33	91	-0.4538354	0.6485052	0.2689647
2PHT	HP34	92	-0.4527691	0.5909099	0.3606001
2PHT	CR35	93	-0.5541190	0.7413566	0.2414384
2PHT	HP36	94	-0.6337504	0.7570678	0.3131888
2PHT	CR37	95	-0.5539690	0.8156041	0.1214841
2PHT	HP38	96	-0.6335700	0.8868990	0.1035484
2PHT	CR39	97	-0.4535388	0.7987094	0.0262945
2PHT	HP40	98	-0.4520432	0.8549138	-0.0661922
2PHT	CQ41	99	-0.3531068	0.7058628	0.0536248
2PHT	CP42	100	-0.2361984	0.6651786	-0.0228674
2PHT	NQ43	101	-0.1714425	0.5690657	0.0534143
2PHT	HQ44	102	-0.0854763	0.5230910	0.0233019
2PHT	NP45	103	-0.1995948	0.7108497	-0.1409401
2PHT	CP46	104	-0.0909918	0.6702116	-0.2072203
2PHT	CQ47	105	-0.0543340	0.7242716	-0.3388779
2PHT	CR48	106	-0.1131183	0.8196576	-0.4208597
2PHT	HP49	107	-0.2043147	0.8696598	-0.3908019
2PHT	CR50	108	-0.0502404	0.8481639	-0.5426955
2PHT	HP51	109	-0.0933575	0.9220868	-0.6091557
2PHT	CR52	110	0.0681390	0.7824249	-0.5803777
2PHT	HP53	111	0.1143272	0.8067983	-0.6753394

```
    2PHT   CR54  112   0.1269908   0.6863237  -0.4972866
    2PHT   HP55  113   0.2181428   0.6349176  -0.5250247
    2PHT   CQ56  114   0.0641758   0.6584174  -0.3765171
    2PHT   CP57  115   0.0959411   0.5662367  -0.2664097
    2PHT   NR58  116   0.0010781   0.5756301  -0.1666170
1.47960  0.47325  1.68177  0.00000  0.00000  0.00000  0.00000 -0.42930  0.00000
```

2: Perylene-3,4,9,10-tetracarboxyl-bis-benzimidazole (PTCBI)

```
PTCBI Unit Cell
58
    1PTC     O1    1   0.2270468   0.4740328   0.5142616
    1PTC     N2    2   0.2730476   0.2766889   0.4039511
    1PTC    NA3    3   0.3323338   0.0781516   0.3103473
    1PTC     C4    4   0.2050671   0.3984484   0.4185253
    1PTC    CA5    5   0.1075602   0.4258479   0.3107789
    1PTC    CB6    6   0.0360083   0.5440599   0.3172729
    1PTC    CB7    7  -0.0575946   0.5762133   0.2188678
    1PTC    CA8    8  -0.0827174   0.4912026   0.1107673
    1PTC    CE9    9  -0.0099051   0.3679865   0.1015880
    1PTC   CA10   10  -0.0308472   0.2763906  -0.0066615
    1PTC   CB11   11   0.0434870   0.1579616  -0.0097170
    1PTC   CB12   12   0.1369320   0.1266914   0.0891353
    1PTC   CA13   13   0.1588310   0.2137396   0.1948063
    1PTC   CC14   14   0.2546025   0.1841330   0.2982126
    1PTC   CF15   15   0.0858571   0.3358016   0.2028672
    1PTC   CG16   16   0.4067010   0.0984953   0.4285287
    1PTC   CB17   17   0.5034886   0.0175917   0.4883097
    1PTC   CB18   18   0.5620456   0.0624468   0.6064849
    1PTC   CB19   19   0.5252314   0.1855030   0.6644361
    1PTC   CB20   20   0.4287245   0.2677288   0.6061975
    1PTC   CD21   21   0.3708659   0.2221291   0.4882744
    1PTC    H22   22   0.0546324   0.6106923   0.4005770
    1PTC    H23   23  -0.1111014   0.6696217   0.2280515
    1PTC    H24   24   0.0295315   0.0872772  -0.0902966
    1PTC    H25   25   0.1936833   0.0345909   0.0852304
    1PTC    H26   26   0.5310274  -0.0766821   0.4429627
    1PTC    H27   27   0.6374589   0.0017673   0.6551209
    1PTC    H28   28   0.5729813   0.2170664   0.7564193
    1PTC    H29   29   0.3988698   0.3623350   0.6486596
    1PTC    O30   30  -0.4390262   0.3265787  -0.5142616
    1PTC    N31   31  -0.4850272   0.5239225  -0.4039511
    1PTC   NA32   32  -0.5443134   0.7224598  -0.3103474
    1PTC    C33   33  -0.4170465   0.4021631  -0.4185254
    1PTC   CA34   34  -0.3195396   0.3747635  -0.3107790
    1PTC   CB35   35  -0.2479878   0.2565516  -0.3172730
    1PTC   CB36   36  -0.1543848   0.2243981  -0.2188679
    1PTC   CA37   37  -0.1292621   0.3094089  -0.1107673
    1PTC   CE38   38  -0.2020745   0.4326250  -0.1015880
    1PTC   CA39   39  -0.1811323   0.5242209   0.0066616
    1PTC   CB40   40  -0.2554666   0.6426499   0.0097170
    1PTC   CB41   41  -0.3489115   0.6739201  -0.0891353
    1PTC   CA42   42  -0.3708106   0.5868718  -0.1948063
    1PTC   CC43   43  -0.4665821   0.6164785  -0.2982126
    1PTC   CF44   44  -0.2978366   0.4648099  -0.2028672
```

```
    1PTC   CG45   45  -0.6186806   0.7021161  -0.4285286
    1PTC   CB46   46  -0.7154683   0.7830197  -0.4883096
    1PTC   CB47   47  -0.7740253   0.7381646  -0.6064848
    1PTC   CB48   48  -0.7372111   0.6151084  -0.6644360
    1PTC   CB49   49  -0.6407041   0.5328827  -0.6061975
    1PTC   CD50   50  -0.5828454   0.5784823  -0.4882745
    1PTC    H51   51  -0.2666118   0.1899193  -0.4005770
    1PTC    H52   52  -0.1008781   0.1309898  -0.2280515
    1PTC    H53   53  -0.2415112   0.7133342   0.0902966
    1PTC    H54   54  -0.4056630   0.7660206  -0.0852304
    1PTC    H55   55  -0.7430071   0.8772935  -0.4429626
    1PTC    H56   56  -0.8494387   0.7988440  -0.6551208
    1PTC    H57   57  -0.7849611   0.5835450  -0.7564192
    1PTC    H58   58  -0.6108494   0.4382764  -0.6486596
   0.47290   0.80061   1.46906   0.00000   0.00000  -0.21198   0.00000  -0.02949   0.00943
```

3: copper phthalocyanine (CuPc)

```
CuPc Unit Cell
114
    1CPC   CUC1    1  -0.0000000  -0.0000000  -0.0000000
    1CPC    CI2    2  -0.1342582  -0.1910137   0.1845938
    1CPC    CJ3    3  -0.2801566  -0.1882659  -0.2526756
    1CPC    CK4    4  -0.3504904  -0.2169228  -0.3697444
    1CPC    CK5    5  -0.4499181  -0.3143536  -0.3631127
    1CPC    CK6    6  -0.4783063  -0.3814899  -0.2425651
    1CPC    CK7    7  -0.4080097  -0.3528451  -0.1256890
    1CPC    CJ8    8  -0.3084798  -0.2552436  -0.1323795
    1CPC    CI9    9  -0.2175254  -0.2005816  -0.0325124
    1CPC   CJ10   10  -0.1331387  -0.2357626   0.3232305
    1CPC   CK11   11  -0.2079934  -0.3314942   0.3918326
    1CPC   CK12   12  -0.1807606  -0.3499273   0.5272559
    1CPC   CK13   13  -0.0812416  -0.2746346   0.5925848
    1CPC   CK14   14  -0.0065157  -0.1790348   0.5240216
    1CPC   CJ15   15  -0.0337922  -0.1606542   0.3883934
    1CPC   CI16   16   0.0232493  -0.0719225   0.2878420
    1CPC   CI17   17  -0.1726539  -0.0944172  -0.2232117
    1CPC   HG18   18  -0.3279239  -0.1646360  -0.4621536
    1CPC   HG19   19  -0.5067875  -0.3392052  -0.4523082
    1CPC   HG20   20  -0.5565317  -0.4569049  -0.2410291
    1CPC   HG21   21  -0.2845054  -0.3891413   0.3407832
    1CPC   HG22   22  -0.2371470  -0.4236726   0.5837384
    1CPC   HG23   23  -0.0626667  -0.2916335   0.6982864
    1CPC   HG24   24   0.0703668  -0.1205209   0.5734985
    1CPC   NI25   25  -0.2165478  -0.2410216   0.0936268
    1CPC   NJ26   26  -0.0394120  -0.0929605   0.1672539
    1CPC   NI27   27   0.1206284   0.0138105   0.3145577
    1CPC   NK28   28   0.1378817   0.1046869   0.0905646
    1CPC   NJ29   29   0.0394120   0.0929605  -0.1672539
    1CPC   NK30   30  -0.1378817  -0.1046869  -0.0905646
    1CPC   NI31   31  -0.1206284  -0.0138105  -0.3145577
    1CPC   CI32   32   0.1726539   0.0944172   0.2232117
    1CPC   CI33   33   0.2175254   0.2005816   0.0325124
    1CPC   CI34   34   0.1342582   0.1910137  -0.1845938
    1CPC   CI35   35  -0.0232493   0.0719225  -0.2878420
```

1CPC	CJ36	36	0.2801566	0.1882659	0.2526756
1CPC	CJ37	37	0.3084798	0.2552436	0.1323795
1CPC	NI38	38	0.2165478	0.2410216	-0.0936268
1CPC	CJ39	39	0.1331387	0.2357626	-0.3232305
1CPC	CJ40	40	0.0337922	0.1606542	-0.3883934
1CPC	CK41	41	0.3504904	0.2169228	0.3697444
1CPC	CK42	42	0.4080097	0.3528451	0.1256890
1CPC	CK43	43	0.2079934	0.3314942	-0.3918326
1CPC	CK44	44	0.0065157	0.1790348	-0.5240216
1CPC	CK45	45	0.4499181	0.3143536	0.3631127
1CPC	HG46	46	0.3279239	0.1646360	0.4621536
1CPC	CK47	47	0.4783063	0.3814899	0.2425651
1CPC	CK48	48	0.1807606	0.3499273	-0.5272559
1CPC	HG49	49	0.2845054	0.3891413	-0.3407832
1CPC	CK50	50	0.0812416	0.2746346	-0.5925848
1CPC	HG51	51	-0.0703668	0.1205209	-0.5734985
1CPC	HG52	52	0.5067875	0.3392052	0.4523082
1CPC	HG53	53	0.5565317	0.4569049	0.2410291
1CPC	HG54	54	0.2371470	0.4236726	-0.5837384
1CPC	HG55	55	0.0626667	0.2916335	-0.6982864
1CPC	HG56	56	-0.4292613	-0.4040422	-0.0323622
1CPC	HG57	57	0.4292613	0.4040422	0.0323622
2CPC	CUC1	58	0.9703500	0.2395000	0.0000000
2CPC	CI2	59	1.1046095	0.0484881	-0.1845948
2CPC	CJ3	60	1.2505049	0.0512317	0.2526756
2CPC	CK4	61	1.3208380	0.0225737	0.3697447
2CPC	CK5	62	1.4202658	-0.0748570	0.3631126
2CPC	CK6	63	1.4486549	-0.1419921	0.2425646
2CPC	CK7	64	1.3783590	-0.1133462	0.1256882
2CPC	CJ8	65	1.2788290	-0.0157448	0.1323791
2CPC	CI9	66	1.1878753	0.0389181	0.0325119
2CPC	CJ10	67	1.1034910	0.0037406	-0.3232320
2CPC	CK11	68	1.1783461	-0.0919903	-0.3918345
2CPC	CK12	69	1.1511142	-0.1104221	-0.5272581
2CPC	CK13	70	1.0515956	-0.0351287	-0.5925869
2CPC	CK14	71	0.9768693	0.0604703	-0.5240233
2CPC	CJ15	72	1.0041449	0.0788497	-0.3883948
2CPC	CI16	73	0.9471026	0.1675803	-0.2878429
2CPC	CI17	74	1.1430024	0.1450807	0.2232120
2CPC	HG18	75	1.2982708	0.0748596	0.4621542
2CPC	HG19	76	1.4771346	-0.0997094	0.4523082
2CPC	HG20	77	1.5268803	-0.2174070	0.2410284
2CPC	HG21	78	1.2548578	-0.1496378	-0.3407851
2CPC	HG22	79	1.2075011	-0.1841668	-0.5837409
2CPC	HG23	80	1.0330215	-0.0521267	-0.6982888
2CPC	HG24	81	0.8999871	0.1189847	-0.5735002
2CPC	NI25	82	1.1868985	-0.0015206	-0.0936277
2CPC	NJ26	83	1.0097632	0.1465412	-0.1672545
2CPC	NI27	84	0.8497237	0.2533135	-0.3145584
2CPC	NK28	85	0.8324689	0.3441877	-0.0905645
2CPC	NJ29	86	0.9309368	0.3324588	0.1672545
2CPC	NK30	87	1.1082311	0.1348123	0.0905645
2CPC	NI31	88	1.0909763	0.2256865	0.3145584
2CPC	CI32	89	0.7976976	0.3339193	-0.2232120

```
    2CPC     CI33   90   0.7528247   0.4400819  -0.0325119
    2CPC     CI34   91   0.8360905   0.4305119   0.1845948
    2CPC     CI35   92   0.9935974   0.3114197   0.2878429
    2CPC     CJ36   93   0.6901951   0.4277683  -0.2526756
    2CPC     CJ37   94   0.6618710   0.4947448  -0.1323791
    2CPC     NI38   95   0.7538015   0.4805206   0.0936277
    2CPC     CJ39   96   0.8372090   0.4752594   0.3232320
    2CPC     CJ40   97   0.9365551   0.4001503   0.3883948
    2CPC     CK41   98   0.6198620   0.4564263  -0.3697447
    2CPC     CK42   99   0.5623410   0.5923462  -0.1256882
    2CPC     CK43  100   0.7623539   0.5709903   0.3918345
    2CPC     CK44  101   0.9638307   0.4185297   0.5240233
    2CPC     CK45  102   0.5204342   0.5538570  -0.3631126
    2CPC     HG46  103   0.6424292   0.4041404  -0.4621542
    2CPC     CK47  104   0.4920451   0.6209921  -0.2425646
    2CPC     CK48  105   0.7895858   0.5894221   0.5272581
    2CPC     HG49  106   0.6858422   0.6286378   0.3407851
    2CPC     CK50  107   0.8891044   0.5141287   0.5925869
    2CPC     HG51  108   1.0407129   0.3600153   0.5735002
    2CPC     HG52  109   0.4635654   0.5787094  -0.4523082
    2CPC     HG53  110   0.4138197   0.6964070  -0.2410284
    2CPC     HG54  111   0.7331989   0.6631668   0.5837409
    2CPC     HG55  112   0.9076785   0.5311267   0.6982888
    2CPC     HG56  113   1.3996112  -0.1645423   0.0323611
    2CPC     HG57  114   0.5410888   0.6435423  -0.0323611
 1.94070  0.47900  1.25478  0.00000  0.00000  0.00000  0.00000 -0.75187  0.00000
```

4: Buckminsterfullerene (C_{60})

```
C60 Unit Cell
240
    1BUK     CU1    1  -0.0541104   0.3125240   0.1593977
    1BUK     CS2    2  -0.0916714   0.3417019   0.0282320
    1BUK     CU3    3   0.0854092   0.2868004   0.1909608
    1BUK     CU4    4  -0.1356722   0.2234286   0.2402285
    1BUK     CS5    5   0.0086470   0.3463715  -0.0767830
    1BUK     CS6    6  -0.2123818   0.2831001  -0.0275472
    1BUK     CR7    7   0.1817632   0.2913200   0.0901176
    1BUK     CU8    8  -0.0465089   0.1425868   0.3216750
    1BUK     CS9    9  -0.0500226   0.2906743  -0.1974977
    1BUK    CP10   10  -0.2516065   0.1670914   0.1866840
    1BUK    CV11   11   0.1593977  -0.0541103   0.3125240
    1BUK    CO12   12   0.0282321  -0.0916714   0.3417018
    1BUK    CV13   13   0.1909608   0.0854092   0.2868004
    1BUK    CV14   14   0.2402285  -0.1356721   0.2234286
    1BUK    CO15   15  -0.0767829   0.0086470   0.3463715
    1BUK    CO16   16  -0.0275471  -0.2123817   0.2831001
    1BUK    CU17   17   0.0901176   0.1817632   0.2913199
    1BUK    CV18   18   0.3216750  -0.0465089   0.1425867
    1BUK    CO19   19  -0.1974977  -0.0500225   0.2906743
    1BUK    CS20   20   0.1866840  -0.2516065   0.1670914
    1BUK    CR21   21   0.3125240   0.1593977  -0.0541104
    1BUK    CP22   22   0.3417018   0.0282320  -0.0916714
    1BUK    CR23   23   0.2868004   0.1909608   0.0854092
    1BUK    CR24   24   0.2234285   0.2402285  -0.1356722
```

1BUK	CP25	25	0.3463715	-0.0767829	0.0086470
1BUK	CP26	26	0.2831001	-0.0275471	-0.2123818
1BUK	CV27	27	0.2913199	0.0901176	0.1817632
1BUK	CR28	28	0.1425868	0.3216749	-0.0465089
1BUK	CP29	29	0.2906744	-0.1974978	-0.0500226
1BUK	CO30	30	0.1670914	0.1866840	-0.2516066
1BUK	CV31	31	-0.1593977	0.0541103	-0.3125240
1BUK	CO32	32	-0.0282321	0.0916714	-0.3417018
1BUK	CV33	33	-0.1909608	-0.0854092	-0.2868004
1BUK	CV34	34	-0.2402285	0.1356721	-0.2234286
1BUK	CO35	35	0.0767829	-0.0086470	-0.3463715
1BUK	CO36	36	0.0275471	0.2123817	-0.2831001
1BUK	CU37	37	-0.0901176	-0.1817632	-0.2913199
1BUK	CV38	38	-0.3216750	0.0465089	-0.1425867
1BUK	CO39	39	0.1974977	0.0500225	-0.2906743
1BUK	CS40	40	-0.1866840	0.2516065	-0.1670914
1BUK	CR41	41	-0.3125240	-0.1593977	0.0541104
1BUK	CP42	42	-0.3417018	-0.0282320	0.0916714
1BUK	CR43	43	-0.2868004	-0.1909608	-0.0854092
1BUK	CR44	44	-0.2234285	-0.2402285	0.1356722
1BUK	CP45	45	-0.3463715	0.0767829	-0.0086470
1BUK	CP46	46	-0.2831001	0.0275471	0.2123818
1BUK	CV47	47	-0.2913199	-0.0901176	-0.1817632
1BUK	CR48	48	-0.1425868	-0.3216749	0.0465089
1BUK	CP49	49	-0.2906744	0.1974978	0.0500226
1BUK	CO50	50	-0.1670914	-0.1866840	0.2516066
1BUK	CU51	51	0.0541104	-0.3125240	-0.1593977
1BUK	CS52	52	0.0916714	-0.3417019	-0.0282320
1BUK	CU53	53	-0.0854092	-0.2868004	-0.1909608
1BUK	CU54	54	0.1356722	-0.2234286	-0.2402285
1BUK	CS55	55	-0.0086470	-0.3463715	0.0767830
1BUK	CS56	56	0.2123818	-0.2831001	0.0275472
1BUK	CR57	57	-0.1817632	-0.2913200	-0.0901176
1BUK	CU58	58	0.0465089	-0.1425868	-0.3216750
1BUK	CS59	59	0.0500226	-0.2906743	0.1974977
1BUK	CP60	60	0.2516065	-0.1670914	-0.1866840
2BUK	CU1	61	0.6484899	0.3125243	0.5432020
2BUK	CS2	62	0.6109286	0.3417019	0.6743679
2BUK	CU3	63	0.7880094	0.2868006	0.5116389
2BUK	CU4	64	0.5669277	0.2234285	0.4623716
2BUK	CS5	65	0.7112468	0.3463713	0.7793832
2BUK	CS6	66	0.4902183	0.2831001	0.7301471
2BUK	CR7	67	0.8843632	0.2913199	0.6124825
2BUK	CU8	68	0.6560913	0.1425869	0.3809248
2BUK	CS9	69	0.6525774	0.2906743	0.9000977
2BUK	CP10	70	0.4509935	0.1670914	0.5159160
2BUK	CV11	71	0.8619980	-0.0541101	0.3900757
2BUK	CO12	72	0.7308321	-0.0916714	0.3608981
2BUK	CV13	73	0.8935611	0.0854094	0.4157994
2BUK	CV14	74	0.9428284	-0.1356723	0.4791715
2BUK	CO15	75	0.6258169	0.0086468	0.3562287
2BUK	CO16	76	0.6750529	-0.2123818	0.4194999
2BUK	CU17	77	0.7927176	0.1817632	0.4112801
2BUK	CV18	78	1.0242751	-0.0465087	0.5600131

2BUK	CO19	79	0.5051023	-0.0500225	0.4119257
2BUK	CS20	80	0.8892840	-0.2516066	0.5355086
2BUK	CR21	81	1.0151243	0.1593980	0.7567101
2BUK	CP22	82	1.0443019	0.0282321	0.7942713
2BUK	CR23	83	0.9894006	0.1909610	0.6171905
2BUK	CR24	84	0.9260284	0.2402284	0.8382723
2BUK	CP25	85	1.0489713	-0.0767831	0.6939533
2BUK	CP26	86	0.9857001	-0.0275471	0.9149818
2BUK	CV27	87	0.9939199	0.0901175	0.5208368
2BUK	CR28	88	0.8451870	0.3216751	0.7491088
2BUK	CP29	89	0.9932744	-0.1974978	0.7526226
2BUK	CO30	90	0.8696914	0.1866840	0.9542066
2BUK	CV31	91	0.5432020	0.0541101	1.0151243
2BUK	CO32	92	0.6743679	0.0916714	1.0443019
2BUK	CV33	93	0.5116389	-0.0854094	0.9894006
2BUK	CV34	94	0.4623716	0.1356723	0.9260285
2BUK	CO35	95	0.7793831	-0.0086468	1.0489713
2BUK	CO36	96	0.7301471	0.2123818	0.9857001
2BUK	CU37	97	0.6124824	-0.1817632	0.9939199
2BUK	CV38	98	0.3809249	0.0465087	0.8451869
2BUK	CO39	99	0.9000977	0.0500225	0.9932743
2BUK	CS40	100	0.5159160	0.2516066	0.8696914
2BUK	CR41	101	0.3900757	-0.1593980	0.6484899
2BUK	CP42	102	0.3608981	-0.0282321	0.6109287
2BUK	CR43	103	0.4157994	-0.1909610	0.7880095
2BUK	CR44	104	0.4791716	-0.2402284	0.5669277
2BUK	CP45	105	0.3562287	0.0767831	0.7112467
2BUK	CP46	106	0.4194999	0.0275471	0.4902182
2BUK	CV47	107	0.4112801	-0.0901175	0.8843632
2BUK	CR48	108	0.5600130	-0.3216751	0.6560912
2BUK	CP49	109	0.4119256	0.1974978	0.6525774
2BUK	CO50	110	0.5355086	-0.1866840	0.4509934
2BUK	CU51	111	0.7567101	-0.3125243	0.8619980
2BUK	CS52	112	0.7942714	-0.3417019	0.7308321
2BUK	CU53	113	0.6171906	-0.2868006	0.8935611
2BUK	CU54	114	0.8382723	-0.2234285	0.9428284
2BUK	CS55	115	0.6939532	-0.3463713	0.6258168
2BUK	CS56	116	0.9149817	-0.2831001	0.6750529
2BUK	CR57	117	0.5208368	-0.2913199	0.7927175
2BUK	CU58	118	0.7491087	-0.1425869	1.0242752
2BUK	CS59	119	0.7526226	-0.2906743	0.5051023
2BUK	CP60	120	0.9542065	-0.1670914	0.8892840
3BUK	CU1	121	0.7567101	1.0151243	0.1593980
3BUK	CS2	122	0.7942713	1.0443019	0.0282320
3BUK	CU3	123	0.6171905	0.9894007	0.1909610
3BUK	CU4	124	0.8382723	0.9260286	0.2402284
3BUK	CS5	125	0.6939532	1.0489713	-0.0767833
3BUK	CS6	126	0.9149817	0.9857001	-0.0275472
3BUK	CR7	127	0.5208368	0.9939199	0.0901174
3BUK	CU8	128	0.7491087	0.8451870	0.3216751
3BUK	CS9	129	0.7526226	0.9932743	-0.1974978
3BUK	CP10	130	0.9542065	0.8696914	0.1866840
3BUK	CV11	131	0.5432020	0.6484900	0.3125243
3BUK	CO12	132	0.6743678	0.6109287	0.3417019

3BUK	CV13	133	0.5116389	0.7880095	0.2868006
3BUK	CV14	134	0.4623716	0.5669278	0.2234285
3BUK	CO15	135	0.7793831	0.7112468	0.3463713
3BUK	CO16	136	0.7301471	0.4902183	0.2831001
3BUK	CU17	137	0.6124824	0.8843632	0.2913198
3BUK	CV18	138	0.3809249	0.6560913	0.1425869
3BUK	CO19	139	0.9000977	0.6525775	0.2906744
3BUK	CS20	140	0.5159160	0.4509935	0.1670914
3BUK	CR21	141	0.3900757	0.8619980	-0.0541102
3BUK	CP22	142	0.3608982	0.7308321	-0.0916714
3BUK	CR23	143	0.4157994	0.8935610	0.0854094
3BUK	CR24	144	0.4791716	0.9428284	-0.1356723
3BUK	CP25	145	0.3562287	0.6258169	0.0086467
3BUK	CP26	146	0.4194999	0.6750529	-0.2123819
3BUK	CV27	147	0.4112801	0.7927175	0.1817631
3BUK	CR28	148	0.5600130	1.0242751	-0.0465088
3BUK	CP29	149	0.4119257	0.5051022	-0.0500226
3BUK	CO30	150	0.5355086	0.8892839	-0.2516066
3BUK	CV31	151	0.8619980	0.7567100	-0.3125243
3BUK	CO32	152	0.7308322	0.7942713	-0.3417019
3BUK	CV33	153	0.8935611	0.6171905	-0.2868006
3BUK	CV34	154	0.9428284	0.8382722	-0.2234285
3BUK	CO35	155	0.6258169	0.6939532	-0.3463713
3BUK	CO36	156	0.6750529	0.9149817	-0.2831001
3BUK	CU37	157	0.7927176	0.5208368	-0.2913198
3BUK	CV38	158	1.0242751	0.7491087	-0.1425869
3BUK	CO39	159	0.5051023	0.7526225	-0.2906744
3BUK	CS40	160	0.8892840	0.9542065	-0.1670914
3BUK	CR41	161	1.0151243	0.5432020	0.0541102
3BUK	CP42	162	1.0443018	0.6743679	0.0916714
3BUK	CR43	163	0.9894006	0.5116390	-0.0854094
3BUK	CR44	164	0.9260284	0.4623716	0.1356723
3BUK	CP45	165	1.0489713	0.7793831	-0.0086467
3BUK	CP46	166	0.9857001	0.7301471	0.2123819
3BUK	CV47	167	0.9939199	0.6124825	-0.1817631
3BUK	CR48	168	0.8451870	0.3809249	0.0465088
3BUK	CP49	169	0.9932743	0.9000978	0.0500226
3BUK	CO50	170	0.8696914	0.5159161	0.2516066
3BUK	CU51	171	0.6484899	0.3900757	-0.1593980
3BUK	CS52	172	0.6109287	0.3608981	-0.0282320
3BUK	CU53	173	0.7880095	0.4157993	-0.1909610
3BUK	CU54	174	0.5669277	0.4791714	-0.2402284
3BUK	CS55	175	0.7112468	0.3562287	0.0767833
3BUK	CS56	176	0.4902183	0.4194999	0.0275472
3BUK	CR57	177	0.8843632	0.4112801	-0.0901174
3BUK	CU58	178	0.6560913	0.5600130	-0.3216751
3BUK	CS59	179	0.6525774	0.4119257	0.1974978
3BUK	CP60	180	0.4509935	0.5355086	-0.1866840
4BUK	CU1	181	0.0541103	1.0151240	0.5432023
4BUK	CS2	182	0.0916714	1.0443019	0.6743680
4BUK	CU3	183	-0.0854092	0.9894004	0.5116392
4BUK	CU4	184	0.1356722	0.9260287	0.4623715
4BUK	CS5	185	-0.0086471	1.0489715	0.7793830
4BUK	CS6	186	0.2123817	0.9857001	0.7301472

4BUK	CR7	187	-0.1817632	0.9939199	0.6124825
4BUK	CU8	188	0.0465089	0.8451868	0.3809250
4BUK	CS9	189	0.0500225	0.9932743	0.9000978
4BUK	CP10	190	0.2516065	0.8696914	0.5159160
4BUK	CV11	191	-0.1593977	0.6484897	0.3900760
4BUK	CO12	192	-0.0282320	0.6109286	0.3608982
4BUK	CV13	193	-0.1909608	0.7880092	0.4157996
4BUK	CV14	194	-0.2402285	0.5669279	0.4791714
4BUK	CO15	195	0.0767829	0.7112471	0.3562285
4BUK	CO16	196	0.0275472	0.4902183	0.4194999
4BUK	CU17	197	-0.0901176	0.8843632	0.4112801
4BUK	CV18	198	-0.3216749	0.6560911	0.5600132
4BUK	CO19	199	0.1974978	0.6525775	0.4119257
4BUK	CS20	200	-0.1866840	0.4509934	0.5355086
4BUK	CR21	201	-0.3125241	0.8619977	0.7567104
4BUK	CP22	202	-0.3417018	0.7308320	0.7942714
4BUK	CR23	203	-0.2868004	0.8935608	0.6171908
4BUK	CR24	204	-0.2234286	0.9428285	0.8382722
4BUK	CP25	205	-0.3463715	0.6258171	0.6939530
4BUK	CP26	206	-0.2831001	0.6750528	0.9149818
4BUK	CV27	207	-0.2913199	0.7927176	0.5208368
4BUK	CR28	208	-0.1425868	1.0242749	0.7491090
4BUK	CP29	209	-0.2906743	0.5051022	0.7526225
4BUK	CO30	210	-0.1670915	0.8892839	0.9542066
4BUK	CV31	211	0.1593977	0.7567103	1.0151240
4BUK	CO32	212	0.0282320	0.7942714	1.0443018
4BUK	CV33	213	0.1909608	0.6171908	0.9894004
4BUK	CV34	214	0.2402285	0.8382721	0.9260286
4BUK	CO35	215	-0.0767829	0.6939529	1.0489715
4BUK	CO36	216	-0.0275472	0.9149817	0.9857001
4BUK	CU37	217	0.0901176	0.5208368	0.9939199
4BUK	CV38	218	0.3216749	0.7491089	0.8451868
4BUK	CO39	219	-0.1974978	0.7526225	0.9932743
4BUK	CS40	220	0.1866840	0.9542066	0.8696914
4BUK	CR41	221	0.3125241	0.5432023	0.6484896
4BUK	CP42	222	0.3417018	0.6743680	0.6109286
4BUK	CR43	223	0.2868004	0.5116392	0.7880092
4BUK	CR44	224	0.2234286	0.4623715	0.5669278
4BUK	CP45	225	0.3463715	0.7793829	0.7112470
4BUK	CP46	226	0.2831001	0.7301472	0.4902182
4BUK	CV47	227	0.2913199	0.6124824	0.8843632
4BUK	CR48	228	0.1425868	0.3809251	0.6560910
4BUK	CP49	229	0.2906743	0.9000978	0.6525775
4BUK	CO50	230	0.1670915	0.5159161	0.4509934
4BUK	CU51	231	-0.0541103	0.3900760	0.8619977
4BUK	CS52	232	-0.0916714	0.3608981	0.7308320
4BUK	CU53	233	0.0854092	0.4157996	0.8935608
4BUK	CU54	234	-0.1356722	0.4791713	0.9428285
4BUK	CS55	235	0.0086471	0.3562285	0.6258170
4BUK	CS56	236	-0.2123817	0.4194999	0.6750528
4BUK	CR57	237	0.1817632	0.4112801	0.7927175
4BUK	CU58	238	-0.0465089	0.5600132	1.0242750
4BUK	CS59	239	-0.0500225	0.4119257	0.5051022
4BUK	CP60	240	-0.2516065	0.5355086	0.8892840

```
1.40520  1.40520  1.40520  0.00000  0.00000  0.00000  0.00000  0.00000  0.00000
```

5: 4-(Dicyanomethylene)-2-methyl-6-(4-dimethylaminostyryl)-4H-pyran (DCM)

```
DCM Unit Cell
320
    1DCM     OD1    1   1.9708726  -0.0670031   0.6000999
    1DCM     NE2    2   1.3511798   0.4425624   0.3293032
    1DCM     NC3    3   2.5037096  -0.1372421   0.8526713
    1DCM     NC4    4   2.3884551   0.2948917   0.8200249
    1DCM     CI5    5   2.0610010  -0.1620890   0.6384230
    1DCM     CJ6    6   2.1785881  -0.1296088   0.6966350
    1DCM     HI7    7   2.2470143  -0.2086376   0.7252036
    1DCM     CK8    8   2.2135138   0.0083076   0.7207947
    1DCM     CJ9    9   2.1160754   0.1041495   0.6791024
    1DCM    HI10   10   2.1345374   0.2099652   0.6937371
    1DCM    CL11   11   1.9985851   0.0657133   0.6204685
    1DCM    CG12   12   1.8962073   0.1564697   0.5758079
    1DCM    HI13   13   1.9194846   0.2613382   0.5918489
    1DCM    CG14   14   1.7790728   0.1187481   0.5185682
    1DCM    HI15   15   1.7614419   0.0120498   0.5063089
    1DCM    CK16   16   1.6724530   0.2047942   0.4712752
    1DCM    CF17   17   1.5548042   0.1471040   0.4194463
    1DCM    HI18   18   1.5464862   0.0386916   0.4159351
    1DCM    CF19   19   1.4488803   0.2235505   0.3733383
    1DCM    HI20   20   1.3608482   0.1732002   0.3352852
    1DCM    CH21   21   1.4550901   0.3650502   0.3757533
    1DCM    CF22   22   1.5733832   0.4238195   0.4279140
    1DCM    HI23   23   1.5832198   0.5315966   0.4325952
    1DCM    CF24   24   1.6779121   0.3457794   0.4737265
    1DCM    HI25   25   1.7662520   0.3958985   0.5122747
    1DCM    CD26   26   1.2275314   0.3797249   0.2855306
    1DCM    HJ27   27   1.1583338   0.4568422   0.2513944
    1DCM    HJ28   28   1.1788019   0.3233022   0.3664088
    1DCM    HJ29   29   1.2450975   0.3109131   0.2018387
    1DCM    CD30   30   1.3573652   0.5874420   0.3407913
    1DCM    HJ31   31   1.2677432   0.6307245   0.2961062
    1DCM    HJ32   32   1.4442651   0.6280298   0.2874699
    1DCM    HJ33   33   1.3629077   0.6206761   0.4454944
    1DCM    CE34   34   2.0124412  -0.2999336   0.6077310
    1DCM    HJ35   35   2.0854828  -0.3743350   0.6402241
    1DCM    HJ36   36   1.9953903  -0.3117331   0.5000512
    1DCM    HJ37   37   1.9171499  -0.3193525   0.6583780
    1DCM    CC38   38   2.3343131   0.0448051   0.7807884
    1DCM    CB39   39   2.4287360  -0.0536774   0.8209811
    1DCM    CB40   40   2.3660357   0.1816535   0.8032999
    2DCM     OD1   41   0.9356080  -0.0670092   0.5272093
    2DCM     NE2   42   1.5553537   0.4425620   0.7978741
    2DCM     NC3   43   0.4026080  -0.1372410   0.2749801
    2DCM     NC4   44   0.5177648   0.2949048   0.3078116
    2DCM     CI5   45   0.8454786  -0.1620966   0.4888923
    2DCM     CJ6   46   0.7278403  -0.1296132   0.4307856
    2DCM     HI7   47   0.6594155  -0.2086435   0.4022174
    2DCM     CK8   48   0.6928583   0.0083083   0.4067369
    2DCM     CJ9   49   0.7903000   0.1041517   0.4484183
```

2DCM	HI10	50	0.7717978	0.2099712	0.4338628
2DCM	CL11	51	0.9078435	0.0657121	0.5069433
2DCM	CG12	52	1.0102281	0.1564694	0.5515862
2DCM	HI13	53	0.9869098	0.2613414	0.5356272
2DCM	CG14	54	1.1274146	0.1187452	0.6087175
2DCM	HI15	55	1.1450844	0.0120443	0.6208978
2DCM	CK16	56	1.2340445	0.2047918	0.6559869
2DCM	CF17	57	1.3517470	0.1471025	0.7076946
2DCM	HI18	58	1.3600980	0.0386903	0.7111324
2DCM	CF19	59	1.4576828	0.2235501	0.7537735
2DCM	HI20	60	1.5457565	0.1732009	0.7917316
2DCM	CH21	61	1.4514316	0.3650495	0.7514510
2DCM	CF22	62	1.3330842	0.4238179	0.6994125
2DCM	HI23	63	1.3232139	0.5315952	0.6948054
2DCM	CF24	64	1.2285441	0.3457770	0.6536272
2DCM	HI25	65	1.1401622	0.3958953	0.6151741
2DCM	CD26	66	1.6790514	0.3797320	0.8415181
2DCM	HJ27	67	1.7482521	0.4568476	0.8756521
2DCM	HJ28	68	1.7277381	0.3233734	0.7605695
2DCM	HJ29	69	1.6615652	0.3108633	0.9251798
2DCM	CD30	70	1.5491193	0.5874470	0.7864805
2DCM	HJ31	71	1.6387615	0.6307269	0.8311276
2DCM	HJ32	72	1.4622467	0.6279772	0.8398901
2DCM	HJ33	73	1.5434916	0.6207446	0.6818022
2DCM	CE34	74	0.8940992	-0.2999466	0.5194634
2DCM	HJ35	75	0.8210551	-0.3743483	0.4869770
2DCM	HJ36	76	0.9112314	-0.3118082	0.6271234
2DCM	HJ37	77	0.9893593	-0.3193073	0.4687353
2DCM	CC38	78	0.5720054	0.0448092	0.3468535
2DCM	CB39	79	0.4775811	-0.0536749	0.3066679
2DCM	CB40	80	0.5402281	0.1816625	0.3244500
3DCM	OD1	81	0.5021226	0.6903319	0.6000999
3DCM	NE2	82	-0.1175702	1.1998974	0.3293032
3DCM	NC3	83	1.0349596	0.6200929	0.8526713
3DCM	NC4	84	0.9197051	1.0522266	0.8200249
3DCM	CI5	85	0.5922510	0.5952460	0.6384230
3DCM	CJ6	86	0.7098381	0.6277262	0.6966350
3DCM	HI7	87	0.7782643	0.5486974	0.7252036
3DCM	CK8	88	0.7447638	0.7656426	0.7207947
3DCM	CJ9	89	0.6473254	0.8614845	0.6791024
3DCM	HI10	90	0.6657874	0.9673002	0.6937371
3DCM	CL11	91	0.5298351	0.8230483	0.6204685
3DCM	CG12	92	0.4274574	0.9138047	0.5758079
3DCM	HI13	93	0.4507347	1.0186732	0.5918489
3DCM	CG14	94	0.3103228	0.8760831	0.5185682
3DCM	HI15	95	0.2926919	0.7693848	0.5063089
3DCM	CK16	96	0.2037030	0.9621292	0.4712752
3DCM	CF17	97	0.0860542	0.9044390	0.4194463
3DCM	HI18	98	0.0777362	0.7960266	0.4159351
3DCM	CF19	99	-0.0198697	0.9808855	0.3733383
3DCM	HI20	100	-0.1079018	0.9305352	0.3352852
3DCM	CH21	101	-0.0136599	1.1223852	0.3757533
3DCM	CF22	102	0.1046332	1.1811545	0.4279140
3DCM	HI23	103	0.1144698	1.2889316	0.4325952

3DCM	CF24	104	0.2091621	1.1031144	0.4737265
3DCM	HI25	105	0.2975020	1.1532335	0.5122747
3DCM	CD26	106	-0.2412186	1.1370599	0.2855306
3DCM	HJ27	107	-0.3104162	1.2141772	0.2513944
3DCM	HJ28	108	-0.2899481	1.0806372	0.3664088
3DCM	HJ29	109	-0.2236525	1.0682481	0.2018387
3DCM	CD30	110	-0.1113848	1.3447770	0.3407913
3DCM	HJ31	111	-0.2010068	1.3880595	0.2961062
3DCM	HJ32	112	-0.0244849	1.3853648	0.2874699
3DCM	HJ33	113	-0.1058423	1.3780111	0.4454944
3DCM	CE34	114	0.5436912	0.4574014	0.6077310
3DCM	HJ35	115	0.6167328	0.3830000	0.6402241
3DCM	HJ36	116	0.5266403	0.4456019	0.5000512
3DCM	HJ37	117	0.4483999	0.4379825	0.6583780
3DCM	CC38	118	0.8655631	0.8021401	0.7807884
3DCM	CB39	119	0.9599860	0.7036576	0.8209811
3DCM	CB40	120	0.8972857	0.9389884	0.8032999
4DCM	OD1	121	2.4043580	0.6903258	0.5272093
4DCM	NE2	122	3.0241037	1.1998970	0.7978741
4DCM	NC3	123	1.8713580	0.6200940	0.2749801
4DCM	NC4	124	1.9865148	1.0522398	0.3078116
4DCM	CI5	125	2.3142286	0.5952384	0.4888923
4DCM	CJ6	126	2.1965903	0.6277218	0.4307856
4DCM	HI7	127	2.1281655	0.5486915	0.4022174
4DCM	CK8	128	2.1616083	0.7656433	0.4067369
4DCM	CJ9	129	2.2590500	0.8614867	0.4484183
4DCM	HI10	130	2.2405478	0.9673062	0.4338628
4DCM	CL11	131	2.3765935	0.8230471	0.5069433
4DCM	CG12	132	2.4789781	0.9138044	0.5515862
4DCM	HI13	133	2.4556598	1.0186764	0.5356272
4DCM	CG14	134	2.5961646	0.8760802	0.6087175
4DCM	HI15	135	2.6138344	0.7693793	0.6208978
4DCM	CK16	136	2.7027945	0.9621268	0.6559869
4DCM	CF17	137	2.8204970	0.9044375	0.7076946
4DCM	HI18	138	2.8288480	0.7960253	0.7111324
4DCM	CF19	139	2.9264328	0.9808851	0.7537735
4DCM	HI20	140	3.0145065	0.9305359	0.7917316
4DCM	CH21	141	2.9201816	1.1223845	0.7514510
4DCM	CF22	142	2.8018342	1.1811529	0.6994125
4DCM	HI23	143	2.7919639	1.2889302	0.6948054
4DCM	CF24	144	2.6972941	1.1031120	0.6536272
4DCM	HI25	145	2.6089122	1.1532303	0.6151741
4DCM	CD26	146	3.1478014	1.1370670	0.8415181
4DCM	HJ27	147	3.2170021	1.2141826	0.8756521
4DCM	HJ28	148	3.1964881	1.0807084	0.7605695
4DCM	HJ29	149	3.1303152	1.0681983	0.9251798
4DCM	CD30	150	3.0178693	1.3447820	0.7864805
4DCM	HJ31	151	3.1075115	1.3880619	0.8311276
4DCM	HJ32	152	2.9309967	1.3853122	0.8398901
4DCM	HJ33	153	3.0122416	1.3780796	0.6818022
4DCM	CE34	154	2.3628492	0.4573884	0.5194634
4DCM	HJ35	155	2.2898051	0.3829867	0.4869770
4DCM	HJ36	156	2.3799814	0.4455268	0.6271234
4DCM	HJ37	157	2.4581093	0.4380277	0.4687353

4DCM	CC38	158	2.0407554	0.8021442	0.3468535
4DCM	CB39	159	1.9463311	0.7036601	0.3066679
4DCM	CB40	160	2.0089781	0.9389975	0.3244500
5DCM	OD1	161	0.9459127	1.5816771	0.1515437
5DCM	NE2	162	1.5656927	1.0720730	0.4220678
5DCM	NC3	163	0.4129956	1.6519524	-0.1008485
5DCM	NC4	164	0.5282618	1.2198141	-0.0683036
5DCM	CI5	165	0.8557718	1.6767685	0.1132634
5DCM	CJ6	166	0.7381665	1.6442967	0.0550837
5DCM	HI7	167	0.6697309	1.7233296	0.0265486
5DCM	CK8	168	0.7032335	1.5063838	0.0309143
5DCM	CJ9	169	0.8006854	1.4105360	0.0725614
5DCM	HI10	170	0.7822192	1.3047224	0.0579167
5DCM	CL11	171	0.9181941	1.4489637	0.1311639
5DCM	CG12	172	1.0205863	1.3582010	0.1757785
5DCM	HI13	173	0.9973043	1.2533348	0.1597291
5DCM	CG14	174	1.1377388	1.3959143	0.2329868
5DCM	HI15	175	1.1553733	1.5026109	0.2452566
5DCM	CK16	176	1.2443739	1.3098615	0.2802332
5DCM	CF17	177	1.3620388	1.3675443	0.3320335
5DCM	HI18	178	1.3703577	1.4759562	0.3355583
5DCM	CF19	179	1.4679776	1.2910913	0.3780965
5DCM	HI20	180	1.5560216	1.3414361	0.4161294
5DCM	CH21	181	1.4617675	1.1495919	0.3756622
5DCM	CF22	182	1.3434581	1.0908301	0.3235301
5DCM	HI23	183	1.3336204	0.9830536	0.3188357
5DCM	CF24	184	1.2389145	1.1688767	0.2777624
5DCM	HI25	185	1.1505625	1.1187630	0.2392346
5DCM	CD26	186	1.6893548	1.1349044	0.4658107
5DCM	HJ27	187	1.7585635	1.0577821	0.4999134
5DCM	HJ28	188	1.7380585	1.1913394	0.3849256
5DCM	HJ29	189	1.6718150	1.2037036	0.5495185
5DCM	CD30	190	1.5595042	0.9271952	0.4105598
5DCM	HJ31	191	1.6491405	0.8839062	0.4552101
5DCM	HJ32	192	1.4726213	0.8865991	0.4639026
5DCM	HJ33	193	1.5539287	0.8939768	0.3058535
5DCM	CE34	194	0.9043409	1.8146087	0.1439608
5DCM	HJ35	195	0.8312888	1.8890147	0.1115020
5DCM	HJ36	196	0.9214258	1.8263921	0.2516369
5DCM	HJ37	197	0.9996161	1.8340355	0.0932865
5DCM	CC38	198	0.5824154	1.4698949	-0.0290466
5DCM	CB39	199	0.4879795	1.5683831	-0.0691947
5DCM	CB40	200	0.5506862	1.3330498	-0.0515686
6DCM	OD1	201	1.9811984	1.5816759	0.2243660
6DCM	NE2	202	1.3614356	1.0721243	-0.0462964
6DCM	NC3	203	2.5141899	1.6518921	0.4766176
6DCM	NC4	204	2.3990085	1.2197511	0.4438089
6DCM	CI5	205	2.0713317	1.6767604	0.2626813
6DCM	CJ6	206	2.1889650	1.6442737	0.3207961
6DCM	HI7	207	2.2573932	1.7233018	0.3493625
6DCM	CK8	208	2.2239374	1.5063517	0.3448557
6DCM	CJ9	209	2.1264920	1.4105115	0.3031757
6DCM	HI10	210	2.1449871	1.3046918	0.3177392
6DCM	CL11	211	2.0089538	1.4489543	0.2446423

6DCM	CG12	212	1.9065660	1.3582002	0.2000002
6DCM	HI13	213	1.9298771	1.2533279	0.2159673
6DCM	CG14	214	1.7893847	1.3959277	0.1428604
6DCM	HI15	215	1.7717220	1.5026289	0.1306721
6DCM	CK16	216	1.6827520	1.3098844	0.0955913
6DCM	CF17	217	1.5650556	1.3675775	0.0438737
6DCM	HI18	218	1.5567113	1.4759900	0.0404283
6DCM	CF19	219	1.4591175	1.2911333	-0.0022055
6DCM	HI20	220	1.3710487	1.3414853	-0.0401713
6DCM	CH21	221	1.4653600	1.1496336	0.0001268
6DCM	CF22	222	1.5837012	1.0908615	0.0521752
6DCM	HI23	223	1.5935646	0.9830839	0.0567900
6DCM	CF24	224	1.6882437	1.1688991	0.0979607
6DCM	HI25	225	1.7766206	1.1187780	0.1364216
6DCM	CD26	226	1.2377439	1.1349589	-0.0899509
6DCM	HJ27	227	1.1685403	1.0578452	-0.1240832
6DCM	HJ28	228	1.1890564	1.1913259	-0.0090085
6DCM	HJ29	229	1.2552385	1.2038210	-0.1736163
6DCM	CD30	230	1.3676605	0.9272397	-0.0348929
6DCM	HJ31	231	1.2780180	0.8839623	-0.0795417
6DCM	HJ32	232	1.4545334	0.8867007	-0.0882953
6DCM	HJ33	233	1.3732809	0.8939487	0.0697880
6DCM	CE34	234	2.0227209	1.8146113	0.2320985
6DCM	HJ35	235	2.0957680	1.8890107	0.2645837
6DCM	HJ36	236	2.0055949	1.8264668	0.1244368
6DCM	HJ37	237	1.9274595	1.8339811	0.2828205
6DCM	CC38	238	2.3447850	1.4698475	0.4047477
6DCM	CB39	239	2.4392133	1.5683285	0.4449316
6DCM	CB40	240	2.3765529	1.3329937	0.4271618
7DCM	OD1	241	2.4146856	0.8243380	0.1514454
7DCM	NE2	242	3.0343564	0.3147861	0.4223180
7DCM	NC3	243	1.8818411	0.8945612	-0.1011144
7DCM	NC4	244	1.9970672	0.4624262	-0.0683834
7DCM	CI5	245	2.3245620	0.9194221	0.1131068
7DCM	CJ6	246	2.2069698	0.8869379	0.0549074
7DCM	HI7	247	2.1385475	0.9659655	0.0263256
7DCM	CK8	248	2.1720332	0.7490189	0.0307782
7DCM	CJ9	249	2.2694671	0.6531790	0.0724858
7DCM	HI10	250	2.2509971	0.5473615	0.0578741
7DCM	CL11	251	2.3869629	0.6916192	0.1311059
7DCM	CG12	252	2.4893366	0.6008651	0.1757804
7DCM	HI13	253	2.4660512	0.4959948	0.1597624
7DCM	CG14	254	2.6064765	0.6385905	0.2330064
7DCM	HI15	255	2.6241155	0.7452902	0.2452426
7DCM	CK16	256	2.7130927	0.5525469	0.2803122
7DCM	CF17	257	2.8307481	0.6102398	0.3321231
7DCM	HI18	258	2.8390738	0.7186524	0.3356113
7DCM	CF19	259	2.9366689	0.5337957	0.3782420
7DCM	HI20	260	3.0247064	0.5841478	0.4162802
7DCM	CH21	261	2.9304493	0.3922959	0.3758569
7DCM	CF22	262	2.8121495	0.3335239	0.3237143
7DCM	HI23	263	2.8023052	0.2257464	0.3190560
7DCM	CF24	264	2.7076238	0.4115616	0.2778906
7DCM	HI25	265	2.6192785	0.3614405	0.2393572

7DCM	CD26	266	3.1580114	0.3776243	0.4660714
7DCM	HJ27	267	3.2272053	0.3005092	0.5002202
7DCM	HJ28	268	3.2067408	0.4340266	0.3851790
7DCM	HJ29	269	3.1404542	0.4464548	0.5497498
7DCM	CD30	270	3.0281605	0.1699046	0.4108604
7DCM	HJ31	271	3.1177816	0.1266252	0.4555502
7DCM	HJ32	272	2.9412604	0.1293340	0.4641947
7DCM	HJ33	273	3.0226105	0.1366490	0.3061646
7DCM	CE34	274	2.3731328	1.0572698	0.1437676
7DCM	HJ35	275	2.3000948	1.1316694	0.1112626
7DCM	HJ36	276	2.3901898	1.0690906	0.2514441
7DCM	HJ37	277	2.4684229	1.0766715	0.0931118
7DCM	CC38	278	2.0512285	0.7125172	-0.0292018
7DCM	CB39	279	1.9568105	0.8109979	-0.0694105
7DCM	CB40	280	2.0194953	0.5756664	-0.0516832
8DCM	OD1	281	0.5124484	0.8243409	0.2243660
8DCM	NE2	282	-0.1073144	0.3147893	-0.0462964
8DCM	NC3	283	1.0454399	0.8945571	0.4766176
8DCM	NC4	284	0.9302585	0.4624161	0.4438089
8DCM	CI5	285	0.6025817	0.9194254	0.2626813
8DCM	CJ6	286	0.7202150	0.8869387	0.3207961
8DCM	HI7	287	0.7886432	0.9659668	0.3493625
8DCM	CK8	288	0.7551874	0.7490167	0.3448557
8DCM	CJ9	289	0.6577420	0.6531765	0.3031757
8DCM	HI10	290	0.6762371	0.5473568	0.3177392
8DCM	CL11	291	0.5402038	0.6916193	0.2446423
8DCM	CG12	292	0.4378160	0.6008652	0.2000002
8DCM	HI13	293	0.4611271	0.4959929	0.2159673
8DCM	CG14	294	0.3206347	0.6385927	0.1428604
8DCM	HI15	295	0.3029720	0.7452939	0.1306721
8DCM	CK16	296	0.2140020	0.5525494	0.0955913
8DCM	CF17	297	0.0963056	0.6102425	0.0438737
8DCM	HI18	298	0.0879613	0.7186550	0.0404283
8DCM	CF19	299	-0.0096325	0.5337983	-0.0022055
8DCM	HI20	300	-0.0977013	0.5841503	-0.0401713
8DCM	CH21	301	-0.0033900	0.3922986	0.0001268
8DCM	CF22	302	0.1149512	0.3335265	0.0521752
8DCM	HI23	303	0.1248146	0.2257489	0.0567900
8DCM	CF24	304	0.2194937	0.4115641	0.0979607
8DCM	HI25	305	0.3078706	0.3614430	0.1364216
8DCM	CD26	306	-0.2310061	0.3776239	-0.0899509
8DCM	HJ27	307	-0.3002097	0.3005102	-0.1240832
8DCM	HJ28	308	-0.2796936	0.4339909	-0.0090085
8DCM	HJ29	309	-0.2135115	0.4464860	-0.1736163
8DCM	CD30	310	-0.1010895	0.1699047	-0.0348929
8DCM	HJ31	311	-0.1907320	0.1266273	-0.0795417
8DCM	HJ32	312	-0.0142166	0.1293657	-0.0882953
8DCM	HJ33	313	-0.0954691	0.1366137	0.0697880
8DCM	CE34	314	0.5539709	1.0572763	0.2320985
8DCM	HJ35	315	0.6270180	1.1316757	0.2645837
8DCM	HJ36	316	0.5368449	1.0691318	0.1244368
8DCM	HJ37	317	0.4587095	1.0766461	0.2828205
8DCM	CC38	318	0.8760350	0.7125125	0.4047477
8DCM	CB39	319	0.9704633	0.8109935	0.4449316

```
   8DCM   CB40  320   0.9078029   0.5756587   0.4271618
2.93750  1.51467  0.75158  0.00000  0.00000  0.00000  0.00000 -0.02072  0.00000
```

Bibliography

[1] S. R. Yost, J. Lee, M. W. B. Wilson, D. McMahon, R. R. Parkhurst, N. J. Thompson, A. Rao, K. Hohnson, M. Sfeir, M. Bawendi, T. M. Swager, R. H. Friend, M. A. Baldo, and T. Van Voorhis. Universal mechanism for singlet exciton fission. Submitted, 2013.

[2] Martin Pope. Surface Ionization Energies of Organic Compounds: Phthalocyanines. *J. Chem. Phys.*, 36(10):2810–2811, 1962.

[3] Dietrich R.T. Zahn, Gianina N Gavrila, and Mihaela Gorgoi. The transport gap of organic semiconductors studied using the combination of direct and inverse photoemission. *Chem. Phys.*, 325(1):99–112, June 2006.

[4] Barry P Rand, Jan Genoe, Paul Heremans, and Jef Poortmans. Solar cells utilizing small molecular weight organic semiconductors. *Prog. Photovoltaics Res. Appl.*, 15(8):659–676, December 2007.

[5] Adolf Goetzberger, Christopher Hebling, and Hans-Werner Schock. Photovoltaic materials, history, status and outlook. *Mater. Sci. Eng., R*, 40(1):1–46, January 2003.

[6] Stephen R Forrest. The path to ubiquitous and low-cost organic electronic appliances on plastic. *Nature*, 428(6986):911–918, April 2004.

[7] R E Fenna and B W Matthews. Chlorophyll arrangement in a bacteriochlorophyll protein from Chlorobium limicola. *Nature*, 258:573–577, 1975.

[8] Rienk van Grondelle, Jan P Dekker, Tomas Gillbro, and Villy Sundstrom. Energy transfer and trapping in photosynthesis. *Biochimica et Biophysica Acta (BBA) - Bioenergetics*, 1187(1):1–65, August 1994.

[9] Yuan-Chung Cheng and Graham R Fleming. Dynamics of light harvesting in photosynthesis. *Annu. Rev. Phys. Chem.*, 60:241–62, January 2009.

[10] Villy Sundström, Tõnu Pullerits, and Rienk van Grondelle. Photosynthetic Light-Harvesting: Reconciling Dynamics and Structure of Purple Bacterial LH2 Reveals Function of Photosynthetic Unit. *J. Phys. Chem. B*, 103(13):2327–2346, April 1999.

[11] Melih K Sener, Craig Jolley, Adam Ben-Shem, Petra Fromme, Nathan Nelson, Roberta Croce, and Klaus Schulten. Comparison of the light-harvesting networks of plant and cyanobacterial photosystem I. *Biophys. J.*, 89(3):1630–42, September 2005.

[12] Larry. Takiff and Steven G Boxer. Phosphorescence spectra of bacteriochlorophylls. *J. Am. Chem. Soc.*, 110(13):4425–4426, June 1988.

[13] Jenny Nelson. *The Physics of Solar Cells*, volume 57. Imperial College Press, London, 2003.

[14] Martin A Green, Keith Emery, Yoshihiro Hishikawa, Wilhelm Warta, and Ewan D Dunlop. Solar cell efficiency tables (version 39). *Progress in photovoltaics: research and applications*, 20(1):12–20, 2012.

[15] William Shockley and Hans J Queisser. Detailed Balance Limit of Efficiency of p-n Junction Solar Cells. *J. Appl. Phys.*, 32(3):510–519, 1961.

[16] Oliver Morton. Solar energy: A new day dawning?: Silicon valley sunrise. *Nature*, 443(7107):19–22, 2006.

[17] Martin A Green. Photovoltaics: technology overview. *Energy Policy*, 28(14):989–998, 2000.

[18] Jin Young Kim, Kwanghee Lee, Nelson E Coates, Daniel Moses, Thuc-Quyen Nguyen, Mark Dante, and Alan J Heeger. Efficient tandem polymer solar cells fabricated by all-solution processing. *Science*, 317(5835):222–5, July 2007.

[19] Sung Heum Park, Anshuman Roy, Serge Beaupré, Shinuk Cho, Nelson Coates, Ji Sun Moon, Daniel Moses, Mario Leclerc, Kwanghee Lee, and Alan J Heeger. Bulk heterojunction solar cells with internal quantum efficiency approaching 100%. *Nat. Photonics*, 3(5):297–302, April 2009.

[20] Michael Grätzel. Dye-sensitized solar cells. *J. Photochem. Photobiol., C*, 4(2):145–153, October 2003.

[21] Brian E Hardin, Henry J Snaith, and Michael D McGehee. The renaissance of dye-sensitized solar cells. *Nat. Photonics*, 6(3):162–169, February 2012.

[22] Aswani Yella, Hsuan-Wei Lee, Hoi Nok Tsao, Chenyi Yi, Aravind Kumar Chandiran, Md Khaja Nazeeruddin, Eric Wei-Guang Diau, Chen-Yu Yeh, Shaik M Zakeeruddin, and Michael Grätzel. Porphyrin-sensitized solar cells with cobalt (II/III)-based redox electrolyte exceed 12 percent efficiency. *Science*, 334(6056):629–34, November 2011.

[23] Martin Pope and Charles E Swenberg. *Electronic Processes of Organic Crystals and Polymers.* Oxford University Press, Oxford, 2 edition, 1999.

[24] M Knupfer. Exciton binding energies in organic semiconductors. *Appl. Phys. A*, 77(5):623–626, October 2003.

[25] Brian A Gregg. Excitonic Solar Cells. *J. Phys. Chem. B*, 107(20):4688–4698, May 2003.

[26] Brian A Gregg and Mark C Hanna. Comparing organic to inorganic photovoltaic cells: Theory, experiment, and simulation. *J. Appl. Phys.*, 93(6):3605–3614, 2003.

[27] Jean-Luc Brédas, Joseph E Norton, Jérôme Cornil, and Veaceslav Coropceanu. Molecular understanding of organic solar cells: the challenges. *Acc. Chem. Res.*, 42(11):1691–1699, November 2009.

[28] Harald Hoppe and Niyazi Serdar Sariciftci. Organic solar cells: An overview. *J. Mater. Res.*, 19(07):1924–1945, March 2011.

[29] L. Jan Anton Koster, Sean E Shaheen, and Jan C Hummelen. Pathways to a New Efficiency Regime for Organic Solar Cells. *Advanced Energy Materials*, 2(10):1246–1253, October 2012.

[30] Peter Peumans, Aharon Yakimov, and Stephen R Forrest. Small molecular weight organic thin-film photodetectors and solar cells. *J. Appl. Phys.*, 93(7):3693–3723, April 2003.

[31] D. Markov, C Tanase, P. Blom, and J Wildeman. Simultaneous enhancement of charge transport and exciton diffusion in poly(p-phenylene vinylene) derivatives. *Phys. Rev. B*, 72(4):045217, July 2005.

[32] Serap Günes, Helmut Neugebauer, and Niyazi Serdar Sariciftci. Conjugated polymer-based organic solar cells. *Chem. Rev.*, 107(4):1324–1338, April 2007.

[33] D Gebeyehu, B Maennig, J Drechsel, K Leo, and M Pfeiffer. Bulk-heterojunction photovoltaic devices based on donoracceptor organic small molecule blends. *Sol. Energy Mater. Sol. Cells*, 79(1):81–92, August 2003.

[34] J J M Halls, C A Walsh, N C Greenham, E A Marseglia, R H Friend, S C Moratti, and A B Holmes. Efficient photodiodes from interpenetrating polymer networks. *Nature*, 376(6540):498–500, August 1995.

[35] Fan Yang, Max Shtein, and Stephen R Forrest. Controlled growth of a molecular bulk heterojunction photovoltaic cell. *Nat. Mater.*, 4(1):37–41, December 2004.

[36] Neal R Armstrong, Weining Wang, Dana M Alloway, Diogenes Placencia, Erin Ratcliff, and Michael Brumbach. Organic/Organic' heterojunctions: organic light emitting diodes and organic photovoltaic devices. *Macromol. Rapid Commun.*, 30(9-10):717–731, May 2009.

[37] Dirk Veldman, Ozlem Ipek, Stefan C J Meskers, Jörgen Sweelssen, Marc M Koetse, Sjoerd C Veenstra, Jan M Kroon, Svetlana S van Bavel, Joachim Loos, and René A J Janssen. Compositional and electric field dependence of the dissociation of charge transfer excitons in alternating polyfluorene copolymer/fullerene blends. *J. Am. Chem. Soc.*, 130(24):7721–7735, June 2008.

[38] Hideo Ohkita, Steffan Cook, Yeni Astuti, Warren Duffy, Steve Tierney, Weimin Zhang, Martin Heeney, Iain McCulloch, Jenny Nelson, Donal D C Bradley, and James R Durrant. Charge carrier formation in polythiophene/fullerene blend films studied by transient absorption spectroscopy. *J. Am. Chem. Soc.*, 130(10):3030–3042, March 2008.

[39] Dan Credgington, Rick Hamilton, Pedro Atienzar, Jenny Nelson, and James R Durrant. Non-Geminate Recombination as the Primary Determinant of Open-Circuit Voltage in Polythiophene:Fullerene Blend Solar Cells: an Analysis of the Influence of Device Processing Conditions. *Adv. Funct. Mater.*, 21(14):2744–2753, July 2011.

[40] M. C. Scharber, D Mühlbacher, M Koppe, P Denk, C Waldauf, A. J. Heeger, and C. J. Brabec. Design Rules for Donors in Bulk-Heterojunction Solar CellsTowards 10 % Energy-Conversion Efficiency. *Adv. Mater.*, 18(6):789–794, March 2006.

[41] Jonathan D Servaites, Sina Yeganeh, Tobin J Marks, and Mark A Ratner. Efficiency Enhancement in Organic Photovoltaic Cells: Consequences of Optimizing Series Resistance. *Adv. Funct. Mater.*, 20(1):97–104, January 2010.

[42] Guangqi Li, Abraham Nitzan, and Mark A Ratner. Yield of exciton dissociation in a donor-acceptor photovoltaic junction. *Phys. Chem. Chem. Phys.*, 14(41):14270–14276, November 2012.

[43] Yongye Liang, Shengqiang Xiao, Danqin Feng, and Luping Yu. Control in energy levels of conjugated polymers for photovoltaic application. *The Journal of Physical Chemistry C*, 112(21):7866–7871, 2008.

[44] Yongye Liang, Yue Wu, Danqin Feng, Szu-Ting Tsai, Hae-Jung Son, Gang Li, and Luping Yu. Development of new semiconducting polymers for high performance solar cells. *Journal of the American Chemical Society*, 131(1):56–57, 2008.

[45] Huaxing Zhou, Liqiang Yang, and Wei You. Rational design of high performance conjugated polymers for organic solar cells. *Macromolecules*, 45(2):607–632, 2012.

[46] Renee Kroon, Martijn Lenes, Jan C Hummelen, Paul W M Blom, and Bert de Boer. Small Bandgap Polymers for Organic Solar Cells (Polymer Material Development in the Last 5 Years). *Polymer Reviews*, 48(3):531–582, August 2008.

[47] William A Tisdale, Kenrick J Williams, Brooke A Timp, David J Norris, Eray S Aydil, and X-Y Zhu. Hot-electron transfer from semiconductor nanocrystals. *Science*, 328(5985):1543–1547, 2010.

[48] Anshu Pandey and Philippe Guyot-Sionnest. Hot electron extraction from colloidal quantum dots. *The Journal of Physical Chemistry Letters*, 1(1):45–47, 2009.

[49] R.E. Merrifield, P Avakian, and R.P. Groff. Fission of singlet excitons into pairs of triplet excitons in tetracene crystals. *Chem. Phys. Lett.*, 3(3):155–157, March 1969.

[50] N Geacintov, M Pope, and F Vogel. Effect of magnetic field on the fluorescence of tetracene crystals: exciton fission. *Physical Review Letters*, 22(12):593–596, 1969.

[51] Randy J Ellingson, Matthew C Beard, Justin C Johnson, Pingrong Yu, Olga I Micic, Arthur J Nozik, Andrew Shabaev, and Alexander L Efros. Highly efficient multiple exciton generation in colloidal pbse and pbs quantum dots. *Nano Letters*, 5(5):865–871, 2005.

[52] Arthur J Nozik. Multiple exciton generation in semiconductor quantum dots. *Chemical Physics Letters*, 457(1):3–11, 2008.

[53] Millicent B Smith and Josef Michl. Singlet fission. *Chem. Rev.*, 110(11):6891–6936, November 2010.

[54] J Lee, P Jadhav, and M A Baldo. High efficiency organic multilayer photodetectors based on singlet exciton fission. *Appl. Phys. Lett.*, 95(3):033301, 2009.

[55] Eric C Greyson, Josh Vura-Weis, Josef Michl, and Mark A Ratner. Maximizing singlet fission in organic dimers: Theoretical investigation of triplet yield in the regime of localized excitation and fast coherent electron transfer. *The Journal of Physical Chemistry B*, 114(45):14168–14177, 2010.

[56] S. Beljonne, H. Yamagata, J. L. Brédas, F. Spano, and Y. Olivier. Charge-transfer excitations steer the davydov splitting and mediate singlet exciton fission in pentacene. Submitted, 2013.

[57] Timothy C Berkelbach, Mark S Hybertsen, and David R Reichman. Microscopic theory of singlet exciton fission. i. general formulation. *arXiv preprint arXiv:1211.6458*, 2012.

[58] Timothy C Berkelbach, Mark S Hybertsen, and David R Reichman. Microscopic theory of singlet exciton fission. ii. application to pentacene dimers and the role of superexchange. *arXiv preprint arXiv:1211.6459*, 2012.

[59] Wai-Lun Chan, Manuel Ligges, Askat Jailaubekov, Loren Kaake, Luis Miaja-Avila, and X-Y Zhu. Observing the multiexciton state in singlet fission and ensuing ultrafast multielectron transfer. *Science*, 334(6062):1541–1545, 2011.

[60] W. L. Chan, M. Ligges, and X. Y. Zhu. The energy barrier in singlet fission can be overcome through coherent coupling and entropic gain. *Nat. Chem.*, 4(10):840–845, 2012.

[61] Mark W B Wilson, Akshay Rao, Jenny Clark, R Sai Santosh Kumar, Daniele Brida, Giulio Cerullo, and Richard H Friend. Ultrafast dynamics of exciton fission in polycrystalline pentacene. *J. Am. Chem. Soc.*, 133(31):11830–3, August 2011.

[62] Akshay Rao, Mark WB Wilson, Sebastian Albert-Seifried, Riccardo Di Pietro, and Richard H Friend. Photophysics of pentacene thin films: The role of exciton fission and heating effects. *Physical Review B*, 84(19):195411, 2011.

[63] Charusheela Ramanan, Amanda L Smeigh, John E Anthony, Tobin J Marks, and Michael R Wasielewski. Competition between singlet fission and charge separation in solution-processed blend films of 6, 13-bis (triisopropylsilylethynyl) pentacene with sterically-encumbered perylene-3, 4: 9, 10-bis (dicarboximide) s. *Journal of the American Chemical Society*, 134(1):386–397, 2011.

[64] Sean T Roberts, R Eric McAnally, Joseph N Mastron, David H Webber, Matthew T Whited, Richard L Brutchey, Mark E Thompson, and Stephen E Bradforth. Efficient singlet fission discovered in a disordered acene film. *Journal of the American Chemical Society*, 134(14):6388–6400, 2012.

[65] Paul M Zimmerman, Franziska Bell, David Casanova, and Martin Head-Gordon. Mechanism for singlet fission in pentacene and tetracene: from single exciton to two triplets. *Journal of the American Chemical Society*, 133(49):19944–19952, 2011.

[66] Richard R Lunt, Noel C Giebink, Anna A Belak, Jay B Benziger, and Stephen R Forrest. Exciton diffusion lengths of organic semiconductor thin films measured by spectrally resolved photoluminescence quenching. *J. Appl. Phys.*, 105(5):053711, 2009.

[67] Brian A Gregg, Julian Sprague, and Mark W Peterson. Long-Range Singlet Energy Transfer in Perylene Bis(phenethylimide) Films. *J. Phys. Chem. B*, 101(27):5362–5369, July 1997.

[68] V Ern. Triplet Exciton Diffusion in Some Aromatic Crystals. *J. Chem. Phys.*, 56(12):6259–6260, 1972.

[69] P Avakian and R. Merrifield. Experimental Determination of the Diffusion Length of Triplet Excitons in Anthracene Crystals. *Phys. Rev. Lett.*, 13(18):541–543, November 1964.

[70] Amal K Ghosh and Tom Feng. Merocynanine organic solar cells. *J. Appl. Phys.*, 49(12):5982–5989, 1978.

[71] H Najafov, B Lee, Q Zhou, L C Feldman, and V Podzorov. Observation of long-range exciton diffusion in highly ordered organic semiconductors. *Nat. Mater.*, 9(11):938–943, November 2010.

[72] G Vaubel and H Kallmann. Diffusion Length and Lifetime of Triplet Excitons and Crystal Absorption Coefficient in Tetracene Determined from Photocurrent Measurements. *Phys. Status Solidi B*, 35(2):789–792, 1969.

[73] R.R. Alfano, S.L. Shapiro, and M Pope. Fission rate of singlet excitons in a tetracene crystal measured with picosecond laser pulses. *Opt. Commun.*, 9(4):388–391, December 1973.

[74] J B Aladekomo, S Arnold, and M Pope. Triplet exciton diffusion and double photon absorption in tetracene. *Phys. Status Solidi B*, 80(1):333–340, March 1977.

[75] D Kurrle and J Pflaum. Exciton diffusion length in the organic semiconductor diindenoperylene. *Appl. Phys. Lett.*, 92(13):133306, 2008.

[76] V Bulović and S.R. Forrest. Excitons in crystalline thin films of 3,4,9,10-perylenetetracarboxylic dianhydride studied by photocurrent response. *Chem. Phys. Lett.*, 238(1-3):88–92, May 1995.

[77] E Engel, K Leo, and M Hoffmann. Ultrafast relaxation and excitonexciton annihilation in PTCDA thin films at high excitation densities. *Chem. Phys.*, 325(1):170–177, June 2006.

[78] Richard C Powell and Zoltán G Soos. Singlet exciton energy transfer in organic solids. *J. Lumin.*, 11(1-2):1–45, September 1975.

[79] A. C. Durr, F Schreiber, M Kelsch, H D Carstanjen, H Dosch, and O H Seeck. Morphology and interdiffusion behavior of evaporated metal films on crystalline diindenoperylene thin films. *J. Appl. Phys.*, 93(9):5201–5209, 2003.

[80] Seung-Bum Rim and Peter Peumans. The effects of optical interference on exciton diffusion length measurements using photocurrent spectroscopy. *J. Appl. Phys.*, 103(12):124515, 2008.

[81] Gregory S Engel, Tessa R Calhoun, Elizabeth L Read, Tae-Kyu Ahn, Tomás Mancal, Yuan-Chung Cheng, Robert E Blankenship, and Graham R Fleming. Evidence for wavelike energy transfer through quantum coherence in photosynthetic systems. *Nature*, 446(7137):782–786, April 2007.

[82] Elisabetta Collini, Cathy Y Wong, Krystyna E Wilk, Paul M G Curmi, Paul Brumer, and Gregory D Scholes. Coherently wired light-harvesting in photosynthetic marine algae at ambient temperature. *Nature*, 463(7281):644–647, February 2010.

[83] Jianlan Wu, Fan Liu, Jian Ma, Robert J Silbey, and Jianshu Cao. Efficient energy transfer in light-harvesting systems: Quantum-classical comparison, flux network, and robustness analysis. *The Journal of chemical physics*, 137(17):174111–174111, 2012.

[84] M Grover and R Silbey. Exciton migration in molecular crystals. *J. Chem. Phys.*, 54:4843, 1971.

[85] H Haken and P Reineker. The coupled coherent and incoherent motion of excitons and its influence on the line shape of optical absorption. *Zeitschrift für Physik*, 249(3):253–268, 1972.

[86] Stephanie Valleau, Semion K. Saikin, Man-Hong Yung, and Alan Aspuru Guzik. Exciton transport in thin-film cyanine dye j-aggregates. *J. Chem. Phys.*, 137(3):034109, 2012.

[87] Conor Madigan and Vladimir Bulović. Modeling of exciton diffusion in amorphous organic thin films. *Phys. Rev. Lett.*, 96:046404, Jan 2006.

[88] Tracey M Clarke, Amy M Ballantyne, Jenny Nelson, Donal D C Bradley, and James R Durrant. Free Energy Control of Charge Photogeneration in Polythiophene/Fullerene Solar Cells: The Influence of Thermal Annealing on P3HT/PCBM Blends. *Adv. Funct. Mater.*, 18(24):4029–4035, December 2008.

[89] X-Y Zhu, Q Yang, and M Muntwiler. Charge-transfer excitons at organic semiconductor surfaces and interfaces. *Acc. Chem. Res.*, 42(11):1779–1787, November 2009.

[90] Matthias Muntwiler, Qingxin Yang, William Tisdale, and X-Y Zhu. Coulomb Barrier for Charge Separation at an Organic Semiconductor Interface. *Phys. Rev. Lett.*, 101(19):196403, November 2008.

[91] Tao Liu and Alessandro Troisi. What makes fullerene acceptors special as electron acceptors in organic solar cells and how to replace them. *Adv. Mater.*, 25(7):1038–41, February 2013.

[92] Jiye Lee, Koen Vandewal, Shane R Yost, Matthias E Bahlke, Ludwig Goris, Marc A Baldo, Jean V Manca, and Troy Van Voorhis. Charge transfer state versus hot exciton dissociation in polymer-fullerene blended solar cells. *J. Am. Chem. Soc.*, 132(34):11878–11880, September 2010.

[93] Artem A Bakulin, Akshay Rao, Vlad G Pavelyev, Paul H M van Loosdrecht, Maxim S Pshenichnikov, Dorota Niedzialek, Jérôme Cornil, David Beljonne, and Richard H Friend. The role of driving energy and delocalized States for charge separation in organic semiconductors. *Science*, 335(6074):1340–1344, March 2012.

[94] Askat E Jailaubekov, Adam P Willard, John R Tritsch, Wai-Lun Chan, Na Sai, Raluca Gearba, Loren G Kaake, Kenrick J Williams, Kevin Leung, Peter J Rossky, and X-Y. Zhu. Hot charge-transfer excitons set the time limit for charge separation at donor/acceptor interfaces in organic photovoltaics. *Nat. Mater.*, 12(1):66–73, January 2013.

[95] Carsten Deibel, Thomas Strobel, and Vladimir Dyakonov. Origin of the Efficient Polaron-Pair Dissociation in Polymer-Fullerene Blends. *Phys. Rev. Lett.*, 103(3):036402, July 2009.

[96] David P. McMahon, David L. Cheung, and Alessandro Troisi. Why Holes and Electrons Separate So Well in Polymer/Fullerene Photovoltaic Cells. *J. Phys. Chem. Lett.*, 2(21):2737–2741, November 2011.

[97] Jiamo Guo, Hideo Ohkita, Hiroaki Benten, and Shinzaburo Ito. Charge generation and recombination dynamics in poly(3-hexylthiophene)/fullerene blend films with different regioregularities and morphologies. *J. Am. Chem. Soc.*, 132(17):6154–6164, May 2010.

[98] H Vázquez, R Oszwaldowski, P Pou, J Ortega, R Pérez, F Flores, and A Kahn. Dipole formation at metal/PTCDA interfaces: Role of the Charge Neutrality Level. *Europhys. Lett.*, 65(6):802–808, March 2004.

[99] H. Vázquez, W Gao, F Flores, and A Kahn. Energy level alignment at organic heterojunctions: Role of the charge neutrality level. *Phys. Rev. B*, 71(4):041306, January 2005.

[100] Slawomir Braun, William R. Salaneck, and Mats Fahlman. Energy-Level Alignment at Organic/Metal and Organic/Organic Interfaces. *Adv. Mater.*, 21(14-15):1450–1472, April 2009.

[101] Shane R Yost, Lee-Ping Wang, and Troy Van Voorhis. Molecular Insight Into the Energy Levels at the Organic Donor/Acceptor Interface: A Quantum Mechanics/Molecular Mechanics Study. *J. Phys. Chem. C*, 115(29):14431–14436, July 2011.

[102] Shane R Yost and Troy Van Voorhis. Electrostatic Effects at Organic Semiconductor Interfaces: A Mechanism for "Cold" Exciton Breakup. *J. Phys. Chem. C*, Accepted, February 2013.

[103] Sébastien Mothy, Maxime Guillaume, Julien Idé, Frédéric Castet, Laurent Ducasse, Jérôme Cornil, and David Beljonne. Tuning the Interfacial Electronic Structure at Organic Heterojunctions by Chemical Design. *The Journal of Physical Chemistry Letters*, 3(17):2374–2378, September 2012.

[104] Igor Avilov, Victor Geskin, and Jérôme Cornil. Quantum-Chemical Characterization of the Origin of Dipole Formation at Molecular Organic/Organic Interfaces. *Adv. Funct. Mater.*, 19(4):624–633, February 2009.

[105] Mathieu Linares, David Beljonne, Jérôme Cornil, Kelly Lancaster, Jean-Luc Brédas, Stijn Verlaak, Alexander Mityashin, Paul Heremans, Andreas Fuchs, Christian Lennartz, Julien Idé, Rapha el Mereau, Philippe Aurel, Laurent Ducasse, and Frédéric Castet. On the Interface Dipole at the PentaceneFullerene Heterojunction: A Theoretical Study. *J. Phys. Chem. C*, 114(7):3215–3224, February 2010.

[106] Julien Idé, Sébastien Mothy, Adrien Savoyant, Alain Fritsch, Philippe Aurel, Raphaël Méreau, Laurent Ducasse, Jérôme Cornil, David Beljonne, and Frédéric Castet. Interfacial dipole and band bending in model pentacene/C 60 heterojunctions. *Int. J. Quantum Chem.*, 113(4):580–584, February 2013.

[107] Attila Szabo and Neil S Ostlund. *Modern Quantum Chemistry: Introduction to Advanced Electronic Structure Theory.* Dover Publications, Mineola, 1996.

[108] Walter Kohn and Lu Jeu Sham. Self-Consistent Equations Including Exchange and Correlation Effects. *Phys. Rev.*, 140(4A):A1133–A1138, November 1965.

[109] Robert G Parr and Yang Weitao. *Density-Functional Theory of Atoms and Molecules*, volume 16. Oxford University Press, New York, 1994.

[110] Walter Kohn, Axel D Becke, and Robert G Parr. Density Functional Theory of Electronic Structure. *J. Phys. Chem.*, 100(31):12974–12980, January 1996.

[111] John P. Perdew and Stefan Kurth. *Density Functionals for Non-relativistic Coulomb Systems in the New Century*, chapter 1, pages 1–55. Springer Verlag, Berlin, 2003.

[112] Gustavo E Scuseria and Viktor N Staroverov. Progress in the development of exchange-correlation functionals. *Theory and Applications of Computational Chemistry: The First Forty Years*, 40:669–724, 2005.

[113] John P Perdew, Kieron Burke, and Matthias Ernzerhof. Generalized Gradient Approximation Made Simple. *Phys. Rev. Lett.*, 77(18):3865–3868, October 1996.

[114] Yan Zhao and Donald G Truhlar. The M06 suite of density functionals for main group thermochemistry, thermochemical kinetics, noncovalent interactions, excited states, and transition elements: two new functionals and systematic testing of four M06-class functionals and 12 other function. *Theor. Chem. Acc.*, 120(1-3):215–241, July 2007.

[115] Yan Zhao and Donald G Truhlar. Hybrid Meta Density Functional Theory Methods for Thermochemistry, Thermochemical Kinetics, and Noncovalent Interactions: The MPW1B95 and MPWB1K Models and Comparative Assessments for Hydrogen Bonding and van der Waals Interactions. *J. Phys. Chem. A*, 108(33):6908–6918, August 2004.

[116] Axel D Becke. A new mixing of HartreeFock and local density-functional theories. *J. Chem. Phys.*, 98(2):1372–1377, 1993.

[117] Yingkai Zhang and Weitao Yang. Comment on Generalized Gradient Approximation Made Simple. *Phys. Rev. Lett.*, 80(4):890–890, January 1998.

[118] Carlo Adamo and Vincenzo Barone. Toward reliable density functional methods without adjustable parameters: The PBE0 model. *J. Chem. Phys.*, 110(13):6158–6169, 1999.

[119] Axel D Becke. Density-functional thermochemistry. III. The role of exact exchange. *J. Chem. Phys.*, 98(7):5648–5652, 1993.

[120] Hisayoshi Iikura, Takao Tsuneda, Takeshi Yanai, and Kimihiko Hirao. A long-range correction scheme for generalized-gradient-approximation exchange functionals. *J. Chem. Phys.*, 115(8):3540–3544, 2001.

[121] Oleg A Vydrov and Gustavo E Scuseria. Assessment of a long-range corrected hybrid functional. *J. Chem. Phys.*, 125(23):234109, December 2006.

[122] Roi Baer, Ester Livshits, and Ulrike Salzner. Tuned range-separated hybrids in density functional theory. *Annu. Rev. Phys. Chem.*, 61:85–109, January 2010.

[123] Mary A Rohrdanz, Katie M Martins, and John M Herbert. A long-range-corrected density functional that performs well for both ground-state properties and time-dependent density functional theory excitation energies, including charge-transfer excited states. *J. Chem. Phys.*, 130(5):054112, February 2009.

[124] Larry A Curtiss, Krishnan Raghavachari, Paul C Redfern, and John A Pople. Assessment of gaussian-3 and density functional theories for a larger experimental test set. *The Journal of Chemical Physics*, 112:7374, 2000.

[125] D. Jacquemin, E. A. Perpete, I. Ciofini, C. Adamo, R. Valero, Y. Zhao, and D. G. Truhlar. On the Performances of the M06 Family of Density Functionals for Electronic Excitation Energies. *J. Chem. Theory Comput.*, 6:2071–2085, 2010.

[126] Y. Zhao and D. G. Truhlar. The M06 suite of density functionals for main group thermochemistry, thermochemical kinetics, noncovalent interactions, excited states, and transition elements: two new functionals and systematic testing of four M06-class functionals and 12 other function. *Theor. Chim. Acta*, 120:215–241, 2008.

[127] Roberto Peverati and Donald G Truhlar. Performance of the m11 and m11-l density functionals for calculations of electronic excitation energies by adiabatic time-dependent density functional theory. *Phys. Chem. Chem. Phys.*, 14(32):11363–11370, 2012.

[128] John P Perdew and Alex Zunger. Self-interaction correction to density-functional approximations for many-electron systems. *Phys. Rev. B*, 23(10):5048–5079, May 1981.

[129] Aron J Cohen, Paula Mori-Sánchez, and Weitao Yang. Insights into current limitations of density functional theory. *Science*, 321(5890):792–794, August 2008.

[130] Sina Yeganeh and Troy Van Voorhis. Triplet Excitation Energy Transfer with Constrained Density Functional Theory . *J. Phys. Chem. C*, 114(48):20756–20763, December 2010.

[131] Paula Mori-Sánchez, Aron J Cohen, and Weitao Yang. Localization and delocalization errors in density functional theory and implications for band-gap prediction. *Physical review letters*, 100(14):146401, 2008.

[132] Anthony P Scott and Leo Radom. Harmonic Vibrational Frequencies: An Evaluation of HartreeFock, MøllerPlesset, Quadratic Configuration Interaction, Density Functional Theory, and Semiempirical Scale Factors. *J. Phys. Chem.*, 100(41):16502–16513, January 1996.

[133] Charles W. Bauschlicher. A comparison of the accuracy of different functionals. *Chem. Phys. Lett.*, 246(1-2):40–44, November 1995.

[134] Rodney Bartlett and Monika Musia. Coupled-cluster theory in quantum chemistry. *Rev. Mod. Phys.*, 79(1):291–352, February 2007.

[135] George D. Purvis and Rodney J. Bartlett. A full coupled-cluster singles and doubles model: The inclusion of disconnected triples. *J. Chem. Phys.*, 76(4):1910, 1982.

[136] Peter J Knowles, Claudia Hampel, and Hans-Joachim Werner. Coupled cluster theory for high spin, open shell reference wave functions. *J. Chem. Phys.*, 99(7):5219–5227, 1993.

[137] Per-Olov Löwdin. Quantum Theory of Many-Particle Systems. I. Physical Interpretations by Means of Density Matrices, Natural Spin-Orbitals, and Convergence Problems in the Method of Configurational Interaction. *Phys. Rev.*, 97(6):1474–1489, March 1955.

[138] Anna I Krylov. Spin-flip configuration interaction: an electronic structure model that is both variational and size-consistent. *Chem. Phys. Lett.*, 350(5-6):522–530, December 2001.

[139] Peter J Knowles and Hans-Joachim Werner. An efficient method for the evaluation of coupling coefficients in configuration interaction calculations. *Chem. Phys. Lett.*, 145(6):514–522, April 1988.

[140] Björn O Roos, Peter R Taylor, and Per E.M. Siegbahn. A complete active space SCF method (CASSCF) using a density matrix formulated super-CI approach. *Chem. Phys.*, 48(2):157–173, May 1980.

[141] Per E M Siegbahn, Jan Almlöf, Anders Heiberg, and Björn O Roos. The complete active space SCF (CASSCF) method in a NewtonRaphson formulation with application to the HNO molecule. *J. Chem. Phys.*, 74(4):2384–2396, 1981.

[142] Martin Head-Gordon, John A Pople, and Michael J Frisch. MP2 energy evaluation by direct methods. *Chem. Phys. Lett.*, 153(6):503–506, December 1988.

[143] Claudia Hampel, Kirk A Peterson, and Hans-Joachim Werner. A comparison of the efficiency and accuracy of the quadratic configuration interaction (QCISD), coupled cluster (CCSD), and Brueckner coupled cluster (BCCD) methods. *Chem. Phys. Lett.*, 190(1-2):1–12, February 1992.

[144] Erich Runge and E K U Gross. Density-Functional Theory for Time-Dependent Systems. *Phys. Rev. Lett.*, 52(12):997–1000, March 1984.

[145] E. Gross and Walter Kohn. Local density-functional theory of frequency-dependent linear response. *Phys. Rev. Lett.*, 55(26):2850–2852, December 1985.

[146] Andreas Dreuw and Martin Head-Gordon. Single-reference ab initio methods for the calculation of excited states of large molecules. *Chem. Rev.*, 105(11):4009–4037, November 2005.

[147] Denis Jacquemin, Valérie Wathelet, Eric A Perpéte, and Carlo Adamo. Extensive TD-DFT Benchmark: Singlet-Excited States of Organic Molecules. *J. Chem. Theory Comput.*, 5(9):2420–2435, September 2009.

[148] Jong-Won Song, Seiken Tokura, Takeshi Sato, Mark A Watson, and Kimihiko Hirao. Erratum: An improved long-range corrected hybrid exchange-correlation functional including a short-range Gaussian attenuation (LCgau-BOP) [J. Chem. Phys. 127, 154109 (2007)]. *J. Chem. Phys.*, 131(5):059901, 2009.

[149] Andreas Dreuw, Jennifer L Weisman, and Martin Head-Gordon. Long-range charge-transfer excited states in time-dependent density functional theory require non-local exchange. *J. Chem. Phys.*, 119(6):2943, 2003.

[150] Yoshihiro Tawada, Takao Tsuneda, Susumu Yanagisawa, Takeshi Yanai, and Kimihiko Hirao. A long-range-corrected time-dependent density functional theory. *J. Chem. Phys.*, 120(18):8425–33, May 2004.

[151] T. Ziegler, A. Rauk, and E. J. Baerends. Calculation of multiplet energies by the hartree-fock-slater method. *Theor. Chim. Acta*, 43:261–271, 1977.

[152] N. A. Besley, A. T. B. Gilbert, and P. M. W. Gill. Self-consistent-field calculations of core excited states. *J. Chem. Phys.*, 130:124308, 2009.

[153] Qin Wu and Troy Van Voorhis. Direct optimization method to study constrained systems within density-functional theory. *Phys. Rev. A*, 72(2):024502, August 2005.

[154] Qin Wu and Troy Van Voorhis. Extracting electron transfer coupling elements from constrained density functional theory. *J. Chem. Phys.*, 125(16):164105, October 2006.

[155] Qin Wu and Troy Van Voorhis. Constrained Density Functional Theory and Its Application in Long-Range Electron Transfer. *J. Chem. Theory Comput.*, 2(3):765–774, May 2006.

[156] B. Kaduk, T. Kowalczyk, and T. Van Voorhis. Constrained density functional theory. *Chem. Rev.*, 112:321–370, 2012.

[157] F. Ding, H. Wang, Q. Wu, T. Van Voorhis, S. Chen, and J. Konopelski. Computational study of bridge-assisted intervalence electron transfer. *J. Phys. Chem. A*, 114:6039–6046, 2010.

[158] T. Kowalczyk, L.-P. Wang, and T. Van Voorhis. Simulation of solution phase electron transfer in a compact donor–acceptor dyad. *J. Phys. Chem. B*, 115:12135–12144, 2011.

[159] John F Stanton and Rodney J Bartlett. The equation of motion coupled-cluster method. a systematic biorthogonal approach to molecular excitation energies, transition probabilities, and excited state properties. *J. Chem. Phys.*, 98:7029, 1993.

[160] Ove Christiansen, Henrik Koch, and Poul Jørgensen. The second-order approximate coupled cluster singles and doubles model cc2. *Chem. Phys. Lett.*, 243(5):409–418, 1995.

[161] Christof Hättig and Florian Weigend. Cc2 excitation energy calculations on large molecules using the resolution of the identity approximation. *J. Chem. Phys.*, 113:5154, 2000.

[162] John A Pople, Martin Head-Gordon, and Krishnan Raghavachari. Quadratic configuration interaction. a general technique for determining electron correlation energies. *J. Chem. Phys.*, 87:5968, 1987.

[163] Kerstin Andersson, Per Aake Malmqvist, Björn O Roos, Andrzej J Sadlej, and Krzysztof Wolinski. Second-order perturbation theory with a casscf reference function. *J. Phys. Chem.*, 94(14):5483–5488, 1990.

[164] Kerstin Andersson, Per-Åke Malmqvist, and Björn O Roos. Second-order perturbation theory with a complete active space self-consistent field reference function. *J. Chem. Phys.*, 96:1218, 1992.

[165] Peter Pulay. A perspective on the caspt2 method. *Int. J. Quant. Chem.*, 111(13):3273–3279, 2011.

[166] Björn O Roos, Kerstin Andersson, Markus P Fülscher, Per-âke Malmqvist, Luis Serrano-Andrés, Kristin Pierloot, and Manuela Merchán. Multiconfigurational perturbation theory: Applications in electronic spectroscopy. *Adv. Chem. Phys.*, 93:219–331, 1996.

[167] K Hirao. Multireference møllerplesset method. *Chem. Phys. Lett.*, 190(3):374–380, 1992.

[168] C Angeli, R Cimiraglia, S Evangelisti, T Leininger, and J-P Malrieu. Introduction of n-electron valence states for multireference perturbation theory. *J. Chem. Phys.*, 114:10252, 2001.

[169] Josef Paldus and Xiangzhu Li. A critical assessment of the coupled cluster method in quantum chemistry. *Adv. Chem. Phys.*, 110:1–176, 1999.

[170] BH Brandow. Formal theory of effective π-electron hamiltonians. *Int. J. Quantum Chem.*, 15(2):207–242, 1979.

[171] Minh Trung Dang, Guillaume Wantz, Habiba Bejbouji, Mathieu Urien, Olivier J Dautel, Laurence Vignau, and Lionel Hirsch. Polymeric solar cells based on P3HT:PCBM: Role of the casting solvent. *Sol. Energy Mater. Sol. Cells*, 95(12):3408–3418, December 2011.

[172] Frederik C Krebs. Fabrication and processing of polymer solar cells: A review of printing and coating techniques. *Sol. Energy Mater. Sol. Cells*, 93(4):394–412, April 2009.

[173] Frank C Spano. The spectral signatures of frenkel polarons in h-and j-aggregates. *Accounts of chemical research*, 43(3):429–439, 2009.

[174] J A Pople. Approximate Self-Consistent Molecular-Orbital Theory. V. Intermediate Neglect of Differential Overlap. *J. Chem. Phys.*, 47(6):2026–2033, 1967.

[175] Michael C Zerner, Gilda H Loew, Robert F Kirchner, and Ulrich T Mueller-Westerhoff. An intermediate neglect of differential overlap technique for spectroscopy of transition-metal complexes. Ferrocene. *J. Am. Chem. Soc.*, 102(2):589–599, January 1980.

[176] Richard C Bingham, Michael J S Dewar, and Donald H Lo. Ground states of molecules. XXV. MINDO/3. Improved version of the MINDO semiempirical SCF-MO method. *J. Am. Chem. Soc.*, 97(6):1285–1293, March 1975.

[177] Michael J S Dewar and Walter Thiel. Ground states of molecules. 38. The MNDO method. Approximations and parameters. *J. Am. Chem. Soc.*, 99(15):4899–4907, June 1977.

[178] James J P Stewart. Optimization of parameters for semiempirical methods I. Method. *J. Comput. Chem.*, 10(2):209–220, March 1989.

[179] James J P Stewart. Comparison of the accuracy of semiempirical and some DFT methods for predicting heats of formation. *J. Mol. Model.*, 10(1):6–12, February 2004.

[180] Kurt W Sattelmeyer, Julian Tirado-Rives, and William L Jorgensen. Comparison of SCC-DFTB and NDDO-based semiempirical molecular orbital methods for organic molecules. *J. Phys. Chem. A*, 110(50):13551–13559, December 2006.

[181] J Cornil, S Vanderdonckt, R Lazzaroni, D. A. dos Santos, G Thys, Herman J Geise, L-M Yu, M Szablewski, D Bloor, M Lögdlund, W. R. Salaneck, N. E. Gruhn, D. L. Lichtenberger, P. A. Lee, N. R. Armstrong, and J. L. Brédas. Valence Electronic Structure of π-Conjugated Materials: Simulation of the Ultraviolet Photoelectron Spectra with Semiempirical HartreeFock Approaches. *Chem. Mater.*, 11(9):2436–2443, September 1999.

[182] Frédéric Castet, Philippe Aurel, Alain Fritsch, Laurent Ducasse, Daniel Liotard, Mathieu Linares, Jérôme Cornil, and David Beljonne. Electronic polarization effects on charge carriers in anthracene: A valence bond study. *Phys. Rev. B*, 77(11):115210, March 2008.

[183] E. Tsiper and Z. Soos. Electronic polarization in pentacene crystals and thin films. *Phys. Rev. B*, 68(8):085301, August 2003.

[184] P Sreearunothai, A. Morteani, I Avilov, J Cornil, D Beljonne, R Friend, R Phillips, C Silva, and L Herz. Influence of Copolymer Interface Orientation on the Optical Emission of Polymeric Semiconductor Heterojunctions. *Phys. Rev. Lett.*, 96(11):117403, March 2006.

[185] David P McMahon and Alessandro Troisi. An ad hoc tight binding method to study the electronic structure of semiconducting polymers. *Chem. Phys. Lett.*, 480(4-6):210–214, October 2009.

[186] Jacopo Tomasi and Maurizio Persico. Molecular Interactions in Solution: An Overview of Methods Based on Continuous Distributions of the Solvent. *Chem. Rev.*, 94(7):2027–2094, November 1994.

[187] A. Klamt and G. Schüürmann. COSMO: a new approach to dielectric screening in solvents with explicit expressions for the screening energy and its gradient. *J. Chem. Soc., Perkin Trans. 2*, (5):799–805, May 1993.

[188] Maurizio Cossi, Nadia Rega, Giovanni Scalmani, and Vincenzo Barone. Energies, structures, and electronic properties of molecules in solution with the C-PCM solvation model. *J. Comput. Chem.*, 24(6):669–81, April 2003.

[189] Seth Difley, Lee-Ping Wang, Sina Yeganeh, Shane R Yost, and Troy Van Voorhis. Electronic properties of disordered organic semiconductors via QM/MM simulations. *Acc. Chem. Res.*, 43(7):995–1004, July 2010.

[190] William L Jorgensen, David S Maxwell, and Julian Tirado-Rives. Development and Testing of the OPLS All-Atom Force Field on Conformational Energetics and Properties of Organic Liquids. *J. Am. Chem. Soc.*, 118(45):11225–11236, January 1996.

[191] R Joseph Kline, Dean M DeLongchamp, Daniel A Fischer, Eric K Lin, Lee J Richter, Michael L Chabinyc, Michael F Toney, Martin Heeney, and Iain McCulloch. Critical Role of Side-Chain Attachment Density on the Order and Device Performance of Polythiophenes. *Macromolecules*, 40(22):7960–7965, October 2007.

[192] T J Prosa, M J Winokur, and R D McCullough. Evidence of a Novel Side Chain Structure in Regioregular Poly(3-alkylthiophenes). *Macromolecules*, 29(10):3654–3656, January 1996.

[193] U Chandra Singh and Peter A Kollman. A combined ab initio quantum mechanical and molecular mechanical method for carrying out simulations on complex molecular systems: Applications to the $CH_3Cl + Cl$ exchange reaction and gas phase protonation of polyethers. *J. Comput. Chem.*, 7(6):718–730, December 1986.

[194] David M Huang, Roland Faller, Khanh Do, and Adam J Moulé. Coarse-Grained Computer Simulations of Polymer/Fullerene Bulk Heterojunctions for Organic Photovoltaic Applications. *J. Chem. Theory Comput.*, 6(2):526–537, February 2010.

[195] Margherita Moreno, Mosè Casalegno, Guido Raos, Stefano V Meille, and Riccardo Po. Molecular modeling of crystalline alkylthiophene oligomers and polymers. *J. Phys. Chem. B*, 114(4):1591–1602, February 2010.

[196] Qin Wu, Chiao-Lun Cheng, and Troy Van Voorhis. Configuration interaction based on constrained density functional theory: a multireference method. *J. Chem. Phys.*, 127(16):164119, October 2007.

[197] Qin Wu, Benjamin Kaduk, and Troy Van Voorhis. Constrained density functional theory based configuration interaction improves the prediction of reaction barrier heights. *J. Chem. Phys.*, 130(3):034109, January 2009.

[198] C.-P. Hsu, Z.-Q. You, and H.-C. Chen. Characterization of the Short-Range Couplings in Excitation Energy Transfer. *J. Phys. Chem. C*, 112(4):1204–1212, January 2008.

[199] Chao-Ping Hsu. The electronic couplings in electron transfer and excitation energy transfer. *Acc. Chem. Res.*, 42(4):509–518, April 2009.

[200] Th. Förster. Zwischenmolekulare Energiewanderung und Fluoreszenz. *Ann. Phys.*, 437(1-2):55–75, 1948.

[201] T Förster. *Delocalized Excitation and Excitation Transfer.* Academic Press, New York, 1965.

[202] Kim F Wong, Biman Bagchi, and Peter J Rossky. Distance and Orientation Dependence of Excitation Transfer Rates in Conjugated Systems: Beyond the Förster Theory. *J. Phys. Chem. A*, 108(27):5752–5763, July 2004.

[203] Sébastien Faure, Christine Stern, Roger Guilard, and Pierre D Harvey. Role of the spacer in the singlet-singlet energy transfer mechanism (Förster vs Dexter) in cofacial bisporphyrins. *J. Am. Chem. Soc.*, 126(4):1253–61, February 2004.

[204] D L Dexter. A Theory of Sensitized Luminescence in Solids. *J. Chem. Phys.*, 21(5):836–850, 1953.

[205] Shammai Speiser, Salah Hassoon, and Mordecai B Rubin. The mechanism of short-range intramolecular electronic energy transfer in bichromophoric molecules. 2. Triplet-triplet transfer. *J. Phys. Chem.*, 90(21):5085–5089, October 1986.

[206] R A Marcus. On the Theory of Oxidation-Reduction Reactions Involving Electron Transfer. I. *J. Chem. Phys.*, 24(5):966, 1956.

[207] J.J. Kwiatkowski, J.M. Frost, and J. Nelson. The effect of morphology on electron field-effect mobility in disordered c60 thin films. *Nano Lett.*, 9(3):1085–1090, 2009.

[208] V Ern, P Avakian, and R. Merrifield. Diffusion of Triplet Excitons in Anthracene Crystals. *Phys. Rev.*, 148(2):862–867, August 1966.

[209] A. Hagfeldt and M. Grätzel. Molecular Photovoltaics. *Acc. Chem. Res.*, 33:269–277, 2000.

[210] N. Robertson. Optimizing dyes for dye-sensitized solar cells. *Angew. Chem. Int. Ed*, 45:2338–2345, 2006.

[211] B. O'Regan and M. Grätzel. A low-cost, high-efficiency solar cell based on dye-sensitized colloidal TiO2 films. *Nature*, 353:737–740, 1991.

[212] J. R. Sheats, H. Antoniadis, M. Hueschen, W. Leonard, J. Miller, R. Moon, D. Roitman, and A. Stocking. Organic Electroluminescent Devices. *Science*, 273:884–888, 1996.

[213] U. Mitschke and P. Bäuerle. The electroluminescence of organic materials. *J. Mater. Chem.*, 10:1471–1507, 2000.

[214] M. A. Baldo, D. F. O'Brien, Y. You, A. Shoustikov, S. Sibley, M. E. Thompson, and S. R. Forrest. Highly efficient phosphorescent emission from organic electroluminescent devices. *Nature*, 395:151–154, 1998.

[215] C. D. Dimitrakopoulos and D. J. Mascaro. Organic thin-film transistors: A review of recent advances. *IBM J. Res. Dev.*, 45:11–27, 2001.

[216] H. Hoppea and N. S. Sariciftci. Organic solar cells: an overview. *J. Mater. Res.*, 19:1924–1945, 2004.

[217] J. Cornil, D. Beljonne, J.-P. Calbert, and J.-L. Brédas. Interchain Interactions in Organic π-Conjugated Materials: Impact on Electronic Structure, Optical Response, and Charge Transport. *Adv. Mater.*, 13:1053–1067, 2001.

[218] I. Kaur, W. Jia, R. P. Kopreski, S. Selvarasah, M. R. Dokmeci, C. Pramanik, N. E. McGruer, and G. P. Miller. Substituent effects in pentacenes: gaining control over HOMO-LUMO gaps and photooxidative resistances. *J. Am. Chem. Soc.*, 130:16274–16286, 2008.

[219] J. A. Pople, D. P. Santry, and G. A. Segal. Approximate Self-Consistent Molecular Orbital Theory. I. Invariant Procedures. *J. Chem. Phys.*, 43:S129, 1965.

[220] J. Linderberg and Y. Ohrn. Derivation and Analysis of the Pariser–Parr–Pople Model. *J. Chem. Phys.*, 49:716, 1968.

[221] Björn 0. Roos. *The Complete Active Space Self-Consistent Field Method and its Applications in Electronic Structure Calculations*, volume 69. John Wiley & Sons, Inc., Hoboken, NJ, USA, 2007.

[222] K. Emrich. An extension of the coupled cluster formalism to excited states. *Nucl. Phys. A*, 351:397–438, 1981.

[223] E. Gross and W. Kohn. Local density-functional theory of frequency-dependent linear response. *Phys. Rev. Lett.*, 55:2850–2852, 1985.

[224] R. Bauernschmitt and R. Ahlrichs. Treatment of electronic excitations within the adiabatic approximation of time dependent density functional theory. *Chem. Phys. Lett.*, 256:454–464, 1996.

[225] F. Furche and R. Ahlrichs. Adiabatic time-dependent density functional methods for excited state properties. *J. Chem. Phys.*, 117:7433, 2002.

[226] M. E. Casida, C. Jamorski, K. C. Casida, and D. R. Salahub. Molecular excitation energies to high-lying bound states from time-dependent density-functional response theory: Characterization and correction of the time-dependent local density approximation ionization threshold. *J. Chem. Phys.*, 108:4439, 1998.

[227] D. J. Tozer and N. C. Handy. On the determination of excitation energies using density functional theory. *Phys. Chem. Chem. Phys.*, 2:2117–2121, 2000.

[228] A. Dreuw and M. Head-Gordon. Failure of time-dependent density functional theory for long-range charge-transfer excited states: The zincbacteriochlorin-bacteriochlorin and bacteriochlorophyllspheroidene complexes. *J. Am. Chem. Soc.*, 126(12):4007–4016, 2004.

[229] M. J. G. Peach, P. Benfield, T. Helgaker, and D. J. Tozer. Excitation energies in density functional theory: an evaluation and a diagnostic test. *J. Chem. Phys.*, 128:044118, 2008.

[230] S. Grimme and M. Parac. Substantial errors from time-dependent density functional theory for the calculation of excited states of large pi systems. *ChemPhysChem*, 4:292–5, 2003.

[231] M Wanko, M Garavelli, F Bernardi, Thomas A Niehaus, Th Frauenheim, and M Elstner. A global investigation of excited state surfaces within time-dependent density-functional response theory. *J. Chem. Phys.*, 120:1674, 2004.

[232] Z.-L. Cai, K. Sendt, and Jeffrey R. Reimers. Failure of density-functional theory and time-dependent density-functional theory for large extended π systems. *J. Chem. Phys.*, 117:5543, 2002.

[233] D. Jacquemin, E. A. Perpète, G. E. Scuseria, I. Ciofini, and C. Adamo. TD-DFT Performance for the Visible Absorption Spectra of Organic Dyes: Conventional versus Long-Range Hybrids. *J. Chem. Theory Comput.*, 4:123–135, 2008.

[234] A. Görling. Density-functional theory for excited states. *Phys. Rev. A*, 54:3912–3915, 1996.

[235] A. K. Theophilou. The energy density functional formalism for excited states. *J. Phys. C*, 12:5419–5430, 1979.

[236] M. Levy and A. Nagy. Variational Density-Functional Theory for an Individual Excited State. *Phys. Rev. Lett.*, 83:4361–4364, 1999.

[237] P. Ayers and M. Levy. Time-independent (static) density-functional theories for pure excited states: Extensions and unification. *Phys. Rev. A*, 80:012508, 2009.

[238] C.-L. Cheng, Q. Wu, and T. Van Voorhis. Rydberg energies using excited state density functional theory. *J. Chem. Phys.*, 129:124112, 2008.

[239] E. Artacho, M. Rohlfing, M. Côté, P. Haynes, R. Needs, and C. Molteni. Structural Relaxations in Electronically Excited Poly(para-phenylene). *Phys. Rev. Lett.*, 93:116401, 2004.

[240] J. Liu and W. Liang. Analytical Hessian of electronic excited states in time-dependent density functional theory with Tamm-Dancoff approximation. *J. Chem. Phys.*, 135:014113, 2011.

[241] T. Ziegler, M. Seth, M. Krykunov, J. Autschbach, and F. Wang. On the relation between time-dependent and variational density functional theory approaches for the determination of excitation energies and transition moments. *J. Chem. Phys.*, 130:154102, 2009.

[242] T. Liu, W.-G. Han, F. Himo, G. M. Ullmann, D. Bashford, A. Toutchkine, K. M. Hahn, and L. Noodleman. Density Functional Vertical Self-Consistent Reaction Field Theory for Solvatochromism Studies of Solvent-Sensitive Dyes. *J. Phys. Chem. A*, 108:3545–3555, 2004.

[243] D. Ceresoli, E. Tosatti, S. Scandolo, G. Santoro, and S. Serra. Trapping of excitons at chemical defects in polyethylene. *J. Chem. Phys.*, 121:6478–6484, 2004.

[244] J. Gavnholt, T. Olsen, M. Engelund, and J. Schiøtz. Δ self-consistent field method to obtain potential energy surfaces of excited molecules on surfaces. *Phys. Rev. B*, 78:075441, 2008.

[245] M. Schreiber, M. R. Silva-Junior, S. P. A Sauer, and W. Thiel. Benchmarks for electronically excited states: CASPT2, CC2, CCSD, and CC3. *J. Chem. Phys.*, 128:134110, 2008.

[246] Lars Goerigk and Stefan Grimme. Assessment of TD-DFT methods and of various spin scaled CIS(D) and CC2 versions for the treatment of low-lying valence excitations of large organic dyes. *J. Chem. Phys.*, 132(18):184103, 2010.

[247] B. Mennucci, R. Cammi, and J. Tomasi. Excited states and solvatochromic shifts within a nonequilibrium solvation approach: A new formulation of the integral equation formalism method at the self-consistent field, configuration interaction, and multiconfiguration self-consistent field level. *J. Chem. Phys.*, 109:2798, 1998.

[248] F. Inagaki, M. Tasumi, and T. Miyazawa. Excitation profile of the resonance Raman effect of β-carotene. *J. Mol. Spectrosc.*, 50:286–303, 1974.

[249] L. Edwards and M. Gouterman. Porphyrins XV. Vapor absorption spectra and stability: phthalocyanines. *J. Mol. Spectrosc.*, 33:292–310, 1970.

[250] H. Mattoussi, H. Murata, C. D. Merritt, Y. Iizumi, J. Kido, and Z. H. Kafafi. Photoluminescence quantum yield of pure and molecularly doped organic solid films. *J. Appl. Phys.*, 86:2642, 1999.

[251] T. Riehm, G. De Paoli, A. E. Konradsson, L. De Cola, H. Wadepohl, and L. H. Gade. Tetraazaperopyrenes: a new class of multifunctional chromophores. *Chem. Eur. J.*, 13:7317–7329, 2007.

[252] K.-Y. Lai, T.-M. Chu, F. C.-N. Hong, A. Elangovan, K.-M. Kao, S.-W. Yang, and T.-I. Ho. Excimer emission from a novel ethyne-based fluorescent dye in organic light-emitting devices. *Surf. Coat. Technol.*, 200:3283–3288, 2006.

[253] K. Tajima, L.-S. Li, and S. I. Stupp. Nanostructured oligo(p-phenylene vinylene)/silicate hybrid films: one-step fabrication and energy transfer studies. *J. Am. Chem. Soc.*, 128:5488–54895, 2006.

[254] J. Rajput, D. B. Rahbek, L. H. Andersen, A. Hirshfeld, M. Sheves, P. Altoè, G. Orlandi, and M. Garavelli. Probing and modeling the absorption of retinal protein chromophores in vacuo. *Angew. Chem. Int. Ed*, 49:1790–1793, 2010.

[255] Y. Lu and A. Penzkofer. Absorption behaviour of methanolic rhodamine 6G solutions at high concentration. *Chem. Phys.*, 107:175–184, 1986.

[256] Z. Ning, Q. Zhang, W. Wu, H. Pei, B. Liu, and H. Tian. Starburst triarylamine based dyes for efficient dye-sensitized solar cells. *J. Org. Chem.*, 73:3791–3797, 2008.

[257] C. Bonnand, J. Bellessa, and J. Plenet. Properties of surface plasmons strongly coupled to excitons in an organic semiconductor near a metallic surface. *Phys. Rev. B*, 73:245330, 2006.

[258] U. Eisner and R. P. Linstead. Chlorophyll and related substances. Part I. The synthesis of chlorin. *J. Chem. Soc.*, page 3742, 1955.

[259] L. Edwards, D. H. Dolphin, M. Gouterman, and A. D. Adler. Porphyrins XVII. Vapor absorption spectra and redox reactions: Tetraphenylporphins and porphin. *J. Mol. Spectrosc.*, 38:16–32, 1971.

[260] D. Biermann and W. Schmidt. Diels-Alder reactivity of polycyclic aromatic hydrocarbons. 1. Acenes and benzologs. *J. Am. Chem. Soc.*, 102:3163–3173, 1980.

[261] M. Dolg, U. Wedig, H. Stoll, and H. Preuss. Energy-adjusted ab initio pseudopotentials for the first row transition elements. *J. Chem. Phys.*, 86:866–872, 1987.

[262] Yihan Shao, Laszlo Fusti Molnar, Yousung Jung, Jörg Kussmann, Christian Ochsenfeld, Shawn T Brown, Andrew T B Gilbert, Lyudmila V Slipchenko, Sergey V Levchenko, Darragh P O'Neill, Robert A DiStasio, Rohini C Lochan, Tao Wang, Gregory J O Beran, Nicholas A Besley, John M Herbert, Ching Yeh Lin, Troy Van Voorhis, Siu Hung Chien, Alex Sodt, Ryan P Steele, Vitaly A Rassolov, Paul E Maslen, Prakashan P Korambath, Ross D Adamson, Brian Austin, Jon Baker, Edward F C Byrd, Holger Dachsel, Robert J Doerksen, Andreas Dreuw, Barry D Dunietz, Anthony D Dutoi, Thomas R Furlani, Steven R Gwaltney, Andreas Heyden, So Hirata, Chao-Ping Hsu, Gary Kedziora, Rustam Z Khalliulin, Phil Klunzinger, Aaron M Lee, Michael S Lee, Wanzhen Liang, Itay Lotan, Nikhil Nair, Baron Peters, Emil I Proynov, Piotr A Pieniazek, Young Min Rhee, Jim Ritchie, Edina Rosta, C David Sherrill, Andrew C Simmonett, Joseph E Subotnik, H Lee Woodcock, Weimin Zhang, Alexis T Bell, Arup K Chakraborty, Daniel M Chipman, Frerich J Keil, Arieh Warshel,

Warren J Hehre, Henry F Schaefer, Jing Kong, Anna I Krylov, Peter M W Gill, and Martin Head-Gordon. Advances in methods and algorithms in a modern quantum chemistry program package. *Phys. Chem. Chem. Phys.*, 8(27):3172–3191, July 2006.

[263] J. Fabian, L. A. Diaz, G. Seifert, and T. Niehaus. Calculation of excitation energies of organic chromophores: a critical evaluation. *J. Mol. Struct. Theochem.*, 594:41–53, 2002.

[264] A. T. B. Gilbert, N. A. Besley, and P. M. W. Gill. Self-consistent field calculations of excited states using the maximum overlap method (MOM). *J. Phys. Chem. A*, 112:13164–13171, 2008.

[265] A. Toutchkine, W.-G. Han, M. Ullmann, T. Liu, D. Bashford, L. Noodleman, and K. M. Hahn. Experimental and DFT studies: novel structural modifications greatly enhance the solvent sensitivity of live cell imaging dyes. *J. Phys. Chem. A*, 111:10849–10860, 2007.

[266] W. Liang, C. M. Isborn, and X. Li. Obtaining Hartree-Fock and density functional theory doubly excited states with Car-Parrinello density matrix search. *J. Chem. Phys.*, 131:204101, 2009.

[267] J. Tao and G. Vignale. Time-dependent density-functional theory beyond the local-density approximation. *Phys. Rev. Lett.*, 97:036403, 2006.

[268] J. Tao, G. Vignale, and I. Tokatly. Time-dependent density functional theory: Derivation of gradient-corrected dynamical exchange-correlational potentials. *Phys. Rev. B*, 76:195126, 2007.

[269] K. Burke, J. Werschnik, and E. K. U. Gross. Time-dependent density functional theory: past, present, and future. *J. Chem. Phys.*, 123:62206, 2005.

[270] G. Onida, L. Reining, and A. Rubio. Electronic excitations: density-functional versus many-body Green's-function approaches. *Rev. Mod. Phys.*, 74:601–659, 2002.

[271] S. Hirata, S. Ivanov, I. Grabowski, and R. J. Bartlett. Time-dependent density functional theory employing optimized effective potentials. *J. Chem. Phys.*, 116:6468, 2002.

[272] M. A. L. Marques and E. K. U. Gross. Time-dependent density functional theory. *Ann. Rev. Phys. Chem.*, 55:427–455, 2004.

[273] Y. Kurzweil and R. Baer. Adapting approximate-memory potentials for time-dependent density functional theory. *Phys. Rev. B*, 77:085121, 2008.

[274] G. Vignale. Real-time resolution of the causality paradox of time-dependent density-functional theory. *Phys. Rev. A*, 77:062511, 2008.

[275] Y. Kurzweil and R. Baer. Generic Galilean-invariant exchange-correlation functionals with quantum memory. *Phys. Rev. B*, 72:035106, 2005.

[276] M. E. Casida. Time-dependent density functional response theory for molecules. In D. P. Chong, editor, *Recent Advances in Density Functional Methods*, pages 155–192. World Scientific, Singapore, 1995.

[277] M. Seth and T. Ziegler. Calculation of excitation energies of open-shell molecules with spatially degenerate ground states. I. Transformed reference via an intermediate configuration Kohn-Sham density-functional theory and applications to d1 and d2 systems with octahedral and te. *J. Chem. Phys.*, 123:144105, 2005.

[278] M. Seth and T. Ziegler. Calculation of excitation energies of open-shell molecules with spatially degenerate ground states. ii. transformed reference via intermediate configuration kohn-sham time dependent density functional theory oscillator strengths and magnetic circular dichroism c terms. *J. Chem. Phys.*, 124:144105, 2006.

[279] F. Wang and T. Ziegler. The performance of time-dependent density functional theory based on a noncollinear exchange-correlation potential in the calculations of excitation energies. *J. Chem. Phys.*, 122:074109, 2005.

[280] Y. Shao, M. Head-Gordon, and A. I. Krylov. The spin–flip approach within time-dependent density functional theory: Theory and applications to diradicals. *J. Chem. Phys.*, 118:4807, 2003.

[281] F. Wang and T. Ziegler. Time-dependent density functional theory based on a noncollinear formulation of the exchange-correlation potential. *J. Chem. Phys.*, 121:12191–12196, 2004.

[282] N. Maitra, K. Burke, and C. Woodward. Memory in Time-Dependent Density Functional Theory. *Phys. Rev. Lett.*, 89:023002, 2002.

[283] R. Gaudoin and K. Burke. Lack of Hohenberg-Kohn Theorem for Excited States. *Phys. Rev. Lett.*, 93:173001, 2004.

[284] A. Görling. Orbital- and state-dependent functionals in density-functional theory. *J. Chem. Phys.*, 123:62203, 2005.

[285] C. Ullrich, U. Gossmann, and E. Gross. Time-dependent optimized effective potential. *Phys. Rev. Lett.*, 74:872–875, 1995.

[286] M. Levy. Universal variational functionals of electron densities, first-order density matrices, and natural spin-orbitals and solution of the v-representability problem. *Proc. Nat'l. Acad. Sci., USA*, 76:6062–6065, 1979.

[287] D. Cremer. Density functional theory: coverage of dynamic and non-dynamic electron correlation effects. *Mol. Phys.*, 99:1899–1940, 2001.

[288] E. Ruiz, J. Cano, S. Alvarez, and P. Alemany. Broken symmetry approach to calculation of exchange coupling constants for homobinuclear and heterobinuclear transition metal complexes. *J. Comput. Chem.*, 20:1391–1400, 1999.

[289] J. Cabrero, N. Ben Amor, C. de Graaf, F. Illas, and R. Caballol. Ab Initio Study of the Exchange Coupling in Oxalato-Bridged Cu(II) Dinuclear Complexes. *J. Phys. Chem. A*, 104:9983–9989, 2000.

[290] E. Ruiz, A. Rodríguez-Fortea, J. Cano, S. Alvarez, and P. Alemany. About the calculation of exchange coupling constants in polynuclear transition metal complexes. *J. Comput. Chem.*, 24:982–989, 2003.

[291] I. Rudra, Q. Wu, and T. Van Voorhis. Predicting exchange coupling constants in frustrated molecular magnets using density functional theory. *Inorg. Chem*, 46:10539–10548, 2007.

[292] M. Filatov and S. Shaik. A spin-restricted ensemble-referenced Kohn–Sham method and its application to diradicaloid situations. *Chem. Phys. Lett.*, 304:429–437, 1999.

[293] I. Frank, J. Hutter, D. Marx, and M. Parrinello. Molecular dynamics in low-spin excited states. *J. Chem. Phys.*, 108:4060, 1998.

[294] M. Filatov and S. Shaik. Application of spin-restricted open-shell Kohn–Sham method to atomic and molecular multiplet states. *J. Chem. Phys.*, 110:116, 1999.

[295] Y. Mochizuki, Y. Komeiji, T. Ishikawa, T. Nakano, and H. Yamataka. A fully quantum mechanical simulation study on the lowest n–π state of hydrated formaldehyde. *Chem. Phys. Lett.*, 437:66–72, 2007.

[296] U. F. Röhrig, I. Frank, J. Hutter, A. Laio, J. VandeVondele, and U. Rothlisberger. QM/MM Car-Parrinello molecular dynamics study of the solvent effects on the ground state and on the first excited singlet state of acetone in water. *ChemPhysChem*, 4:1177–82, 2003.

[297] M. Sulpizi, U. F. Röhrig, J. Hutter, and U. Rothlisberger. Optical properties of molecules in solution via hybrid TDDFT/MM simulations. *Int. J. Quantum Chem.*, 101:671–682, 2005.

[298] Fabrizio Santoro, Alessandro Lami, Roberto Improta, and Vincenzo Barone. Effective method to compute vibrationally resolved optical spectra of large molecules at finite temperature in the gas phase and in solution. *J. Chem. Phys.*, 126(18):184102, May 2007.

[299] Fabrizio Santoro, Alessandro Lami, Roberto Improta, Julien Bloino, and Vincenzo Barone. Effective method for the computation of optical spectra of

large molecules at finite temperature including the Duschinsky and Herzberg-Teller effect: the Qx band of porphyrin as a case study. *J. Chem. Phys.*, 128(22):224311, June 2008.

[300] Tim Kowalczyk, Shane R Yost, and Troy Van Voorhis. Assessment of the ΔSCF density functional theory approach for electronic excitations in organic dyes. *J. Chem. Phys.*, 134(5):054128, February 2011.

[301] NS Sariciftci, L Smilowitz, AJ Heeger, and F Wudl. Photoinduced electron transfer from a conducting polymer to buckminsterfullerene. *Science*, 258(5087):1474–1476, 1992.

[302] C J Brabec, A Cravino, D Meissner, N S Sariciftci, T Fromherz, M T Rispens, L Sanchez, and J C Hummelen. Origin of the Open Circuit Voltage of Plastic Solar Cells. *Adv. Funct. Mater.*, 11(5):374–380, October 2001.

[303] Christoph J Brabec, Gerald Zerza, Giulio Cerullo, Sandro De Silvestri, Silvia Luzzati, Jan C Hummelen, and Serdar Sariciftci. Tracing photoinduced electron transfer process in conjugated polymer/fullerene bulk heterojunctions in real time. *Chem. Phys. Lett.*, 340(3):232–236, 2001.

[304] MA Fox and M Chanon. *Photoduced electron transfer.* Amsterdam: Elsevier, 1988.

[305] CJ Murphy, MR Arkin, Y Jenkins, ND Ghatlia, SH Bossmann, NJ Turro, and JK Barton. Long-range photoinduced electron transfer through a dna helix. *Science*, 262(5136):1025–1029, 1993.

[306] Yosuke Kanai, Varadharajan Srinivasan, Steven K. Meier, K. Peter C. Vollhardt, and Jeffrey C. Grossman. Mechanism of thermal reversal of the (fulvalene)tetracarbonyldiruthenium photoisomerization: Toward molecular solarthermal energy storage. *Angew. Chem. Int. Ed.*, 49(47):8926–8929, 2010.

[307] J.-J. Zou, Y. Liu, L. Pan, L. Wang, and X. Zhang. Photocatalytic isomerization of norbornadiene to quadricyclane over metal (v, fe and cr)-incorporated timcm-41. *Appl. Catal. B-Environ*, 95(3–4):439–445, 2010.

[308] Constantine Philippopoulos, Dimitrios Economou, Constantine Economou, and John Marangozis. Norbornadiene-quadricyclane system in the photochemical conversion and storage of solar energy. *Ind. Eng. Chem. Prod. Res. and Dev.*, 22(4):627–633, 1983.

[309] Roy McWeeny and Brian T Sutcliffe. *Methods of molecular quantum mechanics*, volume 2. Academic Press London, 1989.

[310] Benjamin Kaduk and Troy Van Voorhis. Communication: Conical intersections using constrained density functional theory–configuration interaction. *J. Chem. Phys.*, 133(061102):061102, 2010.

[311] Oleg A Vydrov and Troy Van Voorhis. Nonlocal van der waals density functional: The simpler the better. *J. Chem. Phys.*, 133:244103, 2010.

[312] Jeng-Da Chai and Martin Head-Gordon. Long-range corrected hybrid density functionals with damped atom–atom dispersion corrections. *Phys. Chem. Chem. Phys.*, 10(44):6615–6620, 2008.

[313] Aron J Cohen, Paula Mori-Sánchez, and Weitao Yang. Challenges for density functional theory. *Chem. Rev.*, 112(1):289, 2012.

[314] Monika Musiał, Ajith Perera, and Rodney J Bartlett. Multireference coupled-cluster theory: The easy way. *J. Chem. Phys.*, 134:114108, 2011.

[315] Per Aake Malmqvist, Alistair Rendell, and Bjoern O Roos. The restricted active space self-consistent-field method, implemented with a split graph unitary group approach. *J. Phys. Chem.*, 94(14):5477–5482, 1990.

[316] Krzysztof Wolinski and Peter Pulay. Generalized møller–plesset perturbation theory: Second order results for two-configuration, open-shell excited singlet, and doublet wave functions. *J. Chem. Phys.*, 90:3647, 1989.

[317] Robert B Murphy and Richard P Messmer. Generalized møllerplesset perturbation theory applied to general mcscf reference wave functions. *Chem. Phys. Lett.*, 183(5):443–448, 1991.

[318] Pawel M Kozlowski and Ernest R Davidson. Considerations in constructing a multireference second-order perturbation theory. *J. Chem. Phys.*, 100:3672, 1994.

[319] Joseph JW McDouall, Kathryn Peasley, and Michael A Robb. A simple mc scf perturbation theory: Orthogonal valence bond møller-plesset 2 (ovb mp2). *Chem. Phys. Lett.*, 148(2):183–189, 1988.

[320] NC Handy, PJ Knowles, and K Somasundram. On the convergence of the møller-plesset perturbation series. *Theor. Chim. Acta*, 68(1):87–100, 1985.

[321] J. Olsen, O. Christiansen, H. Koch, and P. Jørgensen. Surprising cases of divergent behavior in møller-plesset perturbation theory. *J. Chem. Phys.*, 105:5082–5090, 1996.

[322] J. Olsen, P. Jørgensen, T. Helgaker, and O. Christiansen. Divergence in møller-plesset theory: A simple explanation based on a two-state model. *J. Chem. Phys.*, 112:9736–9748, 2000.

[323] C David Sherrill. Bond breaking in quantum chemistry. *Annu. Rep. Comp. Chem.*, 1:45–56, 2005.

[324] Kerstin Andersson. Different forms of the zeroth-order hamiltonian in second-order perturbation theory with a complete active space self-consistent field reference function. *Theor. Chim. Acta*, 91(1-2):31–46, 1995.

[325] Giovanni Ghigo, Björn O Roos, and Per-ke Malmqvist. A modified definition of the zeroth-order hamiltonian in multiconfigurational perturbation theory (caspt2). *Chem. Phys. Lett.*, 396(1):142–149, 2004.

[326] Kenneth G Dyall. The choice of a zeroth-order hamiltonian for second-order perturbation theory with a complete active space self-consistent-field reference function. *J. Chem. Phys.*, 102:4909, 1995.

[327] Michael P Deskevich, David J Nesbitt, and Hans-Joachim Werner. Dynamically weighted multiconfiguration self-consistent field: Multistate calculations for f+ ho hf+ oh reaction paths. *J. Chem. Phys.*, 120:7281, 2004.

[328] Bernard Kirtman. Simultaneous calculation of several interacting electronic states by generalized van vleck perturbation theory. *J. Chem. Phys.*, 75:798, 1981.

[329] JP Malrieu, Ph Durand, and JP Daudey. Intermediate hamiltonians as a new class of effective hamiltonians. *J. Phys. A*, 18(5):809, 1985.

[330] Jiří Pittner, Petr Nachtigall, Petr Čársky, Jozef Mášik, and Ivan Hubač. Assessment of the single-root multireference brillouin–wigner coupled-cluster method: test calculations on ch, sih, and twisted ethylene. *J. Chem. Phys.*, 110:10275, 1999.

[331] Anna Engels-Putzka and Michael Hanrath. Multi-reference coupled-cluster study of the potential energy surface of the hydrogen fluoride dissociation including excited states. *J. Mol. Struct. THEOCHEM*, 902(1):59–65, 2009.

[332] Vladimir V Ivanov, Ludwik Adamowicz, and Dmitry I Lyakh. Potential energy surface of the electron excited states in the state-specific multi-reference coupled cluster theory. hydrogen fluoride dissociation. *J. Mol. Struct. THEOCHEM*, 768(1):97–101, 2006.

[333] M. W. D. Hanson-Heine, M. W. George, and N. A. Besley. Calculating excited state properties using kohn-sham density functional theory. *J. Chem. Phys.*, 138:064101, 2013.

[334] Tom Ziegler, Arvi Rauk, and Evert J Baerends. On the calculation of multiplet energies by the hartree-fock-slater method. *Theor. Chim. Acta*, 43(3):261–271, 1977.

[335] R. McWeeny and B. T. Sutcliffe. *Methods of molecular quantum mechanics*. Academic Press, 1969.

[336] S. C. Leasure and G. G. Balint-Kurti. Valence-bond theory and the evaluation of electronic energy matrix elements between nonorthogonal slater determinants. *Phys. Rev. A*, 31(4):2107–2113, 1985.

[337] AT Amos, GG Hall, AT Amos, and GG Hall. Single determinant wave functions. *Proceedings of the Royal Society of London. Series A. Mathematical and Physical Sciences*, 263(1315):483–493, 1961.

[338] Harry F. King, Richard E. Stanton, Hojing Kim, Robert E. Wyatt, and Robert G. Parr. Corresponding orbitals and the nonorthogonality problem in molecular quantum mechanics. *J. Chem. Phys.*, 47(6):1936–1941, 1967.

[339] Nicholas A Besley, Andrew TB Gilbert, and Peter MW Gill. Self-consistent-field calculations of core excited states. *J. Chem. Phys.*, 130:124308, 2009.

[340] Micah L Abrams and C David Sherrill. An assessment of the accuracy of multireference configuration interaction (mrci) and complete-active-space second-order perturbation theory (caspt2) for breaking bonds to hydrogen. *J. of Phys. Chem. A*, 107(29):5611–5616, 2003.

[341] Michael W Schmidt, Kim K Baldridge, Jerry A Boatz, Steven T Elbert, Mark S Gordon, Jan H Jensen, Shiro Koseki, Nikita Matsunaga, Kiet A Nguyen, Shujun Su, T. L. Windus, M. Dupuis, and J. A. Montgomery Jr. General atomic and molecular electronic structure system. *J. Comp. Chem.*, 14(11):1347–1363, 1993.

[342] Jiye Lee, Matthew J Bruzek, Nicholas J Thompson, Matthew Y Sfeir, John E Anthony, and Marc A Baldo. Singlet exciton fission in a hexacene derivative. *Advanced Materials*, 2013.

[343] Jonathan J Burdett and Christopher J Bardeen. Quantum beats in crystalline tetracene delayed fluorescence due to triplet pair coherences produced by direct singlet fission. *Journal of the American Chemical Society*, 134(20):8597–8607, 2012.

[344] Justin C Johnson, Arthur J Nozik, and Josef Michl. High triplet yield from singlet fission in a thin film of 1, 3-diphenylisobenzofuran. *J. Am. Chem. Soc*, 132(46):16302–16303, 2010.

[345] Claudiu C Gradinaru, John Kennis, Emmanouil Papagiannakis, Ivo HM van Stokkum, Richard J Cogdell, Graham R Fleming, Robert A Niederman, and Rienk van Grondelle. An unusual pathway of excitation energy deactivation in carotenoids: singlet-to-triplet conversion on an ultrafast timescale in a photosynthetic antenna. *Proceedings of the National Academy of Sciences*, 98(5):2364–2369, 2001.

[346] D. N. Congreve, J. Lee, N. J. Thompson, E. Hontz, S. R. Yost, P. D. Reusswig, M. E. Bahlke, S. Reineke, T. Van Voorhis, and M. A. Baldo. External quantum efficiency above 100% in a singlet-exciton-fission-based organic photovoltaic cell. *Science*, Accepted, 2013.

[347] Paul M Zimmerman, Zhiyong Zhang, and Charles B Musgrave. Singlet fission in pentacene through multi-exciton quantum states. *Nature Chemistry*, 2(8):648–652, 2010.

[348] Robert Englman and Joshua Jortner. The energy gap law for radiationless transitions in large molecules. *Molecular Physics*, 18(2):145–164, 1970.

[349] John E Anthony, James S Brooks, David L Eaton, Sean R Parkin, et al. Functionalized pentacene: Improved electronic properties from control of solid-state order. *Journal of the American Chemical Society*, 123(38):9482–9483, 2001.

[350] Qian Miao, Xiaoliu Chi, Shengxiong Xiao, Roswitha Zeis, Michael Lefenfeld, Theo Siegrist, Michael L Steigerwald, and Colin Nuckolls. Organization of acenes with a cruciform assembly motif. *Journal of the American Chemical Society*, 128(4):1340–1345, 2006.

[351] Ricardo Ruiz, Alex C Mayer, George G Malliaras, Bert Nickel, Giacinto Scoles, Alexander Kazimirov, Hyunjung Kim, Randall L Headrick, and Zahirul Islam. Structure of pentacene thin films. *Applied physics letters*, 85(21):4926–4928, 2004.

[352] Geoffrey B. Piland, Jonathan J. Burdett, Dharmalingam Kurunthu, and Christopher J. Bardeen. Magnetic field effects on singlet fission and fluorescence decay dynamics in amorphous rubrene. *The Journal of Physical Chemistry C*, 117(3):1224–1236, 2013.

[353] J Burgos, M Pope, Ch E Swenberg, and RR Alfano. Heterofission in pentacene-doped tetracene single crystals. *physica status solidi (b)*, 83(1):249–256, 1977.

[354] L Sebastian, G Weiser, and H Bässler. Charge transfer transitions in solid tetracene and pentacene studied by electroabsorption. *Chemical Physics*, 61(1):125–135, 1981.

[355] H Yamagata, J Norton, E Hontz, Y Olivier, D Beljonne, JL Bredas, RJ Silbey, and FC Spano. The nature of singlet excitons in oligoacene molecular crystals. *The Journal of chemical physics*, 134(20):204703–204703, 2011.

[356] Shane R. Yost, Eric Hontz, Sina Yeganeh, and Troy Van Voorhis. Triplet vs singlet energy transfer in organic semiconductors: The tortoise and the hare. *The Journal of Physical Chemistry C*, 116(33):17369–17377, 2012.

[357] Joshua Jortner and Mordechai Bixon. Intramolecular vibrational excitations accompanying solvent-controlled electron transfer reactions. *The Journal of chemical physics*, 88(1):167–170, 1988.

[358] Massimo Sparpaglione and Shaul Mukamel. Adiabatic vs. nonadiabatic electron transfer and longitudinal solvent dielectric relaxation: beyond the debye model. *Journal of Physical Chemistry*, 91(15):3938–3943, 1987.

[359] A Bree and LE Lyons. 1002. the intensity of ultraviolet-light absorption by monocrystals. part iv. absorption by naphthacene of plane-polarized light. *Journal of the Chemical Society (Resumed)*, pages 5206–5212, 1960.

[360] Stephen F Nelsen, Silas C Blackstock, and Yaesil Kim. Estimation of inner shell marcus terms for amino nitrogen compounds by molecular orbital calculations. *Journal of the American Chemical Society*, 109(3):677–682, 1987.

[361] Steven L Murov, Gordon L Hug, and Ian Carmichael. *Handbook of photochemistry*. CRC Press, 1993.

[362] Wayne M Witzel, Andrew Shabaev, C Stephen Hellberg, Verne L Jacobs, and Alexander L Efros. Quantum simulation of multiple-exciton generation in a nanocrystal by a single photon. *Physical review letters*, 105(13):137401, 2010.

[363] Al Shabaev, Al L Efros, and AJ Nozik. Multiexciton generation by a single photon in nanocrystals. *Nano letters*, 6(12):2856–2863, 2006.

[364] Rienk van Grondelle and Vladimir I Novoderezhkin. Energy transfer in photosynthesis: experimental insights and quantitative models. *Phys. Chem. Chem. Phys.*, 8(7):793–807, February 2006.

[365] P W Anderson. Absence of Diffusion in Certain Random Lattices. *Phys. Rev.*, 109(5):1492–1505, March 1958.

[366] R Silbey. Electronic Energy Transfer in Molecular Crystals. *Annu. Rev. Phys. Chem.*, 27(1):203–223, October 1976.

[367] Serap Günes, Helmut Neugebauer, and Niyazi Serdar Sariciftci. Conjugated polymer-based organic solar cells. *Chem. Rev.*, 107(4):1324–1338, April 2007.

[368] Harald Hoppe and Niyazi Serdar Sariciftci. Morphology of polymer/fullerene bulk heterojunction solar cells. *J. Mater. Chem.*, 16(1):45–61, 2006.

[369] Gregory D Scholes. Long-range resonance energy transfer in molecular systems. *Annu. Rev. Phys. Chem.*, 54(1):57–87, January 2003.

[370] Hiroyoshi Nagae, Toshiaki Kakitani, Tetzuya Katoh, and Mamoru Mimuro. Calculation of the excitation transfer matrix elements between the S2 or S1 state of carotenoid and the S2 or S1 state of bacteriochlorophyll. *J. Chem. Phys.*, 98(10):8012–8023, 1993.

[371] I A Howard, F Zutterman, G Deroover, D Lamoen, and C Van Alsenoy. Approaches to Calculation of Exciton Interaction Energies for a Molecular Dimer. *J. Phys. Chem. B*, 108(50):19155–19162, December 2004.

[372] Brent P Krueger, Gregory D Scholes, and Graham R Fleming. Calculation of Couplings and Energy-Transfer Pathways between the Pigments of LH2 by the ab Initio Transition Density Cube Method. *J. Phys. Chem. B*, 102(27):5378–5386, July 1998.

[373] Aurora Muñoz Losa, Carles Curutchet, Brent P Krueger, Lydia R Hartsell, and Benedetta Mennucci. Fretting about FRET: failure of the ideal dipole approximation. *Biophys. J.*, 96(12):4779–4788, June 2009.

[374] Shammai Speiser. Photophysics and Mechanisms of Intramolecular Electronic Energy Transfer in Bichromophoric Molecular Systems: Solution and Supersonic Jet Studies. *Chem. Rev.*, 96(6):1953–1976, January 1996.

[375] G Vaubel and H Baessler. Diffusion of Singlet Excitons in Tetracene Crystals. *Mol. Cryst. Liq. Cryst.*, 12(1):47–56, December 1970.

[376] Paul Heremans, David Cheyns, and Barry P Rand. Strategies for increasing the efficiency of heterojunction organic solar cells: material selection and device architecture. *Acc. Chem. Res.*, 42(11):1740–1747, November 2009.

[377] Gerhard L Closs, Mark D Johnson, John R Miller, and Piotr Piotrowiak. A connection between intramolecular long-range electron, hole, and triplet energy transfers. *J. Am. Chem. Soc.*, 111(10):3751–3753, May 1989.

[378] Nobuaki Koga, Keiichiro Sameshima, and Keiji Morokuma. Ab initio MO calculations of electronic coupling matrix elements on model systems for intramolecular electron transfer, hole transfer, and triplet energy transfer: distance dependence and pathway in electron transfer and relationship of triplet energy tra. *J. Phys. Chem.*, 97(50):13117–13125, December 1993.

[379] Zhi-Qiang You and Chao-Ping Hsu. The fragment spin difference scheme for triplet-triplet energy transfer coupling. *J. Chem. Phys.*, 133(7):074105, August 2010.

[380] A. Köhler and H. Bässler. Triplet states in organic semiconductors. *Materials Science and Engineering: R: Reports*, 66(4-6):71–109, November 2009.

[381] V Ern. Anisotropy of Triplet Exciton Diffusion in Anthracene. *Phys. Rev. Lett.*, 22(8):343–345, February 1969.

[382] D F Williams, J Adolph, and W G Schneider. Diffusion of Triplet Excitons in Anthracene Crystals. *J. Chem. Phys.*, 45(2):575–577, 1966.

[383] Pavel Irkhin and Ivan Biaggio. Direct Imaging of Anisotropic Exciton Diffusion and Triplet Diffusion Length in Rubrene Single Crystals. *Phys. Rev. Lett.*, 107(1):017402, July 2011.

[384] Iffat H Nayyar, Enrique R Batista, Sergei Tretiak, Avadh Saxena, D L Smith, and Richard L Martin. Localization of Electronic Excitations in Conjugated Polymers Studied by DFT. *The Journal of Physical Chemistry Letters*, 2(6):566–571, March 2011.

[385] Qin Wu and Troy Van Voorhis. Direct calculation of electron transfer parameters through constrained density functional theory. *J. Phys. Chem. A*, 110(29):9212–9218, July 2006.

[386] R E Kellogg. Evidence of FranckCondon Factors in Radiationless Transitions. *J. Chem. Phys.*, 45(8):3156–3158, 1966.

[387] Richard R Lunt, Jay B Benziger, and Stephen R Forrest. Relationship between crystalline order and exciton diffusion length in molecular organic semiconductors. *Adv. Mater.*, 22(11):1233–1236, March 2010.

[388] W Hofberger and H Bässler. Diffusion of triplet excitons in amorphous tetracene. *Physica Status Solidi (b)*, 69(2):725–730, June 1975.

[389] Wade A Luhman and Russell J Holmes. Enhanced exciton diffusion in an organic photovoltaic cell by energy transfer using a phosphorescent sensitizer. *Appl. Phys. Lett.*, 94(15):153304, 2009.

[390] Akshay Rao, Mark W B Wilson, Justin M Hodgkiss, Sebastian Albert-Seifried, Heinz Bässler, and Richard H Friend. Exciton fission and charge generation via triplet excitons in pentacene/C60 bilayers. *J. Am. Chem. Soc.*, 132(36):12698–12703, September 2010.

[391] Jianhua Zhao, Aihua Wang, Martin A Green, and Francesca Ferrazza. 19.8% efficient honeycomb textured multicrystalline and 24.4% monocrystalline silicon solar cells. *Appl. Phys. Lett.*, 73(14):1991–1993, 1998.

[392] Jan Hendrik Petermann, Dimitri Zielke, Jan Schmidt, Felix Haase, Enrique Garralaga Rojas, and Rolf Brendel. 19%-efficient and 43 m-thick crystalline Si solar cell from layer transfer using porous silicon. *Prog. Photovoltaics Res. Appl.*, 20(1):1–5, January 2012.

[393] Ingrid Repins, Miguel A Contreras, Brian Egaas, Clay DeHart, John Scharf, Craig L Perkins, Bobby To, and Rommel Noufi. 199%-efficient ZnO/CdS/CuInGaSe 2 solar cell with 812% fill factor. *Prog. Photovoltaics Res. Appl.*, 16(3):235–239, May 2008.

[394] K Sugiyama, D Yoshimura, E Ito, T Miyazaki, Y Hamatani, I Kawamoto, Y Ouchi, K Seki, and H Ishii. Uv Photoemission Study of 8-Hydroxyquinoline Aluminum (ALQ 3) / Metal Interfaces. *Molecular Crystals and Liquid Crystals Science and Technology. Section A. Molecular Crystals and Liquid Crystals*, 286(1):239–244, July 1996.

[395] I G Hill, A Rajagopal, A Kahn, and Y Hu. Molecular level alignment at organic semiconductor-metal interfaces. *Appl. Phys. Lett.*, 73(5):662, 1998.

[396] H Ishii and K Seki. Energy level alignment at organic/metal interfaces studied by UV photoemission: breakdown of traditional assumption of a common vacuum level at the interface. *IEEE T. Electron. Dev.*, 44(8):1295–1301, 1997.

[397] H Ishii, K Sugiyama, D Yoshimura, E Ito, Y Ouchi, and K Seki. Energy-level alignment at model interfaces of organic electroluminescent devices studied by UV photoemission: trend in the deviation from the traditional way of estimating the interfacial electronic structures. *IEEE J. Sel. Top. Quantum Electron.*, 4(1):24–33, 1998.

[398] J Blochwitz, T Fritz, M Pfeiffer, K Leo, D.M. Alloway, P.A. Lee, and N.R. Armstrong. Interface electronic structure of organic semiconductors with controlled doping levels. *Org. Electron.*, 2(2):97–104, September 2001.

[399] I G Hill and A Kahn. Energy level alignment at interfaces of organic semiconductor heterostructures. *J. Appl. Phys.*, 84(10):5583–5586, 1998.

[400] W Chen, D C Qi, H Huang, X Gao, and A T S Wee. Organic-Organic Heterojunction Interfaces: Effect of Molecular Orientation. *Adv. Funct. Mater.*, 21(3):410–424, 2011.

[401] F.J. Zhang, A Vollmer, J Zhang, Z Xu, J.P. Rabe, and N Koch. Energy level alignment and morphology of interfaces between molecular and polymeric organic semiconductors. *Org. Electron.*, 8(5):606–614, October 2007.

[402] S Hüfner. *Photoelectron Spectroscopy: Principles and Applications.* Springer Verlag, Berlin, 3 edition, 2003.

[403] Y Hirose, A Kahn, V Aristov, P Soukiassian, V Bulovic, and S. Forrest. Chemistry and electronic properties of metal-organic semiconductor interfaces: Al, Ti, In, Sn, Ag, and Au on PTCDA. *Phys. Rev. B*, 54(19):13748–13758, November 1996.

[404] Xavier Crispin, Victor Geskin, Annica Crispin, Jérôme Cornil, Roberto Lazzaroni, William R Salaneck, and Jean-Luc Brédas. Characterization of the Interface Dipole at Organic/ Metal Interfaces. *J. Am. Chem. Soc.*, 124(27):8131–8141, July 2002.

[405] Hisao Ishii, Kiyoshi Sugiyama, Eisuke Ito, and Kazuhiko Seki. Energy Level Alignment and Interfacial Electronic Structures at Organic/Metal and Organic/Organic Interfaces. *Adv. Mater.*, 11(8):605–625, June 1999.

[406] Feng Zhu, Mandy Grobosch, Uwe Treske, Martin Knupfer, Lizhen Huang, Shiliang Ji, and Donghang Yan. Interfacial energy level bending in a crystalline p/p-type organic heterostructure. *Appl. Phys. Lett.*, 98(20):203303, 2011.

[407] S W Cho, L F J Piper, A DeMasi, A R H Preston, K E Smith, K V Chauhan, P Sullivan, R A Hatton, and T S Jones. Electronic Structure of C 60 /Phthalocyanine/ITO Interfaces Studied using Soft X-ray Spectroscopies. *J. Phys. Chem. C*, 114(4):1928–1933, February 2010.

[408] Stijn Verlaak, David Beljonne, David Cheyns, Cedric Rolin, Mathieu Linares, Frédéric Castet, Jérôme Cornil, and Paul Heremans. Electronic Structure and Geminate Pair Energetics at Organic/Organic Interfaces: The Case of Pentacene/C 60 Heterojunctions. *Adv. Funct. Mater.*, 19(23):3809–3814, December 2009.

[409] Toshiyuki Abe, Shouichi Miyakushi, Keiji Nagai, and Takayoshi Norimatsu. Study of the factors affecting the photoelectrode characteristics of a perylene/phthalocyanine bilayer working in the water phase. *Phys. Chem. Chem. Phys.*, 10(11):1562–1568, March 2008.

[410] Ichiro Hiromitsu, Yohei Murakami, and Takashi Ito. Electric field in phthalocyanine/perylene heterojunction solar cells studied by electroabsorption and photocurrent measurements. *J. Appl. Phys.*, 94(4):2434–2439, August 2003.

[411] Kuwat Triyana, Takeshi Yasuda, Katsuhiko Fujita, and Tetsuo Tsutsui. Tandem-type organic solar cells by stacking different heterojunction materials. *Thin Solid Films*, 477(1-2):198–202, April 2005.

[412] S R Forrest, L Y Leu, F F So, and W Y Yoon. Optical and electrical properties of isotype crystalline molecular organic heterojunctions. *J. Appl. Phys.*, 66(12):5908, December 1989.

[413] E. Haskal, Z Shen, P. Burrows, and S. Forrest. Excitons and exciton confinement in crystalline organic thin films grown by organic molecular-beam deposition. *Phys. Rev. B*, 51(7):4449–4462, February 1995.

[414] D Eastwood, L Edwards, M. Gouterman, and J. Steinfeld. Spectra of porphyrins. *J. Mol. Spectrosc.*, 20(4):381–390, August 1966.

[415] Nadia Dozova, Ciaran Murray, John G McCaffrey, Niloufar Shafizadeh, and Claudine Crépin. Amplified emission of phthalocyanine isolated in cryogenic matrices. *Phys. Chem. Chem. Phys.*, 10(16):2167–74, April 2008.

[416] J Mizuguchi and S Matsumoto. Molecular Distortion and Exciton Coupling Effects in β Metal-Free Phthalocyanine. *J. Phys. Chem. A*, 103(5):614–616, February 1999.

[417] Bernard R Brooks, Robert E Bruccoleri, Barry D Olafson, David J States, S Swaminathan, and Martin Karplus. CHARMM: A program for macromolecular energy, minimization, and dynamics calculations. *J. Comput. Chem.*, 4(2):187–217, January 1983.

[418] H Lee Woodcock, Milan Hodoscek, Andrew T B Gilbert, Peter M W Gill, Henry F Schaefer, and Bernard R Brooks. Interfacing Q-Chem and CHARMM to perform QM/MM reaction path calculations. *J. Comput. Chem.*, 28(9):1485–502, July 2007.

[419] Berk Hess, Carsten Kutzner, David van der Spoel, and Erik Lindahl. GROMACS 4: Algorithms for Highly Efficient, Load-Balanced, and Scalable Molecular Simulation. *J. Chem. Theory Comput.*, 4(3):435–447, March 2008.

[420] Reinhart Ahlrichs, Michael Bär, Marco Häser, Hans Horn, and Christoph Kölmel. Electronic structure calculations on workstation computers: The program system turbomole. *Chem. Phys. Lett.*, 162(3):165–169, October 1989.

[421] Lee, J.; Baldo, M.A. personal communication.

[422] Christof Hattig and Andreas Kohn. Transition moments and excited-state first-order properties in the coupled-cluster model CC2 using the resolution-of-the-identity approximation. *J. Chem. Phys.*, 117(15):6939, October 2002.

[423] Martin Head-Gordon, Ana M Grana, David Maurice, and Christopher A White. Analysis of Electronic Transitions as the Difference of Electron Attachment and Detachment Densities. *J. Phys. Chem.*, 99(39):14261–14270, September 1995.

[424] Frank C Spano. Excitons in conjugated oligomer aggregates, films, and crystals. *Annu. Rev. Phys. Chem.*, 57:217–43, January 2006.

[425] J Cornil, D A dos Santos, X Crispin, R Silbey, and J L Brédas. Influence of Interchain Interactions on the Absorption and Luminescence of Conjugated Oligomers and Polymers: A Quantum-Chemical Characterization. *J. Am. Chem. Soc.*, 120(6):1289–1299, February 1998.

[426] Kaushik Mahata and Pritha Mahata. Maximizing Correlation for Supervised Classification. In S Sanei, J A Chambers, J McWhirter, Y Hicks, and A G Constantinides, editors, *2007 15th International Conference on Digital Signal Processing*, pages 107–110. IEEE, July 2007.

[427] Ryan D Pensack and John B Asbury. Barrierless free carrier formation in an organic photovoltaic material measured with ultrafast vibrational spectroscopy. *J. Am. Chem. Soc.*, 131(44):15986–15987, November 2009.

[428] Yi Zhou, Kristofer Tvingstedt, Fengling Zhang, Chunxia Du, Wei-Xin Ni, Mats R Andersson, and Olle Inganäs. Observation of a Charge Transfer State in Low-Bandgap Polymer/Fullerene Blend Systems by Photoluminescence and Electroluminescence Studies. *Adv. Funct. Mater.*, 19(20):3293–3299, October 2009.

[429] Kouki Akaike, Kaname Kanai, Yukio Ouchi, and Kazuhiko Seki. Impact of Ground-State Charge Transfer and Polarization Energy Change on Energy Band Offsets at Donor/Acceptor Interface in Organic Photovoltaics. *Adv. Funct. Mater.*, 20(5):715–721, March 2010.

[430] M Born. Volumen und Hydratationswärme der Ionen. *Zeitschrift für Physik*, 1(1):45–48, February 1920.

[431] Naoki Sato, Kazuhiko Seki, and Hiroo Inokuchi. Polarization energies of organic solids determined by ultraviolet photoelectron spectroscopy. *J. Chem. Soc. Faraday Trans. 2*, 77(9):1621–1633, 1981.

[432] Kaname Kanai, Takahiro Miyazaki, Hiroyuki Suzuki, Mina Inaba, Yukio Ouchi, and Kazuhiko Seki. Effect of annealing on the electronic structure of poly(3-hexylthiophene) thin film. *Phys. Chem. Chem. Phys.*, 12(1):273–82, January 2010.

[433] A. K. Pandey and J.-M. Nunzi. Rubrene/Fullerene Heterostructures with a Half-Gap Electroluminescence Threshold and Large Photovoltage. *Adv. Mater.*, 19(21):3613–3617, November 2007.

[434] Na Sai, Murilo Tiago, James Chelikowsky, and Fernando Reboredo. Optical spectra and exchange-correlation effects in molecular crystals. *Phys. Rev. B*, 77(16):161306, April 2008.

[435] S L Ren, Y. Wang, A M Rao, E McRae, J M Holden, T Hager, KaiAn Wang, Wen-Tse Lee, H F Ni, J Selegue, and P. C. Eklund. Ellipsometric determination of the optical constants of C60 (Buckminsterfullerene) films. *Appl. Phys. Lett.*, 59(21):2678–2680, 1991.

[436] C W Tang. Two-layer organic photovoltaic cell. *Appl. Phys. Lett.*, 48(2):183–185, 1986.

[437] V. P. Singh, R S Singh, B Parthasarathy, A Aguilera, J Anthony, and M Payne. Copper-phthalocyanine-based organic solar cells with high open-circuit voltage. *Appl. Phys. Lett.*, 86(8):082106, February 2005.

[438] P Peumans, V. Bulovic, and S R Forrest. Efficient photon harvesting at high optical intensities in ultrathin organic double-heterostructure photovoltaic diodes. *Appl. Phys. Lett.*, 76(19):2650–2652, 2000.

[439] M K Debe. Variable angle spectroscopic ellipsometry studies of oriented phthalocyanine films. II. Copper phthalocyanine. *J. Vac. Sci. Technol., A*, 10(4):2816, July 1992.

[440] Barry P Rand, Peter Peumans, and Stephen R Forrest. Long-range absorption enhancement in organic tandem thin-film solar cells containing silver nanoclusters. *J. Appl. Phys.*, 96(12):7519, December 2004.

[441] Qinghai Song, Lei Wang, Shumin Xiao, Xinchuan Zhou, Liying Liu, and Lei Xu. Random laser emission from a surface-corrugated waveguide. *Phys. Rev. B*, 72(3):035424, July 2005.

[442] Pavel A. Troshin, Diana K. Susarova, Ekaterina A. Khakina, Andrey A. Goryachev, Oleg V. Borshchev, Sergei A. Ponomarenko, Vladimir F. Razumov, and N Serdar Sariciftci. Material solubility and molecular compatibility effects in

the design of fullerene/polymer composites for organic bulk heterojunction solar cells. *J. Mater. Chem.*, 22(35):18433, 2012.

[443] Toshihiko Kaji, Minlu Zhang, Satoru Nakao, Kai Iketaki, Kazuya Yokoyama, Ching W Tang, and Masahiro Hiramoto. Co-evaporant induced crystalline donor: acceptor blends in organic solar cells. *Advanced M*, 23(29):3320–5, August 2011.

[444] Bin Yang, Yongbo Yuan, Pankaj Sharma, Shashi Poddar, Rafal Korlacki, Stephen Ducharme, Alexei Gruverman, Ravi Saraf, and Jinsong Huang. Tuning the energy level offset between donor and acceptor with ferroelectric dipole layers for increased efficiency in bilayer organic photovoltaic cells. *Adv. Mater.*, 24(11):1455–60, March 2012.

[445] Abay Gadisa, Mattias Svensson, Mats R. Andersson, and Olle Inganäs. Correlation between oxidation potential and open-circuit voltage of composite solar cells based on blends of polythiophenes/ fullerene derivative. *Appl. Phys. Lett.*, 84(9):1609, 2004.

[446] Thomas Kietzke, Daniel A. M. Egbe, Hans-Heinrich Hörhold, and Dieter Neher. Comparative Study of M3EHPPV-Based Bilayer Photovoltaic Devices. *Macromolecules*, 39(12):4018–4022, June 2006.

[447] Floris B Kooistra, Joop Knol, Fredrik Kastenberg, Lacramioara M Popescu, Wiljan J H Verhees, Jan M Kroon, and Jan C Hummelen. Increasing the open circuit voltage of bulk-heterojunction solar cells by raising the LUMO level of the acceptor. *Org. Lett.*, 9(4):551–554, February 2007.

[448] Koen Vandewal, Kristofer Tvingstedt, Abay Gadisa, Olle Inganäs, and Jean V Manca. On the origin of the open-circuit voltage of polymer-fullerene solar cells. *Nat. Mater.*, 8(11):904–9, November 2009.

[449] Bright Walker, Arnold B Tamayo, Xuan-Dung Dang, Peter Zalar, Jung Hwa Seo, Andres Garcia, Mananya Tantiwiwat, and Thuc-Quyen Nguyen. Nanoscale Phase Separation and High Photovoltaic Efficiency in Solution-Processed, Small-Molecule Bulk Heterojunction Solar Cells. *Adv. Funct. Mater.*, 19(19):3063–3069, October 2009.

[450] Svetlana S. van Bavel, Maik Bärenklau, Gijsbertus de With, Harald Hoppe, and Joachim Loos. P3HT/PCBM Bulk Heterojunction Solar Cells: Impact of Blend Composition and 3D Morphology on Device Performance. *Adv. Funct. Mater.*, 20(9):1458–1463, April 2010.

[451] Wanli Ma, Cuiying Yang, Xiong Gong, Kwanghee Lee, and Alan J Heeger. Thermally Stable, Efficient Polymer Solar Cells with Nanoscale Control of the Interpenetrating Network Morphology. *Adv. Funct. Mater.*, 15(10):1617–1622, October 2005.

[452] Guillaume Lamoureux and Benot Roux. Modeling induced polarization with classical Drude oscillators: Theory and molecular dynamics simulation algorithm. *J. Chem. Phys.*, 119(6):3025, 2003.

[453] O.D. Gordan, T Sakurai, M Friedrich, K Akimoto, and D.R.T. Zahn. Ellipsometric study of an organic template effect: H2Pc/PTCDA. *Org. Electron.*, 7(6):521–527, December 2006.

[454] C P Brock and J D Dunitz. Temperature dependence of thermal motion in crystalline anthracene. *Acta Crystallogr., Sect. B: Struct. Sci.*, 46(6):795–806, December 1990.

[455] Daniel Holmes, Sriram Kumaraswamy, Adam J Matzger, and K Peter C Vollhardt. On the Nature of Nonplanarity in the [N]Phenylenes. *Chemistry - A European Journal*, 5(11):3399–3412, November 1999.

[456] Silvia C Capelli, Alberto Albinati, Sax A Mason, and Bertram T M Willis. Molecular motion in crystalline naphthalene: analysis of multi-temperature X-ray and neutron diffraction data. *J. Phys. Chem. A*, 110(41):11695–703, October 2006.

[457] J Trotter. 1,4-Dibromonaphthalene; a redetermination. *Acta Crystallographica Section C Crystal Structure Communications*, 42(3):351–353, March 1986.

[458] I Bulgarovskaya, V Vozzhennikov, S Aleksandrov, and V Belsky. Low-temperature structure of rubrene single crystals grown by vapor transport. *Latv. PSR Zinat. Akad. Vestis Fiz. Teh. Zinat. Ser.*, 4:53–59, 1983.

[459] J Bernstein. Refinement of trans-stilbene: a comparison of two crystallographic studies. *Acta Crystallogr., Sect. B: Struct. Sci.*, 31(5):1268–1271, May 1975.